

Institute of Cancer and Genetics
School of Medicine
Cardiff University



**Investigating the Mechanisms of Telomeric Mutation in Human
Cells**

A thesis submitted to the School of Medicine, Cardiff University in partial
fulfilment for the degree of Doctor of Philosophy

Raniah Saleem Alotibi

2015

DECLARATION

This work has not previously been accepted in substance for any degree and is not concurrently submitted in candidature for any degree.

Signed (candidate) Date

STATEMENT 1

This thesis is being submitted in partial fulfillment of the requirements for the degree of(insert MCh, MD, MPhil, PhD etc, as appropriate)

Signed (candidate) Date

STATEMENT 2

This thesis is the result of my own independent work/investigation, except where otherwise stated.

Other sources are acknowledged by explicit references.

Signed (candidate) Date

STATEMENT 3

I hereby give consent for my thesis, if accepted, to be available for photocopying and for inter-library loan, and for the title and summary to be made available to outside organisations.

Signed (candidate) Date

STATEMENT 4: PREVIOUSLY APPROVED BAR ON ACCESS

I hereby give consent for my thesis, if accepted, to be available for photocopying and for inter-library loans **after expiry of a bar on access previously approved by the Graduate Development Committee.**

Signed (candidate) Date

Acknowledgements

First, I would like to thank Almighty Allah for the perseverance that he has bestowed upon me during this research project and indeed throughout my life.

I am heartily thankful to my supervisor, Professor Duncan M. Baird, for giving me the opportunity to work in his laboratory. I would also like to thank him for his continuous support and guidance throughout the project and throughout my mother illness, which encouraged me to work hard during this PhD.

Furthermore, I would like to thank all the other members of the STELA group: Dr Maira Tankinmanova, Julia Grimstead, Dr Thet Thet Lin, Dr Nicole Heppel, Dr Bethan Britt-Compton, Dr Laureline Roger, Dr Rhiannon Robinson, Dr Biotelo Letsolo, Dr Kevin Norris, Dr Kate Simpson and Dr Kate Liddiard, for all their advice and encouragement in the last four years. A special thank you goes to Maira Tankinmanova and Julia Grimstead which have been a tremendous help in tissue culture and western blot.

I especially would like to thank my family and friends who have been a continual support and encouragement during this PhD. A huge thank you goes to (my mum, my dad, my grandmother, sisters and brothers) whom their love, prayers source of support during this PhD. Most importantly I have to thank Meshari, who has been a source of support and positivity during writing my thesis.

My mum, without you this PhD thesis would not have been possible.

Summary

Telomeres are nucleoprotein structures that contain non-coding (TTAGGG) tandem repeats and associated telomere binding proteins at the end of chromosomes. As a consequence of end-replication losses, telomeres undergo gradual erosion with ongoing cell division. It is hypothesised that in addition to the end-replication problem, mutational mechanisms may contribute to telomere erosion by generating large-scale telomeric deletion events. As short dysfunctional telomeres are capable of fusion to other chromosome ends, large-scale telomeric deletions can lead to genomic instability which in turn may drive tumour progression.

The primary aim of this thesis was to investigate putative mutational mechanisms that could lead to large-scale telomeric deletion. The role of oxidative stress and its potential contribution to telomere dynamics was assessed. The induction of fragility and replication inhibition at telomeres was also examined. Furthermore, the role that G-quadruplex structure within telomere repeat sequences and the possible induction of replication fork stalling and resolution as single or double stranded breaks was also considered as a mutational mechanism that could lead to telomere deletion.

High-resolution analysis of telomere dynamics using Single Telomere Length Analysis (STELA), following the induction of oxidative stress in IMR90 fibroblasts, revealed that oxidative damage does not appear to affect the rate of telomere erosion, or the frequency of large-scale telomeric deletion. The data are more consistent with the view that premature senescence does not arise as a consequence of accelerated telomere erosion, but instead more likely results from stochastic DNA damage across the rest of the genome.

The analysis of telomere dynamics following the induction of chromosome fragility, showed that telomere length in Seckel cell (SCK) fibroblasts were significantly different from those of untreated cells following treatments with aphidicolin with an increase in stochastic telomeric deletion. Whilst in MRC5 fibroblasts, the induction of the telomere fragility impacted on the upper to lower allele ratio, with a loss of the longer telomere length distributions.

The stabilisation of G-quadruplex structures using the G-quadruplex ligand (RHPS4), together with ATRX knockdown, showed that an absence of ATRX sensitised cells to the ligand, but that the stabilisation of G-quadruplexes, did not significantly affect the telomere dynamics as determined using STELA.

Taken together, the data presented in this thesis are not consistent with a role for oxidative stress, or the formation of G-quadruplex structures, in generating large-scale telomeric deletion; however telomeric mutational events may occur following the induction of chromosome fragile sites, specifically in the context of an ATR deficiency.

Contents

Declaration	I
Acknowledgements	II
Summary	III
Contents	IV
Abbreviations	XIII
Chapter 1 Introduction	1
1.1 The History of Telomeres	1
1.2 The Structure of the Telomere	2
• 1.2.1 Diptera	3
• 1.2.2 Protozoa	4
• 1.2.3 Fungi	4
• 1.2.4 Plants	5
• 1.2.5 Mammals	5
1.3 Telomere-associated proteins	6
• 1.3.1 Shelterin	6
• 1.3.1.1 TRF1 and TRF2	7
• 1.3.1.2 TIN2	8
• 1.3.1.3 TPP1	8
• 1.3.1.4 POT1	9
• 1.3.1.5 Rap1	10
• 1.3.2 Transient associated telomeres proteins	10

• 1.3.2.1 PinX1	11
• 1.3.2.2 Tankyrase1 and Tankyrase2	11
• 1.3.2.3 Ataxia Telangiectasia Mutated (ATM)	12
• 1.3.2.4 BLM	12
• 1.3.2.5 WRN	13
1.4 Telomere function	13
• 1.4.1 Chromosome capping and DNA damage response	13
• 1.4.2 Telomeres in mitosis and meiosis	14
• 1.4.3 Senescence	16
• 1.4.3.1 Senescence associated β –galactosidase activity	17
• 1.4.3.2 The end replication problem	17
• 1.4.3.3 Telomere-dependent replicative senescence	19
• 1.4.3.4 Telomere-independent replicative senescence	20
1.5 Telomere Maintenance Mechanisms (TMM)	22
• 1.5.1 Telomerase	22
• 1.5.1.1 Structure	22
• 1.5.1.2 Function	23
• 1.5.1.3 Telomerase regulation	25
• 1.5.2 Alternative Lengthening of Telomere (ALT)	25
1.6 Telomeres and Disease	26
• 1.6.1 Cancer	26

• 1.6.2 Werner Syndrome	28
• 1.6.3 Bloom’s Syndrome	29
• 1.6.4 Dyskeratosis Congenita	29
• 1.6.5 Ataxia Telangiectasia (AT)	30
1.7 DNA repair mechanisms	31
• 1.7.1 Homologous Recombination (HR)	32
• 1.7.2 Non homologous end joining (NHEJ)	33
1.8 Oxidative damage	34
• 1.8.1 Reactive oxygen species ROS ‘Mitochondria’	35
1.9 G-quadruplex formation	37
• 1.9.1 Structure of G-quadruplex	37
• 1.9.2 G4 ligands	38
1.10 Telomeres and Fragile sites	39
• 1.10.1 Fragile sites	39
• 1.10.2 Telomeres considered as fragile site	39
• 1.10.3 Replication fork stalling	40
1.11 Telomere Length Analysis	41
• 1.11.1 Terminal Restriction fragment (TRF) analysis	41
• 1.11.2 Quantitative fluorescence in situ hybridization (Q-FISH)	41
• 1.11.3 Flow FISH	42

• 1.11.4. Quantitative PCR	42
• 1.11.5 Single Telomere Length Analysis (STELA)	44
1.12 This work	45
Chapter 2 Materials and Methods	48
2.1 Chemicals and Reagents	48
2.2 Plastic Labware	48
2.3 Equipment	48
2.4 Oligonucleotides	49
2.5 Cell Culture	50
• 2.5.1 Cells	50
• 2.5.2 Medium	50
• 2.5.3 Seeding and Passage	51
• 2.5.4 Counting Cells and Population Doublings Calculations	51
• 2.5.5 Cell Freezing	52
• 2.5.6 Cell Thawing	52
• 2.5.7 Senescence Assay	52
• 2.5.8 Cell Cycle Analysis Using Propidium Iodide (PI)	53
• 2.5.9 Apoptosis Analysis	53
• 2.5.10 Metaphase Spread Analysis	54
2.6 Single Telomere Length Analysis (STELA)	55

• 2.6.1 Preparation Cells for DNA Extraction	55
• 2.6.2 DNA Extraction	55
• 2.6.2.1 Maxwell	55
• 2.6.2.2 DNA Extraction Using QIAamp DNA Micro Kit	55
• 2.6.3 DNA Quantification	56
• 2.6.4 STELA PCR	56
• 2.6.5 Fusion PCR	57
• 2.6.6 Gel Electrophoresis for STELA and Fusion PCR Products	57
• 2.6.7 Southern Blot	58
• 2.6.8 Southern Hybridisation Probes for STELA and Fusion Assay	58
• 2.6.9 Hybridisation	59
• 2.6.10 Hybridisation Washes	59
• 2.6.11 Visualisation of Radiolabelled DNA Fragments	59
2.7 Protein	60
• 2.7.1 Protein Extraction (Cell Lysis)	60
• 2.7.2 Protein Quantification	60
• 2.7.3 Prepare Samples	61
• 2.7.4 Running Gel	61
• 2.7.5 Prepare Membrane	62
• 2.7.6 Transfer Proteins from Gel to Membrane (Western Blot)	62
• 2.7.7 Membrane Blocking and Antibody Incubation	62
• 2.7.8 Protein Detection	63

2.8 Statistical Analysis	64
• 2.8.1 T-test	64
• 2.8.2 Repeat Measure ANOVA	64
Chapter 3 Oxidative stress and Telomere erosion	65
3.1 Summary	65
3.2 Introduction	66
• 3.2.1 Telomere-Dependent Replicative Senescence	66
• 3.2.2 Telomere-Independent Cellular Senescence	66
• 3.2.3 Telomere Deletion Events	67
• 3.2.4 Oxidative Stress and Telomere Structure	69
• 3.2.5 Reactive Oxygen Species (ROS)	69
• 3.2.6 Oxidative Stress and Cell Culture	71
• 3.2.7 Analysis of Stochastic Deletion Events	72
3.3 This Work	73
3.4 Results	73
• 3.4.1 Effects of Oxidative Stress on Culture Growth	73
• 3.4.2 Effect of Oxidative Damage on Cell Cycle Progression	81
• 3.4.3 Oxidative Damage Induce Cellular Senescence	84
• 3.4.3.a Cellular Morphology	84
• 3.4.3.b Senescence Associated Beta Galactosidase Activity (SA β -gal)	84
• 3.4.4 Analysis of Telomere Dynamics	88

3.5 Discussion	100
• 3.5.1 Culture Growth	100
• 3.5.2 Cell Cycle Progression under Oxidative Stress	101
• 3.5.3 Telomere Dynamics	103
3.6 Conclusion	107
Chapter 4 Telomere Fragile Site	108
4.1 Summary	108
4.2 Introduction	109
• 4.2.1 Telomeres and Fragile Sites	109
• 4.2.2 History of Fragile Site	110
• 4.2.3 Classification of Fragile Sites	112
• 4.2.3.1 Rare Fragile Sites	112
• 4.2.3.2 Common Fragile Site (CFSs)	112
• 4.2.4 Fragile Site Inducers	112
• 4.2.5. Maintenance of Fragile Site Stability	113
• 4.2.6 Fragile Sites as Indicators of Stalled Replication in Cancer	114
• 4.2.7 Analysis of Stochastic Deletion Events	115
4.3 This Work	115
4.4 Results	116
• 4.4.1 Effects of Fragile Site Induction on Culture Growth	116
• 4.4.2 Effect of Fragility Induces on Cell Cycle Checkpoints	120
• 4.4.3 Cellular Senescence	122

• 4.4.3.a Cellular Morphology	122
• 4.4.3.b Senescence Associated Beta galactosidase Activity (SA β -gal)	122
• 4.4.4 Metaphase Chromosomes Analysis (Breaks and gaps)	127
• 4.4.5 Proteins Checkpoint Activation Analysis (Western Blotting)	129
• 4.4.6 Analysis of Telomere Dynamics	131
4.5 Discussion	138
• 4.5.1 Culture Growth	138
• 4.5.2 Checkpoint Activation, Cell Cycle Arresting and Chromosomal Instability	138
• 4.5.3 Telomere Dynamics	140
4.6 Conclusion	143
Chapter 5 Examining the relationship between G-quadruplex stabilisation and telomeric mutation	144
5.1 Summary	144
5.2 Introduction	
• 5.2.1 Formation of G-quadruplex	145
• 5.2.2 Prevalence of G-quadruplexes in the Genome	146
• 5.2.3 Impact of G-quadruplex Formation in the Genome	147
• 5.2.4 G-quadruplex Ligands	148
• 5.2.5 G-quadruplex Unwinding	148
5.3 This Work	150
5.4 Result	152
• 5.4.1 Effects of G-quadruplex Stabilisation on Cell Proliferation	152

• 5.4.2 Effects of G-quadruplex Stabilisation on Cell Cycle Progression	156
• 5.4.3 Cellular Morphology and Senescence Associated Beta galactosidase Activity (SA β -gal)	158
• 5.4.4 G-quadruplex Stabilisation and Cellular Apoptosis	161
• 5.4.5 Checkpoint Activation	163
• 5.4.6 Analysis of Telomere Dynamics	165
5.5 Discussion	181
• 5.5.1 Cellular Proliferation	181
• 5.5.2 Checkpoint Activation and Cell Cycle Arresting	183
• 5.5.3 Telomere Dynamics	184
5.6 Conclusions	188
Chapter 6 General Discussion and Future Investigations	189
6.1 Previous Studies	189
6.2. Research Presented in This Thesis	190
• 6.2.1 Oxidative Stress and Telomere Erosion	190
• 6.2.2 Telomere Fragile Site	191
• 6.2.3 G-quadruplex Structure at Telomere	193
6.3 Future Investigations	195
6.4 Conclusion	198
References	199

Abbreviations

- **53BP1** p53 Binding Protein 1
- **ABC** ATP Binding Cassette
- **A** Adenosine Diphosphate
- **ALT** Alternative Lengthening of Telomeres
- **AMP** Adenosine Monophosphate
- **A-NHEJ** Alternative NHEJ
- **APH** Aphidicolin

- **ARH3** ADP-ribosylhydrolase 3
- **AT** Ataxia Telangiectasia
- **ATLD** Ataxia Telangiectasia-Like Disorder
- **ATM** Ataxia Telangiectasia Mutated
- **ATP** Adenosine Triphosphate
- **ATR** ATM and Rad3 Related
- **BER** Base Excision Repair
- **BFB** Breakage-Fusion-Bridge
- **BLM** Bloom Syndrome Helicase
- **Bp** Base pair
- **BRCA1** Breast Cancer 1
- **BRCT** Breast Cancer C-terminal domain
- **BrdU** Bromodeoxyuridine
- **BS** Bloom Syndrome
- **BSA** Bovine Serum Albumin
- **CD** Cell division
- **Cdc** Cell division cycle
- **CDC25** Cell Division Cycle 25
- **cDNA** Complementary DNA
- **CHK1** Checkpoint kinase 1

• CHK2	Checkpoint kinase 2
• C-NHEJ	Classic NHEJ
• CFSs	Common Fragile Sites
• C-terminus	Carboxyl-terminus
• <i>D melanogaster</i>	<i>Drosophila melanogaster</i>
• DAB	Diaminobenzidine
• DBD	DNA Binding Domain
• DC	Dyskeratosis Congenita
• DDR	DNA Damage Repair
• DIQ	1,5-Isoquinolinediol
• DKC1	Dyskerin
• D-loop	Displacement loop
• DMEM	Dulbecco's Modified Eagle's Medium
• DMS	Dimethylsulfate
• DMSO	Dimethyl Sulfoxide
• DNA	Deoxyribonucleic Acid
• DNA-PKcs	DNA-dependent protein kinase catalytic subunit
• DSB	DNA double Strand break
• EMEM	Eagle's minimum essential medium
• FBS	Foetal Bovine Serum
• FCS	Fetal Calf Serum
• FEN1	Flap Endonuclease 1
• FHD	Fork Head associated Domain
• G0	Quiescence
• G1	Gap phase 1
• G2	Gap phase 2
• GTP	Guanosine triphosphate
• HeLa	Henrietta Lacks
• HeT-A	Drosophila telomeric non-LTR retrotransposon
• HPV	Human Papillomavirus

- **HR** Homologous Recombination
- **HU** Hydroxyurea
- **IR** Ionizing Radiation
- **Kb** Kilo base
- **kDA** Kilo Dalton
- **LTR** Long Terminal-Repeat
- **MBD** Mre11 Binding Domain
- **MDC1** Mediator of DNA damage Checkpoint 1
- **MMEJ** Microhomology Mediated End Joining
- **MRE11** Meiotic recombination II protein
- **MRN** Complex containing MRE11/RAD50/NBS1
- **MRX** Homolog in yeast of MRN
- **NAD** Nicotinamide Adenine Dinucleotide
- **NBS1** Nijmegen Breakage Syndrome protein
- **NHEJ** Non-Homologous End Joining
- **Nt** Nucleotide
- **NTase** Nucleotidyltransferase
- **N-terminus** Ammino-terminus
- **NTP** Nucleoside triphosphate
- **NuMA** Nuclear Mitotic Apparatus protein
- **OB** Oligonucleotide Binding fold
- **pADPr** Poly ADP-ribose
- **PAR** Poly ADP-ribose
- **PARG** Poly (ADP-ribose) glycohydrolase
- **PARP** Poly ADP-ribose polymerase
- **PBS** Phosphate Buffered Saline
- **PCNA** Proliferating Cell Nuclear Antigen
- **PCR** Polymerase Chain Reaction
- **PD** Population Doubling
- **PI** Propidium Iodide

- **PIN2** Protein interacting with NIMA
- **PINX1** Pin2/TRF1 interacting protein
- **PIP1** Pot1 interacting protein
- **PNK** Mammalian polynucleotide kinase
- **POT1** Protein-protection Of Telomeres 1
- **pRB** Retinoblastoma susceptibility gene product
- **PTOP** Pot1 interacting protein
- **RAD50** Radiation sensitive protein
- **RAD51D** RAD51/RecA-related gene
- **RAP1** Repressor Activator Protein 1
- **RNA** Ribonucleic Acid
- **RNase** Ribonulease
- **ROS** Radical Oxygen Species
- **RS** Replicative senescence
- **RT** Room temperature
- ***S cerevisiae*** *Saccharomyces cerevisiae*
- **SCK** Seckel cells
- **S phase** DNA synthesis phase
- ***S pombe*** *Saccharomyces pombe*
- **SA β -gal** Senescence-associated mammalian β -galactosidase
- **SCE** Sister Chromatide Exchange
- **SD** Standard Deviation
- **SE** Standard error
- **SIPS** Stress induced premature senescence
- **STELA** Single Telomere Length Analysis
- ***T brucei*** *Trypanosoma brucei*
- ***T cruzi*** *Trypanosoma cruzi*
- **TAE** Tris-acetat-EDTA
- **TAHR** Drosophila telomeric non-LTR retrotransponson
- **TART** Drosophilia telomeric non-LTR retrotransposons
- **Taz1** Telomere associated in *Schizosaccharomyces pombe*

- **TBE** Tris Borate EDTA
- **TBS** Tris Buffer Saline

- **T-circles** Telomeric circle
- **TERC** Telomerase RNA
- **TERT** Telomerase reverse transcriptase
- **TIN2** TRF interacting protein 2
- **TINT1** TIN2 interacting protein
- **T-loop** Telomere loop
- **TNKS** Tankyrase 1
- **TNKS2** Tankyrase 2
- **TPP1** Thiamine pyrophosphate enzyme
- **TRD** Telomere rapid deletion
- **TRF** Terminal Restriction Fragment
- **TRF1** Telomere Repeat binding Factors 1
- **TRF2** Telomere Repeat binding Factors 2
- **TRFH** TRF homodimerisation domain
- **TVR** Telomere Variant Repeat
- **UV** UltravioletXI
- **WRN** Werners syndrome gene
- **WS** Werner Syndrome
- **XPF** Human nucleotide excision repair protein
- **XRCC** X-ray repair cross-complementing
- **Xrs2** NBS1 homolog in yeast
- **γH2AX Histone** H2AX phosphorylated on serine 139

Chapter 1

Introduction

1.1 The History of Telomeres

During the 1930s, Hermann Muller became the first researcher to notice that the ends of chromosomes had distinct features (Mueller, 1939). Based on their position on chromosomes, Muller named these ends **TELOMERES** (from Greek word *telo*, which means “end” and *mere*, which means “part”). Later, in his *Drosophila* mutagenesis experiments, he used X-rays to create different internal rearrangements such as deletions, inversions and translocations. Muller was surprised to note that the ends of the chromosomes were not being affected by the mutagenic X-rays. He concluded that the genes at these terminal ends could be having a special function, which prevented chromosomal alterations and helped maintain the integrity of the chromosome.

In 1939, two years after Muller’s discovery, Barbara McClintock’s observed that in maize (*Zea Mays*), the loss of these end structures after an X-irradiation stimulated sister chromatid fusion events. These fusion events by sister chromatids resulted in dicentric chromosomes that formed a “bridge” between the two daughter cells in the meiotic anaphase of cell division. At the end of anaphase, dicentric chromosomes break inducing an unequal break site in the two daughter chromosomes. Mitosis of the daughter cells can induce continuous cycles of replication, sister chromatid fusion and unequal breakage events (**Breakage-Fusions-Bridge (BFB)**). Consequently, several BFB cycles can lead to unequal exchange of genetic information causing gene duplications and deletions. McClintock noticed that BFB cycles were only maintained in somatic cells, whereas in

embryonic cells the BFB cycles were interrupted and chromosomal breakage were permanently healed (McClintock,1941).

1.2 The Structure of the Telomere

Telomeres are specialised DNA structures which are located at the chromosomes terminus (Blackburn, 2000). Since the work by Muller (*Muller, 1939*) and McClintock work (McClintock, 1941), telomeres have been shown to offer protection to chromosome ends against end-to-end fusion and degradation. They are made of repetitive G-rich DNA sequences and associated proteins, which distinguish natural chromosome ends from damage caused by DNA breaks.

T-Loop Structure

Telomeric repeats and associated proteins form the **Telomere Loop (T-loop)** structure, in which the extended 3'end single-stranded overhang invades the DNA double strand to protect the chromosomal ends and to become effectively hidden from being considered as DNA damaged (Figure1). T-loop has been observed in protozoa, plants, yeast and human (Griffith et al., 1999).

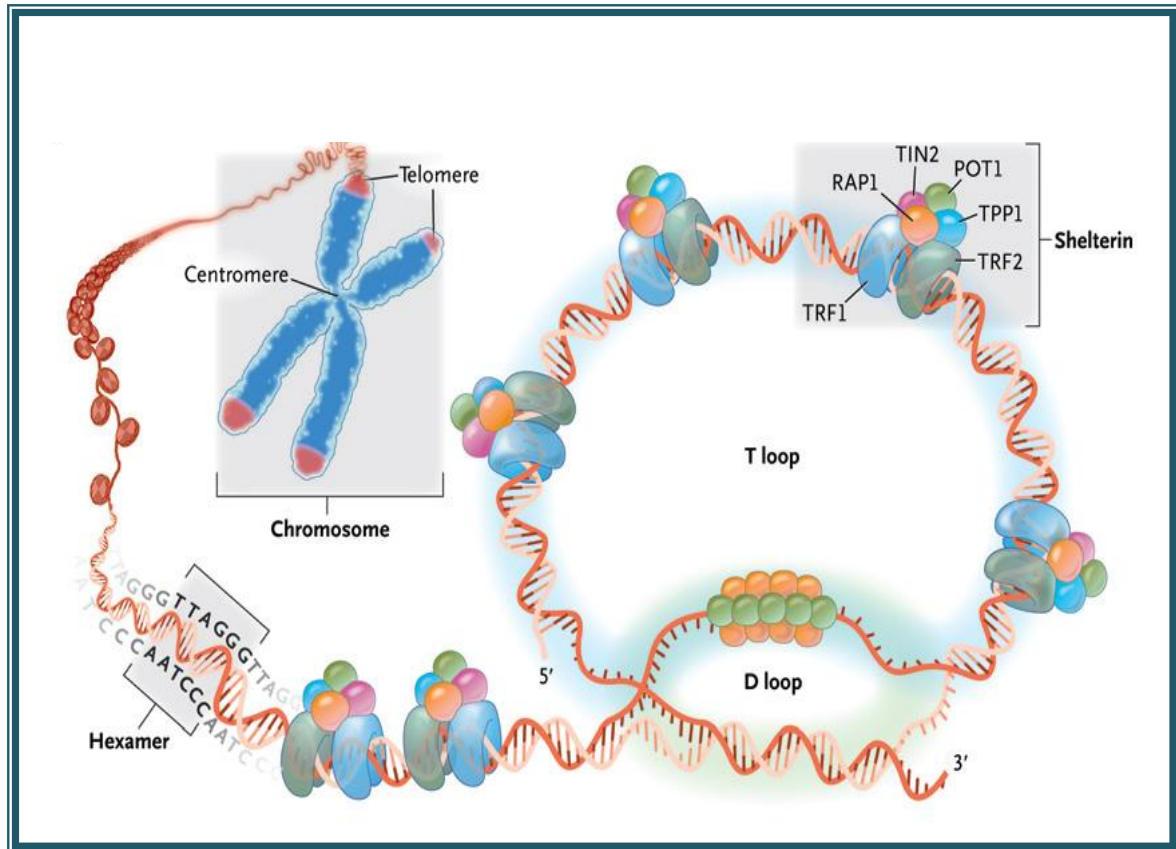


Figure 1: T-Loop structure. Chromosome ends are capped and protected by telomeres and associated proteins which consists of (TRF1, TRF2, TIN2, POT1, TPP1 and RAP1). The leading strand (TTAGGG) overhang invades the double-stranded helix, forming T loop. **(Diagram is reproduced from Calado and Young, 2009).**

1.2.1 Diptera

Drosophila melanogaster telomeres have a unique telomere structure compared to the conserved G-rich structure of eukaryotic telomeres. The chromosome ends of *Drosophila* are formed in arrays of **telomere-specific non-Long Terminal Repeat (LTR)** retrotransposons (Pardue and DeBaryshe, 2003). *Drosophila melanogaster* telomeres are maintained by non-LTR retrotransposons; *HeT-A* and *TART*. *HeT-A* and *TART*

retrotransposons elements transpose to chromosome ends where they arranged head to tail.

1.2.2 Protozoa

In 1978, Blackburn and Gall carried out a study in which they sequenced the termini of *Tetrahymena thermophila* which showed between 20 and 70 repetitive sequences TTGGGG (Blackburn and Gall, 1978). In ciliates such as *Oxytricha fallax* and *Stylonychia pustulata*, the macronuclear DNA is capped by 20 bp of TTTTGGGG telomeric repeats sequence that end in an extra 16 bp 3'-overhang (Chiurillo et al., 1999). T-loop structure has been found in ciliates. Telomeres of *Trypanosome* have TTAGGG repeats similar to those that occur in eukaryotes. Chromosomes from *Trypanosome brucei* terminate in telomeric repeats of 10-20 kb and display a 3'-overhang of 21-250 nucleotides of TTAGGG repeats. The end of *T. brucei* DNA also has a T-loop formation (Munoz-Jordan et al., 2001). In addition to having a comparable structure to *T. brucei*, *T. cruzi* has a G-rich overhang with 9-50 nucleotides (Chiurillo et al., 1999).

1.2.3 Fungi

Telomere sequences of budding yeast *Saccharomyces cerevisiae* found to have a proximal domain containing 120 to a 150 bp of $G_{2-3}(TG)_{1-6}$ repeats and a distal domain containing TG_{1-7} repeats. (Shampay et al., 1984, Wang and Zakian, 1990). On the other hand the telomeres of fission yeast *Schizosaccharomyces pombe* are composed of 300 bp of the degenerated telomeric repeat sequence, $TTAC(A)(C)G_{2-8}$ repeat (Hiraoka et al., 1998). Both budding and fission yeast *S. pombe* and *S.cerevisiae* have a G-rich single stranded overhang at their chromosome termini (Gravel et al., 1998, Tomita et al., 2003).

1.2.4 Plants

In majority of the plants, the telomeres are composed of recognized TTAGGG repeats (Riha and Shippen, 2003). But the telomeres are of different lengths in different plant species. For example in *Arabidopsis*, the length of the telomere measures between 2 and 5 kb, whereas in tobacco, telomere repeats exceed 150 kb (Fajkus et al., 2005). However, the normal TTAGGG repeat seen in other plants is absent in algae such as *Chlamydomonas* and related species. These members of the Asparagales have the six base human-type telomere repeats TTAGGG (Bowers, Chapman, Rong & Paterson, 2003). The *Alliaceae* family (onions) does not have any kind of G-rich telomere repeats and demonstrates an unknown telomere structure (Pich et al., 1996). Similar to telomere length, the G-rich 3'-overhang also possesses variable lengths in plants, which range from 20 to 30 nucleotides in *Arabidopsis* to about 75 kb in *Pisum sativum* (Cesare et al., 2003). The G-rich 3'-overhang does not occur in all plants chromosomal termini, which signifies the presence of unknown telomeric structures in plants (Watson and Riha, 2010).

1.2.5 Mammals

The chromosomal ends in mammals are capped by the same telomere repeat sequence which consist of TTAGGG (Meyne et al., 1989) and telomere length varies in different species and sub-species. The wild *Mus. musculus* and *Mus. spretus* display telomere length vary from 5-20 kb, whereas inbred strains have much longer telomere length ~150Kb. The variation in telomere length has been also observed in mouse strains. For instance, DBA/2 mouse strain has telomere length ranging from 20-150Kb, whereas C57BL/6 strain displays a telomere length of 20-65 kb (Kipling and Cooke, 1990).

Human telomeres consist of TTAGGG repeat arrays, with length varying from 5-20Kb. In addition to TTAGGG repeats, human telomeres contain **Telomere Variant Repeats (TVR)**

such as TTGGGG, TGAGGG and TCAGGG. TVRs are contained within the proximal 1-2Kb of telomere repeat arrays (Baird et al., 1995, Brown et al., 1990 and de Lange et al., 1990).

1.3 Telomere-associated proteins

1.3.1 Shelterin

Human telomere repeats interact with the six protein complex known as **SHELTERIN COMPLEX**. The shelterin complex presents only and abundantly at the chromosomal ends. Telomere and shelterin proteins protect chromosomal ends from being recognised as DNA damage, prevent inappropriate end-to-end fusion and chromosomal abnormalities and maintain telomere length. Shelterin is made up of **Telomeric Repeat Binding protein Factors 1 and 2 (TRF1 and TRF2)**, **TRF1-Interacting Nuclear factor 2 (TIN2)**, **Protection Of Telomeres 1 (POT1)**, **Repressor/Activator Protein 1 (RAP1)** and **(TPP1)** (Diehl et al., 2009) (Figure2).

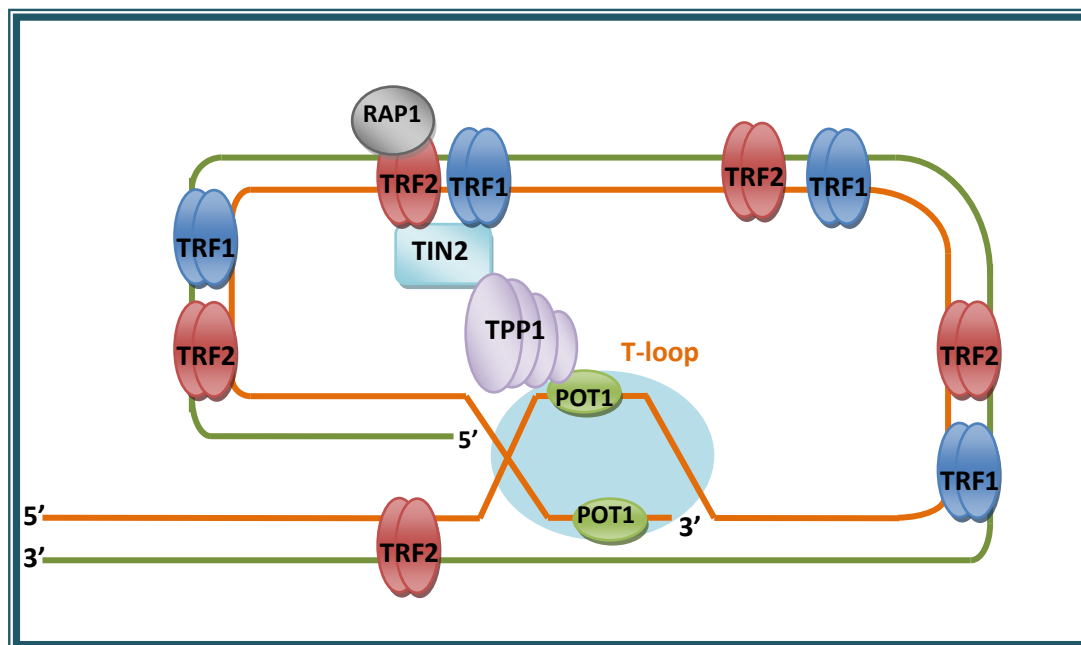


Figure 2: Shelterin complex. TRF1 & TRF2 bind to double-stranded and POT1 binds to 3' end single-stranded and these three proteins are held together by TIN2 & TPP1. (Original diagram using information from Diehl *et al.*, 2009).

1.3.1.1 TRF1 and TRF2

TRF1 was the first binding protein of shelterin complex to be identified (Zhong et al., 1992). TRF2 was identified afterwards as a distant homologue of TRF1 (Broccoli et al., 1997). TRF1 and TRF2 are similar in their structures; both operate as homo-dimers that bind to double stranded TTAGGG repeats via C-terminal helix-turn-helix SANT/Myb DNA-binding motif (Bianchi et al., 1999, Broccoli et al., 1997). Both TRF1 and TRF2 have identical biochemical features, however, their roles in the functioning of the telomere are very different. *In vivo* and *in vitro* studies show that TRF2 facilitates the formation T-loop where the 3' telomeric overhang is occupied into the previous array of duplex telomeric repeat. The overexpression of the dominant-negative TRF2 triggers the ATM/p53 and/or p16/RB pathways. In addition, it prompts cellular apoptosis. Besides, the inhibition of TRF2 triggers end-to-end fusion and chromosomal abnormalities. This is an indication of the critical role played by TRF2 in the “functional telomere structure” and also protects ends of the chromosome.

The role of TRF1 is to negatively regulate the length of the telomere (Steensel & de Lange, 1997). An overproduction of dominant-negative TRF1 triggers advanced elongation of the telomere. However, overproduction of the wild-type TRF1 triggers shortening of the telomere. TRF1 protein appears to be associated with **TANKYRASE 1& 2** that regulate the length of the telomere. Both tankyrase 1 and 2 are polymerases (poly-ADP-ribose), which targets TRF1 and triggers gradual lengthening of the telomere by dissociating TRF1 from the telomeric structures (Smith & de Lange, 2000). On the other hand, TIN2 mimics TRF1 function to negatively regulate telomere length (Kim, Kaminker, & Campisi, 1999). Studies

have suggested that the main function of TRF1 is control telomere length (Steensel & de Lange, 1997).

1.3.1.2 TIN2

TIN2 (TRF1- and TRF2-interacting nuclear factor 2) is a novel protein that binds TRF1 and seems to regulate telomere length. It does this by providing a steadying scaffold for the shelterin complex during its interaction with TRF1, TRF2 and TPP1 (Kim et al., 2004). It binds ssDNA-binding protein TPP1/POT1 to dsDNA-binding protein TRF1 and TRF2 (de Lange, 2005). TIN2 protein has 3 different binding sites for every binding partner (Ye et al., 2004a). For instance, the TRF1 binding site occurs on the C-terminus of TIN2, on the other hand, the N-terminus is related to TRF2 binding. Another role of TIN2 is to recruit TPP1-POT to telomeres through the use of a third binding site, which is found within the N-terminus, by doing so, TIN2 helps link double stranded and single stranded telomere repeats (Houghtaling et al., 2004). In addition, TIN2 prevents the release of TRF1 from the telomere by inhibiting TRF1 poly (ADP-ribosylation using tankyrase1 (Ye et al., 2004b). Moreover, TIN2 forms a bridge between TRF1 and TRF2 to stabilise TRF2 binding to telomere (Kim et al., 2004, Ye et al., 2004a). In human cells, the over-expression of TIN2 inhibits telomere elongation by limiting telomerase access. Based on that, TIN2 is considered as a negative telomere length regulator (Kim et al., 1999).

1.3.1.3 TPP1

TPP1 is also known as TINT1, PTOP or PIP1. TPP1 was first identified through two hybrid screens using TIN2. TPP1 protein is critical in binding between TIN2 and POT1 (Liu et al., 2004b). The TPP1 binds to carboxyl terminus of POT1 in order to recruit it to the telomere

whereas, the carboxyl terminus of TPP1 binds to TIN2 (Ye et al., 2004b). Serine rich region been found between two protein binding domains, thus have multiple potential phosphorylation sites (Palm, de Lange 2008), furthermore, the telomerase-interacting domain found in the N-terminus of TPP1, which indicates that TPP1 plays a role in the recruitment and regulation of telomerase activity at the terminus (Xin et al., 2007, Ye et al., 2004a). The absent of TPP1 leads to the loss of POT1 from the telomere and resulting in telomere de-protection and telomere length alterations, a similar phenotype to the one observed after POT1 loss (Xin et al., 2007).

1.3.1.4 POT1

POT1 (Protection of Telomeres 1) binds specifically to repeats of single-stranded TTAGGG and guards the telomere against rapid degradation (Baumann & Cech, 2001). The HPOT1 has two oligosaccharide/oligonucleotide-binding (OB) folds, which are specific for 5'TTAGGG-3' sequence. One study has indicated that POT1 cannot bind to telomeric DNA when TPP1 is absent (Loayza et al., 2004). However, evidence from a number of other studies showed that POT1 can be localised to the telomere when functional TPP1 is absent (Colgin et al., 2003, He et al., 2006). In a study by Chen et al., (2007), they reported that POT1 needs the presence of TPP1 for its nuclear localisation (Chen et al., 2007). The removal HPOT1 led to the elongation of the telomere and several telomeres fused (Chen et al., 2007). *Arabidopsis thaliana* contains two distinct POT1 paralogs, which do not show telomeric DNA binding and which appear to regulate telomerase rather than be involved in protection of chromosome end (O'Malley, Ecker, 2010). The role of POT1 on telomerase activity at the molecular level remains unknown. However, POT1 appears to play a role in

the stabilization of t-loop formation when it binds to displacement G-strand within the D-loop (Loayza et al., 2004).

1.3.1.5 Rap1

Human Rap1 (Repressor/Activator Protein 1) is recruited by and depends on TRF2 in order to remain stable (Celli and de Lange, 2005). RAP1 is a characteristic sequence-specific DNA-binding protein. Rap1 has different domains; C-terminal domain to interact with TRF2 and Myb domain which enables the binding unknown protein partner (Palm and de Lange, 2008 & Hanaoka et al., 2001). Unlike in yeast, human Rap1 does not bind directly to telomeric DNA (Li and de Lange, 2003). Although the precise function played by hRap1 is not yet understood, its structure suggests that it could be involved in protein-protein interactions (Denchi, 2009). In addition, recent evidence supposes that RAP1 functions in NHEJ inhibition (Sarthi et al., 2009).

1.3.2 Transient associated telomeres proteins

In addition to the shelterin complex, there are a number of additional proteins that have been found in telomeres. Majority of these proteins are involved in DNA signalling and DNA damage repair. They are transiently associated with the telomere during specific phases of the cell cycle. The primary role of every transient associated telomere protein is independent of telomere biology. Examples of these proteins are WRN RecQ helicase (Crabbe et al., 2004, Opresko et al., 2002), bloom syndrome helicase (BLM), Tankyrase1 and Tankyrase2, ATM, and PinX1.

1.3.2.1 PinX1

PinX1 is a novel TRF-binding protein which has a direct inhibition function on telomerase activity. PinX1, together with MCRS2 (cell cycle dependant protein that accumulates in S-phase) are involved in the regulation of telomeric length, and binds directly to TRF1 and TERT (Zhou and Lu, 2001). Human PinX1 contains an N-terminal G-patch domain, which is common among all RNA binding protein (C-terminal TRF1-binding domain) (Chen *et al.*, 2008; Zeng *et al.*, 2010). Ectopic pinX1 has been shown to co localize with ectopic TRF1 leading to the increase of the quantity of TRF1 on the telomeres (Yoo, Oh & Park, 2009). PinX1 is also shown to interact with telomerase RNA and protein subunits, where PinX1 becomes bound to the TERT region that interacts with TERC RNA subunit (Banik and Counter, 2004). Ectopic PinX1 impedes the activity of telomerase (Zhou *et al.*, 2011), while PinX1^{+/-} displays higher telomerase activity. These data are consistent with a role for PinX1 in telomerase regulation (Zhou *et al.*, 2011).

1.3.2.2 Tankyrase1 and Tankyrase2

Tankyrases are proteins containing poly (ADP-ribose) polymerase (Cook et al., 2002). Tankyrase1 is a 140 kD protein that was first discovered in two hybrid screen of yeast (Smith et al., 1998). Tankyrases in human cells post-translationally alter several proteins that are involved in telomere length maintenance and bridging sister telomeres. Both Tankyrase1 and Tankyrase2 bind to poly(ADP-ribosyl)ated TRF1. A poly(ADP-ribosyl)ated TRF1 is inhibited from binding to telomeres, which frees the chromosome termini for telomerase activity (Cook et al., 2002). In addition tankyrase1 associated with NuMA (mitotic apparatus protein) that regulates the function of the mitotic spindle (Chang et al., 2005). Tankyrase1 overexpression within the nucleus facilitates the elongation; this suggests that tankyrase1

could be regulating the contact between telomerase and the telomeric complex. Hsiao and Smith (2008) showed that the inactivation of tankyrase1 from a cell makes it unable to assemble bipolar spindles (Hsiao and Smith, 2008). Moreover, tankyrase1 is critical for the resolution of sister telomeres during the process of mitosis. Deficiency of tankyrase1 causes fusion of the two unprotected sister chromatids. The roles of tankyrase2 within the cell are not very clear; however, it looks like it shares similar roles with tankyrase1 (Cook et al., 2002).

1.3.2.3 Ataxia Telangiectasia Mutated (ATM)

ATM is a gene that encodes a PI3/PI4-kinase family protein. The protein is crucial in cell cycle as it is involved in phosphorylation. Therefore, it works as a regulator of various downstream proteins such as p53, BRCA1, RAD17, RAD9, CHK2, and NBS1 (Meyn, 1999).

1.3.2.4 BLM

BLM is a RecQ helicase (Ellis, Groden, Ye, et al., 1995) involved in homologous recombination (Johnson, Lombard, Neff, Et al., 2000). In addition, BLM can move through Holliday junctions (Walpita, Plug, Neff, German & Ashley, 1999) where it unwinds G4-DNA (Karow, Constantinou, Li, West, & Hickson, 2000), which is formed in vitro at G-rich sequences, for instance, telomeres. When mutations occur in BLM, they cause Bloom syndrome, which is a rare congenital disorder that's characterized by slow growth, low immunity, chromosomal instability and cancer (German, 1993). In human cells, BLM binds to PML bodies (Zhong, Hu, Ye, Stan, Ellis & Pandolfi, 1999). Recent studies have shown that BLM also co-localize with telomeric foci within the ALT cell line (Yankiwski, Marciniak, Guarente & Neff, 2000). However, its role in telomere maintenance is unclear.

1.3.2.5 WRN

WRN plays an essential role in genome stability particularly during DNA replication and in telomere metabolism. WRN encodes a protein that contains a 3' to 5' DNA helicase domain from the RecQ family (Martin and Oshima, 2000). RecQ helicase are involved in numerous biochemical processes such as DNA recombination. The protein also has several other conserved domains such as 3' to 5' exonuclease domain, which is a nuclear localization sequence, and **DNA-protein binding domain (DPBD)**, which interacts with both proteins and DNA (Orren, 2006). WRN interacts with POT1, TRF1 and TRF2. It also interacts with Ku 70 and Ku 80, a protein that's involved in non-homologous-end-joining (NHEJ) that is involved in telomere length maintenance.

According to Johnson et al., (2000), WRN interacts with TRF2 via the DPBD domain. WRN localization to the telomeres seems to be specifically at the S phase of the replication cycle. By interacting with TRF2, WRN's 3'-5' exonuclease and weak 3'-5' helicase activities become induced (Opresko et al., 2002), this activity can resolve telomeric D-loops. Thus, WRN is involved in normal telomere replication by resolving abnormal secondary telomeric structures during the progression of the replication fork.

1.4 Telomere function

1.4.1 Chromosome capping and DNA damage response

Early studies on *Drosophila melanogaster* and *Zea mays* revealed that chromosomes disrupted through treatment with X-ray suffered different forms of chromosomal rearrangements (McClintock, 1939, Mueller, 1938). Muller and McClintock observed that during these alterations, the ends of the chromosomes were never affected. This is where

the idea of “capping” emerged which recognises the natural end of the chromosome from a DNA double strand break. When the chromosome ends were analysed using electron microscopy, it was realised that large duplex loops, the T-loop, were “caps” (Griffith et al., 1999). The formation of this T-loop is dependent on TRF1 and TRF2 that have been suggested to remodel telomeric DNA into large loops (Griffith et al., 1999, Stansel et al., 2001).

The protection of chromosome termini from DNA damage repair and differentiating it from DNA double strand breaks is one of the main functions of the telomeres. TRF2 and POT1, two important members of the shelterin complex, play a critical role in the interaction between telomeres and the DDR. For instance TRF2 dominant negative mutant is expressed as a consequence of the recognition of telomeres as DNA double strand breaks that lead to the stimulation of the ATM/P53 damage response pathway (Karlseider et al., 1999). Furthermore, TRF2 is also assumed to be capable of inhibiting the autophosphorylation and activation of ATM thus abrogating the ATM signalling pathway (Bradshaw et al., 2005). Both POT1 and TRF2 are essential for repressing DNA damage signalling pathways. These two proteins act independent of each other. On one hand, TRF2 inhibits ATM kinase; while on the other hand, POT1 represses ATR (Denchi and de Lange, 2007). Conversely proteins that detect DNA damage, repair, and DDR signalling are also bound to functional telomeres. Evidence from recent studies shows that for telomere replication to occur, the telomeres should have DDR machinery (Verdun et al., 2005).

1.4.2 Telomeres in mitosis and meiosis

Meiosis and mitosis are cell division process common in majority of eukaryotes. Recent evidence points to the involvement of telomeres in homologue pairing during meiotic cell

division. For instance, during meiotic prophase, the ends of the chromosomes are clustered and become attached to the spindle polar body in a process which requires silent chromatin assembly that forms a bouquet-like configuration. This bouquet occurs in many eukaryotes and promotes meiotic pairing and the ensuing homologous recombination through chromosomes alignment.

However, the mechanism through which the “bouquet” is formed is absent in *Caenorhabditis elegans* and *Drosophila* (McKee, 2004, Scherthan, 2001). In addition, studies on maize, mice and human have showed that telomeres become attached to the **Nuclear Envelop (NE)** in a random manner during leptotene and that they continue to move around the nuclear envelop until they come into close contact (Bass et al., 1997). This process is very active and is tightly modulated and switched off during early pachytene. It is suggested that the formation of the bouquet increases the efficiency of meiotic prophase (Harper et al., 2004). In humans, two TRF2 proteins are involved in the tethering of the chromosomes ends to the nuclear envelop (Luderus et al., 1996).

Meiosis occurs in several stages. During the first stage, leptotene, the unfolded bundles of chromatin are organized into long and slender fibres. Towards the end of leptotene and the start of zygotene stage, telomeres become bound to the nuclear envelope and gather together to form a bouquet. In zygotene stage, homologous chromosomes start to come together at the synapse following the installation of the synaptonemal complex's central element. The formation of the bouquet is spread throughout the whole zygotene stage and into the start of pachytene phase. Towards the middle of the pachytene phase, the formation of the synaptonemal complex comes to an end and meiotic recombination among homologues is determined. At this point, the telomeres are no longer huddled together.

Following the dispersion of the bouquet, the cells proceed through diplotene when synaptonemal complex dissociates and chiasmata, which holds the homologs together until anaphase 1, is easily visible. During diakinesis, the chromosomes enter the final stage condensation and shortly after, nuclear envelope breaks down and metaphase starts (Harper et al., 2004).

1.4.3 Senescence

Leonard Hayflick and Paul Moorhead (1961) discovered that normal human fibroblasts possess a limited proliferative capacity, a phenomenon they called replicative senescence. They argued that this predetermined passive potential, later called “**Hayflick limit**” was caused by an asynchronous self-replicating mechanism, and that it forms the basis of the mechanism behind organismal aging. Consistent with this assumption, telomeres shorten as normal cells attain their passage potential, and act as mitotic clocks in modulating replicative senescence (Shay & Hayflick, 2000). Senescent cells are characterised by a perpetual cell-cycle arrest. However, unlike with replicative senescence, cells undergoing senescence do not require telomere deterioration; instead, they can be prompted by various stressors such as UV light, reactive oxygen species, excessive mitogenic signalling, chemotherapeutics, ionizing radiation, and distortion of chromatin structure. Through different signalling pathways, these inducements engage p53 or retinoblastoma protein (RB), or both, subject to the stressor and the level of the stress (Campisi & d’Adda di Fagagna, 2007). Senescent cells that have attained Hayflick limit are large and flat. Oftentimes, they are convoluted and multinucleated. In addition, they show a high frequency of nuclear abnormalities. Their telomeres have eroded lengths and display

characteristics dense foci of heterochromatin. When stained with acidic-galactosidase, they display increased acidic-galactosidase activity at a pH 6.0 and a blue precipitate.

1.4.3.1 Senescence associated β –galactosidase activity

Senescent cells increase with aging in different tissues and organs. This was first discovered in vivo by use of a pH-dependent β -galactosidase, now called **Senescence-Associated- β -Gal (SA β -Gal)**. This is enzyme activity that enables researchers to tell the difference between senescent cells from postmitotic and quiescent cells. The activity is detected at a pH 6.0 and is used in studies which evaluate the induction of senescence in cells and tissues (Itahana, Campisi, Dimri, 2007). Although the method is widely used, there exists conflicting data with regard to the status of SA- β -Gal as a senescence marker. For instance, confluent quiescent presenescent cells show in situ expressions of the SA- β -Gal activity. SA- β -Gal activity arises from increases in lysosomal mass during the aging process within cells. Fibroblasts obtained from patients with lysosomal disorder do not display SA- β -Gal activity. In addition, SA- β -Gal activity is observed in low pH in non-senescent cells that possess high lysosomal content, for instance in vascular smooth muscle and endothelial cells. Thus, it appears that SA- β -Gal activity is not a measure of senescence but a marker of lysosomal changes that occur as a result of senescence (Yang, 2005).

1.4.3.2 The end replication problem

The replication of DNA in a semi-conservative manner causes a distinct problem: the process only functions in a 5' to 3' direction, and DNA polymerase needs to bind to an RNA primer. Even before the discovery of the telomeres, both Olovnikov (1971) and Watson theorised that the consequence of this process and termed it as an end replication process. This occurs due to the expected loss of a small 5' nucleotide segment during DNA synthesis,

followed by a replication-induced shortening of the telomeres (figure 3). While the leading strand is always replicated from a 5' → 3' direction following the firing of the replication origin, the late synthesis of the lagging strand occurs in the form of small defined Okazaki fragments that are 50-150 nucleotides long. DNA polymerase α /primase complex then synthesises a RNA-DNA primer that generates a free 3'-OH group that acts as a base for 5' to 3' elongation by a DNA polymerase δ .

The formation of a novel Okazaki fragment stops after pol δ complex touches the preceding Okazaki fragment. So as to yield an unbroken DNA strand, two enzymes, RNase H1 and FEN1, eliminate the original RNA primer, fills the small gap falling between the two fragments, before the two matured Okazaki fragments are combined together by DNA ligase I (Waga and Stillman, 1998). But, at the chromosome end, the exclusion from the lagging strand of the RNA primer results in an unoccupied gap that ranges from a single RNA primer in size to a whole Okazaki fragment (10 - 150 nucleotides). As a consequence, the shortened lagging strand causes a steady shortening of the chromosome end during every successive replication cycle.

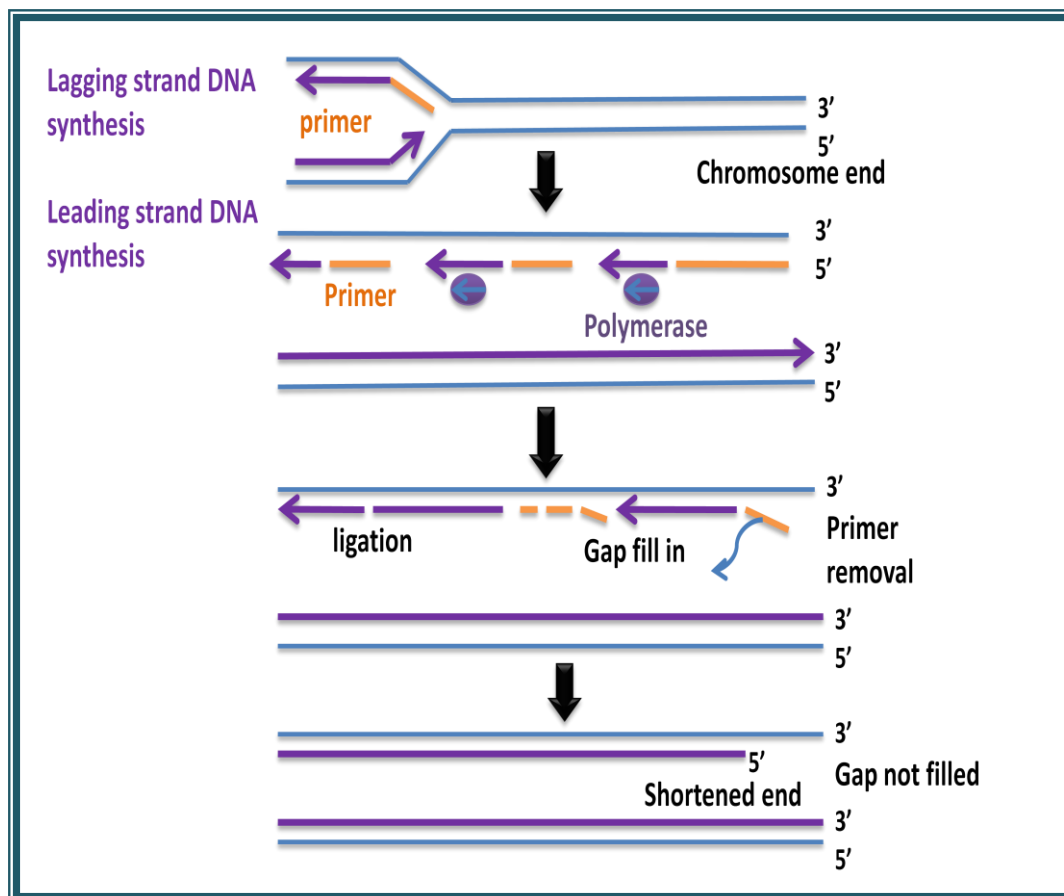


Figure 3: The end-replication problem. During replication process, RNA primer fragments are extended by DNA polymerase, (unidirectional 5' to 3'), in order to synthesis the lagging strand, subsequently the RNA primer are degraded and all the gaps are ligated and filled in by DNA except the region at 5'end, which results in producing 3'end single-stranded overhang. **(Diagram is redrawn from Blackburn *et al.*, 2009).**

1.4.3.3 Telomere-dependent replicative senescence

Various stimuli that cause DNA damage within cells can result in phenotypes that overlap with telomere-dependent replicative senescence. The end replication problem results in a gradual loss of the telomeric DNA following successive cell divisions, until very short, dysfunctional telomeres prompt a DNA damage response (DDR). The stimulated p53 and p16-pRB tumour suppressor pathways lead to a permanent growth arrest (Gire et al., 2004,

Takai et al., 2003). Analogous to DNA double strand breaks, there is a recruitment of DNA damage sensors, which includes mediator of DNA damage checkpoint 1 (MDC1), p53 binding protein 1 (53BP1), Mre11/RAD50/NBS1 complex, and Rad17, to the chromosome end (d'Adda di Fagagna et al., 2003). In turn, the sensor proteins enlist Ataxia Telangiectasia Mutated (ATM), protein kinases and RAD3-related (ATR), to the end of the chromosome (Shiloh, 2006).

In a characteristic positive feedback loop, ATR and ATM activate phosphorylation of **heterochromatin H2AX** (γ H2AX) (Campisi and d'Adda di Fagagna, 2007). The phosphorylation of secondary kinase such as Chk1 and Chk2 causes the amplification of DNA damage signal (Jackson et al., 2002) that in response triggers cell division cycle 25 (CDC25) and p53 pathway. DNA damage response induces replicative senescence using the p53 pathway. Nevertheless, conditional to type of the cell or species, DDR may also arrest cells permanently by utilizing the p16-pRB pathway (Campisi and d'Adda di Fagagna, 2007).

1.4.3.4 Telomere-independent replicative senescence

Replicative senescence is not just caused by telomere erosion alone, DNA damaging agents, oxidative stress and oncogene overexpression can trigger early replicative senescence and thus significantly restrict cell's replicative lifespan (Dumont et al., 2000, Serrano et al., 1997). Replicative senescence resulting from end replication problem can be avoided through ectopic expression of TERT, a catalytic protein constituent of human telomerase (Bodnar et al., 1998). But telomerase alone cannot stop replicative senescence resulting from other senescence triggers (Campisi and d'Adda di Fagagna, 2007).

Many cell types experience senescence as a result of build-up of DNA damage (Di Leonardo et al., 1994, Parrinello et al., 2003). DNA damage triggered by senescence depends on p53

and is complemented by the manifestation of p21 (Di Leonardo et al., 1994, Herbig et al., 2004). This forms the basis of the hypothesis that DNA damage prompting chemotherapy could result in senescence in tumour cells. But, tumour cells which possess functional p53 pathways are expected to undergo senescence than those with mutated p53, particularly in cancer-prone mouse models (Roberson et al., 2005, Schmitt et al., 2002).

Premature senescence is also caused by forced overexpression of active oncogenes within normal cells. The alteration of human cells with Ras, a transducer of mitogenic signals, leads to premature initiation of cellular senescence (Serrano et al., 1997). When other members of the Ras signalling pathway and nuclear proteins such as E2F-1 were used, comparable results were obtained (Zhu et al., 1998; Dimri et al., 2000). Because oncogenes such as member of the Ras signalling pathway induce cell growth and can motivate unmediated cell proliferation, then, oncogene prompted senescence could have risen as a tumour suppressor mechanism, in order to prevent tumourgenesis (Braig and Schmitt, 2006). Oncogene-induced senescence, like telomere-dependent senescence, provokes a DDR. But, the DDR is also active in initiation and maintenance of oncogene-induced senescence, because, when DDR are down regulated, cell proliferation and oncogenic transformation occur (Di Micco et al., 2006).

1.5 Telomere Maintenance Mechanisms (TMM)

1.5.1 Telomerase

1.5.1.1 Structure

The initiation of telomere maintenance process is inexorable for the immortalization of cells. Many cancerous cells preserve their telomeres through the activation of **TELOMERASE**, which is a ribonucleoproteic complex that adds telomeric repeats at the chromosome termini of cancer cells or germline cells. Telomerase was first discovered in *Tetrahymena thermophila* (Greider and Blackburn, 1985). Over time, the activity of telomerase has been identified in protozoa (Zahler and Prescott, 1988), fungi (Lingner et al., 1997) and in mammalian cells.

Dynamic human telomerase is made up of 3 essential elements; **telomerase RNA component (TERC)**, the TERC-binding protein dyskerin (DKC1) and **reverse transcriptase telomerase (TERT)**. Furthermore, there are other elements, which are associated with the telomerase to form a holoenzyme. These are species-specific accessory proteins, which control biogenesis, telomerase function and cellular localization. In human cells, these proteins include NTPase proteins NHP2 and NOP10, ATPases pontin and reptin and **TCAB1 (telomerase Cajal body protein 1)** (Cohen et al., 2007).

Dyskerin, a putative pseudouridine synthase, also distinguishes the H/ACA sequence motif. The motif can occur in TERC (Mitchell et al., 1999). The function of the dyskerin is to provide support to telomerase biogenesis and stability of the TERC (Mitchell et al., 1999). Evidence indicates that dyskerin, NOP10 and NHP2 are essential for the build-up and maintenance of TERC (Fu and Collins, 2007). In addition, Pontin binds directly with dyskerin and TERT. The

quantity of TERT interacting with reptin and pontin is optimum during the S phase of cell division, which provides proof of cell-cycle-dependent TERT regulation. Reduction of reptin and pontin is damages the build-up of TERT, which is an indication of the important role it plays in telomerase assembly (Figure4).

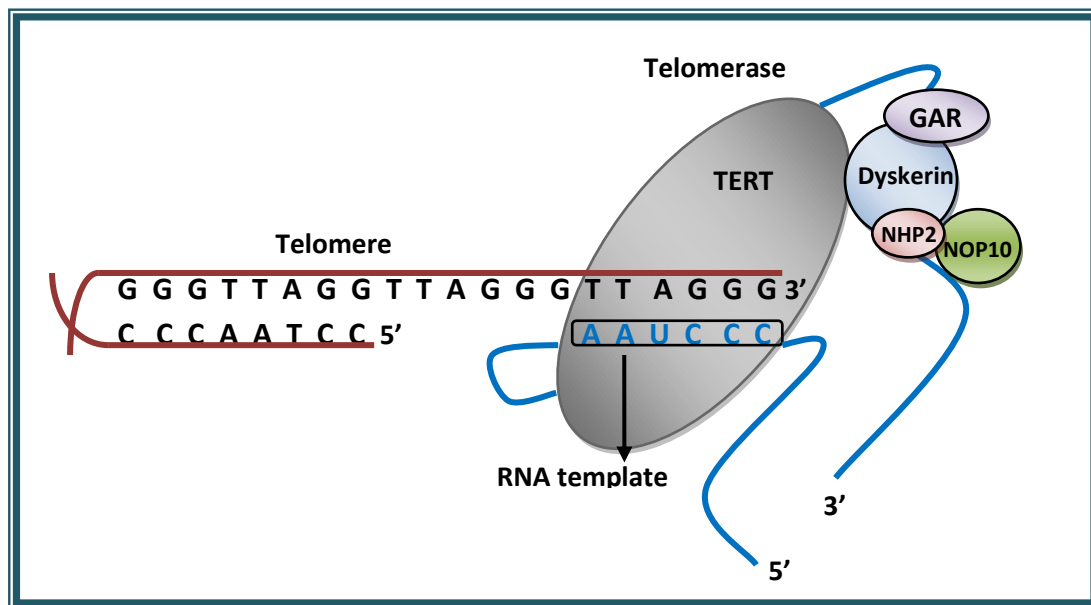


Figure 4: Telomerase structure. Telomerase consists of telomere reverse transcriptase (TERT), RNA template (TERC) and dyskerin with associated proteins (GAR, NHP2 and NOP10) (DKC1). **(Figure is redrawn from Calado and Young, 2009).**

1.5.1.2 Function

Telomerase is severely inhibited in most somatic cells apart from S-phase where it occurs in low activity level, and may take part in the upkeep of the telomeric overhang in typical human cells (Dionne and Wellinger, 1998). Unlike in normal human cells, almost all (90%) human cancer cells exhibit reactivation of telomerase (Broccoli et al., 1997). TERC is manifested in all tissues; whereas TERT expression is highly regulated (Masutomi and Hahn, 2003). Nonetheless, telomere length and the extent of telomerase activity are not associated with the expression levels of either hTERT or hTERC (Swiggers et al., 2004).

Telomerase extends telomeres through catalysis of numerous copying rounds of its own RNA template. During the initial step, the RNA template of the telomere anneals to 3' end of the DNA substrate. In the next phase, new nucleotides are synthesised onto the growing DNA substrate to the point where the template's 5' end is reached. In the final stage, telomerase moves and readjusts to the freshly produced 3' end, and initiates another round of telomere synthesis (Greider and Blackburn, 1996) (Figure 5).

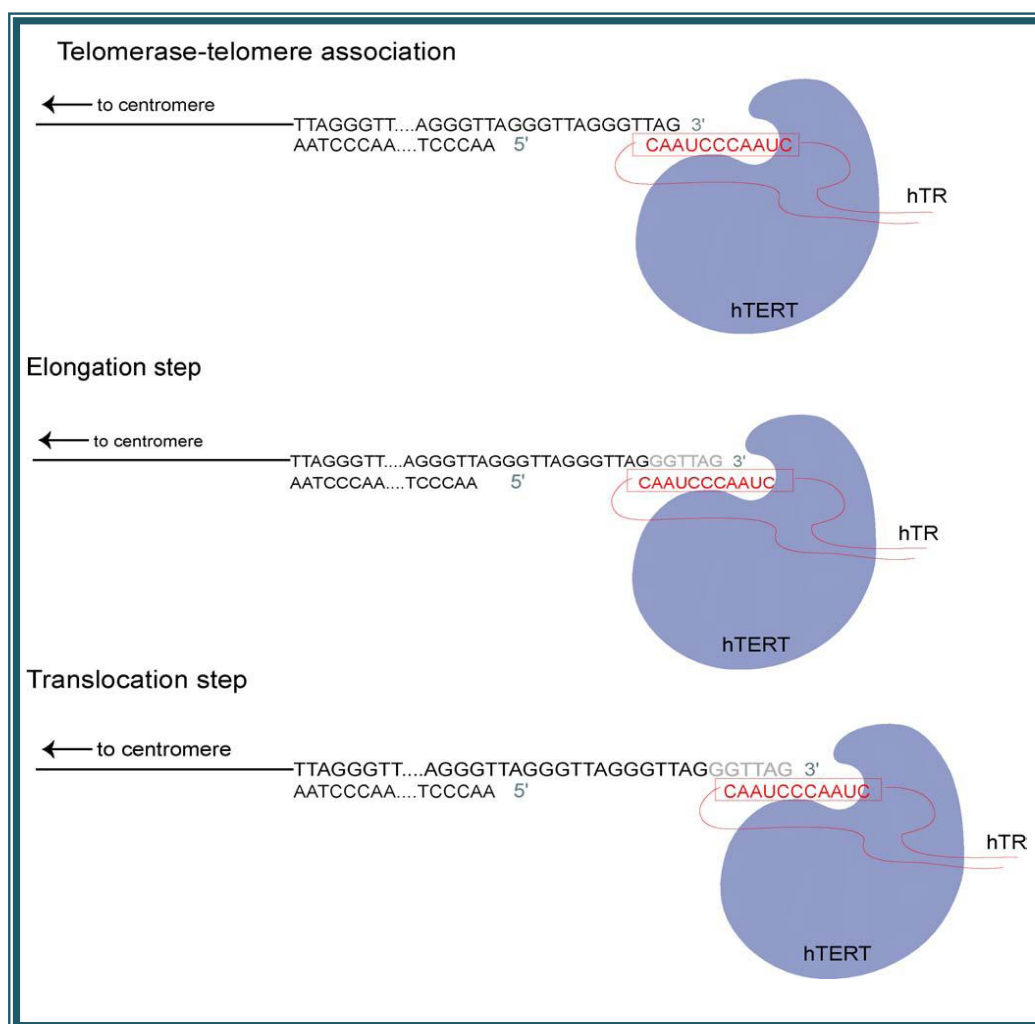


Figure 5: Telomerase function. 1- (Telomerase-telomere association): the telomeric single strand recognised and hybridized to RNA template (hTR), subsequently **2- (Elongation step):** where nucleotides are added by catalytic reverse transcriptase (hTERT) by copying its RNA sequences to extend the strand and **3- (Translocation step):** where telomerase repositions then the 3' end of the strand are hybridised to (hTR) again and extend the strand. (Figure is reproduced from Olausson *et al.*, 2006).

1.5.1.3 Telomerase regulation

Telomerase activity is highly regulated and its activity is limited to cells which extend proliferation potential such as the germ line cells, self-renewing stem cell, embryonic tissues, and skin. In human cells, the activity of telomerase is stringently regulated during oncogenesis and development. TERT and the telomerase's RNA subunit are implicated in the regulation of telomerase. The reduction of TCAB1 through RNA interference stops TERC from interacting with Cajal bodies, disturbs telomerase-telomere interaction, and repeals telomere production by telomerase. Therefore, TCAB1 regulates telomerase trafficking and is necessary for the synthesis of telomere cancerous human cells (Venteicher et al., 2009).

1.5.2 Alternative Lengthening of Telomere (ALT)

The **Alternative Lengthening of Telomere (ALT)** is a telomere length maintenance mechanism which does not rely on telomerase activity. The process occurs in 15% of all human cancers in which the activity of telomerase is not evident. In these cancers, the preservation of telomere length is achieved through homologous recombination and mis-regulation of the usual telomere homeostasis (Bryan et al., 1997, Dunham et al., 2000). ALT cell lines and tumours are characterised by an abundance of extrachromosomal telomeric DNA that presents itself in the form of telomeric circles (t-circles) (Cesare and Griffith, 2004) (Figure 6).

Telomeric DNA and related proteins occur in promyelocytic leukaemia nuclear bodies (PML nuclear bodies). PML bodies comprise of telomeric chromatin and usually occur in ALT cells, thus, they are sometimes called ALT-associated PML bodies (APBs) (Yeager et al., 1999). PML proteins are important in the accretion of p53 as a reaction to DNA damage. In addition, APBs encompass replicative factor A, RAD52, RAD51 and the MRN complex, which

are all engaged in DNA recombination and synthesis (Wu et al., 2000). These APBs may stimulate the homologous recombination leading to ALT, even though a debate rages on the exact function of APBs.

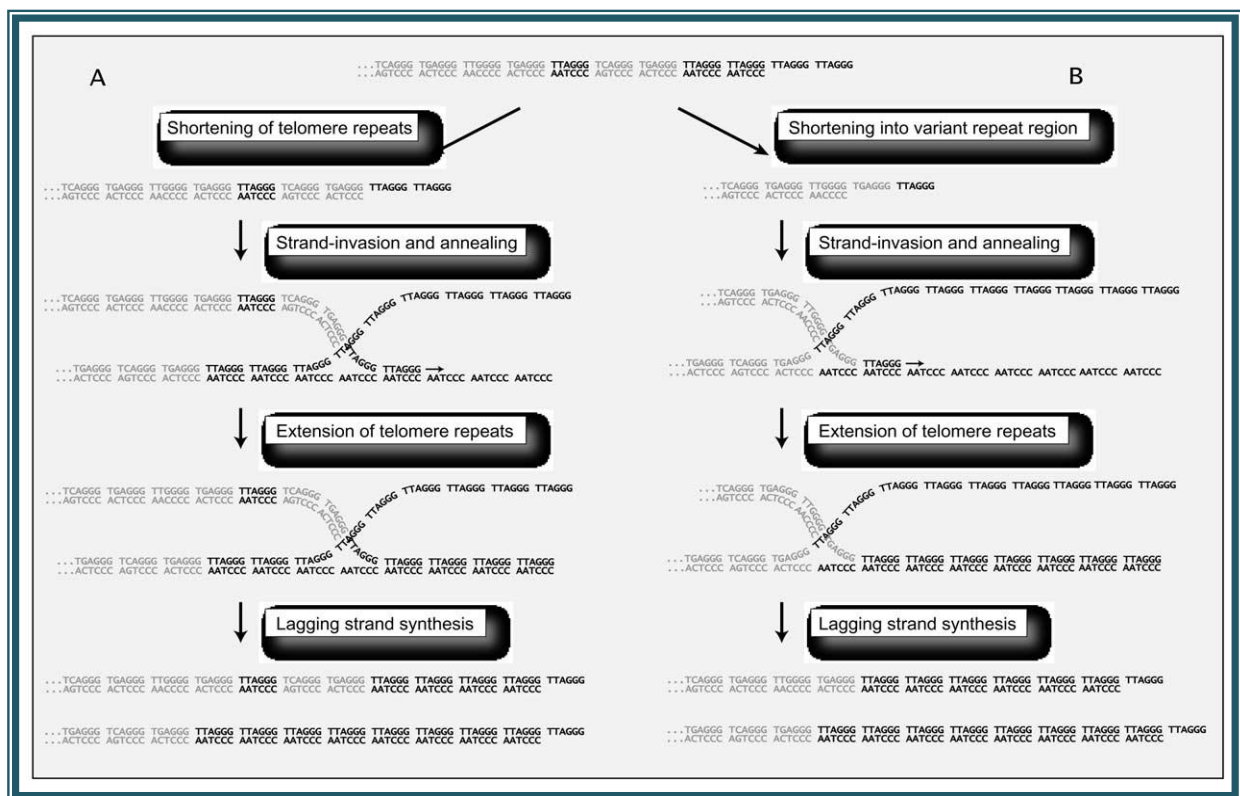


Figure 6: Recombinational Telomere Elongation (RTE) in ALT cells. A Shortened telomere invades another telomere and anneals with its complementary strand, that works as template and extend the shortened telomere, subsequently its lagging strand can be synthesis and filled in. **B** shortening telomere extends to subtelomeric repeats, that replaced by telomeric repeats (TTAGGG) by RTE process in ALT cells (**Diagram is reproduced from Reddel, 2003**).

1.6 Telomeres and Disease

1.6.1 Cancer

Age is one of the greatest risk factors associated with the development of cancer, with the incidence rising steadily in midlife in both man and mice. A cancer cell is one that grows uncontrollably by disregarding signals to discontinue dividing and is incapable of recognising

its natural limits. The progression of cancer is said to be a somatic evolution, where certain mutagens lead to the production of a cell that possesses selective proliferative benefits (Cahill et al., 1999). It is argued that most cancers originate from stem cells which are capable of proliferating indefinitely.

The cells that facilitate carcinogenesis by homeostatic processes that manage tissue repair and cell self-renewal (Beachy et al., 2004, Reya et al., 2001). Telomerase negative cells have lost their telomeric function as a result of progressive erosion of their telomeres that arises in chromosomal fusion events and non-reciprocal translocations. Such cells avoid replicative senescence by sidestepping the pRB and p53 pathway checkpoints and thus causing the formation of cancer (Artandi and DePinho, 2000) (Figure7).

The majority of cancerous cells preserve their telomeric length by the re-activation of the telomerase enzyme or ALT pathway (Holt and Shay, 1999). The manifestation of both hTERC and hTERT subunits of telomerase is increased in nearly all human and mouse malignant tumours. Thus, telomerase activity is an important pointer of consequence and development of cancer (Hiyama, 2002). As such, telomerase is a significant focus in the development of anti-cancer therapies (Keith et al., 2004).

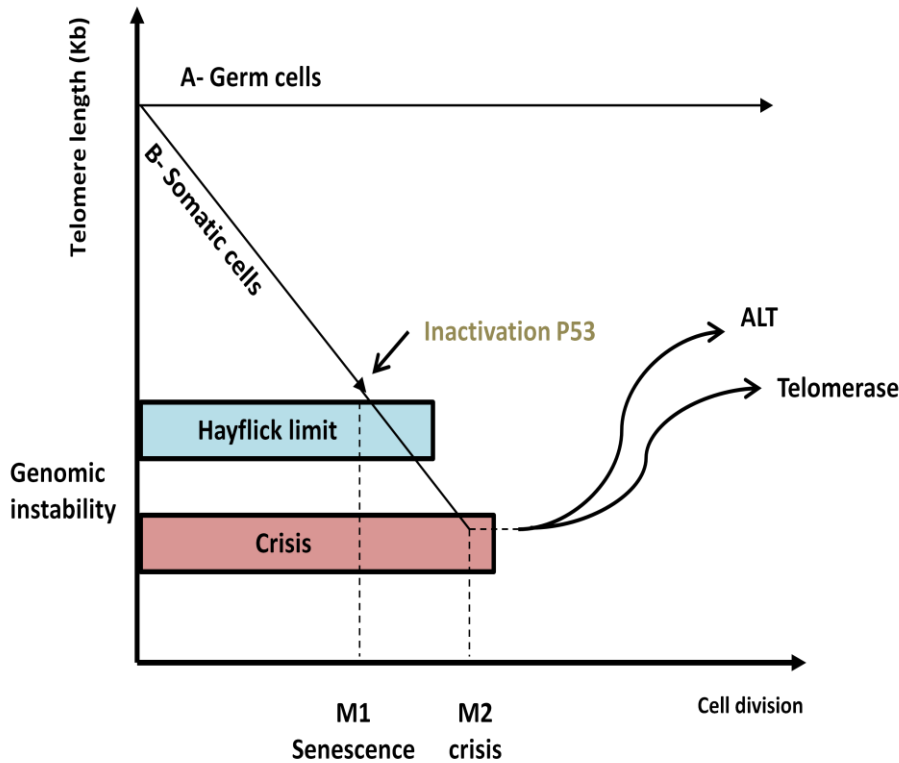


Figure 7: Telomere erosion. A- Germ cells maintain their telomeres length over cell division by telomerase enzyme. B- Telomere length shortens in the somatic cells over cell division reaching to the critical length (Hayflick limit), when cells arrested by p53 (cellular senescence M1). If p53 inactive, cells bypass the senescence to (crisis M2), cancer cells emerge from crisis and their telomere length replenished by telomerase or ALT. (Original figure using information from Diehl *et al.*, 2009 and Reddel, 2003).

1.6.2 Werner Syndrome

Werner Syndrome (WS) also known as “adult progeria” is an erratic autosomal recessive syndrome that occurs as a result of mutations in the *WRN* gene. The disease is characterized by the appearance of premature aging, signified by cataracts, skin atrophy, type II diabetes, atherosclerosis, soft tissue calcifications and osteoporosis (Martin, 1982). Furthermore, the disease is linked to genomic instability and an early cancer onset (Davis and Kipling, 2009). In individuals with the disease, over 90% of all WS cells display premature senescence

(Tollefsbol and Cohen, 1984). WS cells have a tendency to developing chromosomal rearrangements such as inversions, translocations, and deletion (Salk, 1982). They also show a higher incidence of chromosomal deletions (Fukuchi et al., 1989).

1.6.3 Bloom's Syndrome

Bloom's syndrome (BS) is an inherited disorder and is characterized by short stature, sun sensitive telangiectasia skin, compromised immune response and a higher risk of developing cancer (Bloom, 1954). The disease is caused by mutations in the *BLM* gene which provides the instructions for synthesizing proteins called RecQ helicases. Helicases are enzymes which interact with DNA and help the DNA's unwind the two spiral strands. This event is crucial in DNA replication, repair and cell division. BS patients have increased levels of Sister Chromatid Exchange (SCE) following treatment with DNA damaging agents (German et al., 1977). At homologous sites, there are symmetrical quadriradials, which are chromosomal re-arrangements among homologous chromosomes (German et al., 1965). A RecQ ATP-dependent DNA helicase is the affected protein in BS (Ellis et al., 1995). BLM helicase is essential in Holliday branch migration, homologous recombination and stability of the genome (Wu et al., 2001). POT1 induces both WRN and BLM to relax D-loop structures and long telomeric duplexes.

1.6.4 Dyskeratosis Congenita

Dyskeratosis Congenita (DC) is congenital disorder which affects many parts of the body. It is characterised by fingernails and toenails dystrophy, changes in skin pigmentation and bone marrow failure (Marrone and Mason, 2003). There are two different types of the disease; X-linked recessive Dyskeratosis Congenita and autosomal dominant Dyskeratosis Congenita.

The X-linked DC is associated with mutations of the *DKC1* gene at Xq28. Dyskerin, the encoded protein, interacts with a sub group of small nucleolar RNAs and TERC (Mitchell et al., 1999). The autosomal dominant Dyskeratosis Congenita occurs as a result of mutations in TERC itself (Vulliamy et al., 2001). Both forms of dyskeratosis congenital are characterised by undersized dysfunctional telomeres.

1.6.5 Ataxia Telangiectasia (AT)

This is a rare inherited disease that affects the immune system, nervous system, and related body systems. The disorder is characterised by progressive challenges in controlling movements (ataxia) and starts as early as 5 years of age. Ataxia Telangiectasia occurs as consequence of mutations in the ataxia telangiectasia mutated *ATM* gene found on chromosome 11q22 (Savitsky et al., 1995). The ATM kinase plays an important role in DNA damage response, mitogenic signal transduction and cell cycle control (Hoekstra, 1997). Patients of AT seems to have augmented telomere erosion and an increased number of chromosomal fusions (Metcalf et al., 1996).

1.7 DNA repair mechanisms

DNA double strand breaks (DSBs) and single-strand breaks (SSBs) occur continuously in cells and are primarily caused by ionizing radiation, ultraviolet light, reactive oxygen species ROS, errors during DNA replication, and enzymes during meiosis. The repair of these DSBs and SSBs is essential to maintain genomic fidelity and stability. In order to combat DSBs and SSBs, cells have developed multiple distinct DNA repair mechanisms which detect damaged DNA, signal its presence and promote the repair of the damage (Jackson and Bartek, 2009). One of these mechanisms is base excision repair (BER). BER is a multi-step process that corrects non-bulky damage to bases resulting from oxidation, methylation, deamination, or spontaneous loss of the DNA base itself. In BER, DNA glycosylase recognises the damaged base and mediates base removal before proliferating cell nuclear antigen (PCNA), polymerase β and DNA ligase I or DNA Ligase III complete the repair process (Jackson and Bartek, 2009, David et al., 2007). Nucleotide excision repair (NER) is perhaps the most flexible of the DNA repair pathways. NER recognizes and repairs lesions which are caused by helical distortion of the DNA duplex and pyrimidine dimers (cyclobutane pyrimidine dimers and 6-4 photoproducts) which are caused by the UV component of sunlight. Other NER substrates include bulky chemical adducts, DNA intrastrand crosslinks, and some forms of oxidative damage. Two distinct NER pathways exist: transcription-coupled NER which focuses on lesion blocking transcriptions and global genome NER which surveys the entire genome for distorting damage (Jackson and Bartek, 2009, David et al., 2007). DNA mismatch repair (MMR) pathway plays an essential role in the correction of replication mistakes such as base-base mismatches resulting from errors of DNA polymerases which escaped the proof reading function and insertion/deletion loops caused by template slippage. In eukaryotes, DSBs are repaired by either homologous recombination (HR) or non-

homologous end joining (NHEJ). Both pathways require the MRN complex to bind to unprocessed DNA breaks, tethering the ends and aligning them for DSB repair (Williams et al., 2008). The error-free HR is limited to late S and G2 phase and utilises homologous repeat sequences like the sister chromatids to repair DNA damage. NHEJ-mediated DNA repair is relatively error-prone and is composed of two distinct pathways termed classic NHEJ (C-NHEJ) and alternative NHEJ (A-NHEJ). C-NHEJ can be observed throughout the cell cycle and is dependent on Ku70/80 and DNA Ligase IV/XRCC4. In contrast, A-NHEJ is associated with G2 phase and requires PARP1 and DNA ligase III/XRCC1 or DNA ligase I (Weterings and Chen, 2008).

1.7.1 Homologous Recombination (HR)

DNA repair by Homologous recombination (HR) occurs in all life forms and is important in the repair of damaged chromosomes which avoids termination of broken replication forks, and for several other aspects of chromosome maintenance. HR is responsible for genome integrity, but ought to be regulated to prevent deleterious events in DNA which may lead to diseases like breast and ovarian cancer, Bloom's syndrome and Fanconi anaemia (Hunters, 2007). In addition HR plays a prominent role in faithfully duplicating the genome by providing critical support for DNA replication and telomere maintenance (Li and Heyer, 2008). DNA replication involves the separation of homologous chromosomes in meiosis. Programmed DNA double-strand breaks (DSBs) that occur in meiosis are thought to stimulate HR. Recombination also occurs in response to unscheduled DSBs and other DNA lesions and is restricted to the S and G2 phase of the cell cycle (Hartlerode and Scully, 2009). Certain types of DNA damage pose a strong impediment to the DNA-replication machinery,

and recombination of a damaged DNA with its sister chromatid re-establishes the DNA replication fork (Li and Heyer, 2008).

After the DSB formation, the DNA ends are processed by nucleolytic resection to give single-strand tails with free 3'-OH ends. These ends become the substrate for the HR protein machinery in order to form the recombinase filament on the single stranded DNA end. After a successful homology search, strand invasion occurs to form a nascent D-loop intermediate. DNA polymerase synthesizes new DNA and thereby extends from the 3' end of the invading strand. The second DSB is captured to form a D-loop intermediate, which contains two crossed strands or Holliday junctions. The reaction is completed by gap-filling DNA synthesis and ligation. Finally Holliday junctions are resolved to give a crossover and non-crossover product (Weterings and Chen, 2008, Rass et al., 2010).

1.7.2 Non homologous end joining (NHEJ)

The core elements in mammalian classic NHEJ are the heterodimer Ku70/80, the catalytic subunit of DNA-dependent protein kinase (DNA-Pkcs), and the DNA Ligase IV – XRCC4 complex. C-NHEJ is initiated by the binding of the Ku70/80 heterodimer to two broken ends of the DSB. The two Ku heterodimers are presumed to provide a scaffold for the members of C-NHEJ and thereby allowing the modification of both DNA ends in preparation for joining. The two Ku proteins in turn recruit DNA-PKcs, thus linking the two DNA ends and thereby forming the active DNA-PK complex. Active DNA-PK interacts with different nucleases and polymerases and starts DNA processing by phosphorylating several proteins including Ku and itself. In a final step, the DNA ligase IV/XRCC4 complex is recruited, further stabilising the broken DNA ends and finally mediating the rejoining of the modified break side.

1.8 Oxidative damage

The large proportions of guanines in telomeres are considered to cause sensitivity to damage by oxidative stress. Moreover, nucleobase damage due to oxidation has been shown to increase in the life a cell or an organism, causing high chances of senescence. Senescent cells are characterized by 30% more oxidized guanine in their DNA and presence of four times free 8-oxodG bases (8-oxo-deoxyguanosine) (Nasir et al., 2014). In addition, there is production of single-strand breaks by oxygen free radicals and ROS, especially hydroxyl radicals cause oxidative base changes.

The causing features for oxidative stress may be many, starting with inheritance or genetic problems or environmental changes to pure stochastic happenings such as metabolic problems.

The effects of Reactive Oxygen Species are counteracted by a variety of antioxidants, by both enzymatic and non-enzymatic mechanisms. Oxidative stress is considered to be the result of an imbalance of ROS and antioxidants where by the effects of ROS are more powerful than the compensatory ability of antioxidants. In the case of mitochondrial-derived ROS, superoxide is the first radical produced (Loft and Polsen, 1996). Because the main site of superoxide production is the inner mitochondrial membrane, the mitochondrial DNA (mtDNA) has been thought to be a major target for ROS damage. Hydrogen peroxide is another mitochondrially derived ROS which arises from superoxide detoxification by manganese superoxide dismutase (MnSOD) (Loft and Polsen, 1996). Although H₂O₂ lacks free electrons, its role in ROS-mediated damage is extremely important. H₂O₂ is used as a substrate in many biochemical and abnormal chemical pathways. Because of its small size and relatively high reactivity, compared to the rest of the ROS, H₂O₂ is able to diffuse fast

cross several cells and cause toxic effects far from the site of its production (Ames, 1989) Mitochondria do not contain catalase, hence their only defence against toxic properties of H₂O₂ is glutathione peroxidase (GSPx) which requires reduced glutathione (GSH) as a cofactor and which acts H₂O₂ converting it to water hence detoxifying ROS. The in the presence of reduced transition metals, H₂O₂ can produce the reactive hydroxyl ions which may cause extensive damage to DNA, proteins, and lipids as argued by Loft et al., (1992).

1.8.1 Reactive oxygen species ROS 'Mitochondria'

In Mitochondria there are numerous oxidative pathways. Mitochondria are crowded with various redox carriers that can potentially liberate electrons to oxygen and change it into superoxide anion which is a Reactive oxygen species (ROS). Mitochondria are unique organelles, as they are the main site of oxygen metabolism and most of the oxygen produced in the cell is used by Mitochondria. Release of free electrons due to partial use of oxygen will result in the formation of free radicals. Mitochondria continuously metabolize oxygen leading to production of reactive oxygen species (ROS) as a by product (Ames, 1989). Mitochondria have their own their own ROS scavenging mechanisms required for cell survival. It has been shown, however, that mitochondria produce ROS faster than their scavenging capacity. By products of incomplete oxygen metabolism are superoxide ions, hydrogen peroxide, and hydroxyl radical. These reactions usually occur at specific sites of the electron transport chain (ETC), in the inner mitochondrial membrane (Chandel et al., 1998). ETC complexes I (NADH dehydrogenase) and III (ubisemiquinone) produce most of the superoxide which is then acted upon by the mitochondrial enzyme manganese superoxide dismutase (MnSOD) to produce H₂O₂ (Chandel et al. 1998). Other important free radical includes nitric oxide (NO) and peroxynitrite (ONOO⁻). Nitric oxide has also been

involved in ROS mediated damage (Turrens, 2003). It may be involved in inflammatory, neurodegenerative, and cardiovascular pathological processes. Nitric Oxide (NO) can regulate aerobic respiration by reversible inhibition of cytochrome c oxidase. NO short half-life and the ability to diffuse any cell that produces excess NO may inhibit its own respiration and respiration of surrounding cells, which may lead to the cytotoxic effects of NO. Peroxynitrite is a highly damaging agent with many targets and harmful cellular effects. ONOO⁻ changes proteins by nitrating tyrosine residues, forming dityrosine, and oxidizing tryptophan and cysteine. Main mitochondrial targets of peroxynitrite are complexes I, II, IV and V, aconitase, creatine kinase, superoxide dismutase. Recent findings have shown that mitochondria has its own nitric oxide synthase and can release endogenous NO and ONOO⁻ (Chandel et al., 1998; Turren, 2003).

1.9 G-quadruplex formation

G-quadruplexes are secondary structures which are formed in guanine-rich DNA sequences. Two or more guanine tetrads in DNA can stack upon each other forming a four-stranded structure known as G-quadruplexes (Blackburn, 1991). Sequences that exhibit G-quadruplex formation motifs are extensively found in eukaryotic genomes. However there is no evidence to support the occurrence of such motifs in prokaryotes. Telomeres can form G-quadruplex structure with its guanine-rich sequences (Blackburn, 1994). Similarly immunoglobulin switch regions, promoter regions of *c-myc* and other oncogenes, retinoblastoma susceptibility gene are also known to possess elements responsible for the formation of G-quadruplex structures (Sen and Gilbert, 1990; Simonsson *et al.*, 2002).

1.9.1 Structure of G-quadruplex

G-quadruplex consists of two parallel strands and have four thymine loops which lie diagonally at the top and bottom of the G-quadruplex structure. Guanine bases are held in G-quadruplex by hydrogen bonds. The guanine glycosidic angles show alternating pattern along the strands of G-quadruplex. In the two ends of the G-quadruplex structure, one guanine base is tilted more compared to the others to increase the stack with the thymine loop. The four grooves have water bridges which link to phosphate groups with amino group of guanine to increase its strength and stability (Haider *et al.*, 2003; Han and Hurley, 2000) (Figure 8).

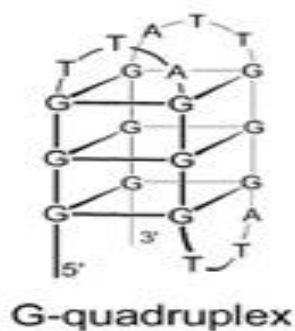


Figure 8: (A) G-quadruplex structure (Leonetti *et al.*, 2004)

1.9.2 G4 ligands

A group of small ligands show ability to stabilize G-quadruplex structure. These ligands all contain pronounced planar aromatic electron deficient chromophores. Example of these ligands include: di-substituted aminoalkylamido acridine, pentacyclic acridine (RHPS4) (Figure 9), potassium ions, small molecules and proteins besides others. RAPI is a protein produced by *Saccharomyces cerevisiae* which is known to bind to G-quadruplex while Gq1 is an artificially derived protein which as acts as a G-quadruplex ligand. Many of the features of both ligand-bound quadruplex and native quadruplex structure are shared, but the ligand will induce some conformation changes in quadruplex structure (Haider *et al.*, 2003).

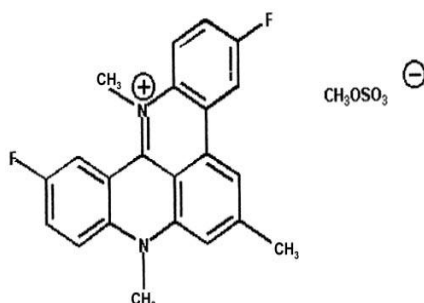


Figure 9: RHPS4 structure (G4 ligand) (Leonetti *et al.*, 2004).

1.10 Telomeres and Fragile sites

1.10.1 Fragile sites

Fragile sites are heritable chromosome loci that have high frequency of gaps, constrictions or breaks when chromosomes are exposed to partial DNA replication inhibition (Sfeir et al., 1999). They are found in areas of chromatin which fail to compact in mitosis. They can either be common or rare based on their frequency in the population. They are divided further depending on the basis of their specific induction chemistry into various groups. Example of fragile sites inducers include: Andaphidicolin, bromodeoxyuridine and 5-azacytidine(Sutherland et al, 1998). Most of the known inducers of fragility share in common their capability to slow down DNA replication notably in the fragile sites.

1.10.2 Telomeres considered as fragile site

Expression of fragile sites shows a genetic instability at specific sites on the chromosomes and may lead to chromosome breakage and unwanted recombination events. The telomere repeat sequence present in eukaryotic cells also found in non-telomeric sites called intrachromosomal telomeric sequences (ITs)(Coquelle et al., 1997) which are said to be remnants of ancestral chromosome arrangements (Finato et al., 2000). Of late it has been argued that telomeres are similar to fragile sites, and shelterin, specifically TRF1, is essential for preventing telomere breakage that is associated with replication fork stalling at telomeres. Since fragile sites are susceptible to breakage, it is expected that on oncogenic signaling telomeres are potential sites of which trigger genome instability. Oncogenic signaling telomeres have been shown to be involved in the in vivo occurrence of duplications or other chromosomal changes related to human congenital diseases (Coquelle et al., 1997). Hence there is evidence that these loci are concerned in the in vivo

chromosomal rearrangements observed in tumour cells. Fragile sites have been shown to colocalize with breakpoints leading to deletions and translocations in various tumours. Understanding fragile sites is thus vital for the management of a series of human diseases (Ruiz-Herrera et al., 2004).

1.10.3 Replication fork stalling

Maintaining replication fork integrity is important to conserve genomic stability and avoid serious genetic diseases. DNA damage and distorted nucleotide or proteins indicate replication challenges. Various cellular responses have emerged to make sure that there is successful DNA replication despite various obstacles. Comprehending such responses is vital to prevent genetic diseases notably cancer (Mirkin and Mirkin, 2007). Re-priming is a mechanism which makes it possible for DNA replication to resume past a fork-stalling lesion. This explains why gaps are formed during DNA replication on injured DNA. The break left behind a re-primed fork must be stabilized to keep off replication fall down. In bacterial cells, replication forks often come across damaged DNA template and this inactivates the DNA replication process. Replication forks are occasionally inactivated under growth conditions. The replication forks initiating at the bacterial origin, oriC, encounter damage under normal growth conditions along the way and which inactivate the replication forks which prompts for re-priming (Torres at al.,2004).

1.11 Telomere Length Analysis

1.11.1 Terminal Restriction fragment (TRF) analysis

TRF method used to determine telomere length utilizes Southern blotting technique to analyse terminal restriction fragments (TRF) obtained following the digestion of genomic DNA with restriction enzymes such as; *HinfI* and *RsaI*. The resulting TRFs usually contain DNA with telomeric (TTAGGG) repeats and other degenerate DNA repeats (Dunburn et al., 2000). After digestion, the DNA fragments are separated by gel electrophoresis and then subjected to southern blotting. TRFs are visualized directly or indirectly by hybridization with labelled oligonucleotides corresponding to the TTAGGG repeat sequence. Size distribution of the TRFs is then compared to a standard DNA strand of known length (Dunburn et al., 2000).

TRF analysis has been viewed as fast, reliable and broadly applicable to different type of tissues (Kitts, 2001). Despite its advantages, TRF method has disadvantages; it requires large numbers of cells, which is difficult to achieve within senescent cells. As TRF is a hybridisation based technique, very short telomere will produce lower hybridisation signal that might be undetectable.

1.11.2 Quantitative fluorescence in situ hybridization (Q-FISH)

Fluorescence *In Situ* Hybridization is a method involving microscopy observation of specific hybridized DNA. FISH is based on the hybridization of labeled nucleic acid probes to metaphase chromosome preparation which can be detected via fluorescence microscopy. Besides, the FISH procedure can be done in a short period of time which allows rapid *in situ* analysis (Amann and Fuchs, 2008; Justé et al., 2008). Peptide Nucleic Acid (PNA) (CCCTAA)

probes is frequently used in Quantitative FISH for individual telomeres which are highly specific to complementary sequences chromosomes.

Q-FISH technique quantifies the telomere length and telomere lengths are measured as Telomere Fluorescent Units (TFU). TFU is measured and translated to value number by (TFL-TELO) computer program software. However, the translation of TFU accurately into telomere length is difficult. Moreover, as TRF is a hybridisation based technique, very short telomere might be undetectable. Q-FISH requires metaphase chromosomes which is a problematic in senescent cells. However, Q-FISH has been highly successfully used in many different research fields.

1.11.3 Flow FISH

It is another method for determining the lengths of telomeres. Flow FISH is adapted from Q-FISH which uses interphase telomere FISH with flow cytometry and its procedure as following; cell separation, denaturation, hybridization to probe, washing and flow cytometry analysis. Telomere lengths are measured and assessed by the multicolor produced by flow FISH. Flow FISH is able to detect telomere length in cycling and non-cycling cell of metaphase. Moreover, flow FISH is used to measure telomere length as prognostic tool for hematopoietic stems cells diseases. However, it is required high level of florescence to analyse and detect telomere length which is difficult to achieve in senescent cells (Lansdorp, 1996).

1.11.4. Quantitative PCR

Quantitative PCR (qPCR) involves primers labeled with a fluorescent dye and a quencher, designed such in a way that reduce the formation of dimers. One of the most common techniques for measuring telomere length by means of qPCR is Cawthon's method

(Telomere/Single Copy Gene ratio also known as T/S method) (Cawthon, 2002). This method measures the how the ratio of the TTAGGG telomere repeat copy number to single-gene copy number varies between the sample tested and a control sample. Cawthon method relies on the evaluation of the kinetics of the amplification of a telomere fragment and a single-copy gene fragment so as to come up with a telomere/single-copy gene ratio. Sample tested is then compared to the standard control sample whose length is known. The number of telomere repeats in the sample tested is calculated using the level of dilution of the control DNA that would make the number of cycles of PCR required to produce a given amount of telomere PCR product from the sample tested comparable to the number of cycles needed to come up with the same amount of telomere product from the control sample. Other variations of the qPCR method for measuring telomere length use internal oligomer standards with known number of telomere repeats sequences to avoid relative quantification by comparison with a control of known length (Cawthon et al., 2003). Q-PCR is often used for measurement of telomere length since it demands relatively small amounts of DNA. Moreover, Q-PCR is rapid and high-throughput. However, since PCR is sensitive technique, the qPCR method for measurement of telomere length has a danger of contamination among samples and this may produce biased results. In addition, due to the nature of PCR, shorter telomeres are preferentially amplified whereas larger fragments may not be amplified to the point of visualized. Furthermore, the exact shorter telomere length may be hard to estimate as this method provides no information on telomere length distribution.

1.11.5 Single Telomere Length Analysis (STELA)

STELA was invented and developed to overcome the limitations of other telomere determination techniques. High quality resolution, the accuracy and sensitivity of analysis telomere length and the applicability to numerous cell and different type of tissue samples; those are STELA technique advantages.

STELA is a long-range single-molecule PCR technique that determines the length of the telomeric repeats from specific chromosome ends (Baird, 2005). STELA utilises a linker 'Telorette' that contains TTAGGG sequences followed by 20 nucleotides of non-complimentary tail that ligates to the 5' end of the C-rich telomeric strand. Teltail primer is the second requirement, which is annealed to the 20 nucleotides of non-complimentary tail of telorette. A third requirement is chromosome specific upstream primer, is located in the subtelomeric region. By all three requirements, STELA PCR can be performed across the double-straded telomere repeat region (Figure10).

In each STELA PCR reaction, DNA is diluted to 4-10 amplifiable molecules to detect single telomere length accurately. PCR products are resolved by agarose gel electrophoresis and detected by southern hybridisation with a telomere repeat probe.

The end of chromosome XpYp was the first telomere analysed by STELA. STELA has since been further developed and designed to be able to analyse other chromosomes ends such as; 2p, 9p, 11q, 12q, 16q, 17p and 18q (Britt-compton et al., 2006). STELA has facilitated and demonstrated detailed of telomere loss through the process of the end replication problem. Furthermore, by its sensitivity and ability to detect extremely short telomere, STELA has defined a new mean senescent telomere length of 1Kb, when telomere has eroded and

become dysfunctional, whereas 4 Kb was the previous telomere length threshold described by TRF method (Baird et al., 2003).

In STELA, primers have been designed to extensive sequence polymorphisms in telomere adjacent of the chromosomes, which makes STELA limited to that primers sequence designed. Technique demands high quality DNA sample, is unlikely to be applicable to egraded or fixed samples (Baird, 2005).

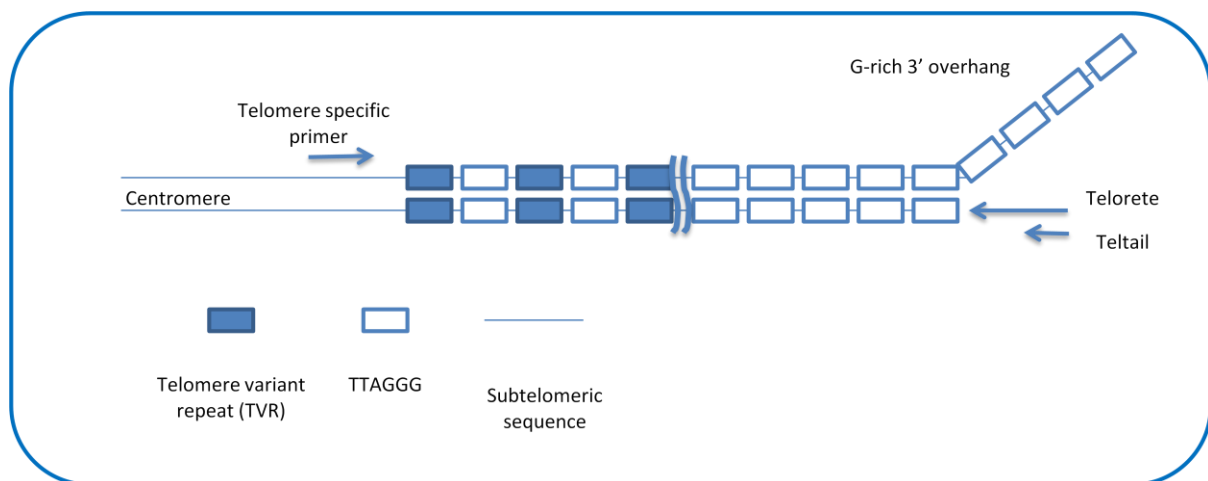


Figure 10: STELA method. Telorette ligates to the 5' end of the C-rich telomeric strand, then teltail anneals to the 20 nucleotides of non-complimentary tail of telorette. Together telorette, teltail with telomere specific primers designed within subtelomeric sequence are making telomere amplification. (Baird et al., 2003)

1.12 This work

Short dysfunctional telomeres are capable of fusion to other chromosome ends; this can lead to genomic instability that may drive tumour progression. As a consequence of end-replication losses, telomeres undergo gradual erosion with ongoing cell division. However this erosion is superimposed by large-scale telomeric deletion events. These deletions were

not consistent with end replication losses, but instead must arise via as yet unknown additional mutational mechanisms. These events have been detected in normal human cells and tissues (Figure 11).

Our hypothesis that oxidative damage, replication fork stalling and G-quadruplex structures at telomeric DNA could act as mutational mechanisms that may participate in the induction of large scale telomeric deletion and dysfunction.

The triplet guanines within telomeric repeats (TTAGGG) make telomeres more susceptible to oxidative damage and oxidative guanine damage may be induced preferentially in telomeres (Rhee *et al.*, 2011); thus oxidative stress is one hypothesised mutational mechanism that may result in deletion.

Moreover, telomeres have been described as fragile sites, which may arise due to the inability of DNA polymerases to replicate telomere repeat sequences resulting in replication fork stalling. Consequently polymerase dissociation from DNA and the cessation of replication, may result in telomeres that are not fully replicated and may cause telomeric deletion.

Furthermore, telomeric strands tend to form G-quadruplex structures, these structures are difficult to resolve. Replication fork stalling and resolution as a double-stranded DNA breaks may result in telomeric mutation.

In this study will investigate these putative mutational mechanisms that may underlie telomeric deletion, using STELA technique, due to its ability to detect the extremely short telomeres of the length at which both senescence can be triggered and telomere fusion can occur.

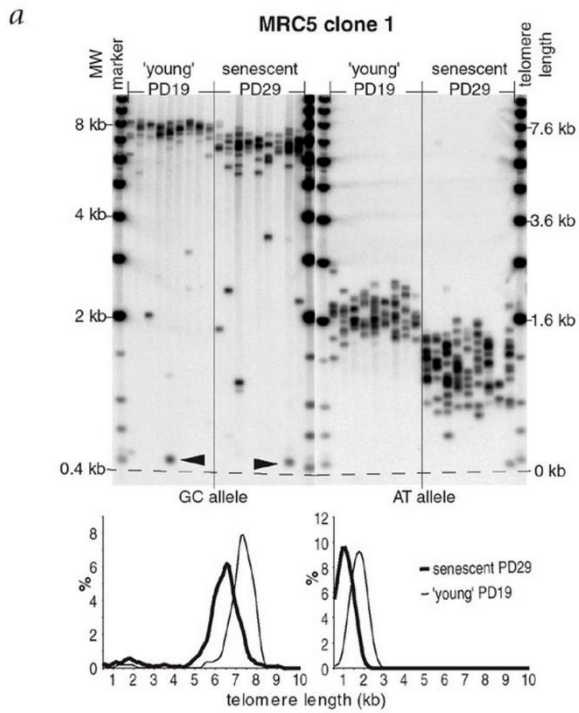


Figure 11: STELA reveals gradual telomere erosion with on-going cell division, superimposed by stochastic deletion events (arrowed) (taken from Baird et al Nat Genet. 2003)

Chapter 2

Materials and Methods

2.1 Chemicals and Reagents

Chemicals and reagents used in the experiments were obtained from: Fisher Scientific, Thermo Scientific, Bio-Rad, Abcam, Sigma-Aldrich, Roche, Amersham Biosciences/GE healthcare, Invitrogen, Applied Biosystems, and New England Biolabs. Table 2.1 showed drugs used during study.

Drug	Formula	Molecular Weight	Product No.
Hydrogen Peroxides	H ₂ O ₂	34.01g/mol	216763Sigma-Aldrich
Aphidicolin (APH)	C ₂₀ H ₃₄ O ₄	338.48g/mol	A0781 Sigma-Aldrich
Hydroxyurea (HU)	CH ₄ N ₂ O ₂	76.05g/mol	H8627 Sigma-Aldrich
RHPS4	CH ₃ OSO ₃	458.48g/mol	Sigma-Aldrich

Table2.1: Drugs used during study

2.2 Plastic Labware

Plastic and glassware were obtained from Becton Dickson labware, Gilson, thermo Electron Corporation and Eppendorf.

2.3 Equipment

Specialised equipment was from Bio-Rad, MJ research, MSE, Limited, Hybaid, Bioquell Ltd, DJB Labcare Ltd/Heraeus, Labcold, Patterson scientific, GRANT instruments Ltd, Thermo electron corporation, Amersham Biosciences, IBS integrated biosciences, Molecular

dynamics, Qiagen and scientific laboratory supplies Ltd. Microscopes were supplied by Olympus UK Ltd.

2.4 Oligonucleotides

Primers were designed based on human DNA sequences obtained from H. Reithman at Wistar institute and the national centre for Biotechnology information (NCBI). They were synthesised by MWG-Biotech AG (Ebersberg, Germany). Table 2.2 showed all primers were used in this project.

1- STELA Primers

Telorette2	5'-TGCTCCGTGCATCTGGCATCTAACCT-3'
Teltail	5'-TGCTCCGTGCATCTGGCATC-3'
XpYpE2	5'-TTGTCTCAGGGTCCTAGTG-3' (406 bp)
17pseqrev1	5'-GAATCCACGGATTGCTTTGTGTAC-3' (311bp)

2- Fusion Assay Primers

XpYpM	5'-ACCAGGTTTTCCAGTGTGTT-3'
17p6	5'-GGCTGAACTATAGCCTCTGC-3'
21q1	5'-CTTGGTGTGAGAGAGGTAG-3'

3- Fusion Reamplification Primers

17p7	5'-CCTGGCATGGTATTGACATG-3'
21qseq1	5'-TGGTCTTATACTGTGTTC-3'
XpYpO	5'-CCTGTAACGCTGTTAGGTAC-3'

Table 2.2: Oligonucleotide sequences used during study.

2.5 Cell Culture

2.5.1 Cells

IMR90, MRC5 and Seckel cells human diploid fibroblasts were obtained from Coriell Cell Repository (Institute for Medical Research, Camden, New Jersey, USA). U138 cells and HeLa cells were obtained from Prof. Paul Smith (school of Medicine, Cardiff University). Ntera cells were obtained from Prof. Peter Andrews (Department of Biomedical Science, The University of Sheffield). For further details see table 2.3.

Name / ID	IMR90	MRC5	SCK	U138	Hela	Ntera
Description			Seckel Syndrome (ATR-)	glioblastoma	Cervix carcinoma	embryonal carcinoma of the testis
Cell Type	fibroblast	fibroblast	fibroblast	glioblastoma	epithelial	epithelial
Tissue Type	Lung	Lung	Skin	brain	cervix	Testis (lung metastasis)
Species	Homo sapiens	Homo sapiens	Homo sapiens	Homo sapiens	Homo sapiens	Homo sapiens
Age	16 weeks	14 weeks	6 years	47 years	31 years	22years
Sex	female	male	male	male	female	male
Race	Caucasian	Caucasian	Indian	Caucasian	Black	Caucasian

Table 2.3 Cell lines used in this study

2.5.2 Medium

IMR90, MRC5, U138 and Seckel (SCK) cells were cultured in Eagle's minimum essential medium (EMEM, Invitrogen) supplemented with Earle's salts containing Sodium Bicarbonate (7.5% solution, Gibco), 2x nonessential amino acids (Sigma), 10% (v/v) fetal calf serum (Autogenbioclear), 25mM HEPES Buffer, 1x10⁵ U/l penicillin, 100 mg/l streptomycin and 2

mM L-Glutamine (all Sigma). In SCK cells, 1X vitamins were added to medium. Hela cells were cultured in Dulbecco's Modified Eagle's Medium DMEM (Invitrogen) with 1×10^5 U/l penicillin, 100 mg/l streptomycin and 2 mM L-Glutamine (all Sigma) and 10% (v/v) fetal calf serum (Autogenbioclear). Ntera cells were cultured in Dulbecco's Modified Eagle's Medium DMEM (Gibco) containing 4.5 g/L glucose with 10% Foetal Bovine Serum (FBS), 2mM L-Glutamine and Pen/Strep (1×10^5 U/l penicillin, 100 mg/l streptomycin). Cells were incubated in 5% CO_2 at 37 °C and medium was changed every 2-3 days and cells were passaged when ~80% confluence was reached.

2.5.3 Seeding and Passage

Medium were removed from flask and cells were washed once with fresh trypsin (0.05% trypsin and 0.2% EDTA (Gibco)) to remove all remaining serum. An appropriate volume of pre-warmed trypsin was added to the flask and cells were incubated at 37 °C for 5 minutes or until the cells were detached. Fresh medium was added to stop trypsinisation and cells suspension was transferred into a 15ml falcon tube. For re-plating sufficient numbers of cells and fresh medium were added to a new flask or well. Cells were passed at different densities adjusting according to the shape and type of cells and size of the dish or flask were used.

2.5.4 Counting Cells and Population Doublings Calculations

To monitor population doublings (PDs) of the cells, cells were counted at every passage with haemocytometer (Improved Neubauer, Hawksley). Total cell number was calculated as follow: number of counted cells $\times 10^4 \times$ volume of cell suspension (in mL)

Population doublings (PDs) then could be calculated as follow;

$$PD = [\text{Log (total cell number)} - \text{log (seeded cell number)}] / \text{Log}2$$

2.5.5 Cell Freezing

Cells were frequently frozen to enable the cells to re-grow and works as a back-up for further experiments or in case of infection or contamination of the original cell culture. For freezing; cells were centrifuged and re-suspended in 0.5ml of medium and equal amount of freezing mixture (1:4 dimethyl- sulphoxide (DMSO, Sigma); foetal calf serum). The suspension then transferred to freezing ampoule and stored at (-80 °C) for short term storage or in liquid nitrogen (-196 °C) for long term storage, in a freezing box containing isopropanol. This method facilitates gradual freezing and reduces the ice damage of the cells by preventing ice crystal formation in the cells.

2.5.6 Cell Thawing

Ampoules of cell suspensions was removed from the -80°C freezer or from liquid nitrogen and thawed quickly in water bath (Grant) at 37°C to prevent ice crystal formation. Thawed cell suspension was transferred to 15ml falcon tube and 9ml of fresh medium was added drop wise to avoid the damage through osmotic shock. The falcon tube of the cell suspension was centrifuged at 1000 rpm for 5 minutes and supernatant was removed and an appropriate volume of fresh medium was added for re-plating.

2.5.7 Senescence Assay

Senescent cells were measured by using Senescence Detection Kit (Abcam). Cells were cultured overnight in a 12- well plate then, medium was removed and the cells were washed once with 1xPBS. Culture was fixed with fixative solution for 15 minutes at room temperature. Fixative solution was removed and culture washed twice with 1xPBS. Cells

were stained overnight at 37°C with staining solution mix (staining solution, staining supplement and X-gal in dimethyl-sulphoxide DMSO (1mg/ml)). Percentage of senescent cells was calculated by counting number of blue staining cells in a total cell number of 500. Percentage of senescent cells (%) = (number of stained cells / total number of cells) x 100.

2.5.8 Cell Cycle Analysis Using Propidium Iodide (PI)

Harvested cells were washed twice in (PBS + 0.1% BSA) buffer and 1×10^6 cell/ml was re-suspended in buffer. 1ml of 70% cold ethanol was added as drop wise while vortexing to avoid cell loss or clumping. Cells were fixed for at least one hour at -20°C or several days prior to PI staining. Fixed cells were washed in PBS and then centrifuged at 12000 rpm for 5 minutes. 0.5ml of PI staining solution (50µg/ml PI in PBS) and 50µl of RNase A were added to cell pellet and were mixed well and incubated for one hour at 4°C. Then the sample was analysed by flow cytometry (BD Bioscience accuri c6 flow cytometer) and cells in the different phases of cell cycle was determined by flow cytometry.

2.5.9 Apoptosis Analysis

Annexin V Staining kit from (eBioscience) was used. 10X binding buffer was diluted to 1X using distilled water. Cells were washed once in PBS, then once in 1x binding buffer. Cells were resuspended in 1x binding buffer at $1-5 \times 10^6$ /ml. 5µl of fluorochrome-conjugated Annexin V was added to 100µl of cell suspension and then were incubated at room temperature for 10-15 minutes. Suspension were washed in 1x binding buffer and resuspended in 200µl of 1x binding buffer and then 5µl of Propidium Iodide (PI) staining solution was added to suspension. Suspension were incubated at 4°C for 2 hours and then apoptotic cells fractions were analysed and determined by flow cytometry.

2.5.10 Metaphase Spread Analysis

Cultured cells were incubated one hour to two hours in regular medium with 0.1µg/ml demecolcin (colcemid solution from Sigma-Aldrich). Cells were checked under microscope rounded and refractile cells with blebby membrane were seen as effects of colcemid. Cells were harvested and trypsinised and collected in conical tube and centrifuged at 1000 rpm for 5 minutes. Supernatant was removed following centrifugation, pellet was resuspended in 5ml of (0.075M KCl pre-warmed to 37°C), and incubated for 10-30 minutes at 37°C, in this step cells were swollen. Suspension was centrifuged at 1000 rpm for 5 minutes. Supernatant was removed following centrifugation, pellet was resuspended again in small volume of KCl. 1ml of fixative solution (3:1 methanol and glacial acetic acid) was added as drop wise, suspension was kept overnight at 4°C. Slides (Fisher Scientific) were prepared and placed in cold water. The hot block was set to 70°C and wet paper towels were placed on top of the block. Resuspended cells were dropped using (Pasteur pipette) from a couple of inches on each end of wet slides. Fresh fixative solution was dropped across the slides, all cytoplasmic membrane washed off and nuclei stayed. Slides were checked under light microscope for spreading efficiency. Slides were dried overnight in a fume hood, fixed in methanol for 10 minutes and air dried. Then the slides were immersed for 45 minutes in Giemsa stain (Giemsa stain solution from (Sigma-Aldrich) were diluted 1:20 with distilled water), and were rinsed with distilled water. Slides were checked under microscope (100X magnification) in (Medical Genetics Department, Cardiff University). Breaks and gaps in chromosomes were visualised under microscope and counted in 50 metaphases.

2.6 Single Telomere Length Analysis (STELA)

2.6.1 Preparation Cells for DNA Extraction

Cells were alternatively either frozen or sampled for single telomere length analysis (STELA). Cells were centrifuged at 1000 rpm for 5 minutes at room temperature, then supernatant was removed and cell pellet was washed twice with PBS to remove any trypsin and culture medium and centrifuged again at the same conditions. After centrifugation supernatant was removed and cell pellet was stored at -20 °C for up to 12 months.

2.6.2 DNA Extraction

2.6.2.1 Maxwell

DNA was extracted from cell pellets by using the Maxwell 16 LEV Blood DNA Kit (Promega) along with the Maxwell 16 machine. Cells were lysed by 300µl of lysis buffer and 30µl of proteinase K at 56°C for at least one hour. After a quick centrifugation cell lysates were loaded into the cartridges and placed into the Maxwell 16 machine. The research mode with LEV hardware was adjusted to extract the DNA from cell lysates. DNA was eluted with elution buffer into 50µl.

2.6.2.2 DNA Extraction Using QIAamp DNA Micro Kit

For cell samples which contained less than 1×10^5 cells, genomic DNA was extracted using QIAamp DNA Micro Kit. The kit enables the purification of genomic DNA from small samples sizes by binding the DNA to a silica-based membrane. DNA was extracted from the cell pellets by adding 100µl of the provided ATL buffer (tissue lysis buffer) and 10µl of the provided Proteinase K solution. After adding 100µl of the provided AL buffer (containing

guanidinium chloride to denature proteins), the samples were pulse-vortexed for 15s. The lysis of the samples was carried out at 45°C for 10 min. After a quick spin to remove all condensation from the tube lid, 50µl 100% ethanol was added to the sample. Afterward the sample was pulse-vortexed for 15s and incubated at RT for 3 min. The entire lysate was transferred to the QIAamp MinElute Column. The samples were centrifuged for 1 min at 6000x g in a Heraeus centrifuge to bind the DNA to the silica-based membrane. Residual contaminations were removed by washing twice with the provided buffers AW1 (containing guanidinium chloride to denature proteins) and AW2 (70% ethanol to remove salt). The DNA was eluted from the column with 30µl 10mM Tris-HCl pH 8.0.

2.6.3 DNA Quantification

DNA concentration was quantified in triplicate using Hoechst 33258 fluorometry (Bio Rad) as described previously (Baird *et al.*, 2003), NanoDrop-100 system (Thermo Scientific) supplied by (Central Biotechnology Service (CBS) Cardiff University) or by performing a pilot STELA to determine band number, after which relative DNA quantities to add to reactions were then calculated.

2.6.4 STELA PCR

To enable the accurate detection of telomere length within STELA, the DNA was diluted to 10ng/µl in 10mM Tris-HCl pH 8, leaving typically 4-10 amplifiable molecules per reaction. Firstly, 40µl of Tel2/DNA working dilution was prepared containing: (1µl of diluted DNA (10ng), 38µl of Tris-HCl (10mM, pH 8) (Sigma) and 1µl of telorette2 primer (10µM)). Typically 6 PCR reactions were carried out per sample in a volume of 10µl containing: Taq reaction buffer (Tris-HCl (75mM, pH8.8), (NH₄)₂SO₄ (20mM), 0.01% Tween-20) (Abgene),

MgCl₂ (2mM), dNTPs (1.2mM), telomere specific primer (0.5μM), teltail primer (0.5μM) and 0.5U *Taq* (Abgene)/*PWO* (Roche) at ratio of 10:1. Finally, 1μl of telorette2-linked DNA (250pg) was added to each reaction and 10μl drop of mineral oil on top of the reaction was added as well to prevent evaporation through the program cycles. All PCR reaction steps were prepared on ice. The reactions were then cycled in a Bio-Rad DNA Engine Tetrad Thermal Cycler using following program: denaturation at 94°C for (20 second), annealing at 59°C for (17peseqrev1 primer) or at 65°C for (XpYpE2 primer) for (30 second) and elongation at 68°C for (8 minutes)X 22 cycles.

2.6.5 Fusion PCR

DNA was diluted to 50ng/μl in Tris-HCL (10mM, pH 8). 18 PCR reactions were carried out per sample in a volume of 10μl containing: 50ng DNA, *Taq* reaction buffer (Tris-HCL (75mM, PH8.8), (NH₄)₂SO₄ (20mM), 0.01% Tween-20) (Abgene), MgCl₂ (2mM), dNTPs (1.2mM), telomere adjacent primers (17p6, XpYpM, & 21q1) (0.5μM), teltail primer (0.5μM) and 0.5U *Taq* (Abgene)/*PWO* (Roche) at ratio of 10:1. 10μl drop of mineral oil was added on top of the reaction. All PCR reaction steps were prepared on ice. The reactions were then cycled in a Bio-Rad DNA Engine Tetrad Thermal Cycler using following program: denaturation at 94°C for (20 second), annealing at 59°C for (30 second) and elongation at 68°C for (8 minutes) X 25 cycles.

2.6.6 Gel Electrophoresis for STELA and Fusion PCR Products

Amplified DNA fragments generated by STELA or fusion PCR were resolved by submarine gel electrophoresis using 0.5% Tris-acetate-EDTA agarose gel containing 0.1% ethidium bromide. 2μl of a Ficol based gel loading dye (5% bromophenol blue, 5% xylene and 15%

ficol) were added to PCR reactions, then 5µl of STELA PCR reactions were loaded and run onto 40 cm long gel at 120V for overnight or at least for 16 hours under circulating cooling system at 4°C. 0.5µl of 1Kb DNA ladder and 0.5µl of 2.5Kb DNA ladder (Stratagene) were run (to track the molecular weight of PCR products). Fusion products were loaded and run a third to half the length of the 40cm gel at 50V for 16hours.

2.6.7 Southern Blot

DNA ladder bands were stained by ethidium bromide and were visualised under UV transilluminator and gels were cut to the ladder size. Gels were washed twice for 6 minutes with depurination (0.25M HCl), gels were rinsed in ddH₂O, and then DNA fragments for STELA or for fusion were denaturated in 1.5M NaCl, 0.5M NaOH for 15 minutes. DNA fragments then were transferred to a positively charged membrane (Hybond XL (Amersham)) by alkaline southern blotting for 4-6 hours; denaturation buffer was used as transfer buffer. Membrane was washed with H₂O and left to dry at room temperature.

2.6.8 Southern Hybridisation Probes for STELA and Fusion Assay

The hybridisation probe for STELA and fusion was labelled by using rediprime random hexamer labelling beads (Ready-To-Go DNA, GE Healthcare). 1µl of 25ng of probe template in 44µl of TE buffer (10mM Tris-HCl and 1mM EDTA) was denatured at 96°C for 5 minutes and then chilled on ice for 5 minutes. Denatured DNA was added to ready-made labelling mix containing random hexanucleotides, the klenow fragment of DNA polymerase, NTPs and [α -³²P]dCTP. The reaction mix was incubated at 37°C for 15 minutes at water bath, resulted in DNA synthesis and incorporation of ³²P radioactive label. To detect molecular

weight markers on the blots, 1µl of [α -³³P] labelled 1Kb and 2.5Kb DNA markers was added to the reaction mix of telomere specific probe.

2.6.9 Hybridisation

After 4-6 hours of Southern blotting, the apparatus was dismantled and the membrane was rotated at 60°C in a hybridisation oven with 15 ml of church buffer (0.5M sodium phosphate buffer [1M disodium hydrogen phosphate and 1M sodium dihydrogen phosphate], 1mM EDTA, 1% BSA and 7% SDS, (pH 7.2)) for 15 minutes. The labelled telomere specific probe was denatured again at 96°C for 5 minutes and then 25µl of probe was added to hybridisation bottle. Hybridisation was carried out overnight at 60°C in a hybridisation oven.

2.6.10 Hybridisation Washes

After the hybridisation process, the hybridised membrane was washed several times with 0.1X sodium chloride sodium citrate (SSC)/ 0.1% sodium dodecyl sulphate (SDS) at 60°C in hybridisation oven for 1-2 hours, to remove all non-specific bound hybridisation probe. Washed membrane was dried for 30 minutes in the oven.

2.6.11 Visualisation of Radiolabelled DNA Fragments

Dried membrane was placed in a cassette with a phosphoimager screen (Amersham) for 24 hours. Phosphoimager screen was scanned by using Typhoon 9419 biomolecular imager (GE healthcare). Prior to re-hybridisation with a second probe, STELA and fusion blots were stripped with boiling 0.1% SDS for at least 6 hours.

2.7 Protein

2.7.1 Protein Extraction (Cell Lysis)

Protein was extracted from cells seeded in 100mm dish which containing 70-80% of confluence. Cells were washed twice with 5ml of ice cold sterile PBS, to remove any culture medium. Cells were scraped and transferred from the dish into 15ml falcon tube with 2ml of ice cold sterile STE buffer (10mM Tris-Hcl, 150mM NaCl and 1mM EDTA (pH8.0)). Cell suspension was centrifuged at 1000rpm, 4°C for 5 minutes. Supernatant was removed carefully. Cells were lysed by 30µl of ice-cooled lysis buffer (1ml of cell lysis buffer (150mM NaCl, 50mM Tris, 5mM EDTA and 1% NP40 (pH8.0)), 30µl of (phenylmethylsulfonyl fluoride (PMSF)), 10µl of phosphatase inhibitor and 10µl of protease inhibitor), tubes were kept on ice for 5 minutes. Samples were centrifuged at 1000rpm, -5°C for 30 minutes. Tubes were gently removed from the centrifuge and placed on ice, the supernatant was aspirated and placed in a fresh tube and kept on ice, and the pellet was discarded. Protein was stored at -80 °C.

2.7.2 Protein Quantification

Bradford method, was used to determine protein concentration, it depends on quantitating the binding of a dye coomassie blue to unknown protein (samples) and comparing this binding to different amounts of a standard protein (BSA). Coomassie Plus Protein Assay Reagent (Pierce No 23236) kit was used in the experiment. Samples were prepared and diluted in H₂O (1/10). Standards were also prepared from BSA and lysis buffer as in (table 2.4) in triplicate, ranging from 0, 100, 200, 300 and 400µg/ml, allowing for comparing.

BSA	Lysis Buffer	Concentration
0µl	150µl	0µg/ml
7.5µl	142.5µl	100µg/ml
15µl	135µl	200µg/ml
22.5µl	127.5µl	300µg/ml
30µl	120µl	400µg/ml

Table 2.4 Standard concentrations that used in the experiment.

From each standard or sample, 40µl was taken into semi-micro cuvettes and 1ml of the coomassie blue reagent was added. Standards and samples were mixed well and were read on spectrophotometer at 595 nm. Standards were carried out in triplicate, and samples in duplicate. Protein concentrations were calculated using excel software.

2.7.3 Prepare Samples

3X loading buffer and lysis buffer were added to samples. 3X loading buffer was prepared from (0.5M Tris 300µl, Glycerol 300µl, 10% SDS 300µl and 1% bromophenol blue 60µl) and fresh 5µl of 2-mercaptoethanol blue was added to 160µl of 3X loading buffer mixture. Then, mixtures were incubated for 5 minutes in hot block 100 °C before loading.

2.7.4 Running Gel

10% Gel precast gel from (BioRad) with 15 wells and loading capacity 15µl and the system Mini-protean II Electrophoresis from (BioRad) was used. 250mM of running buffer was prepared (15g of Tris base, 94g of Glycine, 5g of SDS and 1 litter H₂O) pH 8, buffer was kept at 4°C. 15µl of mixtures (samples, 3X loading buffer and lysis buffer) were loaded into

precast gel. 5 μ l of molecular weight marker (rainbow marker from Amersham) and 10 μ l of loading buffer was run along with the samples. Gel was run at 100-200V for one hour.

2.7.5 Prepare Membrane

Millipore Immobolin-P (IPVH30470), PVDF transfer membrane (BioRad), was used. Membrane was immersed for 3 seconds in methanol, and then washed for 2 minutes in H₂O. Membrane was kept in transfer buffer (4.6g of Tris base, 21.6g of Glycine, 300ml of methanol and 1.5 liters H₂O, pH 8). Clamp, pads (x2) and 3MM paper (x4) were kept soaked in transfer buffer as well.

2.7.6 Transfer Proteins from Gel to Membrane (Western Blot)

Mini Trans-blot Electrophoresis Transfer Cell, the same tank that was used for electrophoresis was used for transfer as well. Gel was removed from plates, and one corner was nicked to help orientation. Gel was placed in transfer buffer. The immunoblot sandwich was assembled as (1- white face of clamp, 2- pad, 3- 2X 3MM papers, 4- membrane, 5- gel, 6- pad, 7- 2X 3MM papers any bubbles were rolled out and 8- black face of clamp). The immunoblot sandwich was clamped together and placed in holder black face was next to black side of holder and white face next to red side of holder. Transfer buffer was poured and stir bar/flea was placed at bottom and ice block was placed as well in holder. Holder was placed on stirrer and transferred at 20-30V over night.

2.7.7 Membrane Blocking and Antibody Incubation

Membrane was washed with Tris Buffer Saline (TBS) for 5 minutes at room temperature. One liter x10 TBS was prepared as (24.2g Tris base, 80g NaCl and pH was adjusted to 7.6 with HCl and was stored at 4°C. x1 of TBS was used. Membrane was incubated for one hour

with blocking buffer at room temperature. Blocking buffer was prepared previously as (1X TBS, 0.1% Tween-20 with 5% nonfat dry milk). Following blocking, membrane was washed three times for 5 minutes with washing buffer (1X TBS 0.1% Tween-20). Then, membrane was incubated with diluted primary antibody from (Cell Signaling) over night at 4°C, table 2.5 showed antibodies and dilutions used. Primary antibodies were diluted in primary antibody dilution buffer (1x TBS, 0.1% Tween-20 with 5% BSA). Then, membrane was washed three times for 5 minutes with washing buffer. Membrane was incubated with diluted HRP-conjugated secondary antibodies (anti-rabbit or anti-mouse depending on type of primary antibody used) (Cell Signaling) for one hour at room temperature. Secondary antibodies were diluted (1:2000) in (1x TBS, 0.1% Tween-20 with 5% BSA). Then, membrane was washed three times for 5 minutes with washing buffer.

Antibodies used	Molecular weight	Isotype	Dilution	Product No.
Phospho-Chk1 (Ser345)	56 KDa	Rabbit	1:500	2348
Phospho-Chk2 (Thr68)	62 KDa	Rabbit	1:500	2661
Phospho-p53 (Ser15)	53 KDa	Mouse	1:1000	9286

Table 2.5: Antibodies used during study.

2.7.8 Protein Detection

Membrane was incubated with developing solution from (Amersham) for 5 minutes, and then excess solution was removed from membrane. Membrane was wrapped in plastic and exposed to x-ray film (Amersham) for 1 minute to 5 minutes, then membrane was removed to develop.

2.8 Statistical Analysis

Scanned STELA blots were analysed using Molecular Dynamics ImageQuant 5.0 (GE). The calculation of the molecular weight of the DNA fragments was carried out by using Phoretix 1Dsoftware (Nonlinear Dynamics). Telomere length measurements were exported to Microsoft Excel where the distance between telomere adjacent primer and telomere repeat array was subtracted and giving an accurate telomere length measurement. All mean values, standard derivations (SD), standard errors (SE) and median values were calculated with Microsoft Excel and GraphPad Prism. All presented diagrams were generated in Microsoft Excel, Power Point and GraphPad Prism.

2.8.1 T-test

The t-test was calculated in GraphPad Prism using unpaired t-test. The calculated p-value is the probability of the null hypothesis being true. At a p-value below 0.05 the null hypothesis was rejected.

2.8.2 Repeat Measure ANOVA

A repeat measure ANOVA (analysis of variance) was used to determine if there was a significant difference between one sample subjected to three or more different concentrations. No difference between the different concentrations was stated as the null hypothesis. The repeat measure ANOVA was calculated in GraphPAD Prism. At a p-value below 0.05 the null hypothesis was rejected.

Chapter 3

Oxidative Stress and Telomere Erosion

3.1 Summary

Telomeres are nucleoprotein structures that contain non-coding (TTAGGG) tandem repeats and associated telomere binding proteins at the end of chromosomes. As a consequence of end-replication losses, telomeres undergo gradual erosion with ongoing cell division. It is hypothesised that in addition to the end-replication problem, mutational mechanisms may contribute to telomere erosion by generating large-scale telomeric deletion events. As short dysfunctional telomeres are capable of fusion to other chromosome ends, large-scale telomeric deletions can lead to genomic instability which in turn may drive tumour progression. The aim of this chapter is to observe if oxidative stress contributes to telomere erosion and large-scale telomeric deletion.

By undertaking a comprehensive analysis of telomere dynamics following the induction of oxidative stress, the data presented here showed that oxidative damage does not appear to affect the rate of telomere erosion or the frequency of large-scale telomeric deletions. Instead prolonged exposure to oxidative stress results in the preferential loss of sub-populations of cells exhibiting short telomeres from the culture. We conclude that loss of these cells from the culture may be due to a preferential sensitivity to damage that may be related to these cells being closer to their replicative limit. These data are more consistent with the view that premature senescence does not arise as a consequence of accelerated telomere erosion, but instead more likely results from stochastic DNA damage across the rest of the genome.

3.2 Introduction

3.2.1 Telomere-Dependent Replicative Senescence

The ends of eukaryotic chromosomes are capped by telomeric sequences that are lost as a result of the end replication problem with each cell division in telomerase negative cells (Henderson *et al.*, 1996). Cell division and telomeric erosion occur until critically short uncapped telomeres predominate resulting in the triggering of a DNA damage response (Fagagna *et al.*, 2003). This response includes the ATM/p53 and the Rb/p16 pathways that serve as the signals of the DNA damage response and lead to a permanent cell-cycle arrest (Fagagna *et al.*, 2003). The termination of cell growth, commonly referred to as Replicative Senescence and the repression of the proliferation promoting genes are also involved (Hayflick, 1965). Replicative cellular senescence is a non-dividing but biologically active state, that represents a limit to the number of times cells can divide referred to as the Hayflick limit (Hayflick, 1965; Allsopp *et al.*, 1995). Replicative senescence can provide a tumour suppressive mechanism, preventing end-to-end fusions and chromosomal abnormalities (Campisi, 2005; Krtolica *et al.*, 2001). Replicative senescence resulting from the end-replication problem can be circumvented in telomerase negative cells by forced expression of the catalytic subunit of telomerase (Bodnar *et al.*, 1998). However, telomerase expression alone cannot completely prevent the occurrence of senescent cells resulting from other senescence triggers (Campisi and d'Adda di Fagagna, 2007).

3.2.2 Telomere-Independent Cellular Senescence

Cellular senescence is not just caused by telomere erosion alone. In some cases, cell stress has been associated with triggering of early replicative senescence (Dumont *et al.*, 2000;

Serrano *et al.*, 1997). For example, *in vitro* stresses of tissue culture conditions including hyperoxia, the distributions of cells in a culture, cell-to-cell contact and the medium to cell ratios all considerably restrict a cell's replicative lifespan (Sherr and DePinho, 2000). A number of cell types have been observed to undergo senescence in a telomere independent manner, for example, the telomerase positive Human fetal ventricular cardiomyocytes (HFC) (Ball and Levine, 2005) and Syrian hamster embryonic cells (Carman *et al.*, 1998). Moreover, oxidative stress, oncogene over-expression and DNA damaging agents can also induce early replicative senescence (Dumont *et al.*, 2000; Serrano *et al.*, 1997). Oxidative stress can be induced by H₂O₂ treatment. H₂O₂ is considered as a reactive oxygen species and can react with intracellular iron to produce the hydroxyl radicals (Liu *et al.*, 2002). Hydroxyl radicals are highly reactive species that can lead to DNA attack, breaking single strands and subsequently causing a premature senescence (Dumont *et al.*, 2000). Cellular senescence can also be induced by the over-expression of active oncogenes within normal cells, for example the expression of mutant RAS oncogene leads to a senescence response (Serrano *et al.*, 1997). Furthermore, human cells have been observed to undergo cellular senescence as a result of the build-up of DNA damage (Di Leonardo *et al.*, 1994). Telomere independent senescence has probably evolved as a tumour suppressor mechanism, preventing on-going cell division of damaged cells.

3.2.3 Telomere Deletion Events

Single Telomere Length Analysis (STELA) is a single molecule approach to determine telomere length distributions at specific chromosome ends (Baird *et al.*, 2003). Through this technique, it has been observed that telomere erosion with ongoing cell division results in a decrease in the mean and an increase in the variance of the telomere length distribution

that is entirely consistent with gradual telomere erosion arising as a consequence of the end-replication problem (Baird *et al.*, 2003). However, this was superimposed by the occurrence of stochastic deletion events resulting in extremely short telomeres (Baird *et al.*, 2003). These have been observed in both telomerase positive and negative cells (Baird *et al.*, 2003; Britt-compton *et al.*, 2006). These events result in dysfunctional telomeres that are capable of fusion, even in normal cells in which the mean telomere lengths are consistent with long-stable telomeres (Capper *et al* 2007; Letsolo *et al.* 2009). Such events have the potential to trigger genomic instability which may lead to tumourgenesis or aging phenotypes. A telomere deletion phenomenon, telomere rapid deletion (TRD), was first described in yeast (Li and Lustig, 1996) and was considered to arise from an intra-telomeric recombination event. TRD as described in yeast results in the deletion of artificially lengthened telomeres resetting them to the length of the genome average (Li and Lustig, 1996). In contrast Human (hTRD) events result in the deletion of telomeres from genome average to a critically short length (< 1kb). Thus the mutational mechanisms underlying TRD in yeast may be distinct from those observed in human (hTRD). The mechanisms generating hTRD events are unclear. Possible mechanisms for TRD include oxidative stress (Von Zglinicki *et al.*, 1995) replication fork stalling (Crabbe *et al.*, 2004) unequal sister chromatid exchange (Bailey *et al*, 2004) and intra-allelic mechanisms that may include replication slippage (Baird *et al.*, 1995). Other mechanisms for TRD include the fragility of telomere repeat region and stability of G-quadruplex structures in the telomeres may also be involved in generating hTRD, both of which are investigated in chapters 4 and 5.

In human cells TRD events do not increase with on-going cell division implying that they may either be repaired back to mean telomere length, or that the cells may have exited the cell-cycle or that fusion event may occur rendering the molecules undetectable with STELA

(Baird *et al.*, 2003). hTRD events at the XpYp telomere were estimated to occur at a rate of 3%. Assuming that hTRD events occurs at the same frequency at the other telomeres, hTRD may represent a significant contributor to genome-wide telomere losses which have the potential to result in genome instability (Baird *et al.*, 2003; Britt-compton *et al.*, 2006).

3.2.4 Oxidative Stress and Telomere Structure

The canonical telomere repeat sequence contains a triple guanine sequence that has been shown to be sensitive to damage by oxidative stress. Oxidised guanine increases in senescent cells that are characterised by an increase of up to four times in free 8-oxodG bases (8-oxo-deoxyguanosine) (Nasir *et al.*, 2014). 8-oxodG bases can be very mutagenic if unrepaired, 8-oxoG base pairs with adenine resulting in a GC to AT transversion just after two replication cycles. These mutations can lower the affinity of the telomere binding proteins and result in telomere uncapping and increased rate of recombination (Boiteux and Radicella, 1999).

3.2.5 Reactive Oxygen Species (ROS)

The effects of Reactive Oxygen Species can be counteracted by a number of antioxidants through both enzymatic and non-enzymatic mechanisms. Oxidative stress is related to the imbalance of ROS and antioxidants whereby the effects of ROS can overwhelm the compensatory ability of antioxidants. In the case of mitochondrial-derived ROS, a superoxide is the first radical produced (Loft and Polsen, 1996). Based on the fact that the main site of superoxide production is in the inner mitochondrial membrane, the mitochondrial DNA (mtDNA) has been regarded as the major target for ROS damage.

Reactive oxygen species such as superoxide radical anion, hydrogen peroxide, hydroxyl radical, peroxynitrite, hypochlorous acid can all be formed within cells. Transfer of electrons to oxygen from mitochondrial Electron Transport Chains leads to the formation of superoxide ions (Liu *et al.*, 2002). Reaction of superoxide radicals with MnSOD produces hydrogen peroxide. Within cells, several oxidases also produce hydrogen peroxide. Catalase and glutathione peroxidase react with hydrogen peroxide and change it to water. At times reaction of hydrogen peroxide with superoxide radical can form more superoxide radicals. In the presence of heavy metals and UV, lysis of hydrogen peroxide can react with the heavy metals leading to formation of hydroxyl radicals. Hydroxyl radicals are highly reactive and can disturb the integrity of DNA (Liu *et al.*, 2002). Formation of nitric oxide is catalysed by nitric oxide synthase may produce highly reactive peroxynitrite radical when reacted with superoxide ions. In addition, peroxynitrite radical is able to form various reactive oxygen species. For instance, the conjugate acid of the peroxynitrite, i.e. ONOOH may dissociate and form reactive free radicals like NO₂ and OH (Chandel *et al.*, 1998).

Telomeres are considered to be extremely sensitive to oxidative damage and this may be due to the sensitivity of the GGG repeat regions to ROS and the reduced capacity for DNA repair within telomeres. The high rate of telomere erosion that has been reported in cell cultures subjected to high oxygen tensions has been reported to occur as a consequence of the apparent low antioxidant capacity of the cell strains. This is considered to result in an accumulation of single stranded breaks and elevated rates of telomere shortening (Von Zglinicki, 1995).

3.2.6 Oxidative Stress and Cell Culture

The proliferative capacity of human fibroblasts in culture is modulated by oxygen concentrations and seeding densities (Balin *et al.*, 1984). It has been shown that lowering oxygen concentrations from 20% to around 5% and/or adding antioxidants to growth media can facilitate an increase in replicative lifespan of the cell cultures from human colorectal mucosa, amniotic fluid and primary melanoma cells (Pritchett *et al.*, 1985; Brackertz *et al.*, 1983). Several studies have been demonstrated that IMR90 fibroblasts can enter premature senescence early in their replicative lifespan following the treatment with hydrogen peroxide (H₂O₂) (Chen *et al.*, 2004). Premature senescence induced due to the effect of oxidative stress. Reactive oxygen species (ROS) are the source of oxidative stress which constitutes the majority of DNA damage in human cells. Oxidative stress induces DNA damage response via p53, p21 and p16 activation and result in cell cycle arrest (Chen *et al.*, 2004; Itahana *et al.*, 2001).

A link between oxidative damage and telomere biology has been observed. This observation has been emerged from the growth fibroblast cells such as WI38 cells in 20% and 40% oxygen. WI38 in 40% oxygen underwent premature senescence but this was associated with an increased rate of telomere erosion compared to cells cultured at the 20% oxygen. This leads to the hypothesis that the oxidative stress and oxygen tension in the culture was the primary driver of telomere erosion in WI38 cells (Von Zglinicki, 2002). In contrast to WI38 strains, BJ and MRC5 fibroblast strains showed no observable difference in cell proliferation and telomere shortening at varying oxygen tension. Thus it was concluded that different cell strains react differently to varying oxygen tensions and that such differences may be due to differing antioxidant capacities (Lorenz, 2001; Britt-Compton, 2009). Further observations

using G6PD deficient primary foreskin fibroblasts HFF1 and HFF3 showed that these cells prematurely senesce after H₂O₂ treatment without significant telomere loss (Cheng *et al.*, 2004). Therefore the role that oxidative stress plays in driving telomere erosion is controversial.

3.2.7 Analysis of Stochastic Deletion Events

STELA is a single telomere length analysis technology that determines the distributions of telomere lengths at a specific chromosome ends (Baird, 2005). The technique is considered as a sensitive method that can detect telomere lengths up to 28 kb and can also detect telomeres which have almost completely lost their telomeric sequences, thus revealing full spectrum of telomere length at specific chromosome ends. Critical short telomeres that have potential to trigger replicative senescence or initiate chromosome instability now are detectable with the technique. The technique was first developed for the analysis of the dynamics at XpYp telomere (Baird, 2003) and has since been extended for 2p, 9p, 11q, 12q, 16q, 17p and 18q chromosomes end (Britt-Compton *et al.*, 2006) and also *C. elegans* (Cheung *et al.*, 2004).

Analysis of clonal populations of human cells with STELA shows that with on-going cell division a decrease in the mean and an increase in variance of the telomere length distributions. These dynamics were consistent with the predicted losses as a consequence of the end replication problem, with a requirement to invoke additional mutational process such that those that occur as a consequence of oxidative damage. However superimposed on the gradual telomere erosion, were large-scale telomere deletion events resulting in truncated telomeres (Baird, 2003). These stochastic deletion events are not predicted as a consequence of end-replication losses, instead it is likely that they arise as a consequence of

some additional mutational process. One example of which may be telomere specific oxidative damage.

3.3 This Work

In this chapter, I have examined whether oxidative stress has the potential to drive stochastic telomere deletion events and therefore resulting in extremely short telomeres which are detectable with STELA. In order to do so, I analysed the effect of different concentrations of hydrogen peroxide (H_2O_2) on cell growth and on telomere dynamics in IMR90 and U138 cancer cells. IMR90 cells were previously described to be subjected to higher rates of telomere erosion compared to other fibroblasts. To investigate whether this is due to oxidative stress, cells were cultured in different concentrations of H_2O_2 in a parallel with cells cultured in normal conditions. DNA samples were taken at various points during proliferation of the cultures (recover period), enabling detailed analysis of telomere dynamics using STELA.

3.4 Results

3.4.1 Effects of Oxidative Stress on Culture Growth

In order to monitor the influence of oxidative stress on fibroblast cultures, human diploid fibroblast IMR90, derived from human foetal lung, were cultured at PD 28 in 6 well plates (35-mm dish) and treated with different concentrations of hydrogen peroxide H_2O_2 (25 μ M, 50 μ M, 150 μ M & 300 μ M) for two hours. Afterwards the cells were allowed to recover for seven days before the next treatment. Three serial treatments were undertaken. Before each treatment cells were collected for DNA extraction, after 7 days, 14 days and 21 days of recovery, allowing detailed analysis of telomere dynamics. Figure 3.1 illustrate the experimental plan.

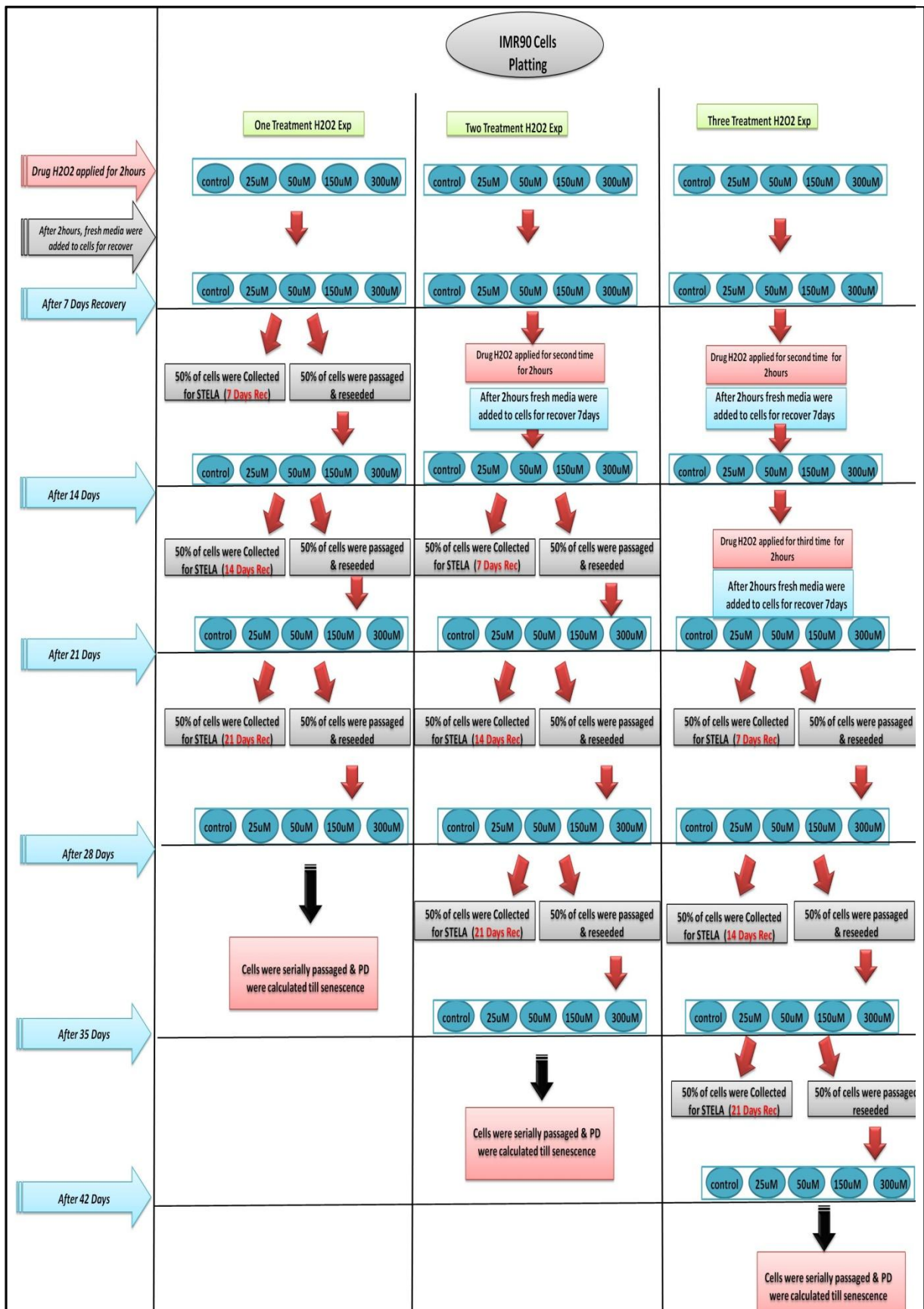


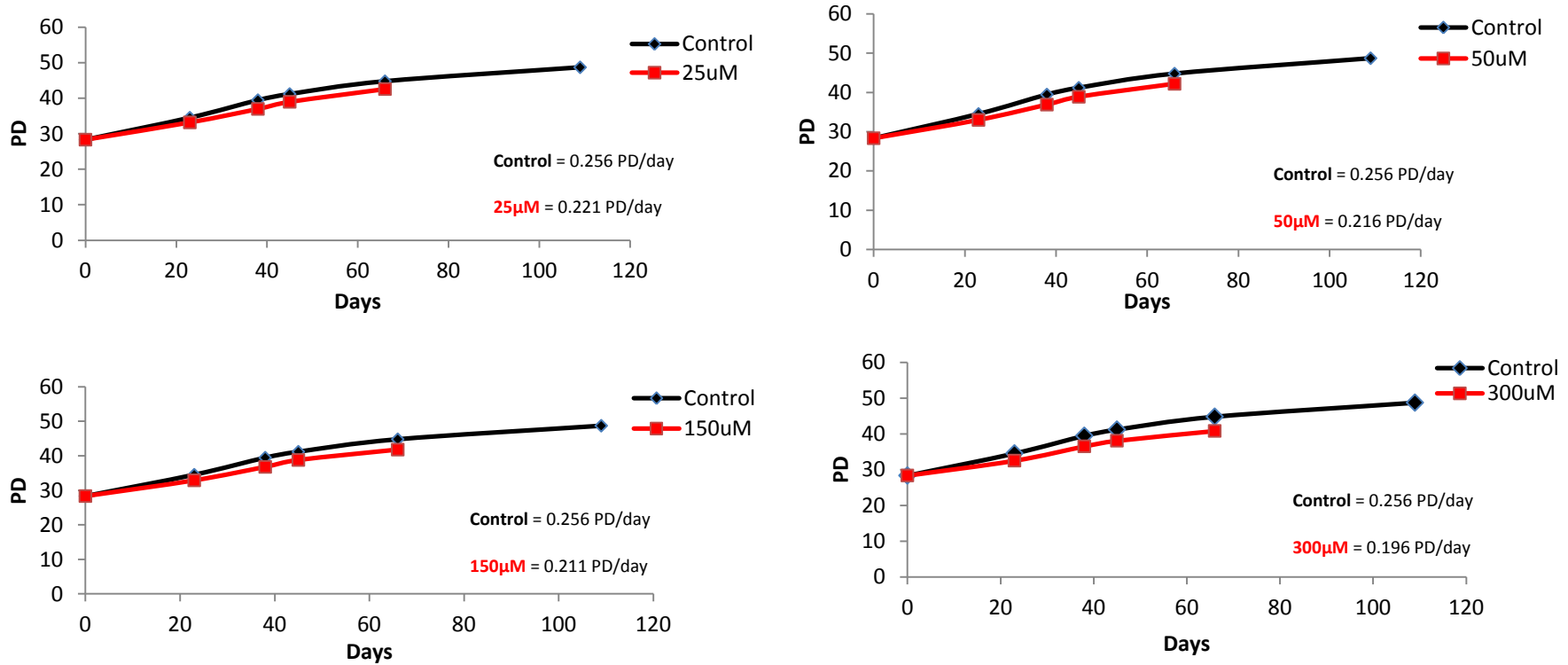
Figure 3.1: The experimental plan. IMR90 fibroblast treated with different concentrations of H₂O₂ for two hours, then the cells were allowed to recover seven days before the next treatment. For each of the three different treatments cells were collected for STELA analysis.

The cells were passaged serially after treatments and the average of population doublings (PDs) was calculated and plotted as a function of time (Figures 3.2, 3.3 and 3.4)

The data showed that the replicative capacity of IMR90 fibroblasts in standard culture conditions was PD 48.72. Whereas, treated IMR90 cells exhibited a truncated replicative lifespan compared to normal control fibroblasts (~ 40.5 PD's were achieved for cells treated with 25 μ M & 50 μ M H₂O₂) and (~39.5 PD's for those treated with 150 μ M & 300 μ M) at the third treatments. Thus normal control of IMR90 fibroblasts grew on average 8 additional PDs compared to those treated with (H₂O₂) for first, second and third treatments (p<0.0001; ANOVA), the H₂O₂ treated cells became senescent and stopped growing in cultures earlier than the control.

The overall growth rates were determined to be on average of ~ 0.256 PD/day for the normal control and ~ 0.163 PD/day for (300 μ M H₂O₂ third treatments). It was obvious that with cells approaching the end of their replicative lifespan, the growth rates slowed at both normal and recovered cultures. This data is in line with previous observations, as fibroblast cell cultures reach their replicative capacity, the growth rate slows with an increasing proportion of cells senescent and fewer cells capable of cell division.

Figure 3.2: PDs of IMR90 Clone 4 (First Treatment H₂O₂)

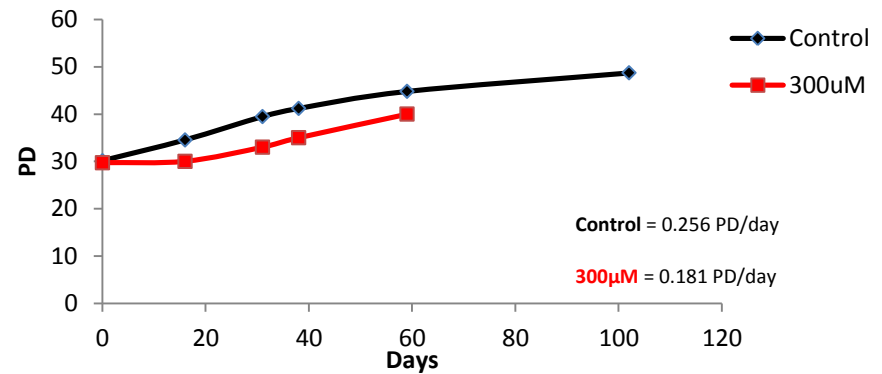
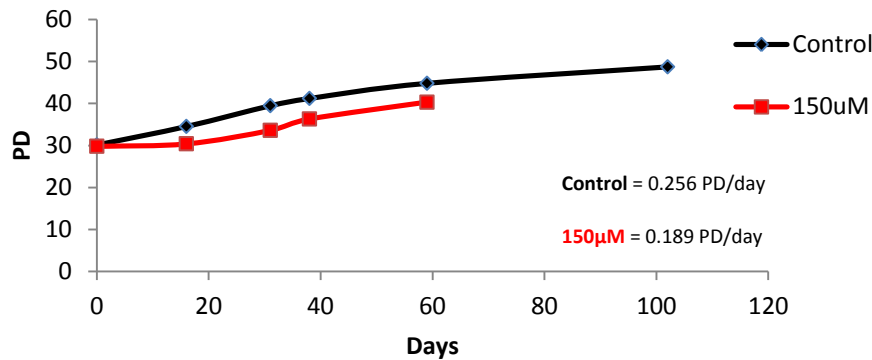
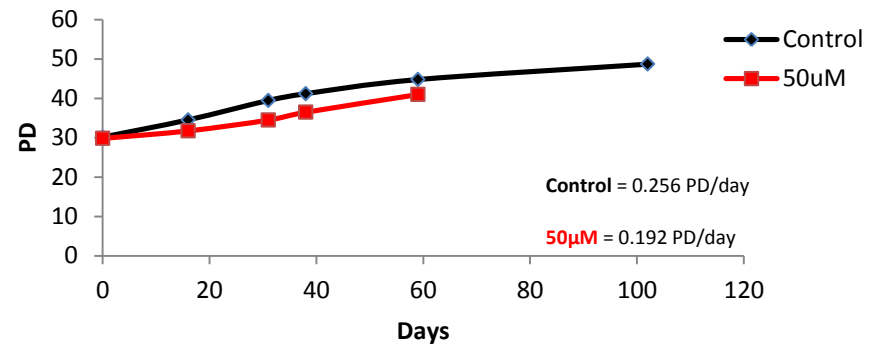
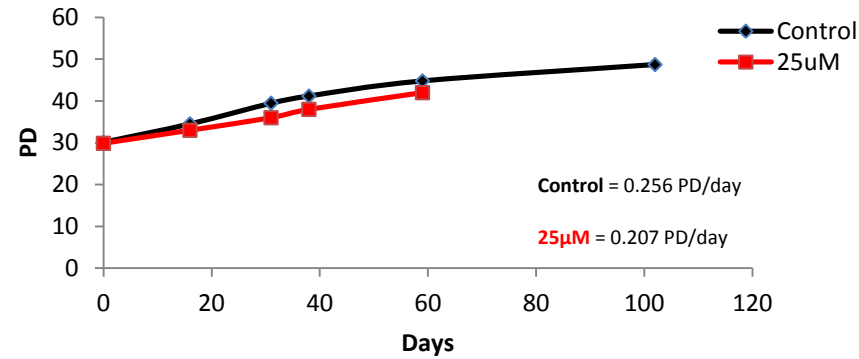


First Treatment	Growth Rate PD/day	Total PD's
Control	0.256 PD/day	48.72
25µM (H ₂ O ₂)	0.221 PD/day	42.60
50µM (H ₂ O ₂)	0.216 PD/day	42.20
150µM (H ₂ O ₂)	0.211 PD/day	41.80
300µM (H ₂ O ₂)	0.196 PD/day	40.99

Figure 3.2: Growth curves of IMR90 clone 4 (First Treatment).

IMR90 control (untreated) (Black Line) was compared to treated (Red Line) with different concentrations of H₂O₂ (25µM, 50µM, 150µM & 300µM) for 2hours. Plotting growth curves as function of population doublings (PD) versus time in days. Treated cells were senesced and stopped growing earlier than control.

Figure 3.3: PDs of IMR90 Clone 4 (Second Treatment H₂O₂)



Second Treatment	Growth Rate PD/day	Total PD's
Control	0.256 PD/day	48.72
25μM (H ₂ O ₂)	0.207 PD/day	42.00
50μM (H ₂ O ₂)	0.192 PD/day	41.50
150μM (H ₂ O ₂)	0.189 PD/day	40.30
300μM (H ₂ O ₂)	0.181 PD/day	40.00

Figure 3.3: Growth curves of IMR90 clone 4 (Second Treatment). IMR90 control (untreated) (Black Line) was compared to treated (Red Line) with different concentrations of H₂O₂ (25μM, 50μM, 150μM & 300μM) for 2hours. Plotting growth curves as function of population doublings (PD) versus time in days. Treated cells were senesced and stopped growing earlier than control.

Figure 3.4: PDs of IMR90 Clone 4 (Third Treatment H₂O₂)

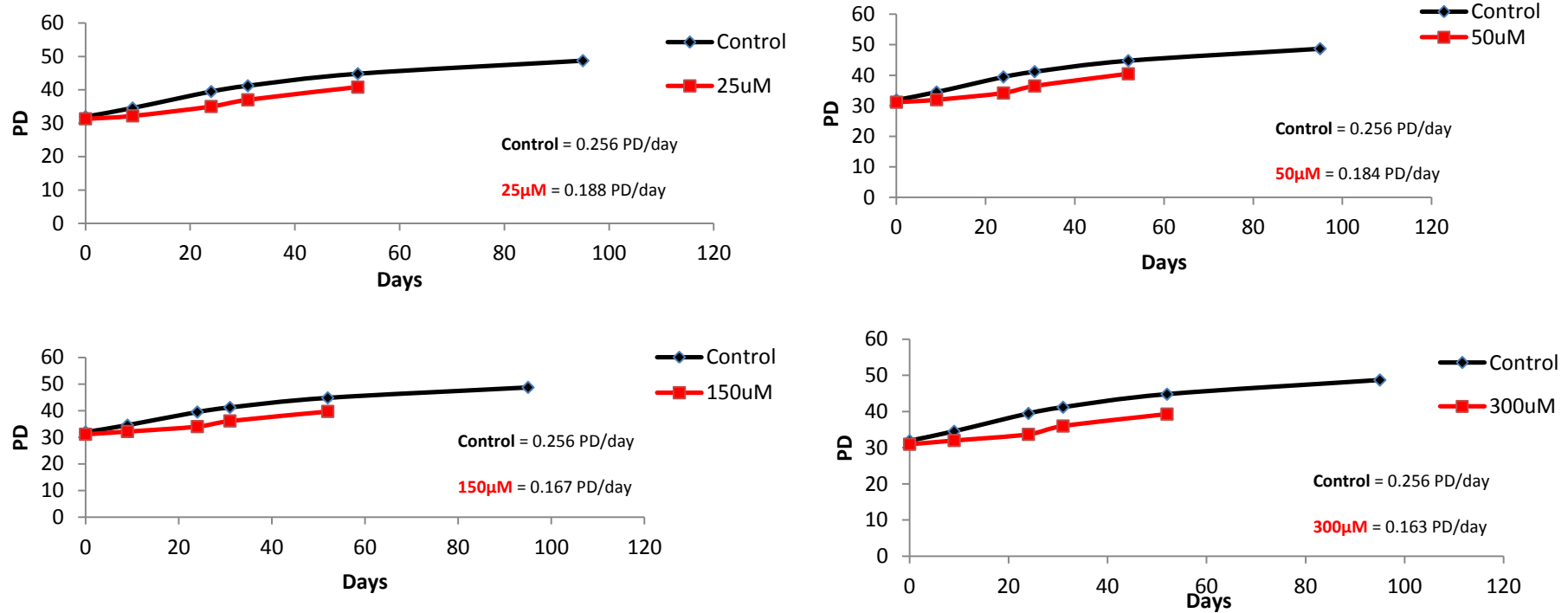


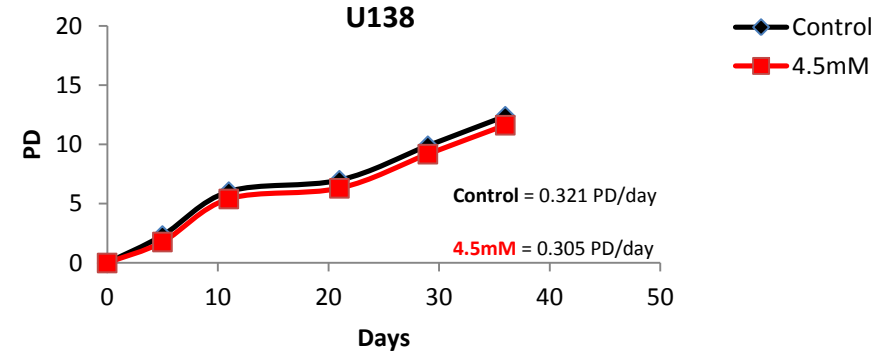
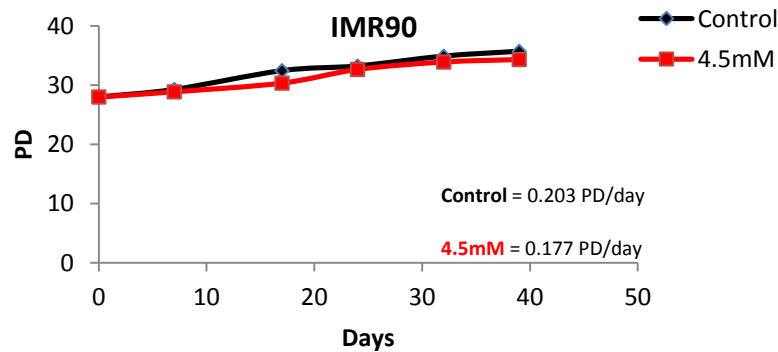
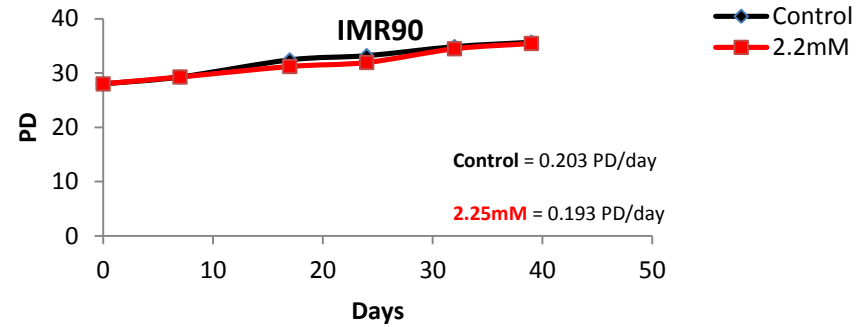
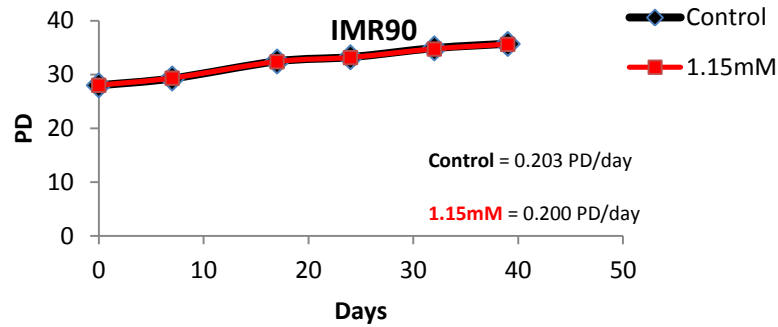
Figure 3.4: Growth curves of IMR90 clone 4 (Third Treatment). IMR90 control (untreated) (Black Line) was compared to treated (Red Line) with different concentrations of H₂O₂ (25µM, 50µM, 150µM & 300µM) for 2hours. Plotting growth curves as function of population doublings (PD) versus time in days. Treated cells were senesced and stopped growing earlier than control.

Another set of experiments was carried out using a higher concentration of H₂O₂ and lower duration of exposure. IMR90 fibroblasts were cultured at PD28 in 6 well plates and were treated with different H₂O₂ concentrations (1.15mM, 2.25mM and 4.5mM) for 10 minutes. U138 cancer cells (mutant *p53*) were cultured and treated as well with 4.5mM H₂O₂ for 10 minutes. After treatment cells were counted and half were collected for DNA extraction and the remaining half were reseeded in normal media allowing the cells to recover, cells were collected for DNA extraction after 7 days, 14 days, 21 days and 27 days of recovery.

The cells were passaged serially after treatments and the average of population doublings (PDs) was calculated and plotted as a function of time (Figure 3.5).

The overall growth rates during experiment were determined to be 0.177 PD/day in IMR90 treated with 4.5mM and 0.203 PD/day in the control. The growth rates of U138 cancer cells were slightly higher than IMR90 fibroblasts. U138 treated with 4.5mM was 0.305 PD/day and 0.321 PD/day for the control of U138.

Figure 3.5: PDs of IMR90 and U138 (Treatment 4.5mM H₂O₂)



Treatment	Growth Rate PD/day
Control IMR90	0.203 PD/day
1.15mM (H ₂ O ₂)	0.200 PD/day
2.25mM (H ₂ O ₂)	0.193 PD/day
4.5mM (H ₂ O ₂)	0.177 PD/day
Control U138	0.321 PD/day
4.5mM (H ₂ O ₂)	0.305 PD/day

Figure 3.5: Growth curves of IMR90 fibroblasts and U138 cancer cells. Control (untreated) cells (Black Line) was compared to treated cells (Red Line) with different concentrations of H₂O₂ (1.15mM, 2.25mM & 4.5mM) IMR90 for 10 minutes. U138 cancer cells were treated with 4.5mM H₂O₂ concentration only for 10 minutes. Plotting growth curves as function of population doublings (PD) versus time in days.

3.4.2 Effect of Oxidative Damage on Cell Cycle Progression

In order to examine the effects of oxidative damage on the cell cycle progression, cell cultures were collected and fixed on the seventh days of the cell's recovery and then the cell cycle progression was investigated after the first, second and third treatment (Figure 3.6)

In the control IMR90 fibroblasts, which were cultured without H₂O₂, the cell cycle proceeded without interruptions in G₁, S and G₂ phases. These checkpoints monitor of the movement through cell cycle and they generate pause in cell cycle progression when damage occurs. If the cells treated with H₂O₂ suffer damage, they may arrest temporarily in G₁, S or G₂ phase depending on the point in the cell cycle in which the damage occurred.

Treatment with hydrogen peroxide resulted in a reduction in the number of cells in G₂/M phase, as shown in (Figure 3.6), where only 8% of treated IMR90 with 300 μ M H₂O₂ (third treatments) in G₂/M phase compared to IMR90 untreated cells were 24% in G₂/M phase.

Moreover, the oxidative stress that was induced by the exposure to hydrogen peroxide diminished the DNA synthesis in treated cells compared to the control cells. Only 1% of the IMR90 cells treated with 150 μ M H₂O₂ (second treatment) were in S phase compared to ~4% of control cells.

In contrast, the percentage of control cells in G₀/G₁ phase were about 70%, whereas around 83% of IMR90 fibroblasts treated with 300 μ M H₂O₂ (first treatment) were in G₀/G₁. This percentage increased even further after the third treatment where 90% of treated cells arrested in G₀/G₁.

This data is in line with previous studies (Chen *et al.*, 1998; Chen *et al.*, 2000) which showed that H₂O₂ induced senescence in human fibroblasts results in a permanent cell cycle arrest

in G1 phase. Other studies have demonstrated that the arrest in G1 phase is related to protection of the cell against oxidative damage and apoptosis (Barzilai and Yamamoto, 2004).

Figure 3.6: Cell cycle of IMR90 Clone 4 (H₂O₂)

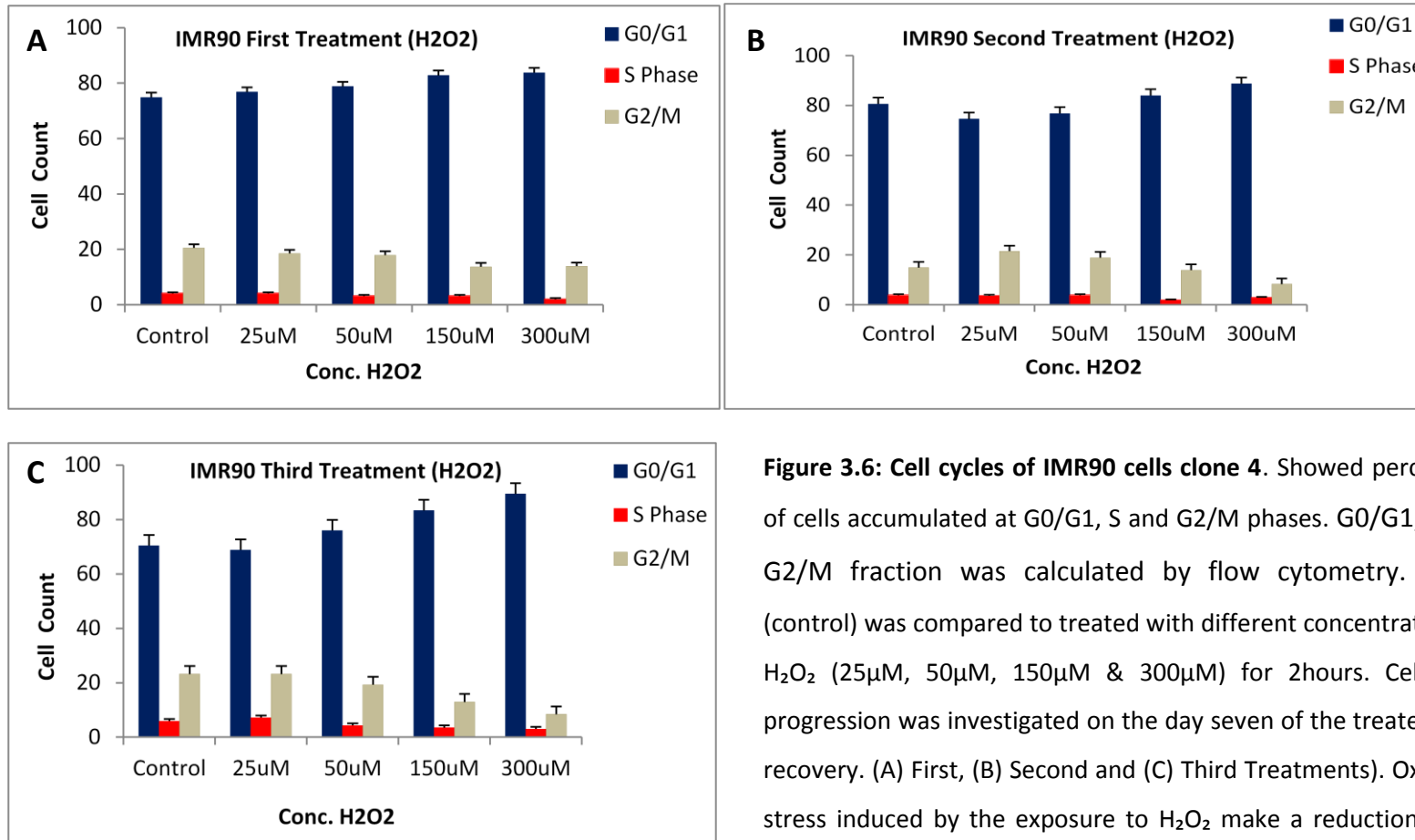


Figure 3.6: Cell cycles of IMR90 cells clone 4. Showed percentage of cells accumulated at G0/G1, S and G2/M phases. G0/G1, S and G2/M fraction was calculated by flow cytometry. IMR90 (control) was compared to treated with different concentrations of H₂O₂ (25μM, 50μM, 150μM & 300μM) for 2hours. Cell cycle progression was investigated on the day seven of the treated cell's recovery. (A) First, (B) Second and (C) Third Treatments). Oxidative stress induced by the exposure to H₂O₂ make a reduction in the number of cells in the synthesis phase, G2/M phase & more cells were accumulated and arrested in G0/G1 phase. Error bars represent standard error (SE).

In order to examine the effect of fragile site induction on cell cycle checkpoints, MRC5, SCK and U138 cells were cultured with APH (1 μ M) and HU (1mM) and incubated for 24 hours in 100mm dishes. Controls and treated cells were collected from culture and fixed in 70% ethanol then were stained with Propidium Iodide (PI) and the G1, S and G2/M fraction was determined by flow cytometry.

3.4.3 Oxidative Damage Induce Cellular Senescence

- **3.4.3.a Cellular Morphology**

Morphological changes were investigated in treated cells and were compared to morphological changes in control cells under the microscope (X20). Treated cells lost their original morphology as shown in (figure 3.7), became larger than their untreated control with a much larger flattened cytoplasm and bigger nuclei. These features are typical of the morphological characteristics of senescent cells (Toussaint *et al.*, 2000; Chainiaux *et al.*, 2002).

- **3.4.3.b Senescence Associated Beta Galactosidase Activity (SA β -gal)**

In order to examine the impact of H₂O₂ treatment on the cellular senescence, the activation of senescence-associated β -galactosidase enzyme was investigated on control and treated IMR90 cells using the Senescence Detection Kit ('ab65351 Abcam'). SA β -gal activity was determined by counting positive stained cells under microscope (X20). The proportions of positive cells were given as percentages of the total counted cells.

It was observed that the activation of senescence-associated β -galactosidase enzyme (cellular senescence marker) in treated cells increased with higher H_2O_2 concentrations. This can be clearly seen from the result of the SA β -gal assay (Figure 3.8.a). The average of senescent untreated cells at 34.5 PDs was 40% of the total counted cells whereas the average of senescent 25 μ M H_2O_2 treated cells was 58% after the third time of treatment and the cells were at (~32.4 PDs). This average activity increased with higher concentrations of H_2O_2 reaching 92% for those cells treated with 300 μ M at PD32.

IMR90 fibroblasts at 28 PDs which were treated with 4.5mM H_2O_2 for 10 minutes showed an average of 47% of senescent cells (Figure 3.8.b).

These data strongly indicate that H_2O_2 treatment successfully induced cellular senescence in IMR90 fibroblasts. In contrast cell cultures derived from p53 deficient (U138 tumour cells) showed no induction of senescence markers despite exposure high concentration of (H_2O_2) (Figure 3.7.b).

Figure 3.7: Cellular Senescence of IMR90 (H₂O₂)


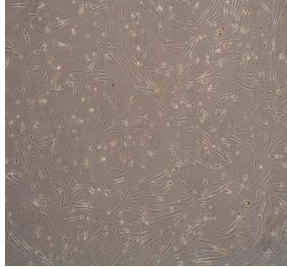


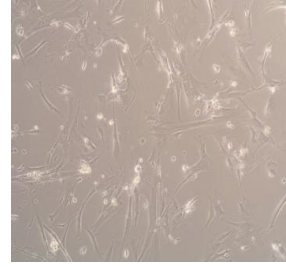
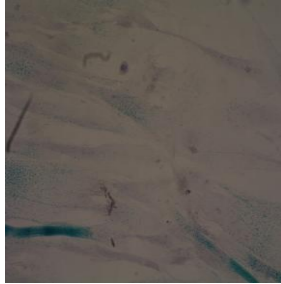
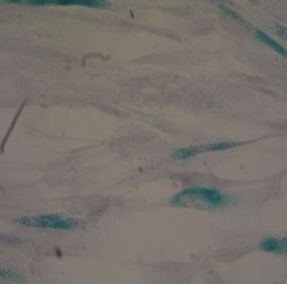


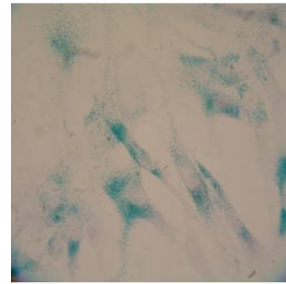
	Control IMR90	IMR90 (25µM H ₂ O ₂)	IMR90 (50µM H ₂ O ₂)	IMR90 (150µM H ₂ O ₂)	IMR90 (300µM H ₂ O ₂)
(A) Cellular morphology					
(B) SAβ-gal					

Figure 3.7: A Cellular Morphology. Morphological changes were monitored in treated cells and were compared regularly to the morphological changes in control cells. Treated cells displayed features similar to those observed in senescent cells; became larger, they had a flattened cytoplasm and bigger nuclei. **B Senescence-associated-beta-galactosidase (SAβ-gal) activity** is detectable at pH6 and produces a blue colour in positive senescent cells; as shown the number of blue positive cells increased with higher H₂O₂ concentrations.

Figure 3.8: Senescence-Associated β -galactosidase Activity (H_2O_2)

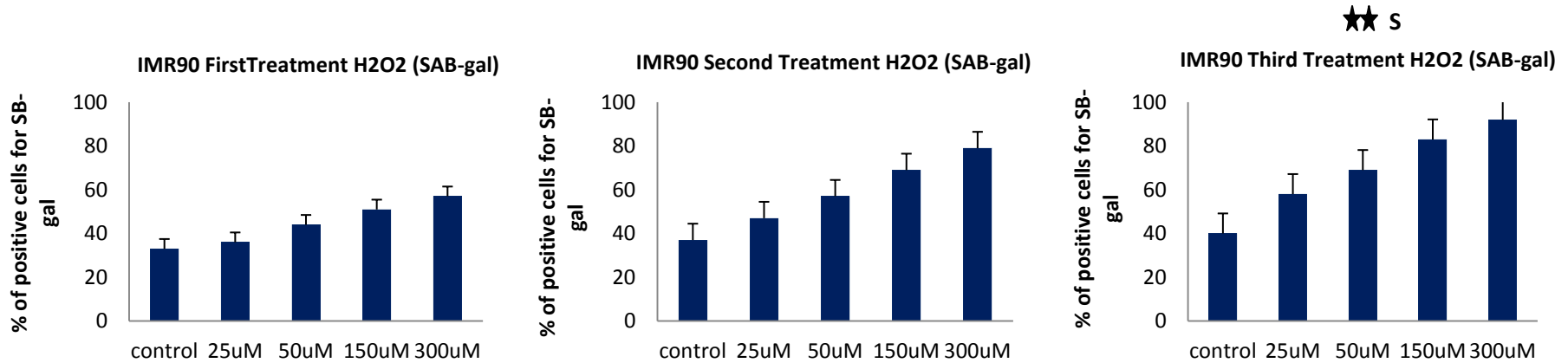


Figure 3.8.a: Senescence-Associated β -galactosidase Activity of IMR90 cells. Shows percentages of positive cells for SA β -gal assay. SA β -gal activity was determined by counting positive stained cells under microscope (X20). The proportions of positive cells were given as percentages of the total counted cells. cells treated with different concentrations of H_2O_2 (25 μ M, 50 μ M, 150 μ M & 300 μ M) for 2 hours first, second and third treatment respectively. Error bars represent standard error (SE). ★★ (SIGNIFICANT) ($p < 0.0001$, ANOVA)

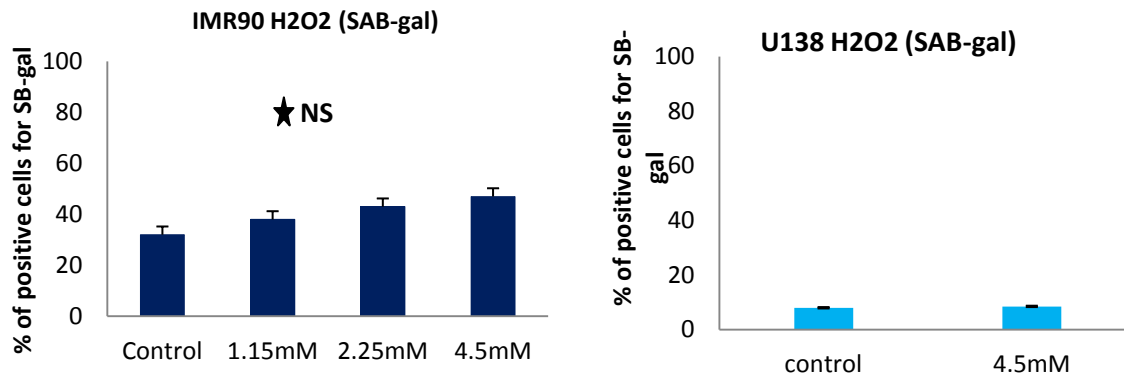


Figure 3.8.b: Senescence-Associated β -galactosidase Activity of IMR90 fibroblasts and U138 cancer cells. Shows percentages of positive cells for SA β -gal assay; IMR90 treated with different concentrations of H_2O_2 (1.15mM, 2.25mM & 4.5mM) for 10 minutes ★ (NOT SIGNIFICANT; ANOVA). U138 cancer cells treated with 4.5mM H_2O_2 for 10 minutes. Error bars represent standard error (SE).

3.4.4 Analysis of Telomere Dynamics

In order to examine if oxidative damage induced by exposure to H₂O₂ result in large-scale changes to telomere length, the XpYp telomere length distributions of IMR90 and U138 treated with hydrogen peroxide were investigated using single telomere length analysis (STELA) (Baird *et al.*, 2003). In line with previous studies in the group (Baird *et al.*, 2003), the XpYp telomere was analysed because it is considered to be representative for average chromosomal telomere length and average telomere erosion rates resulting from the end-replication problem. Multiple cell samples were taken during the course of the experiment. STELA was used to track the telomere dynamics and detect any stochastic shorter telomeres with ongoing cell division. STELA for the experiment are shown in figures (3.9, 3.10, 3.11 and 3.12).

It has been previously defined that stochastically shorter telomeres as those which deviate significantly from the normal distribution of expected telomere length. However we have observed that both control and treated IMR90 fibroblasts clone 4 displayed bimodal distributions at the XpYp telomere. The bimodal distributions made it more difficult to determine these deleted telomeres and thus for the purposes of this study short deleted telomeres were defined as those that were shorter than 2kb.

In treated IMR90 fibroblasts, an apparent change in the bimodal distributions could be observed after approximately 14 days of recovery periods after three treatments. The lower modal distribution disappeared which was consistent across all four different treatments. For example the loss of the lower distribution was clearly seen and was statistically significant in IMR90 fibroblasts treated with 50µM H₂O₂ after the 21 days recovery period following the third treatment ($p < 0.0001$; Figures 3.10 and 3.13).

By looking at Figure 3.14 the proportion of short telomere that were calculated below 2kb showed that IMR90 after the second treatment had a higher short telomeres frequency compared to those after the third treatment indicating that thus cells with short telomeres had disappeared after three treatments. Interestingly, IMR90 fibroblasts treated with 50 μ M had the highest frequency of short telomeres. This means that IMR90 treated with 50 μ M H₂O₂ after 21 days recovery in culture from the third treatments drastically lost their lower model distribution.

In IMR90 fibroblasts treated with higher concentration (1.15mM, 2.25mM & 4.5mM) of H₂O₂ and lower duration (10 minutes), cells remained in culture up to 27 days after treatment, the mean telomere length declined in both control and treated IMR90 over time. IMR90 treated with 2.25mM displayed a higher short telomere frequency (~4.14%) compared to the control (2.25%) and the cells treated with 1.15mM (2.19%) and 4.5mM (1.69%) (Figures 3.15 and 3.16).

Cultures derived from p53 deficient (U138 tumour cells) showed no significant differences in mean telomere length between treated and untreated U138 tumour cells. Both treated and untreated cultures slightly reduced in mean telomere length as a result of the end replication problem (Figure 3.17 and 3.18). Short telomere frequency was higher in control cultures.

Figure 3.9: STELA of Treated IMR90 Clone 4 at XpYp Telomere (25µM H₂O₂) for (First, Second &Third treatments)

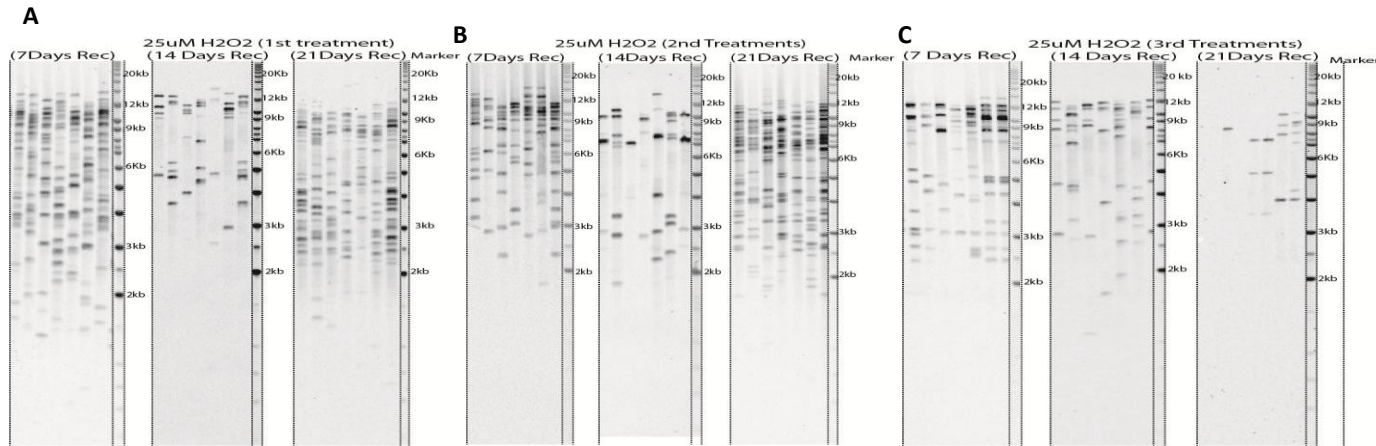
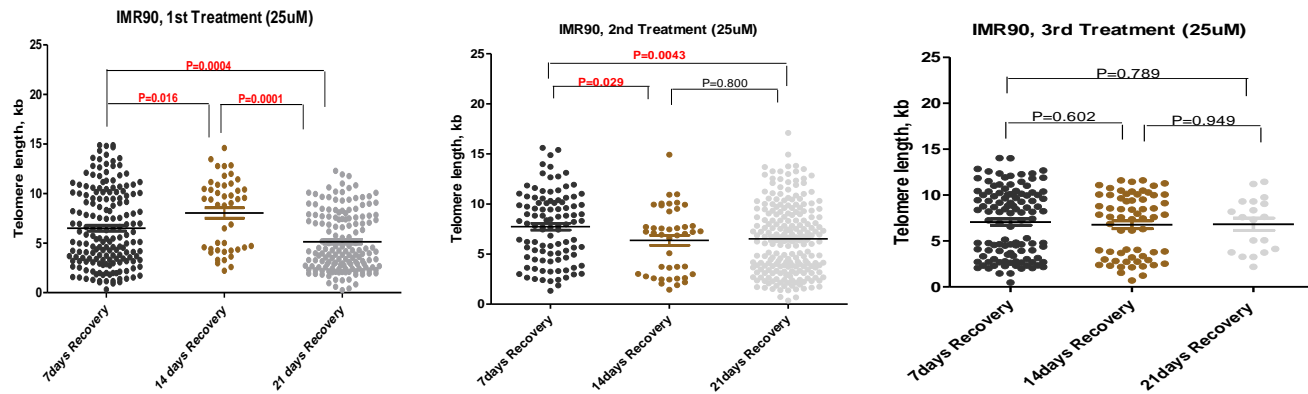


Figure 3.9: STELA gels of XpYp telomere in the IMR90 clone 4 treated with 25µM H₂O₂ for 2 hours and the tables of descriptive data for telomeres. The gels illustrate the telomere length distributions while the tables give the mean, standard deviations (SD) and population doublings (PD), (PD) was calculated after cells harvested. **(A)** IMR90 fibroblasts were treated with 25µM H₂O₂ for 2 hours **once**, then cells were refreshed with normal media and recovered for 7 days, 14 days, 21 days, cells were collected for DNA extraction subsequently. **(B)** IMR90 fibroblasts were treated with 25µM H₂O₂ for 2 hours **twice**. **(C)** IMR90 fibroblasts were treated with 25µM H₂O₂ for 2 hours **three times**. Dot Plot made in (Prism) represent dot plots (Telomere length distributions) from the gels, were quantified using Phortetix software, then they were compared (Days of recovery) and p value was calculated using t-test in Prism (P value in Red is Significant) (in Black is NS).



1 st Treat	7 Days	14 Days	21 Days	2 nd Treat	7 Days	14 Days	21 Days	3 rd Treat	7 Days	14 Days	21 Days
PD	29.88	31.43	33	PD	31.4	32.66	34.22	PD	32.63	33.95	35.26
Mean	6.50	8.04	5.13	Mean	7.706	6.376	6.523	Mean	7.05	6.76	6.82
SD	3.85	3.56	2.98	SD	3.49	3.26	3.52	SD	3.66	3.37	2.89

Figure 3.10: STELA of Treated IMR90 Clone 4 at XpYp Telomere (50µM H₂O₂) for (First, Second &Third treatments)

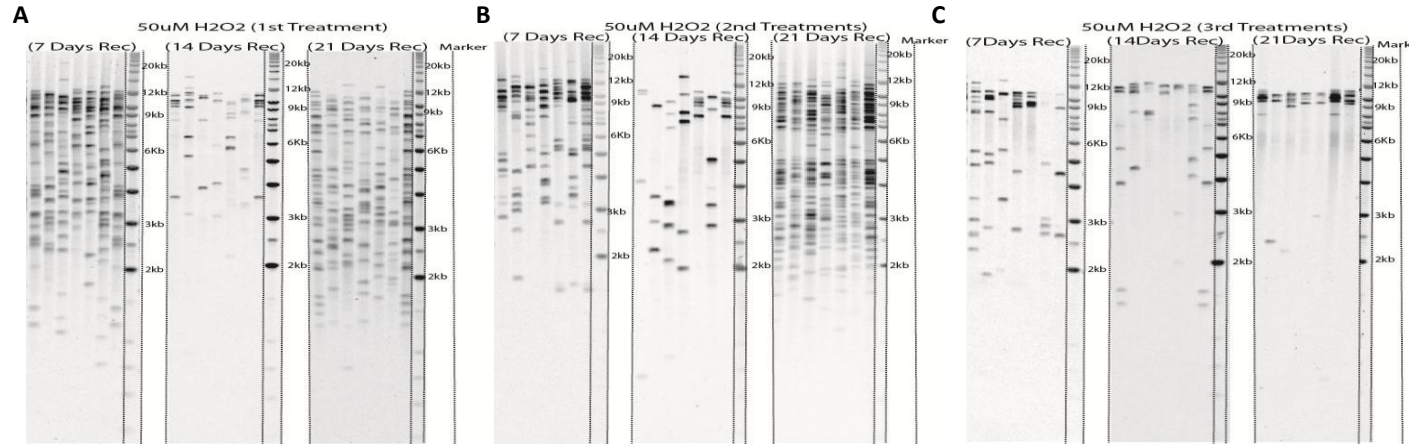
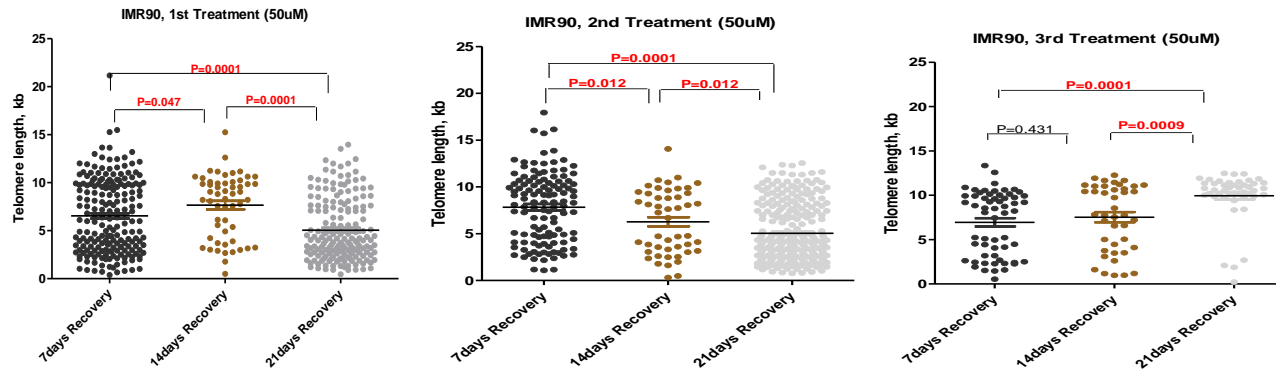


Figure 3.10: STELA gels of XpYp telomere in the IMR90 clone 4 treated with 50µM H₂O₂ for 2 hours and the tables of descriptive data for telomeres. The gels illustrate the telomere length distributions while the tables give the mean, standard deviations (SD) and population doublings (PD), (PD) was calculated after cells harvested. **(A)** IMR90 fibroblasts were treated with 50µM H₂O₂ for 2 hours **once**, then cells were refreshed with normal media and recovered for 7 days, 14 days, 21 days, cells were collected for DNA extraction subsequently. **(B)** IMR90 fibroblasts were treated with 50µM H₂O₂ for 2 hours **twice**. **(C)** IMR90 fibroblasts were treated with 50µM H₂O₂ for 2 hours **three times**. Dot Plot made in (Prism) represent dot plots (Telomere length distributions) from the gels, were quantified using Phortetix software, then they were compared (Days of recovery) and p value was calculated using t-test in Prism (P value in Red is Significant) (in Black is NS).



1 st Treat	7 Days	14 Days	21 Days	2 nd Treat	7 Days	14 Days	21 Days	3 rd Treat	7 Days	14 Days	21 Days
PD	29.85	31.36	32.87	PD	31.19	32.53	33.88	PD	32.47	33.76	35.05
Mean	6.53	7.66	5.05	Mean	7.507	6.272	5.577	Mean	6.95	7.53	9.94
SD	3.83	3.29	3.26	SD	3.88	3.41	3.74	SD	3.57	3.70	2.76

Figure 3.11: STELA of Treated IMR90 Clone 4 at XpYp Telomere (150µM H₂O₂) for (First, Second &Third treatments)

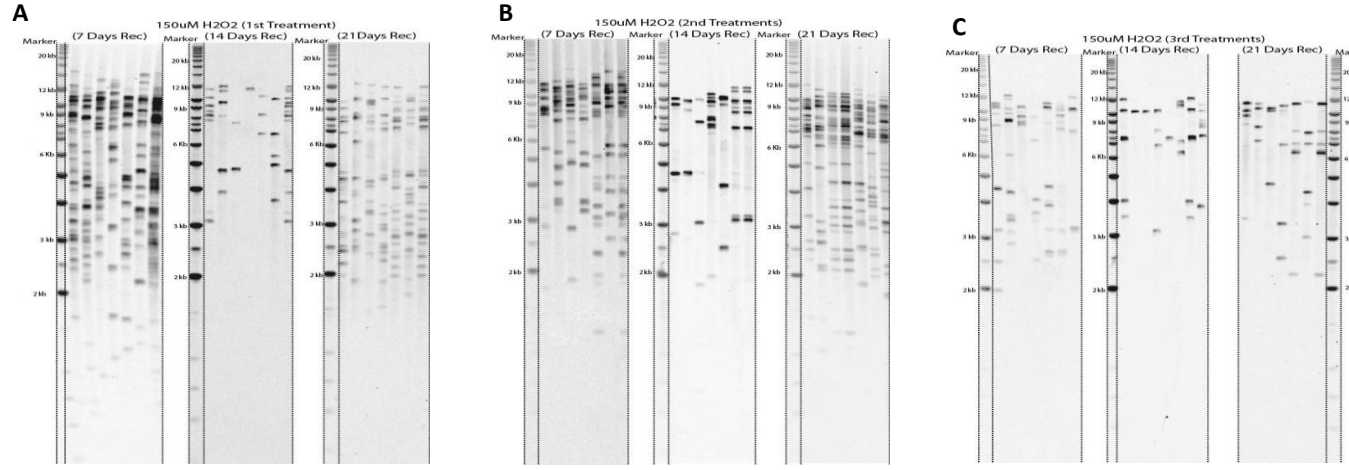
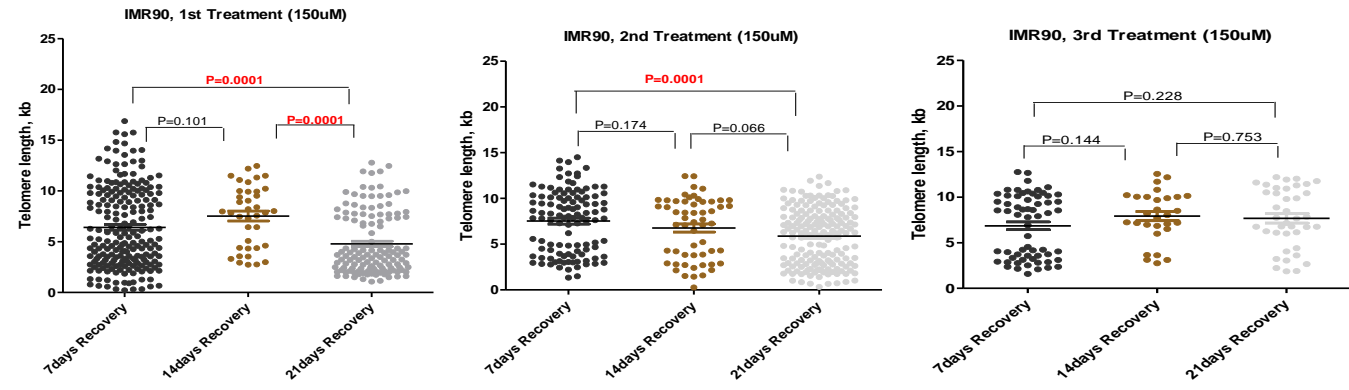
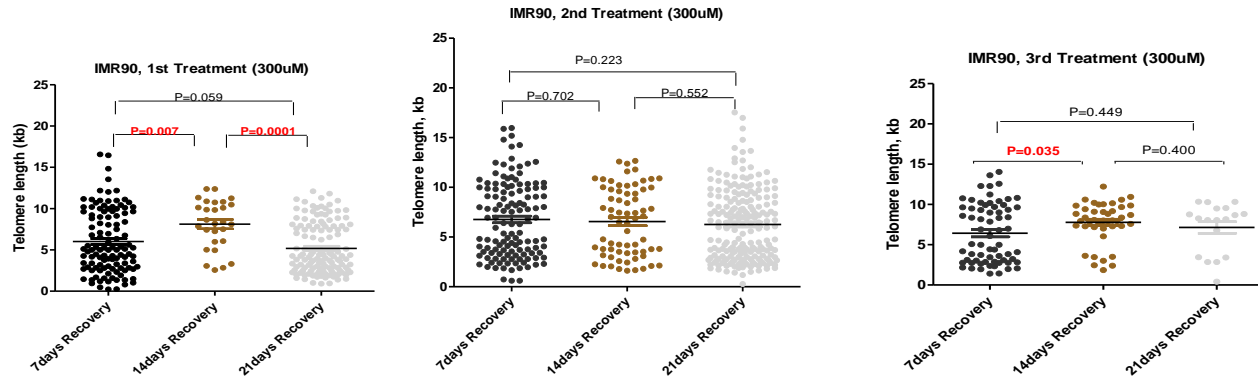
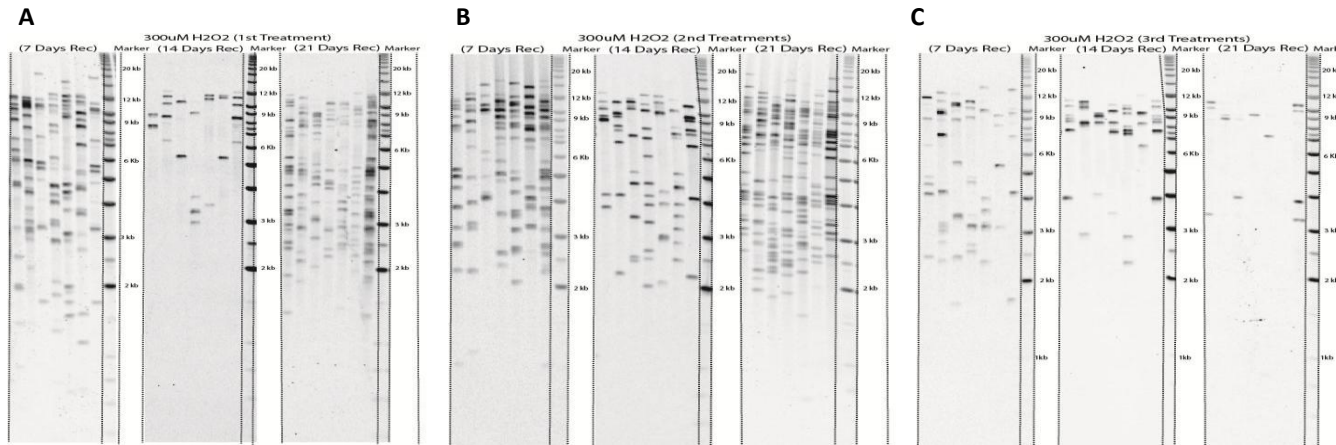


Figure 3.11: STELA gels of XpYp telomere in the IMR90 clone 4 treated with 150µM H₂O₂ for 2 hours and the tables of descriptive data for telomeres. The gels illustrate the telomere length distributions while the tables give the mean, standard deviations (SD) and population doublings (PD), (PD) was calculated after cells harvested. **(A)** IMR90 fibroblasts were treated with 150µM H₂O₂ for 2 hours **once**, then cells were refreshed with normal media and recovered for 7 days, 14 days, 21 days, cells were collected for DNA extraction subsequently. **(B)** IMR90 fibroblasts were treated with 150µM H₂O₂ for 2 hours **twice**. **(C)** IMR90 fibroblasts were treated with 150µM H₂O₂ for 2 hours **three** times. Dot Plot made in (Prism) represent dot plots (Telomere length distributions) from the gels, were quantified using Phortetix software, then they were compared (Days of recovery) and p value was calculated using t-test in Prism (P value in Red is Significant) (in Black is NS).



1 st Treat	7 Days	14 Days	21 Days	2 nd Treat	7 Days	14 Days	21 Days	3 rd Treat	7 Days	14 Days	21 Days
PD	29.81	31.29	32.77	PD	31.13	32.45	34	PD	32.29	33.46	34.63
Mean	6.40	7.524	4.785	Mean	6.97	6.76	5.87	Mean	6.8	7.9	7.6
SD	3.97	3.02	3.08	SD	3.67	3.32	3.08	SD	3.4	2.7	3.2

Figure 3.12: STELA of Treated IMR90 Clone 4 at XpYp Telomere (300µM H₂O₂) for (First, Second &Third treatments)



1 st Treat	7Days	14 Days	21 Days	2 nd Treat	7 Days	14 Days	21 Days	3 rd Treat	7 Days	14 Days	21 Days
PD	29.71	31.08	32.45	PD	30.97	32.24	33.51	PD	32.11	33.25	34.39
Mean	6.01	8.11	5.18	Mean	6.76	6.55	6.26	Mean	6.42	7.78	7.14
SD	3.81	2.95	3.06	SD	3.79	3.42	3.56	SD	3.65	2.52	3.09

Figure 3.12: STELA gels of XpYp telomere in the IMR90 clone 4 treated with 300µM H₂O₂ for 2 hours and the tables of descriptive data for telomeres. The gels illustrate the telomere length distributions while the tables give the mean, standard deviations (SD) and population doublings (PD), (PD) was calculated after cells harvested. **(A)** IMR90 fibroblasts were treated with 300µM H₂O₂ for 2 hours **once**, then cells were refreshed with normal media and recovered for 7 days, 14 days, 21 days, cells were collected for DNA extraction subsequently. **(B)** IMR90 fibroblasts were treated with 300µM H₂O₂ for 2 hours **twice**. **(C)** IMR90 fibroblasts were treated with 300µM H₂O₂ for 2 hours **three** times. Dot Plot made in (Prism) represent dot plots (Telomere length distributions) from the gels, were quantified using Phortetix software, then they were compared (Days of recovery) and p value was calculated using t-test in Prism (P value in Red is Significant) (in Black is NS).

Figure 3.13: Comparison of Mean Telomere Length between Control and Treated IMR90

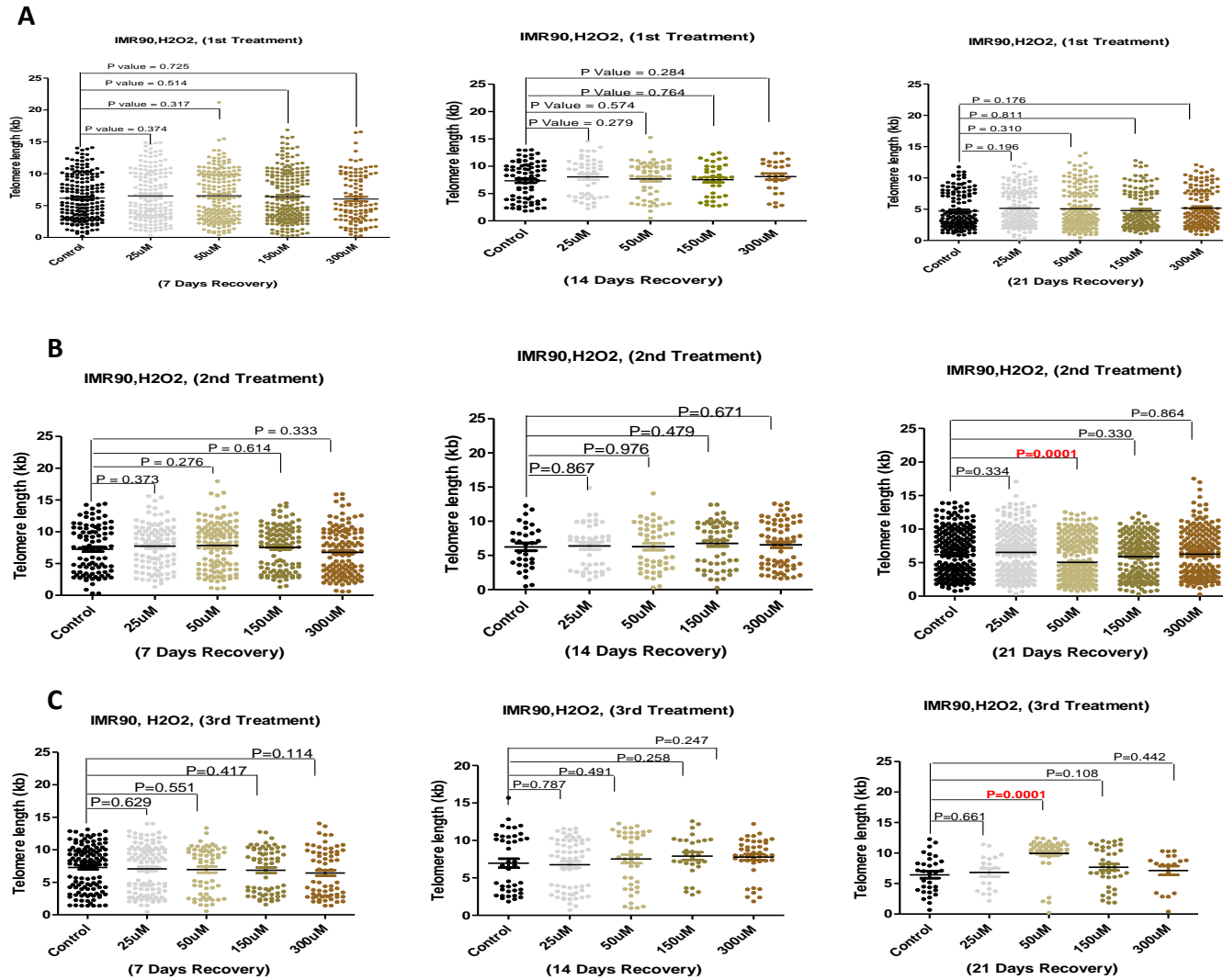


Figure 3.13: Comparison between mean XpYp telomere length distributions in IMR90 control and treated (25 μ M, 50 μ M, 150 μ M & 300 μ M H₂O₂) for (A) first treatment; after 7 days recovery, 14 days recovery and 21 days recovery. (B) Second treatments; after 7 days recovery, 14 days recovery and 21 days recovery. (C) Third treatments; after 7 days recovery, 14 days recovery and 21 days recovery.. Differences in mean telomere length between control and treated cells were measured by t-test. IMR90 treated with 50 μ M H₂O₂ had a significantly shorter mean telomere length compared to the control in the second time treatments (21 days recovery). The same cells when treated for the third time (50 μ M H₂O₂ third treatments) (21 days recovery) they had significantly longer mean telomere length. Dot Plot made in (Prism) represent dot plots (Telomere length distributions) from the gels, were quantified using Phortetix software, then they were compared (control and treated samples) and p value was calculated using t-test in Prism (P value in Red is Significant) (in Black is NS).

Figure 3.14: The proportion of Short Telomere frequency (IMR90, H2O2)

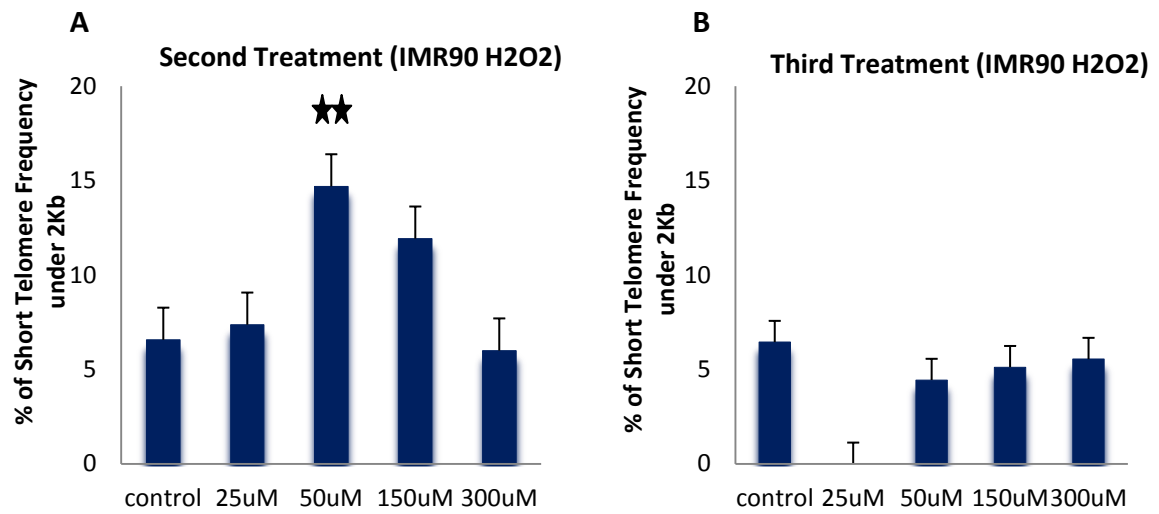
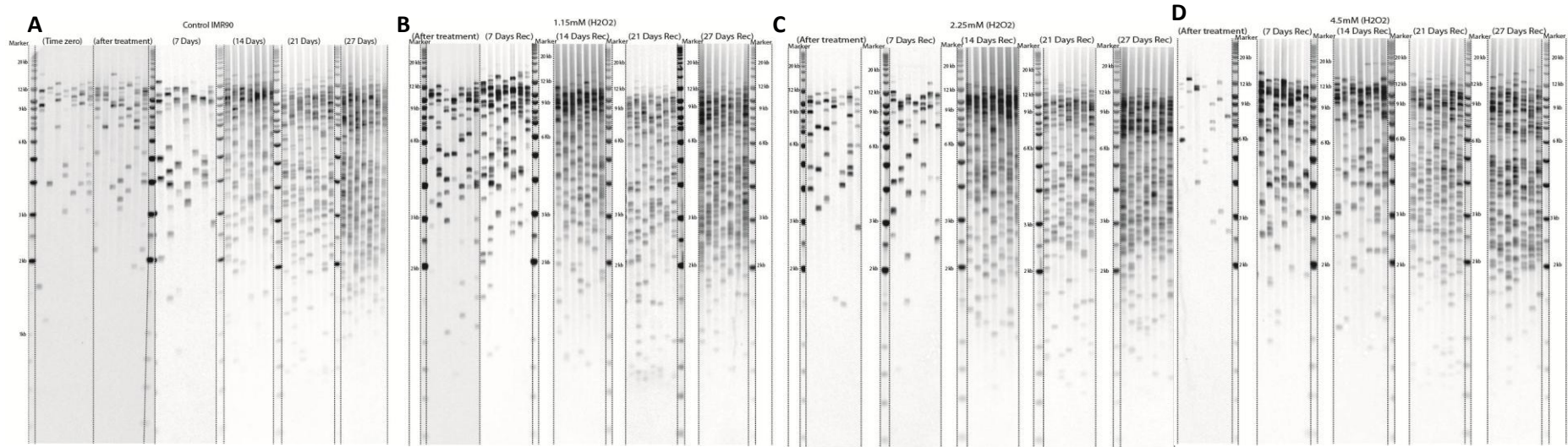


Figure 3.14: The proportion of short telomere frequency was calculated under 2kb. IMR90 fibroblasts displayed a high proportion of short telomeres after 21 days recovery of H₂O₂ treatment in second treatment (A) more than those in the third treatments (B). The cells with short telomeres disappeared after third treatments. ★★(Significant) p value was calculated using (ANOVA). Error bars represent standard error (SE).

Figure 3.15: STELA of IMR90 Clone 4 at XpYp Telomere (Control, 1.15mM, 2.25mM & 4.5mM H₂O₂)



Control	PD	Mean	SD	1.15mM	PD	Mean	SD	2.25mM	PD	Mean	SD	4.5mM	PD	Mean	SD
Time 0	28	8.407	3.76												
AT	28	7.97	3.58	AT	28	6.36	3.52	AT	28	7.76	3.28	AT	28	7.66	3.36
7Days	29.42	7.10	3.80	7Days	29.4	7.45	3.93	7Days	29.35	7.78	3.27	7Days	29.23	6.54	3.47
14Days	30.84	6.40	3.75	14Days	30.8	6.10	3.59	14Days	30.7	5.84	3.62	14Days	30.47	6.84	3.92
21 Days	32.26	5.95	3.79	21 Days	32.2	5.42	3.53	21 Days	32.05	6.14	4.10	21 Days	31.71	5.39	3.60
27 Days	33.48	5.52	3.54	27 Days	33.4	5.77	3.49	27 Days	33.21	5.66	3.19	27 Days	32.77	5.48	3.32

Figure 3.15: STELA gels of XpYp telomere in the IMR90 clone 4 treated with H₂O₂ for 10 minutes and the tables of descriptive data for telomeres. The gels illustrate the telomere length distributions while the tables give the mean, standard deviations (SD) and population doublings (PD), (PD) was calculated after cells harvested. **(A)** Control IMR90 fibroblasts. **(B)** IMR90 fibroblasts were treated with **1.15mM** H₂O₂ for 10 minutes, then cells were washed with PBS and trypsinised and spilt into half, half were collected for DNA extraction after treatment directly and the remaining half were reseeded in normal media and recovered for 7 days, 14 days, 21 days and 27 days, cells were collected for DNA extraction subsequently. **(C)** IMR90 fibroblasts were treated with **2.25mM** H₂O₂. **(D)** IMR90 fibroblasts were treated with **4.5mM** H₂O₂.

Figure 3.16: IMR90 Clone 4 at XpYp Telomere Length Distributions (Control, 1.15mM, 2.25mM & 4.5mM H₂O₂)

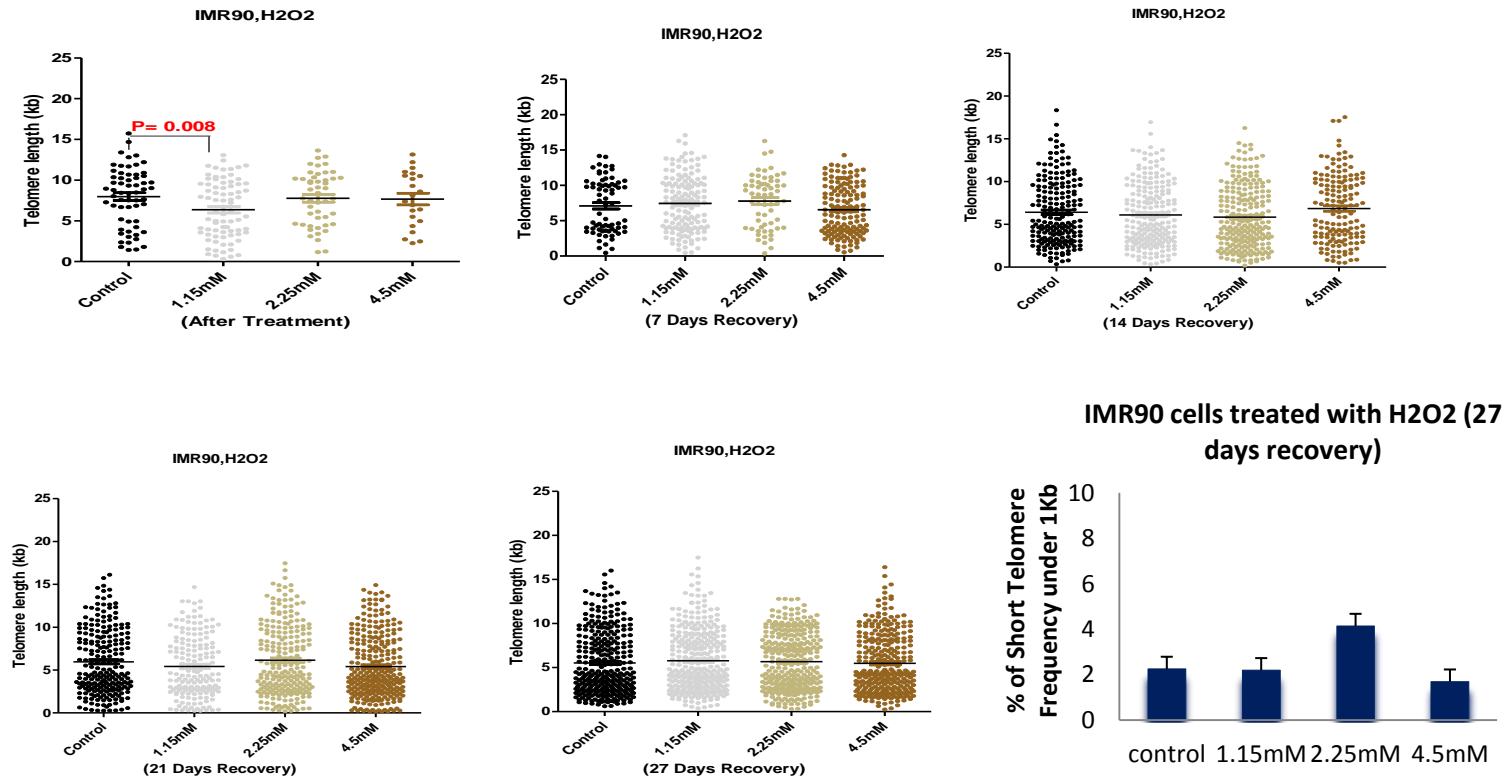


Figure 3.16: Dot Plot made in (Prism) represent dot plots (Telomere length distributions) from the gels, were quantified using Phortetix software. Any significant differences in mean telomere length between control and treated cells as measured by t-test were highlighted. **Bar chart showed the proportion of short telomere frequency**, calculated below 1kb, IMR90 treated with 2.25mM had high short telomere frequency compared to the control and the cells treated with 1.15mM and 4.5mM. Error bars represent standard error (SE).

Figure 3.17: STELA of U138 at XpYp Telomere Control and treated with (4.5mM H₂O₂)

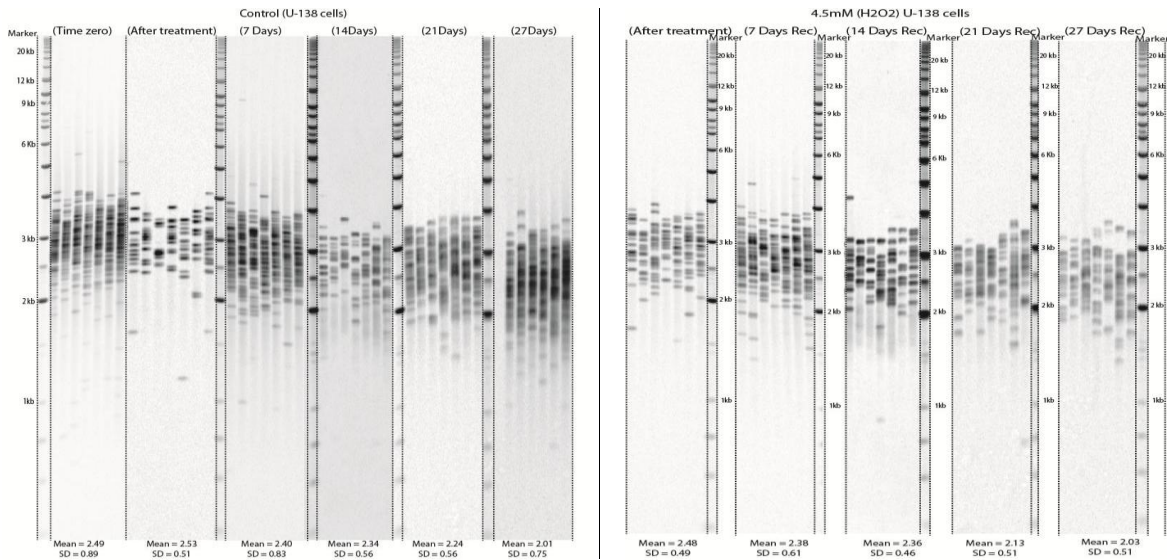


Figure 3.17: STELA gels of XpYp telomere in U138 treated with H₂O₂ for 10 minutes. The gels illustrate the telomere length distributions, (mean, and standard deviations (SD) displayed under the gels. Control U138 cells gel on the RIGHT and U138 treated with 4.5mM H₂O₂ gel on the LEFT. Cells were recovered for 7 days, 14 days, 21 days and 27 days, cells were collected for DNA extraction subsequently.

Figure 3.18: Telomere length distributions of U138 at XpYp Telomere (comparison between control and treated)
(4.5mM H₂O₂)

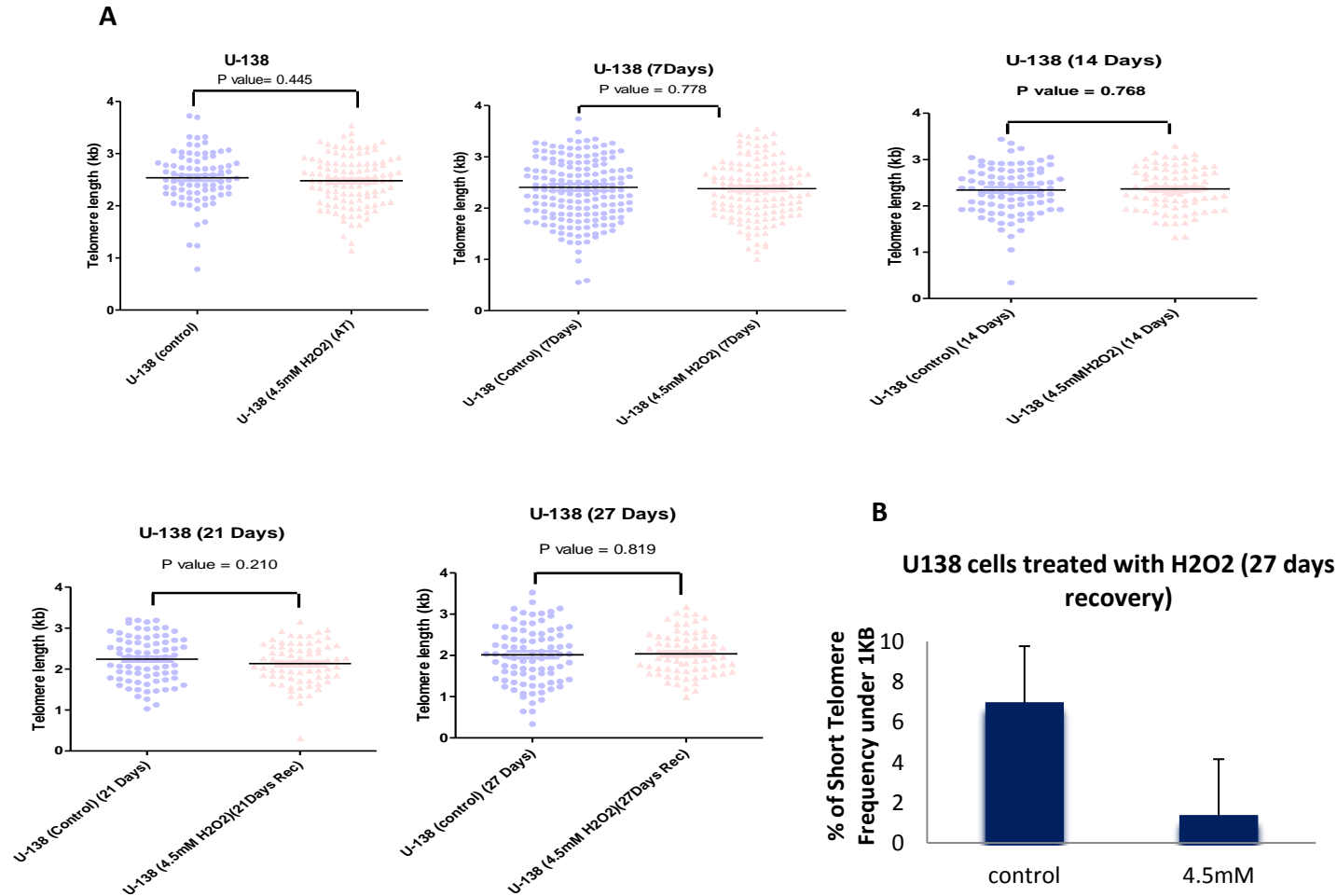


Figure 3.18: A- Telomere length distributions were quantified using Phoretix software, comparison between mean telomere length of control and treated cells revealed no significant differences as measured by t-test.

B- Bar chart showed the proportion of short telomere frequency after 27 days recovery, it was calculated below 1kb. Control cells had higher short telomere frequency than treated cells. Error bars represent standard error (SE).

3.5 Discussion

3.5.1 Culture Growth

In the study presented here, IMR90 foetal lung fibroblasts treated with various concentrations of H₂O₂ displayed a truncated replicative lifespan (~39-42 PDs) compared to the cells grown in normal conditions (~48.72 PDs). Moreover, it was obvious that with cells reaching the end of their replicative lifespan, the growth rates slowed at both normal and recovered cultures. This data is in line with previous observations, as fibroblast cell cultures reach their end of their replicative capacity, the growth rate slows with an increasing proportion of cells senescing and fewer cells capable of cell division.

In IMR90 fibroblasts treated with 4.5mM H₂O₂ the growth rate was determined to be 0.177 PD/day and 0.203 PD/day were in the control. U138 cancer cells were higher in their growth rate compared to IMR90 fibroblasts. U138 treated with 4.5mM was 0.305 PD/day and 0.321 PD/day for control.

Such observations illustrate that levels of oxidative stress influences the replicative life span of primary human cell culture. IMR90 cells appears to be sensitive to oxidative stress, as previously observed, many studies have shown that IMR90 cells in conditions of low oxidative stress, their replicative lifespan is significantly increased (Packer and Fuehr 1977; Chen *et al.*, 1995; Saito *et al.*, 1995). It was also observed that when the media was supplemented with free radical scavengers, IMR90 cells significantly extended their replicative capacity (Britt-Compton *et al.*, 2006).

Our data, together with previous studies using IMR90 (Chen *et al.*, 1995; Saito *et al.*, 1995; Forsyth *et al.*, 2003), indicate that these cells may be less able to adapt to conditions of

oxidative stress which is obvious from their limited replicative capacity in culture. A study suggested that the reason behind the attenuation of replicative lifespan of IMR90 cultures in conditions of high oxidative stress is that the telomeres structure of IMR90 cells are more sensitive to oxidative damage. This damage accelerates telomere erosion which in turn reduces the replicative capacity (Von Zglinicki, 2002). A Previous study from our laboratory showed that the ectopic expression of telomerase in IMR90 cells results in IMR90 immortalised in conditions of lower levels of oxidative stress, but not in conditions of high oxidative stress (Britt-Compton, 2009). Thus it was concluded that telomerase is incapable of counteracting telomeric specific damage resulting from oxidative stress. In contrast to IMR90 cells, MRC5 fibroblasts have previously been shown to be immortalised with telomerase in high oxidative stress (20% oxygen) (McSharry *et al.*, 2001). Different cell strains react differently to varying oxygen tensions and that such differences may be due to differing antioxidant capacities (Lorenz, 2001; Britt-Compton, 2009).

3.5.2 Cell Cycle Progression under Oxidative Stress

Previous studies have observed that hyperoxia initiates growth arrest. Depending upon the cell type, cell cycle arrest may occur in G1, S or G2 phase of the cell cycle. Furthermore the arrest may be transient, permanent or can even lead to apoptosis or necrosis (Boonstra and Andries Post, 2004). These checkpoint responses allow damaged cells to either repair the damage, enter a permanently growth-arrested state (G0) or if the damage is too severe, cells can undergo apoptosis. Thus depending on the level of oxidative stress, cells display a broad spectrum of responses.

The usage of Hydrogen peroxide in the concentration of 300 μ M on Fibroblast cells has shown that cells were not been able to adapt to the oxidative stress and therefore entered a permanently growth-arrested state (Barzilai and Yamamoto, 2004).

It has been observed that severe DNA damage inhibits the activity of CDK-cyclin complexes. (Barzilai and Yamamoto, 2004). These complexes are responsible for the cellular progression through the cell cycle. Their inhibition will result in cells arresting at G1 phase. The Inhibition of CDK-cyclin is modulated by p53, which in turn activates protein p21. p21 will bind to CDK-cyclin complex in the cells and prevents the phosphorylation of the proteins and thus inhibits the kinase activity of the complex. The cells will not be able to progress in the cell cycle and result in cells arrested at G1 (Barzilai and Yamamoto, 2004).

Around 24% of untreated IMR90 cells were in G2/M phase. This percentage was drastically decreased in treated cells with 300 μ M H₂O₂ (third treatment) where only 8% of treated cells were in G2/M phase. Moreover, Hydrogen peroxide treatment results in a reduction of cells in synthesis phase (S phase) as well. IMR90 fibroblasts which were treated with 150 μ M H₂O₂ (second treatment) displayed around 1% of cells in S phase.

In contrast, in this study we have shown that oxidative stress induced by H₂O₂ results in the increased frequency of cells arresting in G0/G1 phase.

These findings suggest that the cells had been injured severely by hydrogen peroxide and they were not been able to re-enter the cell cycle again. Furthermore, the data obtained from SA β -gal assay support this observation, where a high percentage of IMR90 cells were senescent and positive for SA β -gal (senescence marker) after the exposure to H₂O₂. Furthermore population doublings (PDs) and growth rate were decreased after treatment

with hydrogen peroxide. These data indicate that oxidative damage induced by exposure to H_2O_2 result in a premature senescence while the percentages of senescent cells produced vary dependent upon the H_2O_2 concentrations.

3.5.3 Telomere Dynamics

Telomere deletion events have been observed in primary culture fibroblasts (Baird *et al.*, 2003), these represent a significant mutational mechanism creating dysfunctional telomere that are capable of fusion (Capper *et al.*, 2007). The objective of this study was to determine if oxidative stress plays a role in generating telomere deletion events.

In order to examine this hypothesis, the XpYp telomere length distributions of IMR90 and U138 cancer cells treated with hydrogen peroxide were investigated using STELA (Baird *et al.*, 2003). In line with previous studies in the group (Baird *et al.*, 2003), the XpYp telomere were analysed as the average telomere length and the average telomere erosion rates resulting from the end-replication problem is similar at most chromosome ends. Multiple samples were taken during the proliferative lifespan of the cultures and subjected to STELA. STELA was used to track the telomere dynamics and detect any stochastic shorter telomeres with ongoing cell division.

IMR90 control and treated cells displayed bimodal distributions at XpYp telomere. However bimodal distributions make it difficult to determine these deleted telomeres. Bimodal distributions or extensive telomere length variation could arise from inter-allelic differences, which are set in zygote and resulting of contribution of maternal and paternal telomere alleles, or they may be due to the presence of sub populations of cells with shorter telomeres that may have a shorter replicative capacity.

Allelic variation has been previously described. Previous studies have shown that MRC5 fibroblasts display bimodal distributions at XpYp. These distributions were a consequence of allelic variation as determined using allele-specific amplification (allele-specific STELA) (Baird *et al.*, 2003). In contrast IMR90 fibroblasts were characterised having a uni-modal allelic distribution at XpYp. A smaller subset of these telomeres was not consistent with allelic variation instead represented a sub-population of cells with shorter telomeres.

The IMR90 cultures used in this study also displayed bimodal distributions at XpYp. Reproducible changes in these distributions were observed after approximately 14 days of recovery periods specifically after the third treatments; i.e. the cells with shorter telomeres disappeared from the culture. This was clearly seen and statistically significant in IMR90 treated with 50 μ M H₂O₂ after 21 days of recover periods after the third treatment.

Our data showed that IMR90 in the third treatment had a lower frequency of short telomeres compared to those after the second treatment. These short telomeres had probably disappeared as those cells reach the end of their replicative capacity.

In IMR90 fibroblasts, treated with higher concentration of H₂O₂ and a shorter duration, the mean telomere length declined in both control and treated cells over time. IMR90 treated with 2.25mM had higher short telomere frequency.

U138 tumour cells showed no significant differences in mean telomere length between treated and untreated cells. Both control and treated cultures decreased in mean telomere length.

Taken together these data suggest that the cells had been damaged by exposure to hydrogen peroxide and they were prematurely senescent. From data obtained from cell

cycle analysis showed that higher numbers of treated cells accumulated at G1. The SA β -gal assay showed high percentage of treated cells was senescent. Furthermore population doublings (PDs) and growth rate of the cells were decreased in treated cells.

In this data we made the key observation that the telomere length in IMR90 cells was longer after the third treatment of H₂O₂ compared to the untreated cells and the lower modal distributions had disappeared. This could be explained by different scenarios (Figure 3.19). Firstly, that oxidative stress preferentially damages short telomeres and therefore they had disappeared. As described previously, telomeres are considered to be sensitive to oxidative damage. This might be due to the sensitivity of the GGG repeat regions to ROS and in turn might induce premature senescence in effected cell. However it difficult to conceptualise how, given the apparent sensitivity to the oxidative stress, short telomeres would be preferentially subjected to the oxidative damage compared to longer telomeres that represent a larger target for damage. A second and potentially more plausible scenario could be that the cells with short telomeres are closer to the point of replicative senescence and are more sensitive to exposure to hydrogen peroxide and thus undergo premature senescence or apoptosis, such that they are no longer detectable in the culture.

Moreover, our data showed that exposure IMR90 fibroblasts to hydrogen peroxide treatments did not produce an increase in the proportions of short deleted telomeres and telomeric deletion events were not detectable under different levels of oxidative stress. The role of p53 has been also investigated. p53 were knockdown in IMR90 cells and hydrogen peroxide treatment was carried out; telomere deletion events were undetectable at 17p telomere (data not shown). Furthermore, U138 tumour cells (p53 deficient) showed no significant differences in telomere deletion events were not seen in treated cells as well.

The original hypothesis that oxidative stress might work as a mutational mechanism and result in telomeric deletion events has not been substantiated with the data presented here. However it remains formally possible that telomeric deletion events may still occur but that they render the telomere undetectable with STELA.

Together these data are consistent with the previous observations that IMR90 cells had longer telomere length at higher oxidative stress (20% oxygen) than at 3% oxygen (Britt-Compton *et al.*, 2006). Thus it was concluded that senescence of IMR90 at high level of oxidative stress is telomere-independent manner and telomere dependent in case of low level of oxidative stress (Britt-Compton *et al.*, 2006). Other study by Chen *et al.* (2001) used H₂O₂ and induced premature senescence in IMR90 cells and no telomere erosion was detectable.

Our present data, and data from others may be important because others have argued that oxidative stress drives the majority of telomere erosion (Von Zglinicki 2002). Our data are not consistent with this view and indeed others have concluded that premature senescence does not arise as a consequence of accelerated telomere erosion, but instead more likely results from stochastic DNA damage across the rest of the genome (Dumont *et al.*, 2001; de Magalhaes *et al.*, 2002).

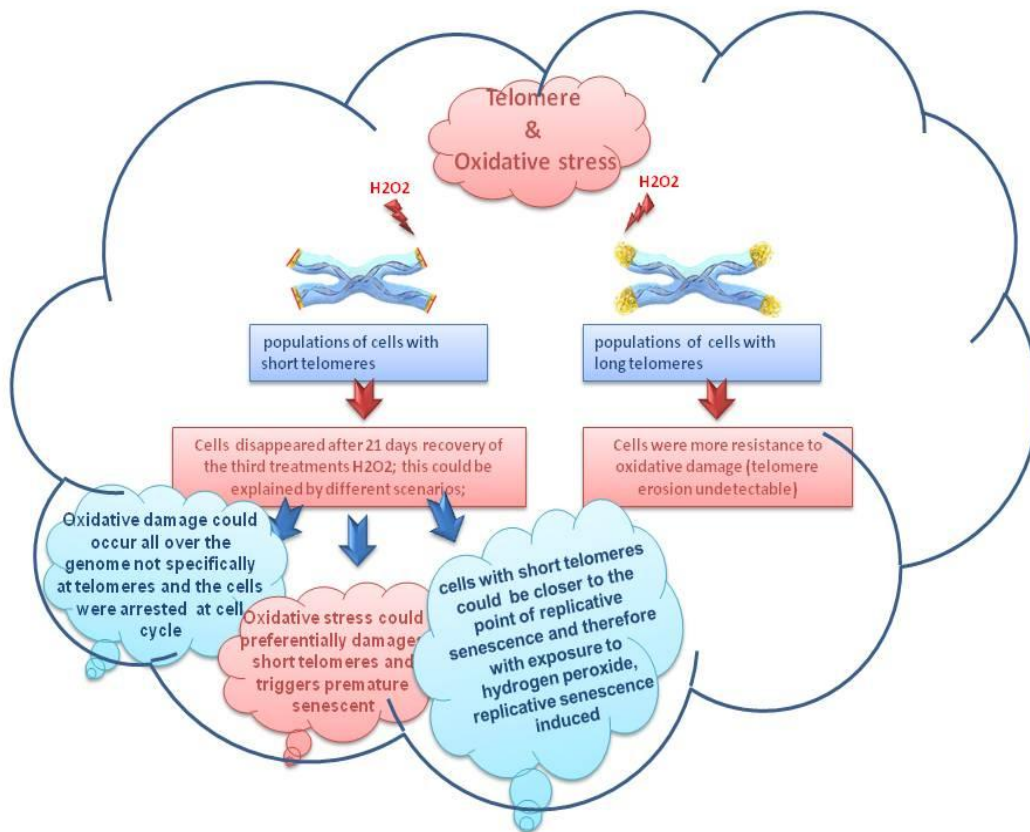


Figure 3.19: illustrate scenarios that might explain losing of lower modal distributions in IMR90 fibroblast after the exposure to oxidative stress.

3.6 Conclusion

The data generated in this study indicates that the original hypothesis that oxidative stress might work as a mutational mechanism and result in telomeric deletion events was not valid. Instead these data are more consistent with the view that premature senescence does not arise as a consequence of accelerated telomere erosion, but instead more likely results from stochastic DNA damage across the rest of the genome.

Chapter 4

Telomere Fragile Site

4.1 Summary

Telomeres can resemble fragile sites and can pose a challenge to the replication fork machinery. Moreover, replication fork stalling is a characteristic of fragile site that may be resolved as single or double-stranded breaks within telomeres, potentially resulting in telomeric-deletion events. The aim of this work was to investigate if the induction of telomere fragility has the potential to drive stochastic telomeric deletion events.

In order to test this hypothesis, chromosome fragility was induced in cultured MRC5 fibroblasts, Seckel cell fibroblasts (SCK) and U138 cancer cells using the DNA replication inhibitors Aphidicolin (APH) and Hydroxyurea (HU).

The induction of chromosome fragility was monitored in metaphase chromosomes. Cell-cycle checkpoints, cell growth and the induction of senescence were also documented. Telomere dynamics and stochastic telomeric deletion events were investigated using STELA. The telomere dynamics in treated SCK fibroblasts were significantly different from those untreated SCK fibroblasts following treatments with APH, with an increase in stochastic telomeric deletion. Whilst in MRC5 fibroblasts, the induction of the telomere fragility impacted on the upper to lower allele ratio, with a loss of the longer telomere length distributions. The induction of fragility in U138 cancer cells did not produce any significant differences in the mean telomere length or the frequency of telomeric deletion events.

Taken together these data indicate that fragile site induction can modulate telomere dynamics. Moreover MRC5 fibroblasts were more resistance to the induction of fragility than SCK fibroblasts where the fragility appeared to be enhanced by ATR deficiency.

4.2 Introduction

In order to minimise mutation, the process of DNA replication needs to be as accurate as possible, but it is clear that some regions of the human genome, such as Common Fragile Sites (CFSs), are difficult to replicate and this can lead to mutation (Toledo *et al.*, 2000). Recently, the role of common fragile sites in the generation of chromosome instability has become clear, so that they are now implicated in chromosomal aberrations in tumour cells (Lukusa and Fryns, 2008). The fragility of CFSs appears to arise as a consequence of mitotic entry prior to the completion of the replication process. However, the mechanisms behind these aberrations and incomplete replication are still unclear (Tallec *et al.*, 2014).

Chromosomal fragile sites are defined as specific regions of the genome that are prone to gaps or breaks within metaphase chromosomes following the partial inhibition of DNA replication (Glover, 2006). Late replication is a characteristic of these sites and it was found that the mutational expansion of nucleotide repeats (CGG or AT) at these sites could form secondary structures that can lead to replication fork stalling (Figure 4.1) (Durkin and Glover, 2007). Stalled forks are the most common cause of breakage at these sites and are a source of chromosome rearrangements and instability, which is important for tumorigenesis (Tallec *et al.*, 2014).

4.2.1 Telomeres and Fragile Sites

Recently, telomeres have been characterised as fragile sites. Telomeric sequences, which are composed of long arrays (2–10 kb) of TTAGGG repeats, present a challenge for DNA replication, leading to phenotype similar to those seen at common fragile sites (Sfeir *et al.*, 2009). Specific protein complex (shelterin) proteins protect telomeres from DNA damage response and preventing potential chromosomal fragility at these sites (de Lange, 2005). A study by Sfeir *et al.*, 2009 demonstrated that DNA replication is compromised at telomere

repeats and telomeres resemble the common fragile sites. Moreover, they reported that the shelterin protein TRF1 is important to protect telomere from breakage associated with replication fork stalling at telomeric sequences. The deletion of TRF1 led to unprotected telomeres and increased number of fusions and activation of the ATR protein, which is responsible for stabilising stalled replication forks during replication and prevents chromosomal breaks at fragile sites (Verdun and Karlseder, 2006). ATR has been found to be abundant at mammalian telomeres during late replication (Verdun and Karlseder, 2006).

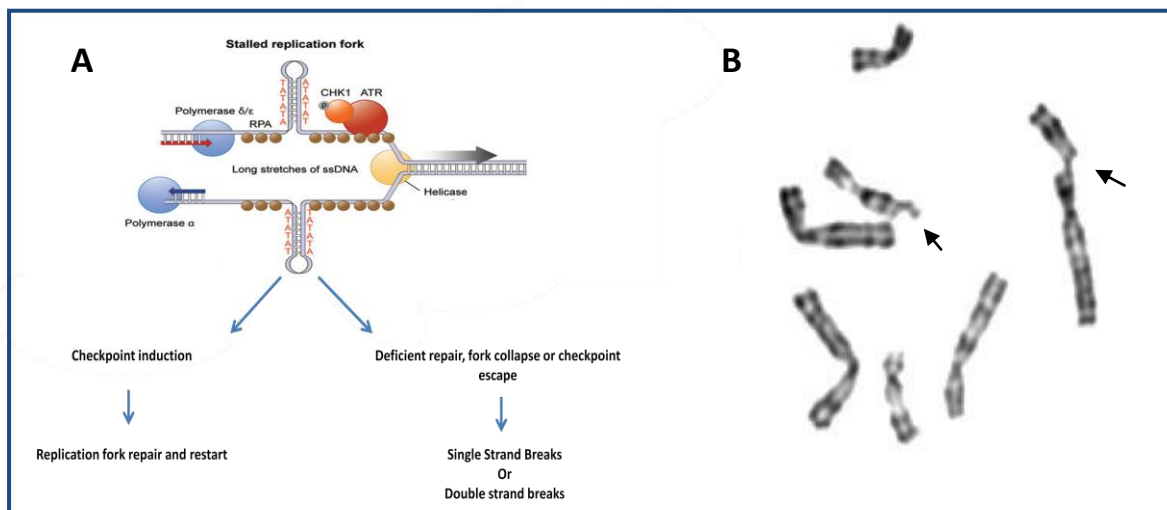


Figure 4.1. Fragile site. (A) Fragile sites originate from unreplicated DNA, when replication fork stalled, RPA, single strand DNA binding protein, binds to unreplicated ssDNA and activates DNA damage response. ATR activates S-phase or G2/M checkpoints in order to repair these regions. However, sometimes these sites escape checkpoint and left unrepaired and displayed as breakage and gap on metaphase chromosomes (B). Redrawn from (Durkin and Glover, 2007).

4.2.2 History of Fragile Site

The identification of chromosomal fragile sites had a major impact on the understanding of the molecular basis of genetics disease, for example fragile X disorder and the other

mutational expansions of nucleotide repeats (Durkin and Glover, 2007). Fragile sites have been also involved in activation of DNA damage response to stalled replication and in genome instability in tumour cells (Durkin and Glover, 2007). In 1970, the term of fragile site was first described, when breaks on the long arm of chromosome 16 were found to segregate in a large family (Magenis *et al.*, 1970). Since that time, more fragile sites have been identified and observed to segregate in pedigrees, for example the fragile site at Xq28 in families with X-linked mental retardation (Turner *et al.*, 1978). Fragile sites are stable in cell culture, but under certain conditions they form breaks and gaps on metaphase spreads chromosomes (Sutherland, 1977). For example a rare autosomal fragile site, in Australian families, and the fragile X in males, were induced follow culturing of cells in media containing low folic acid (Sutherland, 1979). This study and others observations identified that folate stress can lead to fragile sites expression. This work led to the identification of the essential conditions to diagnose individuals with fragile X disorder utilising a cytogenetic assay and also facilitate to discover other fragile sites over the genome. Nowadays, more than hundred fragile sites have been reported and identified.

Un-replicated single stranded DNA, arising from replication fork stalling after partial inhibition of DNA synthesis, is most likely it is related to the localised DNA sequence and replication dynamics (Zlotorynski *et al.*, 2003). DNA repair of single-stranded regions in fragile sites require DNA-directed homologous repair. They are recognised and arrested by ATR protein (S phase and/or G2/M checkpoints), however some fragile sites in normal cells can escape the ATR checkpoints and displayed as breakages on metaphase chromosomes (Casper *et al.*, 2002). Sister chromatid exchange can be found within fragile sites, moreover deletions and translocations also can be seen and they usually as a result of DNA double stranded breaks at damaged forks (Casper *et al.*, 2002). These breaks are recognised by ATM

checkpoints. Previous research has proposed that alterations found in replication checkpoint in tumour cells will display a high number of chromosomal rearrangements at fragile sites (Tallec *et al.*, 2014; Casper *et al.*, 2002).

4.2.3 Classification of Fragile Sites

Fragile sites are divided into two main groups: rare or common on the basis of their frequency within the population.

4.2.3.1 Rare Fragile Sites

They are the sites which are seen in less than 5% of population and nucleotide repeat expansion is the main cause of the gaps and breakages at these regions (Kremer *et al.*, 1991). Rare fragile sites are subdivided depending on their particular induction chemistry into as folate sensitive or non-folate sensitive fragile sites. The folate sensitive group are characterised by the expansion of CGG repeats and they are the most common group of rare fragile site. On the other hand, non-folate sensitive rare fragile sites are less in their frequency and are associated with the expansion of AT minisatellite repeats. Bromodeoxyuridine (BrdU) or distamycin A usually induce non-folate sensitive rare fragile sites (Kremer *et al.*, 1991; Sutherland *et al.*, 1998).

4.2.3.2 Common Fragile Site (CFSs)

(CFSs) are classified as the largest group among fragile sites, and are seen in the whole population. Unlike rare fragile sites, CFSs are not associated with nucleotide repeats expansion, CFSs display normal chromosome structure (Durkin and Glover, 2007).

4.2.4 Fragile Site Inducers

Most of inducers of chromosomal fragility (Table 4.1) share in common their ability to partially inhibit of DNA synthesis, specifically at fragile site loci.

Fragile site inducer	Number of loci	Sequence
aphidicolin	76	AT rich repeats
Bromodeoxyuridine (BrdU)	9	AT rich repeats
distamycin A	5	AT rich repeats
5-azacytidine,	4	

Table 4.1 fragile site inducer. Modified from (Durkin and Glover, 2007).

4.2.5. Maintenance of Fragile Site Stability

Little was known about the mechanisms of fragile site stability until 2002, when a study was carried out by Casper and his colleagues, who were the first who report the crucial role of the Ataxia-Telangiectasia and Rad3 Related (ATR) checkpoint in the maintenance of fragile site stability (Casper *et al.*, 2002). They found that cells with ATR deficiency have high number of breaks and gaps at fragile sites even without the addition of aphidicolin, hydroxyurea or any other replication inhibitor agents (Casper *et al.*, 2002). Moreover, they noticed that cultured cells with (ATR knockdown) in the presence of aphidicolin have increased fragile sites instability (Casper *et al.*, 2002). These results are important, as they indicated that replication fork inhibition that can occur at fragile sites is common and that ATR activation in response to fork stalling at these sites delays cell division and allows for repair the damage. In the absence of ATR, fragile site expression is observed as deletions, translocation and/or other rearrangements in metaphase chromosomes (Casper *et al.*, 2002).

They have subsequently found that Seckel cells which have a mutation in ATR show high frequencies of chromosome breakages at fragile sites (O'Driscoll *et al.*, 2003; Casper *et al.*, 2004). They have reported that Seckel disorder is the first human genetic disease has high susceptibility to fragile site instability (Casper *et al.*, 2004).

In contrast, ATM-deficient cells did not display fragile site breaks or any of chromosome rearrangements. This suggests that DNA double stranded breaks, the lesion to which ATM responds to, are not the initial cause of fragile sites expression (Durkin and Glover, 2007).

However, ATM plays an important role in modulating downstream events at fragile sites mainly in the resolution of double stranded breaks that happen at these sites. These double stranded breaks arise at these sites via action of nucleases (Durkin and Glover, 2007).

In 1996, ATR was identified and found in all eukaryotic cells (Keegan *et al.*, 1996). It is an important and critical activator in signalling responses to DNA damage and replicative stress, that induces S-phase checkpoint and G2 checkpoints and block cell cycle progression into mitosis (Keegan *et al.*, 1996). Subsequent studies have investigated and characterised other mechanisms could involved in fragile site stability; they have found that Chk1 and BRCA1 play a role in the maintenance of these sites (Arlt *et al.*, 2002). BRCA1, like ATR activates, Chk1 which in turn regulates CDC2/cyclin complex and thus manages the G2 checkpoint and progression into mitosis (Arlt *et al.*, 2002). Durkin *et al.*, 2006 reported the effect of depletion of Chk1 on fragile sites expression following APH treatment.

4.2.6 Fragile Sites as Indicators of Stalled Replication in Cancer

It has been found that the rate of the recombination is increased at fragile sites compared to other regions in the genome. In cancer, fragile sites are the hotspots for deletions, translocation and other chromosomes rearrangements (Yunis and Soreng, 1984; LeBeau and Rowley, 1984). It has been reported that high frequencies of fragile site instability is considered as indicator of replication fork stalling in tumour cells (Durkin and Glover, 2007). This is associated with deficiencies in ATR or related repair genes during tumorigenesis. Previous studies have found phosphorylated ATR, Chk1 and P53 in precancerous lesions from bladder, breast, colorectal and lung (Gorgoulis *et al.*, 2005). These results

demonstrated that replication forks stalling in premalignant cells leads to ATR activation and deletions preferentially target fragile sites in cells that escape the DNA damage checkpoints (Durkin and Glover, 2007).

4.2.7 Analysis of Stochastic Deletion Events

Telomeres were not originally classified as fragile sites, perhaps due to their terminal position, at the end of chromosomes, rendering it difficult to detect these events (Sfeir *et al.*, 2009). However it is now clear that telomeres do resemble fragile sites and pose a challenge to the replication fork machinery (Sfeir *et al.*, 2009). Stalled replication forks within telomeres could be resolved as single-stranded DNA breaks that result in truncated telomeres. Therefore, the characteristic of telomere fragility could play a role and have the potential to drive stochastic telomeric deletion events, resulting in the extremely short telomeres. Sensitive techniques, such as STELA, are able to detect mutational events in telomeric DNA, the resulting critically short telomeres have the potential to trigger replicative senescence or initiate chromosome instability (Baird *et al.*, 2003).

4.3 This Work

In this chapter, I have examined whether the induction of chromosome fragility at telomeres has the potential to drive stochastic telomeric deletion events, resulting in the extremely short telomeres that can be detected with STELA. In order to test this hypothesis, fragile sites were induced with using Aphidicolin (APH) and Hydroxyurea (HU) (DNA synthesis inhibitors). The effects of fragility on the cell growth and on telomere dynamics were examined in MRC5 fibroblasts, Seckel cell fibroblasts (SCK) and U138 cancer cells. Cells were cultured in different concentrations of APH and HU in a parallel with cells grown in

normal conditions. DNA samples were taken during proliferation of the cultures, enabling detailed analysis of telomere dynamics using STELA.

4.4 Results

4.4.1 Effects of Fragile Site Induction on Culture Growth

In order to examine the effect of fragile site induction on cells in culture, MRC5 cultured at PD 34.86, Seckel cells (ATR deficient cells) at PD 26 and U138 cancer cells (mutated P53), cells were cultured in 6-well plates (35-mm dish) and treated with different concentrations of APH (0.3 μ M) & (1 μ M) and HU (1mM) & (5mM) for 24 hours. After treatment cells were counted and half were collected for DNA extraction and the remaining half were reseeded in normal media for recovery, cells were later collected for DNA extraction after 5days of recovery. STELA was carried out allowing detailed analysis of telomere dynamics.

The cells were passaged serially after treatments and the average of population doublings (PDs) was calculated and plotted as a function of time (Figures 4.2 & 4.3).

These data showed the growth rate which was determined to be on average of 0.35 PD/day for MRC5 fibroblasts (Figure 4.2) in standard culture conditions and this average declined in cells cultured with APH and HU. It was about 0.24PD/day for those treated with 0.3 μ M APH and 0.14PD/day for cells cultured with 5mM HU.

Figure 4.3 showed the growth rate of Seckel cells (SCK) control and treated. The growth rate of normal control SCK cells was lower than the normal growth rate of MRC5 cells, it was about 0.24PD/day. SCK cells cultured with 1 μ M APH was 0.19PD/day and it was 0.16PD/day for those treated with 5mM HU. Thus in both SCK and MRC5 fibroblast cultures the treatment with APH or HU resulted in clear reduction in the rate of growth.

The overall growth rates of U138 cells control and treated were higher than MRC5 fibroblasts and SCK cells. In contrast to the SCK and MRC5 cells there was no difference between control and recovered U138 cells.

Figure 4.2: PDs of MRC5 cells (APH & HU)

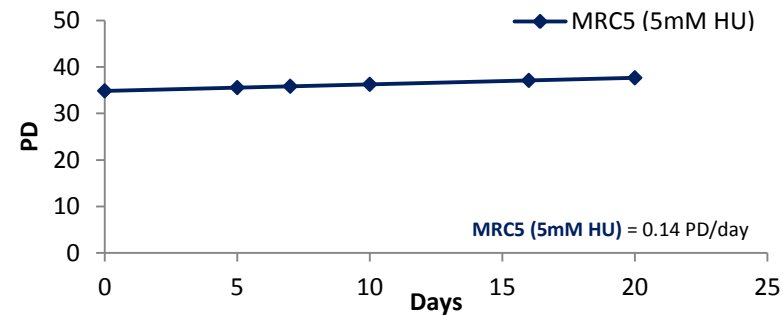
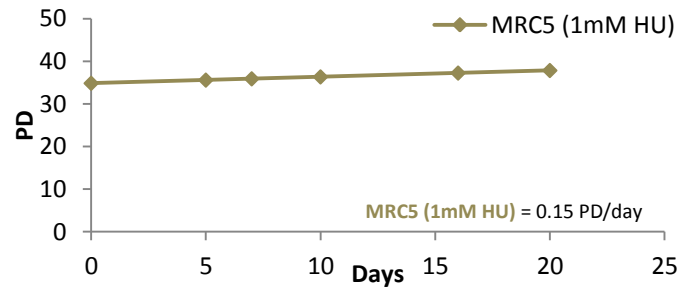
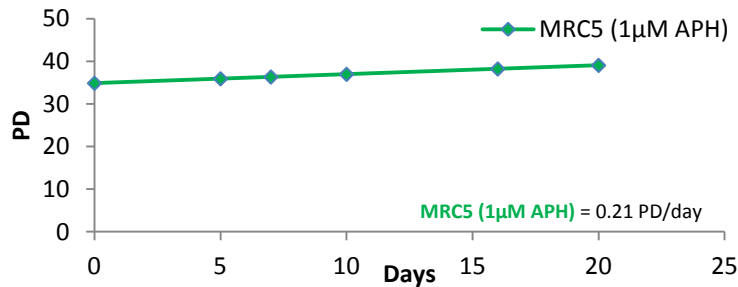
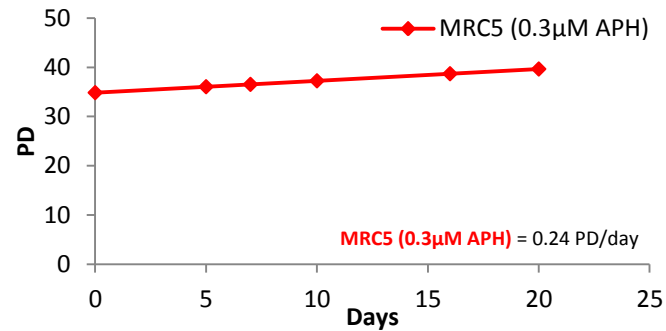
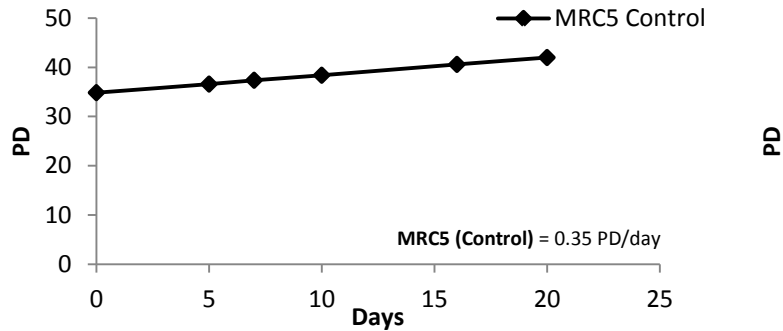


Figure 4.2: Growth curves of MRC5 cells. MRC5 control (untreated) (Black Line) and (treated) with different concentrations of APH (0.3µM (Red Line) & 1µM (Green Line) & HU (1mM (Gray Line) & 5mM (Blue Line)) for 24 hours. Plotting growth curves as function of population doublings (PD) versus time in days.

Control & Treatment	Growth Rate PD/day	Total PD's
Control	0.35 PD/day	42.00
0.3µM APH	0.24 PD/day	39.66
1µM APH	0.21 PD/day	39.06
1mM HU	0.15 PD/day	37.86
5mM HU	0.14 PD/day	37.66

Figure 4.3: PDs of SCK cells (APH & HU)

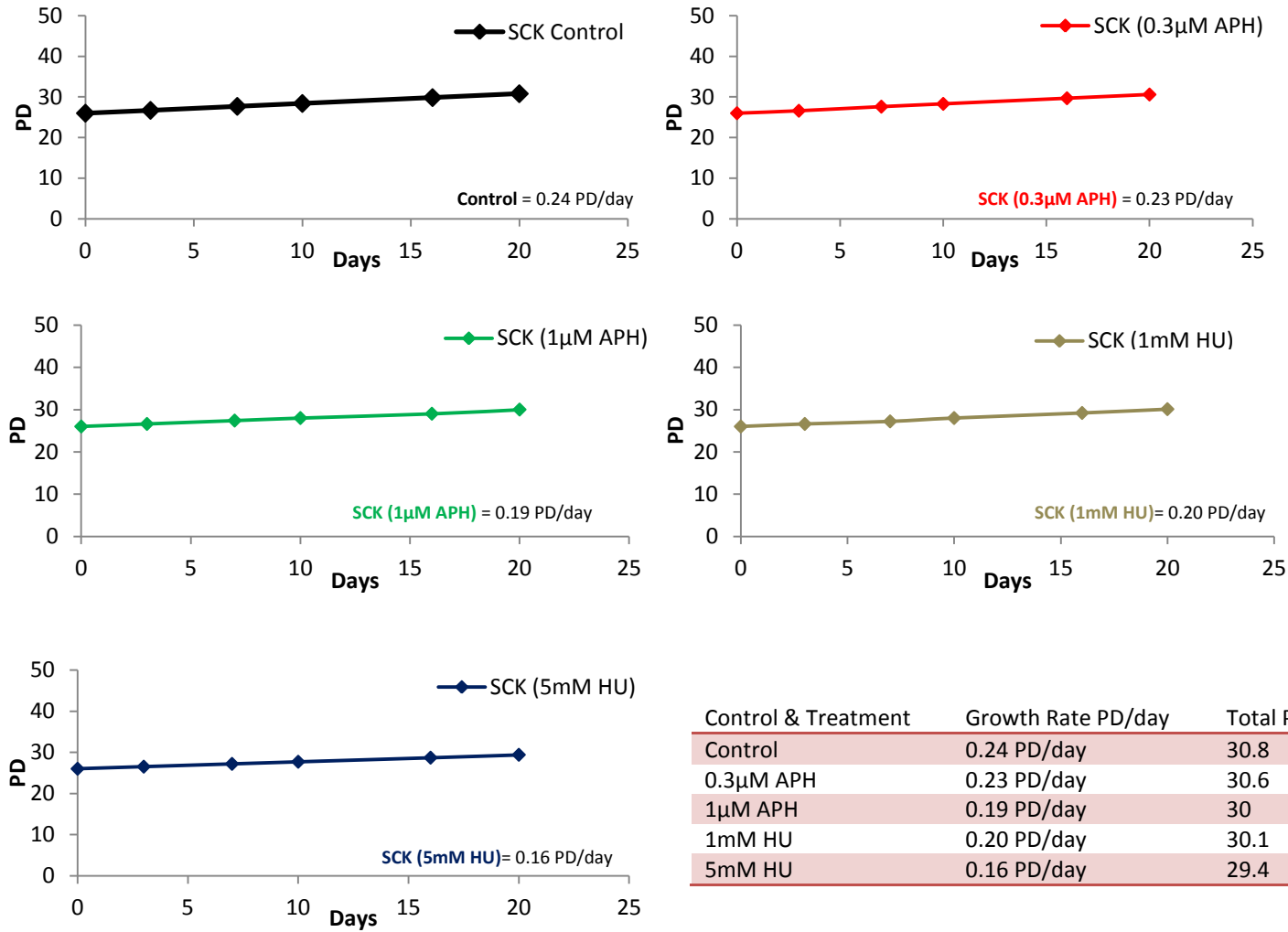


Figure 4.3: Growth curves of SCK cells. SCK control (untreated) (Black Line) and (treated) with different concentrations of APH (0.3µM (Red Line) & 1µM (Green Line)) & HU (1mM (Gray Line) & 5mM (Blue Line)) for 24 hours. Plotting growth curves as function of population doublings (PD) versus time in days.

4.4.2 Effect of Fragility Induces on Cell Cycle Checkpoints

In order to examine the effect of fragile site induction on cell cycle checkpoints, MRC5, SCK and U138 cells were cultured with APH (1 μ M) and HU (1mM) and incubated for 24 hours in 100mm dishes. Controls and treated cells were collected from culture and fixed in 70% ethanol then were stained with Propidium Iodide (PI) and the G1, S and G2/M fraction was determined by flow cytometry.

Treatment with APH and HU resulted in an increase in the number of cells in S-phase compared to controls in MRC5, SCK & U138 cells, as shown in (Figure 4.4). 10.4% and 9.1% of treated MRC5 cells with 1 μ M of APH and 1mM of HU respectively were in S-phase, compared to the control which were only 3.3% of cells were in S-phase (Figure 4.4.A).

The fragility induced by the exposure to APH and HU, also increased the number of cells in S-phase in ATR deficient cells (SCK cells). 14.7% of treated SCK cells with 1 μ M of APH and 15.8% of treated cells with 1mM of HU were in S phase, where the control was only 8.3% in DNA synthesis phase (Figure 4.4.B).

U138 cancer cells also showed an increase in the number of treated cells in S phase (Figure 4.4.C).

These observations were consistent with the action of APH and HU that induce a partial inhibition of DNA synthesis; thus treated cells were accumulated in S phase compared to their controls in all the cultures tested MRC5, SCK and U138.

Figure 4.4: Cell cycle of MRC5, SCK & U138 cells (Treatments (APH & HU))

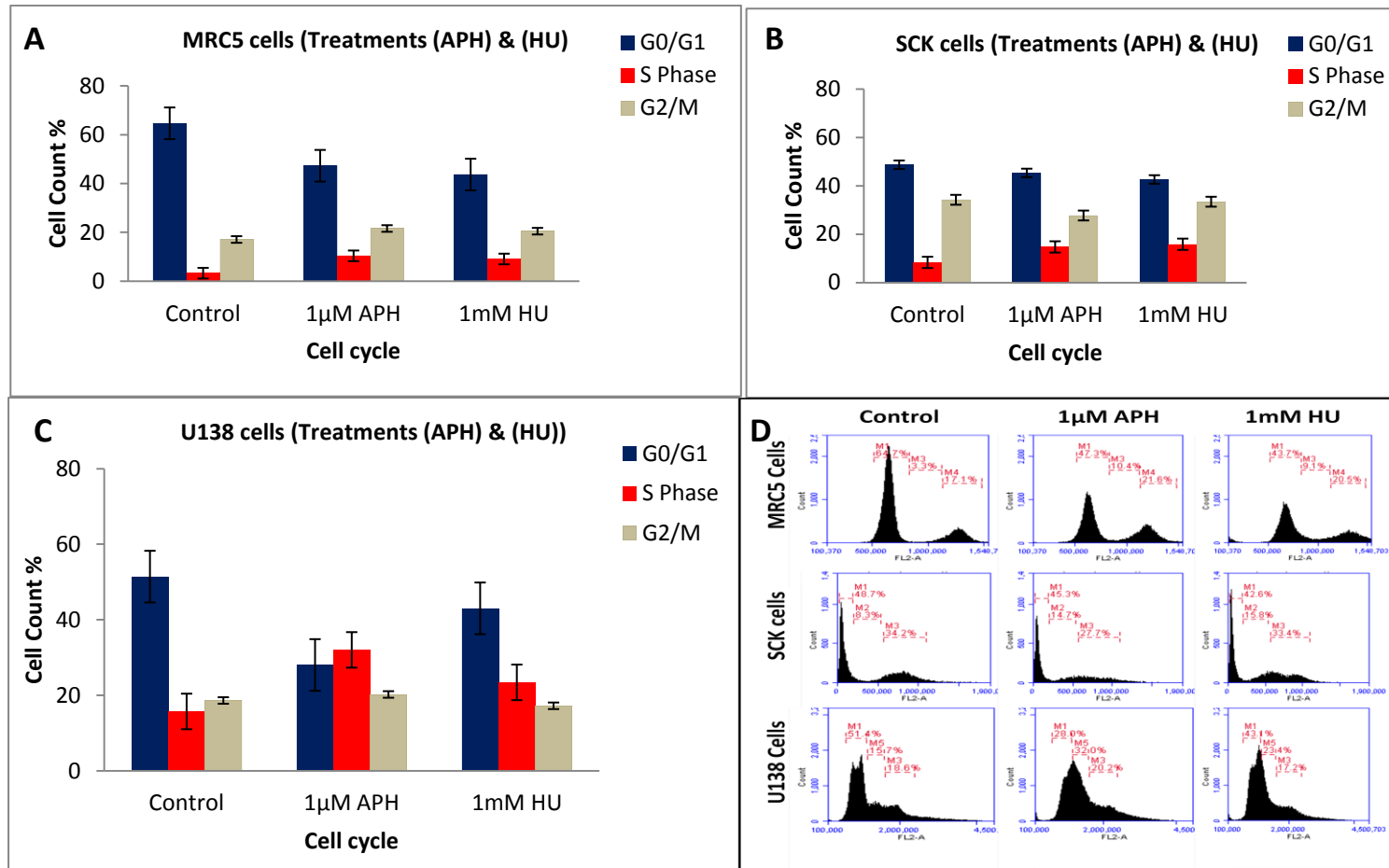


Figure 4.4: Cell cycle progression of (A) MRC5, (B) SCK (C) U138 cells & (D) plots from flow cytometry. Percentage of cells accumulated at G0/G1, S and G2/M phases and fraction was calculated by flow cytometry. Controls were compared to treated cells with 1µM of APH & 1mM of HU for 24 hours. Cell cycle progression was investigated after (24 hours) of treatments. Treated cells with (APH & HU) were accumulated more in S phase compared to controls, due to drug induction partial inhibition of DNA synthesis. Error bars represent standard error (SE). 121

4.4.3 Cellular Senescence

Cellular Morphology

In order to examine the impact of the induction of fragility on cellular senescence, morphological changes were monitored in cells (MRC5, SCK & U138 cells) treated with APH and HU and compared to their controls (Figures 4.5, 4.6 & 4.7). The cellular morphology of treated cells (MRC5 & SCK cells) changed as shown in figure (4.5.A & 4.6.A). They became larger than their controls and had bigger flattened cytoplasm and larger nuclei, consistent with cells undergoing cellular senescence (Toussaint *et al.*, 2000). In contrast, U138 treated cells did not display any changes in their morphology compared to their control neither with APH nor with HU (Figure 4.7).

Senescence Associated Beta galactosidase Activity (SA β -gal)

A chemical assay based on production of blue stain at pH 6.0 was developed, results from accumulation of the endogenous lysosomal β -galactosidase. In senescent cells, hydrolase enzyme catalyses β -galactosidase into monosaccharides and precipitate blue dyed. Senescence-associated beta-galactosidase is the most common reliable biomarker assay used for senescent detection. (Toussaint *et al.*, 2000; Chainiaux *et al.*, 2002; Dimri *et al.*, 1995).

Senescence-associated β -galactosidase assay was used to investigate cellular senescence induction in cells treated with APH and HU and compared with untreated controls. Positive senescent cells were determined by counting 500 cells and the proportions of positive cells were given as percentages of the total counted cells.

It was observed that treated cells (MRC5 and SCK cells) had higher percentages of activation of senescence-associated β -galactosidase enzyme compared to their controls: this can be clearly seen from the result in figures (4.5.B & 4.6.B). Moreover, controls and treated of SCK cells had higher percentage of positive senescent cells compared to MRC5 cells.

The average of senescent cells in the 1 μ M APH treated SCK and MRC5 cells was 49% and 36% respectively; this average increased and reaching 56% and 39% for those cells treated with 5mM of HU; whereas control SCK cells was 18% and 8% for MRC5 senescent of the total counted cells.

In contrast to the SCK and MRC5 cells, senescence-associated β -galactosidase activity could not be detected in U138 cancer cells, irrespective of the treatments with HU or APH.

Taken together these data strongly indicate that APH and HU treatments successfully induced cellular senescence in SCK and MRC5 cells. In contrast U138 cells showed no sign of cellular senescence induction with either APH or HU treatments.

Figure 4.5: Cellular Morphology & Senescence-Associated β - galactosidase Activity of MRC5 Cells (APH & HU)

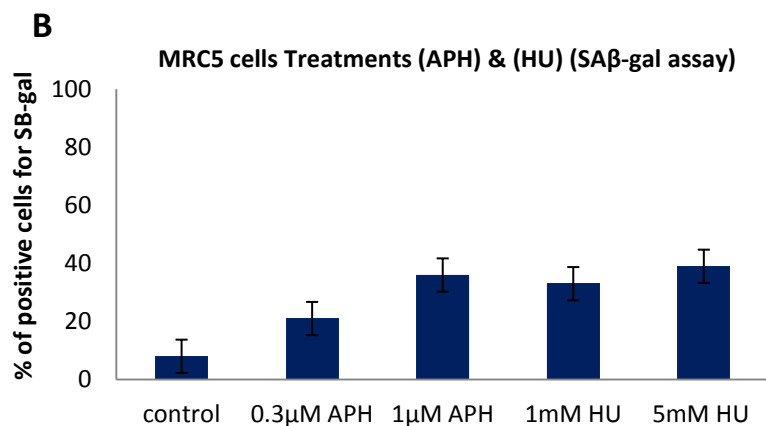
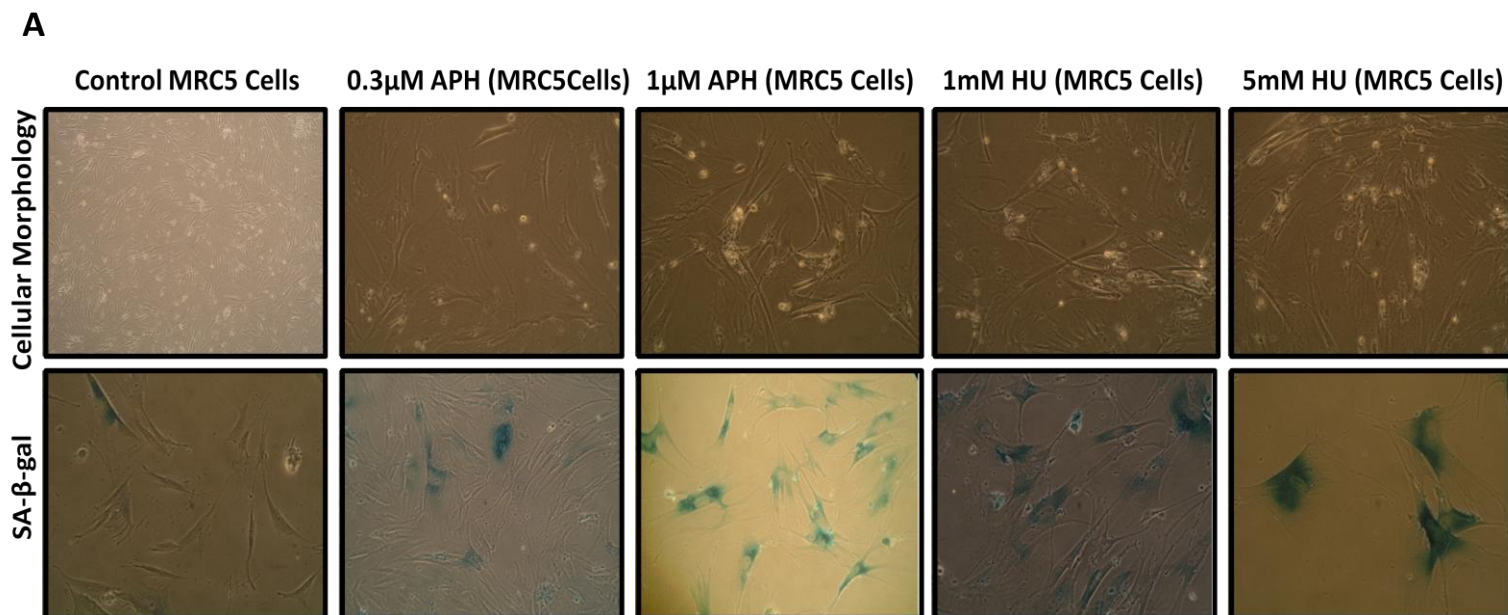


Figure 4.5: Cellular Morphology and SA β -gal assay of MRC5 Cells. (A) Morphological changes for MRC5 cells were monitored and treated cells with APH (0.3 μ M & 1 μ M) & HU (1mM & 5mM) were compared to the morphological changes in control cells after 24 hours of treatments. **Senescence-associated-beta-galactosidase (SA β -gal) activity** is detectable at pH 6 and produces a blue colour in positive senescent cells; as shown in the bars chart **(B)** the quantification of positive cells for SA β -gal assay was determined by counting positive stained cells under microscope (X20). The proportions of positive cells were given as percentages of the total counted cells. Error bars represent standard error (SE).

Figure 4.6: Cellular Morphology & Senescence-Associated β - galactosidase Activity of Seckel cells (SCK) (APH & HU)

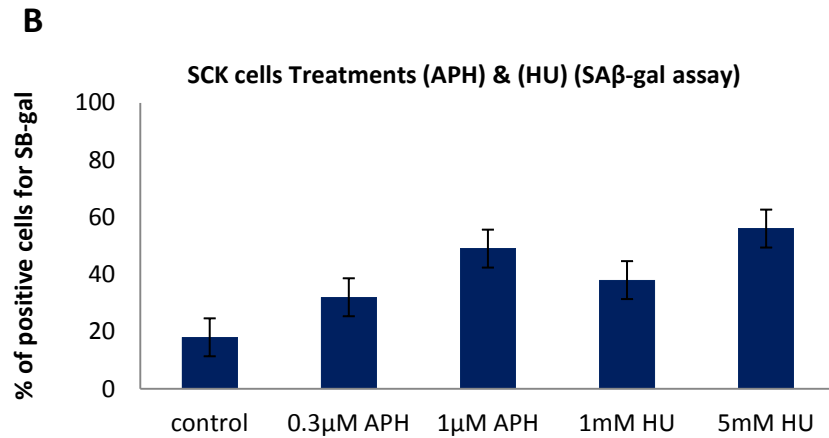
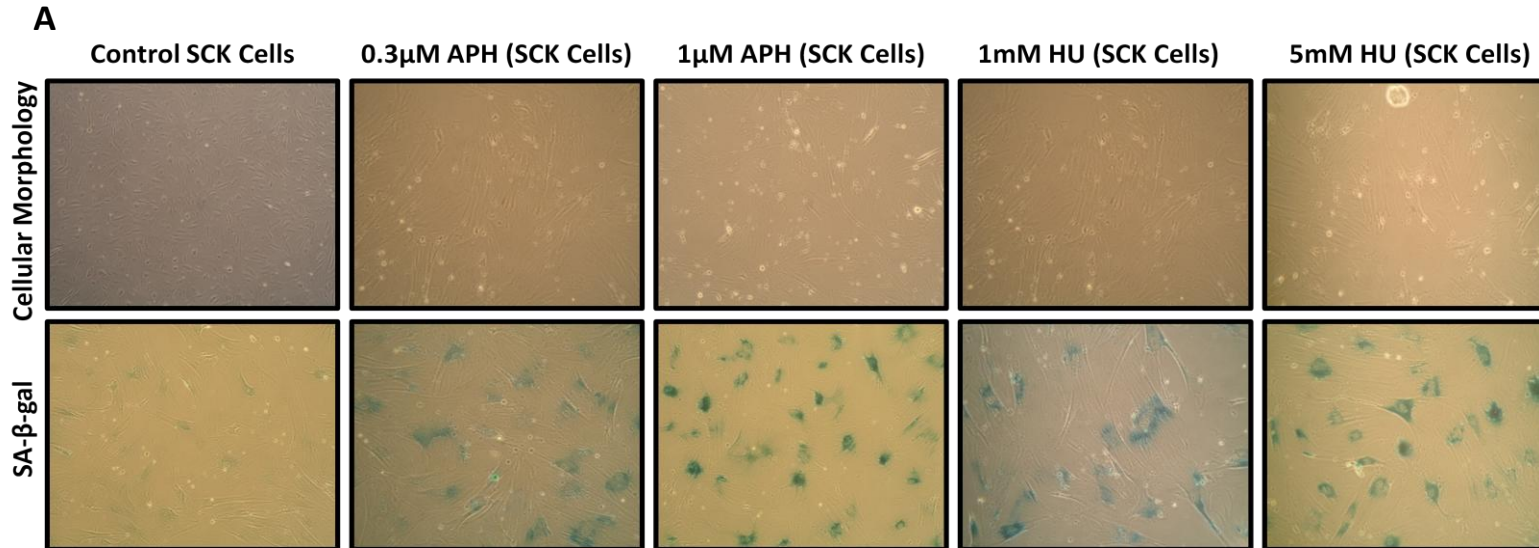


Figure 4.6: Cellular Morphology and SA β -gal assay of SCK Cells. (A) Morphological changes were monitored and treated cells were compared to the control post-treatments (24 hours). **(SA β -gal images)** representative images of senescence-associated β -gal staining in the cells. Bars chart **(B)** is the quantification of senescence-associated β -gal-positive cells of total counted 500 cells. Error bars represent standard error (SE).

Figure 4.7: Cellular Morphology & Senescence-Associated β - galactosidase Activity of U138 (APH & HU)

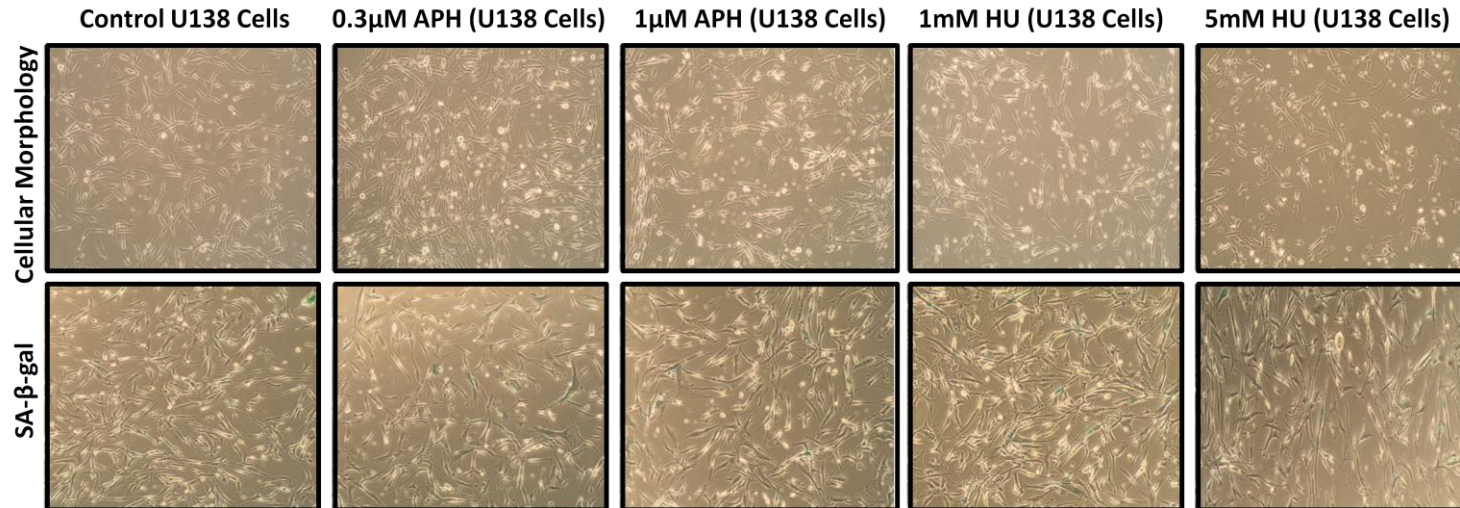


Figure 4.7: Cellular Morphology and SA β -gal assay of U138 Cells. Morphological changes for U138 cells were monitored and treated cells with APH (0.3 μ M & 1 μ M) and HU (1mM & 5mM) were compared to the morphological changes in control post-treatments (24 hours). **Senescence-associated-beta-galactosidase (SA β -gal) activity** was not detectable in these cells as shown in the images.

4.4.4 Metaphase Chromosomes Analysis (Breaks and gaps)

In order to test the impact of inducing fragility on chromosomal breaks and gaps at fragile sites, MRC5, SCK and U138 cells were cultured with APH (0.3 μ M & 1 μ M) and HU (1mM & 5mM) incubated for 24 hours in 100mm dishes. After treatment, demecolcin (colcemid) were added to controls and treated cells and incubated for one-two hours then cells were trypsinised and KCl was added for 10-30 minutes, cells were fixed in (fixative solution 3:1 methanol and glacial acetic acid) and can be kept at 4°C. Slides were prepared, metaphase chromosomes were stained with Giemsa. Then, breaks and gaps were counted in 50 metaphases and was given as proportions as shown in figure 4.8.

We did not observe any chromosomal instability in untreated MRC5 cells. However both the SCK and U138 untreated cells had chromosomal breaks and gaps in 9% and 32% of the cells respectively. U138 cancer cells having mutated *p53* and SCK cells fibroblast cells with *ATR* deficient, for these mutations might be that the chromosomal instability displayed more common in these cells, since *p53* and *ATR* are important proteins play a crucial role in modulating DNA damage response.

Following aphidicolin and hydroxyurea treatments, the average total gaps and breaks was increased in MRC5, SCK and U138 cells, as compared with their controls (Figure 4.8). In MRC5 treated cells an increase in gaps and breaks was observed from 0% in untreated cells to 26% in MRC5 cells treated with (1 μ M APH) and 21% for those treated with (5mM HU). SCK and U138 cells were treated with 0.3 μ M APH had 32% & 42% of breaks respectively; this average rose to 39% & 47% with cells treated with HU (5mM). These data clearly demonstrate that treatment of MRC5, SCK and U138 cells with APH and HU induces chromosomal fragility.

Figure 4.8 Metaphase Chromosomes Analysis in MRC5, SCK & U138 cells treated with (APH) and (HU)

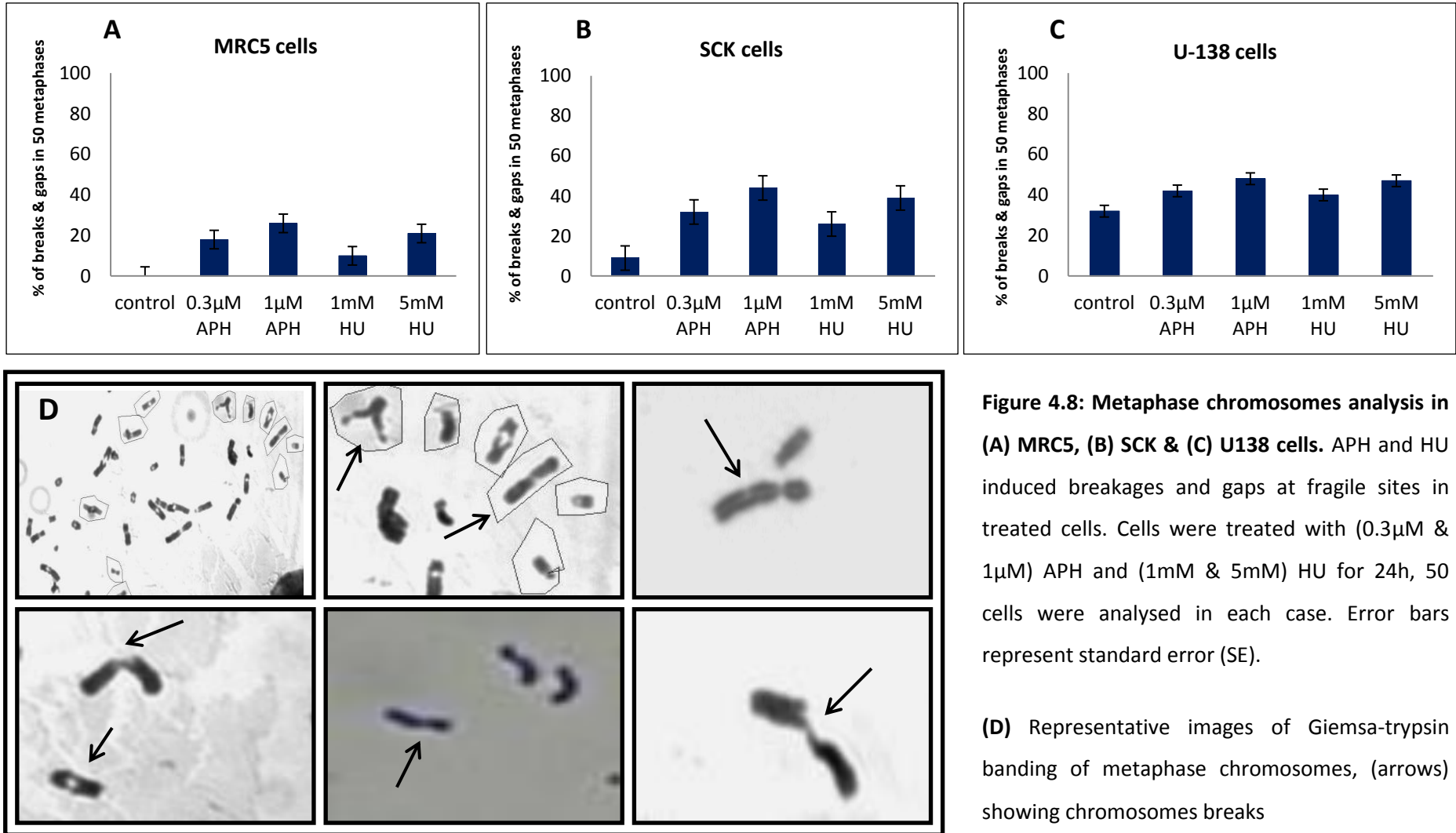


Figure 4.8: Metaphase chromosomes analysis in (A) MRC5, (B) SCK & (C) U138 cells. APH and HU induced breakages and gaps at fragile sites in treated cells. Cells were treated with (0.3µM & 1µM) APH and (1mM & 5mM) HU for 24h, 50 cells were analysed in each case. Error bars represent standard error (SE).

(D) Representative images of Giemsa-trypsin banded metaphase chromosomes, (arrows) showing chromosomes breaks

4.4.5 Proteins Checkpoint Activation Analysis (Western Blotting)

In order to investigate the effect of fragile site induction on key proteins involved with cell cycle checkpoint control, MRC5, SCK and U138 cells were cultured untreated and treated with APH (0.3 μ M & 1 μ M) and HU (1mM & 5mM) in 100mm dishes for 24 hours. Treated and untreated cells were trypsinised and collected for protein extraction. Western blots were carried out and phosphorylation of P53, Chk1 and Chk2 was investigated in treated cells and compared to untreated. Phosphorylations were determined by probing with anti-phospho P53 Ser15, anti-phospho Chk1 Ser345 and anti-phospho Chk2 Thr68 antibodies (Figure 4.9).

Both Chk1 and Chk2 were phosphorylated following exposure to the higher concentration of APH (1 μ M) and at both concentrations of HU (1mM and 5mM) in MRC5 and U138 cells (Figure 4.9).

In SCK cells (ATR deficient cells), it was observed that Chk1 was not fully phosphorylated or activated; Chk1 is an important ATR substrate regulating cell cycle checkpoint arrest. In contrast, Chk2, which is regulated by ATM, was phosphorylated in these cells after treatment with HU in both concentrations were used (Figure 4.9).

Following exposure to HU (1mM and 5mM), P53 was phosphorylated in MRC5 cells and SCK cells but was not activated after treatment with APH in both concentrations were used in MRC5 cells.

These data are consistent with the observed induction of cellular senescence and reduction in growth rates as a consequence of DNA damage arising following the induction of fragile site in the APH and HU treated cells.

Figure 4.9: Activation of key proteins required for cell cycle checkpoint control in MRC5, SCK & U138 cells treated with (APH) and (HU) (Western Blotting)

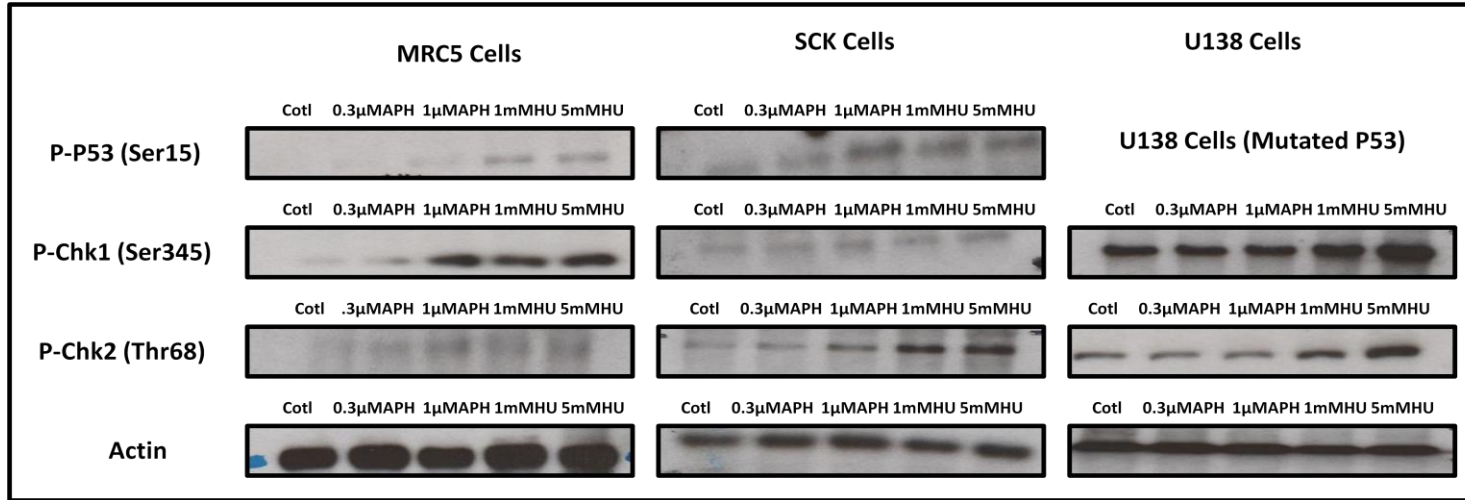


Figure 4.9: Checkpoints Activation Analysis. Western blot of MRC5, SCK and U138 cells, phosphorylations were determined by probing with antiphospho P53 Ser15, antiphospho Chk1 Ser345 and antiphospho Chk2 Thr68 antibodies. Cells treated with APH (0.3μM & 1μM) and HU (1mM & 5mM) for 24 hours Western blot was carried out for untreated and treated cells allowing comparison. Equal loading was confirmed by probing with Actin specific antibody.

4.4.6 Analysis of Telomere Dynamics

It was clear that the treatments of MRC5, SCK and U138 cells with either APH or HU was sufficient to induce chromosome fragility. In order to examine if the fragility induced by exposure to APH and HU resulted in large-scale changes to telomere length, the XpYp telomere length distributions of untreated MRC5, SCK and U138 cells and those treated with APH and HU were determined using single telomere length analysis (STELA). The XpYp telomere was analysed because it is considered to be representative for average chromosomal telomere length and average telomere erosion rates resulting from the end-replication problem (Baird and Farr, 2006; Baird *et al.*, 2003; Britt-Compton *et al.*, 2006). Following treatments and 5 days recovery cell samples were taken in parallel with untreated cells and subjected to STELA to track the telomere dynamics and to detect any stochastic telomeric deletion events with ongoing cell division. STELA southern blots for the experiment are shown in figures (4.10, 4.12 & 4.13).

As expected MRC5 fibroblasts displayed a bi-modal distribution at the XpYp telomere (Figure 4.10), and it is consistent with previous studies that MRC5 containing two differently lengths alleles at XpYp telomere, these distributions are a consequence of allelic variation in telomere length.

Whilst no significant differences were observed in the telomere length distributions of the MRC5 cells following treatment, the proportion of molecules detected the upper and lower alleles appeared to change (Figure 4.11).

Fewer molecules were detected in the upper alleles compared to the lower alleles following treatment. This appeared to be enhanced following 5 days of recovery after treatment of the MRC5 cells with 1 μ M APH. These changes are illustrated in Figure 4.11 that shows the

proportions of the long alleles to short alleles. Directly after treatment the proportions were 41.66% to 58.33%, following 5 days of recovery the average for long allele decreased to 32.8% whereas short allele increased to become 67.17%.

The SCK fibroblasts displayed a uni-modal distribution at the XpYp telomere and displayed a more homogenous distribution. By looking at (figure 4.12) an apparent change in the mean telomere length distributions was observed in SCK fibroblasts after APH treatments directly. The shorter molecules observed in the control SCK disappeared in the cells treated with APH in both concentrations 0.3 μ M and 1 μ M and this resulted in a statistically significant change to the mean telomere lengths distributions (p value 0.0001 and 0.0191 respectively).

U138 cancer cells displayed a slight difference in mean telomere length between treated either with APH or with HU and untreated U138 cells (Figure 4.13) however this was not statistically significant.

U138 cells short telomere frequency was determined to be 19.4% below 3kb in control cultures while it was higher in cultures recovered from 1 μ M of APH was about 22.66%, similar average showed after treatment of 5mM HU (Figure 4.13).

Figure 4.14 showed the proportion of short telomeres which was determined and calculated below 1kb for the MRC5 cells and below 3kb for the SCK cells, this due to the differences in the modal distributions between these cells. In MRC5 cells treated with 1mM HU showed 4% of short telomere frequency while cells treated with 1 μ M APH was 0%. Moreover, in SCK cells post treatment with 0.3 μ M APH showed 0 % of short telomere and in SCK cells treated with 5mM of HU, short telomere frequency was 6.8% only.

Figure 4.10: STELA of MRC5 XpYp Telomere (Untreated, After treatment & Recovered) (APH & HU)

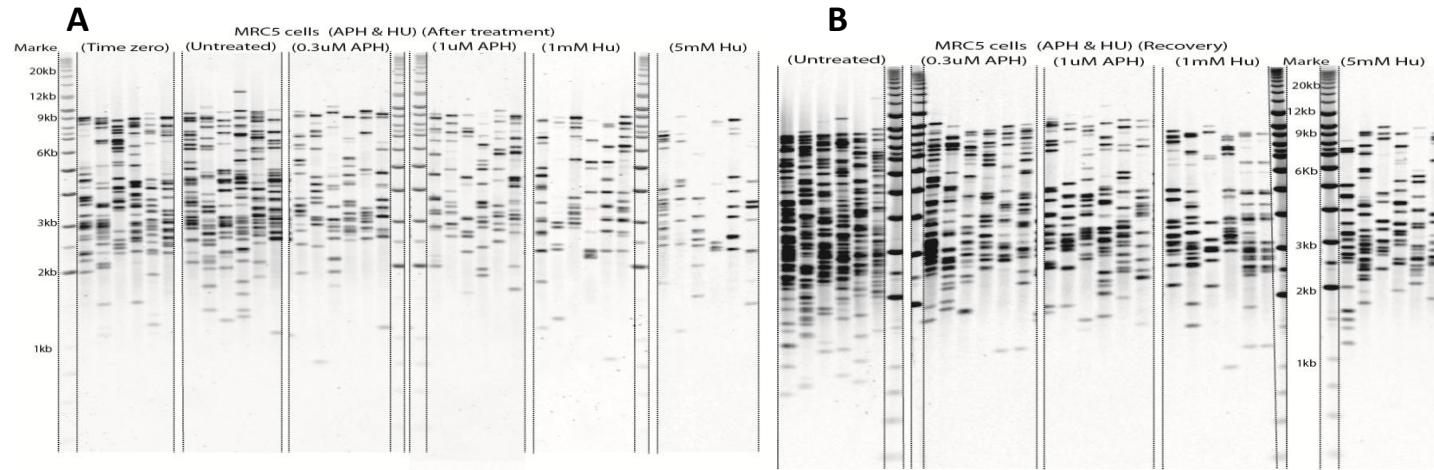
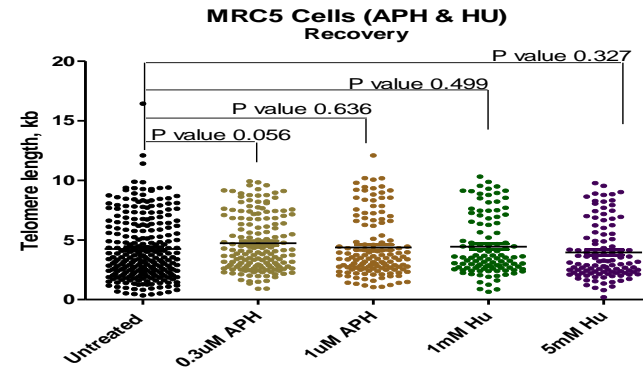
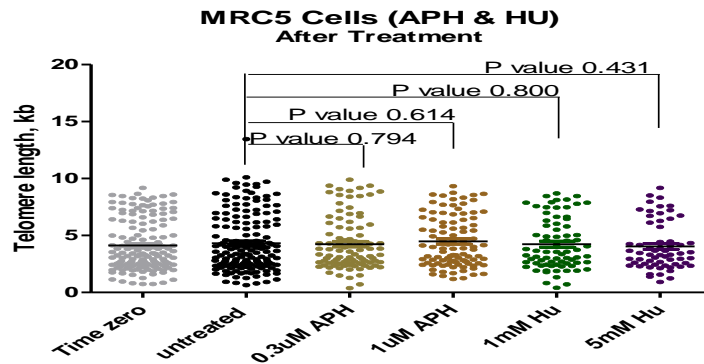


Figure 4.10: STELA gels of XpYp telomere in the MRC5 untreated and treated with APH (0.3 μ M & 1 μ M) and HU (1mM & 5mM) for 24 hours and the tables of descriptive data for telomeres. The gels illustrate the telomere length distributions while the tables give the mean, standard deviations (SD), standard error (SE) and population doublings (PD), (PD) was calculated after cells harvested. **(A)** 50% of MRC5 fibroblasts were collected for DNA extraction after 24h of treatments (APH & HU). **(B)** The remaining 50% of cells were refreshed with normal media and recovered for 5 days. Dot Plot made in (Prism) represent dot plots (Telomere length distributions) from the gels, were quantified using Phortetix software, then they were compared (control and treated samples) and p value was calculated using t-test in Prism (P value in Red is Significant) (in Black is NS).



AT	Time zero	Untreated	0.3uM APH	1uM APH	1mM HU	5mM HU
PD	34.86	35.21	35.1	35.07	35.01	35
Mean	4.160	4.32	4.236	4.472	4.231	4.036
SD	2.24	2.50	2.34	2.23	2.25	2.10
SE	0.18	0.19	0.24	0.23	0.26	0.27

Rec	Untreated	0.3uM APH	1uM APH	1mM HU	5mM HU
PD	36.6	36.06	35.91	35.61	35.56
Mean	4.24	4.733	4.376	4.444	3.956
SD	2.63	2.35	2.55	2.46	2.35
SE	0.16	0.19	0.22	0.24	0.23

**Figure 4.11: The proportion of long to short alleles of MRC5 XpYp telomere
(Untreated, After treatment & Recovered) (APH & HU)**

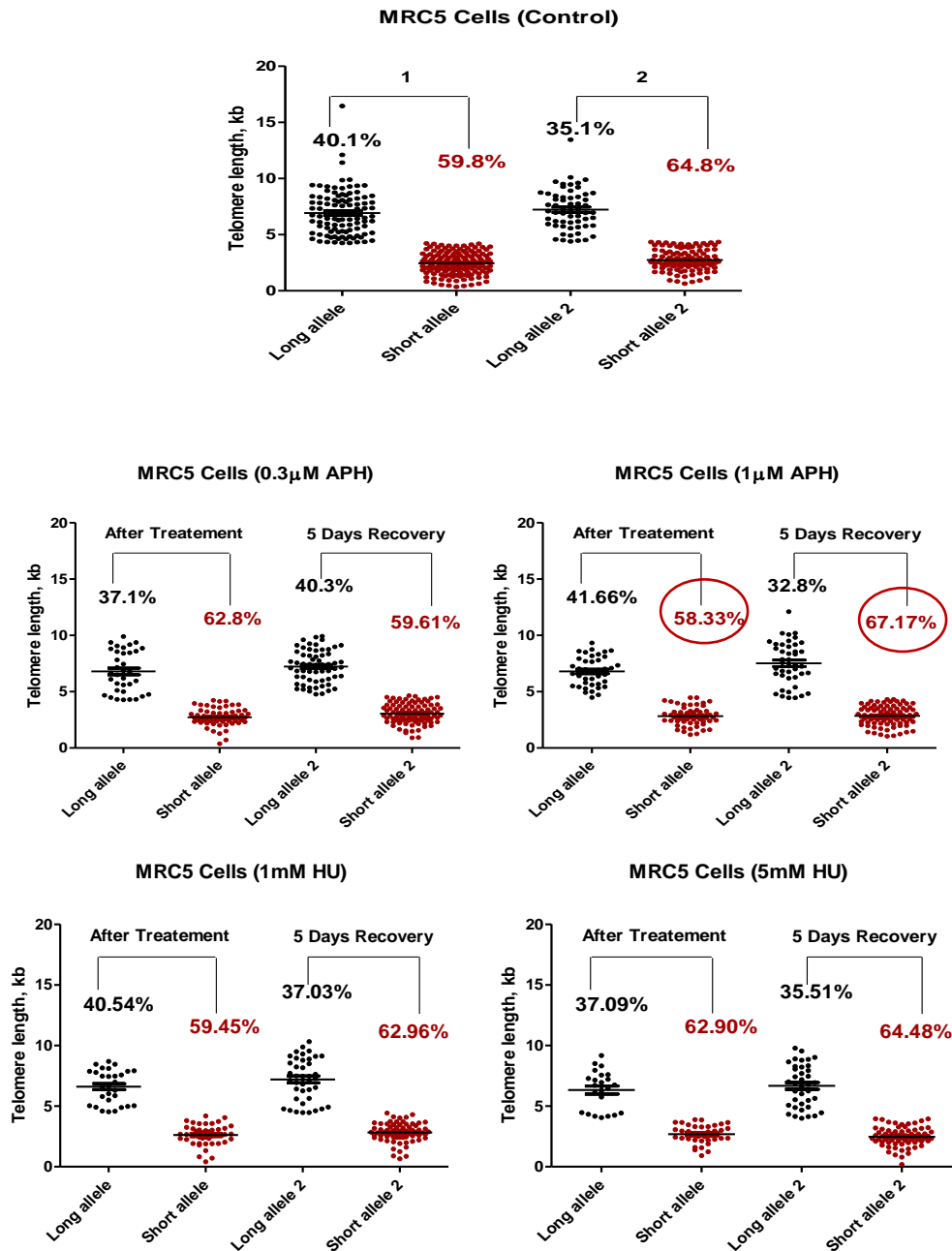


Figure 4.11: The proportion of long to short alleles of MRC5 XpYp telomere. MRC5 fibroblasts had the highest proportion of short alleles in cultures treated with 1µM APH following 5 days recovery.

Figure 4.12: STELA of Seckel cells (SCK) XpYp Telomere (Untreated, After treatment & Recovered) (APH & HU)

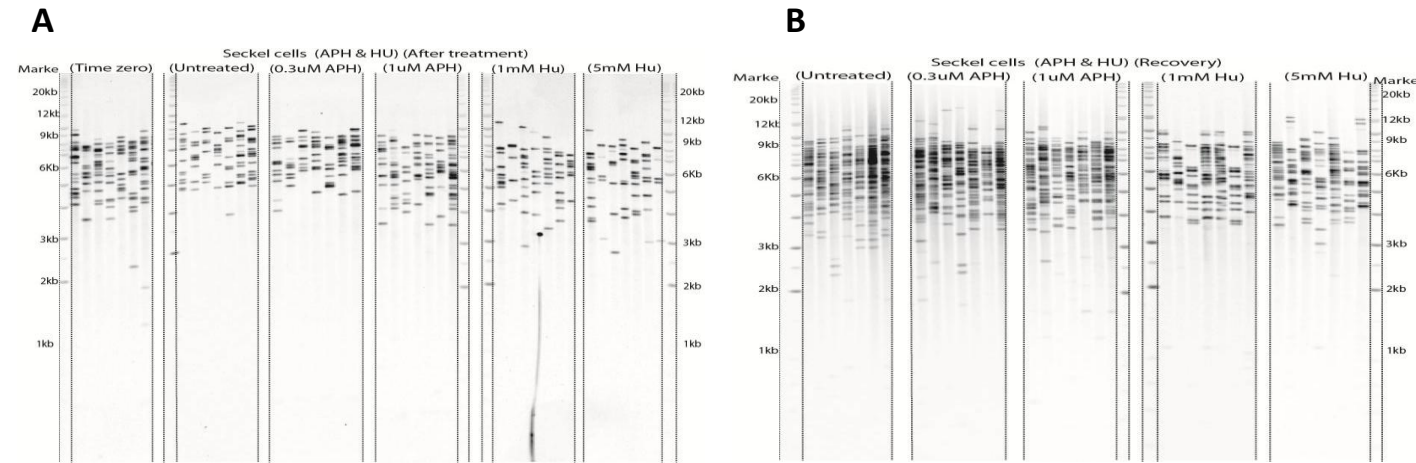
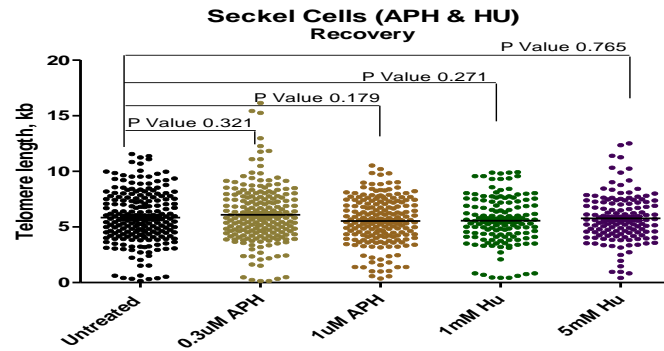
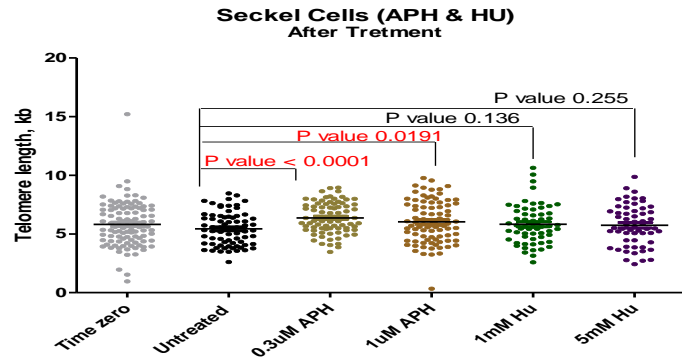


Figure 4.12: STELA gels of XpYp telomere in the SCK untreated and treated with APH (0.3µM & 1µM) and HU (1mM & 5mM) for 24 hours and the tables of descriptive data for telomeres. The gels illustrate the telomere length distributions while the tables give the mean, standard deviations (SD), standard error (SE) and population doublings (PD), (PD) was calculated after cells harvested. **(A)** 50% of SCK cells were collected for DNA extraction after 24h of treatments (APH & HU). **(B)** The remaining 50% of cells were refreshed with normal media and recovered for 5 days. Dot Plot made in (Prism) represent dot plots (Telomere length distributions) from the gels, were quantified using Phortetix software, then they were compared (control and treated samples) and p value was calculated using t-test in Prism (P value in Red is Significant) (in Black is NS).



AT	Time zero	Untreated	0.3uM APH	1uM APH	1mM HU	5mM HU
PD	26	26.24	26.23	26.19	26.2	26.16
Mean	5.815	5.43	6.370	6.036	5.825	5.744
SD	1.90	1.39	1.33	1.77	1.65	1.74
SE	0.18	0.16	0.15	0.19	0.21	0.23

Rec	Untreated	0.3uM APH	1uM APH	1mM HU	5mM HU
PD	27.2	27.15	26.95	27	26.8
Mean	5.84	6.088	5.539	5.564	5.769
SD	2.37	2.58	2.10	2.17	2.14
SE	0.17	0.18	0.15	0.19	0.18

Figure 4.13: STELA of U138 cells XpYp Telomere (Untreated, After treatment & Recovered) (APH & HU)

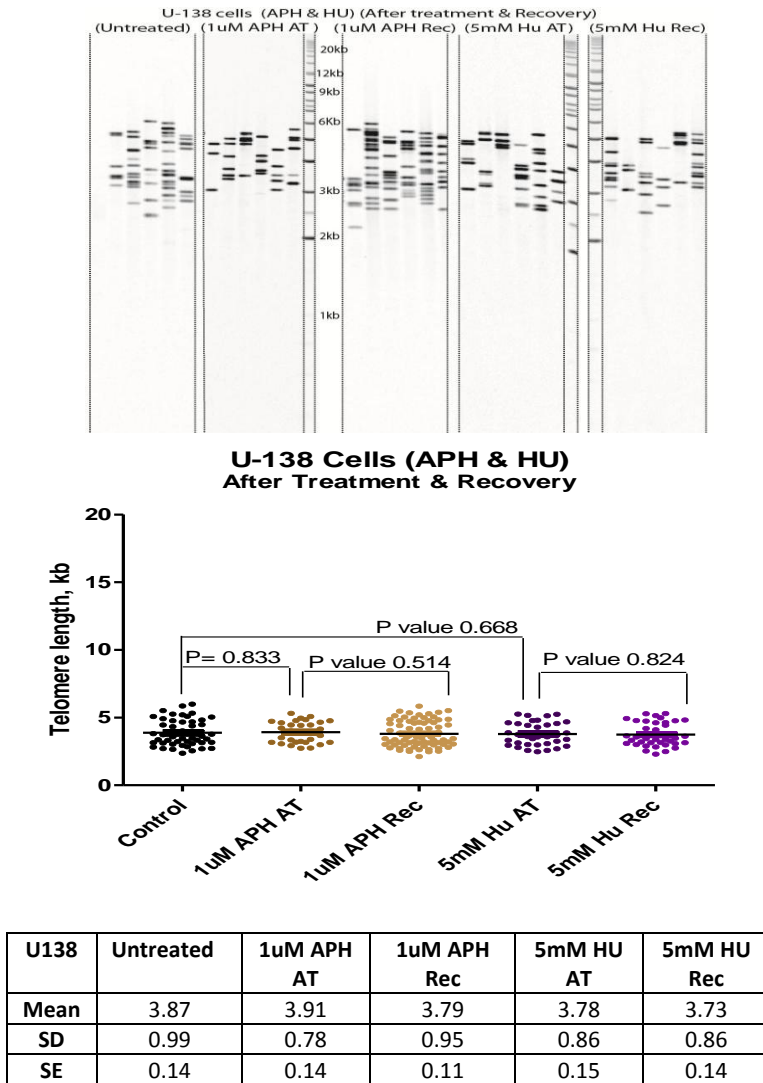
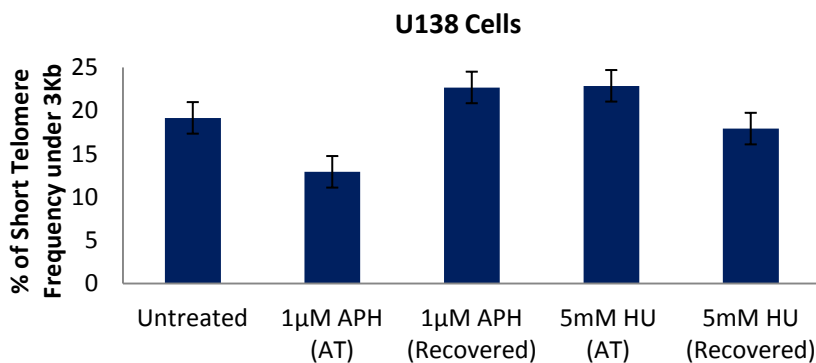


Figure 4.13: STELA gels of XpYp telomere in the U138 untreated and treated with APH (1µM) and HU (5mM) for 24 hours and the tables of descriptive data for telomeres. The gels illustrate the telomere length distributions while the tables give the mean, standard deviations (SD) and standard error (SE). 50% of U138 cells were collected for DNA extraction after 24h of treatments (APH & HU). The remaining 50% of cells were refreshed with normal media and recovered for 5 days. Dot Plot made in (Prism) represent dot plots (Telomere length distributions) from the gels, were quantified using Phortetix software, then they were compared (control and treated samples) and p value was calculated using t-test in Prism (P value in Red is Significant) (in Black is NS). Bar charts showed the proportion of short telomere frequency of U138 cells were calculated below 3kb for cells untreated, after treatment and 5days recovery, there were no significant differences observed. Error bars represent standard error (SE).



**Figure 4.14: The proportion of Short Telomere frequency (MRC5, SCK cells)
(Untreated, AT & Recovered) (APH & HU)**

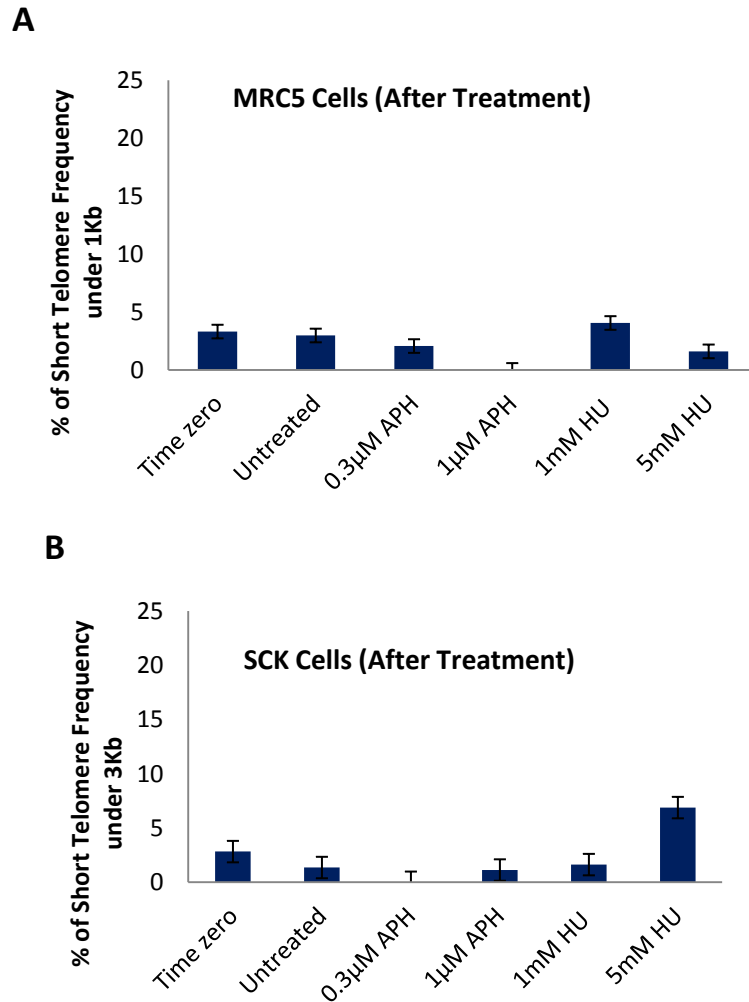


Figure 4.14: The proportion of short telomere frequency. The proportion of short telomere frequency of MRC5 cells (**A**) were calculated below 1kb and SCK cells (**B**) were calculated below 3kb for cells untreated and after treatment. SCK cells post treatment with 0.3µM APH showed 0 % of short telomere; this increased reaching 6.8% in cells treated with 5mM HU. In MRC5 cells treated with 1mM HU showed 4% of short telomere frequency while cells treated with 1µM APH was 0%. Error bars represent standard error (SE).

4.5 Discussion

4.5.1 Culture Growth

In the study presented here, chromosome fragility was successfully induced in MRC5, SCK and U138 cells following treatment with APH or HU. These treatments slowed the growth rates of the treated cultures in MRC5 and SCK. Data also showed that the growth rate of normal control SCK cells was lower than the normal growth rate of MRC5 cells. The overall growth rates of U138 cells control and treated were higher than MRC5 and SCK fibroblasts cells. Moreover, there was no difference in its growth rate between control and recovered U138 cells.

These data are consistent with previous observations that the growth rate slows with an increasing proportion of cells damaged or senescent and fewer cells capable of division.

4.5.2 Checkpoint Activation, Cell Cycle Arresting and Chromosomal Instability

ATR and ATM, directly regulate Chk1 and Chk2. Chk1 and Chk2 are structurally distinct, however they have overlapping functions. Chk1 is placed downstream of ATR and is phosphorylation and activated in response to replication fork stalling and regulates cell cycle checkpoints in S phase and G2 phase of the cell cycle (Durkin *et al.*, 2006). Chk1 has been shown to stabilise replication during the DNA synthesis phase in DT40 B-lymphoma cells. Chk2 is downstream target of ATM, and activated by double strand breaks, although it was argued that it may also be activated independently of ATM in some circumstances (Durkin *et al.*, 2006). It was reported that Chk1 and Chk2 are activated during S phase in response to high doses of APH, suggesting that Chk1, and Chk2, regulate common fragile site stability (Durkin *et al.*, 2006).

The Ser345 site in Chk1 and Thr68 site in Chk2 are known to be preferred domains for phosphorylations by ATR and ATM respectively, after DNA damage or replication forks stalled (Zhao and Piwnica, 2001; Bartek *et al.*, 2001). There has been controversy concerning what Chk1 and/or Chk2 respond to, also whether these kinases activated in response to genotoxic stress. It has been reported that Chk1 is inducibly phosphorylated in response to single strand breaks while Chk2 respond to double stranded breaks (Zhao and Piwnica, 2001; Casper *et al.*, 2002).

Our data showed that in the MRC5 fibroblasts, the effects of low dose of Aphdicolin (0.3 μ M) concentration was able to induce the fragile site breakages and SA β -gal activity, but did not signal efficiently to activate and phosphorylate Chk1. In contrast, the higher dose (1 μ M) concentration of APH was sufficient to induce Chk1 phosphorylation. This can illustrate that a higher concentration of APH leads to more widespread damage across the genome and they are more likely as single stranded breaks which in turn activate the Chk1 phosphorylation but not Chk2.

Our data also showed that ATR deficiency in SCK fibroblasts interfere with the phosphorylation of Chk1 on its target domain Ser 345 either with APH or HU.

Previous findings have showed that ATM does not play a role in phosphorylation following replication stalling (Durkin *et al.*, 2006), however in contrast our data showed that Chk2 was fully activated and phosphorylated after treatments mainly in the cultures where HU were applied. HU in both concentrations (1mM and 5mM) were able to induce Chk2 phosphorylation successfully on Thr68 domain more than what we have seen in APH treatment, this suggest that the damages produced from HU are more likely as double stranded breaks.

The occurrence of breaks at fragile sites is enhanced when replication stress is combined with deficiency in the ATR mechanism. ATR respond to the replication stress and delays the cell cycle progression.

Our data showed that MRC5, SCK and U138 cells had a significant increase (p value 0.005 ANOVA) in fragile site expression following treatments. Moreover, untreated SCK fibroblasts and U138 cells displayed fragile sites expressions, this suggests the frequency of fragile site instability in cultures lacking ATR or P53 and demonstrates the important role for ATR and P53 in regulating fragile sites. Moreover, SCK cells displayed higher proportions of chromosomal breaks and gaps compared to MRC5 cells following exposure to APH and HU. This is due to ATR deficiency. ATR which plays an important role in response to replication stalling following APH and HU treatments, delays the cell cycle progression at the S phase or G2/M checkpoints, allowing for repair the damages and prevents improper progression into mitosis. In SCK fibroblasts where this important kinase is absent, improper progression into mitosis occurs and chromosomal instability is more common in these cells. While in MRC5 fibroblasts, where the checkpoints proteins are proficient and the progression through cell cycle are monitored, the chromosomal instability were less frequent.

4.5.3 Telomere Dynamics

Different mutational mechanisms may contribute to telomere erosion and generate large-scale telomeric deletions. The aim of this chapter was to observe if the induction of chromosome fragility could contribute to telomere erosion and large-scale telomeric deletion. In order to examine this hypothesis, the XpYp telomere length distributions of MRC5, SCK and U138 cells treated with APH and HU were investigated using STELA (Baird *et al.*, 2003). In line with previous studies in the group (Baird *et al.*, 2003), the XpYp telomere

was analysed because it is considered to be representative for average chromosomal telomere length and average telomere erosion rates resulting from the end-replication problem.

SCK fibroblasts showed uni-modal distribution at the XpYp telomere and displayed a more homogenous distribution compared to MRC5 cells. In contrast, MRC5 fibroblasts displayed bi-modal distributions at the XpYp telomere, and it is consistent with previous studies that MRC5 containing two differently lengths alleles at XpYp telomere, arise from inter-allelic differences which are set in zygote and resulting of contribution of maternal and paternal telomere alleles (Baird *et al.*, 2003).

SCK cells showed significant differences in mean telomere length between treated with 0.3 μ M, 1 μ M APH and untreated cells. Treated SCK fibroblasts with APH displayed higher mean telomere length (~ 6Kb) compared to control (~5Kb). This suggests that cells with shorter telomeres in treated SCK fibroblasts disappeared from the culture; this lost made the mean telomere length higher in these cells than their control statistically significant. This could be explained by that Aphidicolin preferentially damages the cells with shorter telomeres in cultures of Seckel fibroblasts and that cells in which this occurs subsequent disappear from the culture. As described previously; TTAGGG repeat of telomeres pose a challenge to replication process and they resemble the fragile sites characteristics (Sfeir *et al.*, 2009) accordingly, telomeres considered being sensitive to replication inhibition and forks stalling that induced by exposure to APH. To sum up, the fragility of telomere repeats, and consequently exposure to APH, which is a replication inhibitor, and the SCK fibroblasts its self containing ATR deficiency, which is playing an important role in DNA damage

response, all these factors play as a synergetic effect and induce damages preferentially in these cells.

In contrast, the mean of telomere length showed no significant differences between treated either with APH or with HU in both cells MRC5 and U138 cells. However, the proportion of molecules detected in the upper and lower alleles in the MRC5 following treatments appeared to change. More molecules were observed in the lower alleles compared to the upper alleles; this increasing were observed following 5 days of recovery and were mainly seen in the cells treated with 1 μ M of APH. This could be explained by that, MRC5 fibroblasts are more resistance to APH treatment compared to SCK fibroblasts. Unlike SCK fibroblasts, exposure to APH treatment in MRC5 did not induce a statistically significant change in the mean telomere length distribution. However a change in the proportions of long to short alleles was induced. It is possible that the upper alleles in MRC5 may have been preferentially targeted by APH treatment and that replication fork stalled that induced by exposure to APH in these upper alleles were resolved as breaks resulting in a reduction in the length of these alleles. Moreover, our western blot data was consistent with this suggestion; as Chk1 was phosphorylated and activated following 1 μ M of APH treatment in MRC5 fibroblasts indicating that replication stress induced DNA-damage occurred.

Furthermore, our data showed that exposure of U138 cancer cells to APH and HU treatments did not produce a detectible increase in the proportions of short deleted telomeres. This could be explained by the type of damage induced by exposure to APH or HU treatments in such type of aggressive cancer cells U138 are more likely to be in form of telomeres fusions, chromosomes translocations etc rather than deleted short telomere and these are un-detectable by STELA. This can be clearly seen in metaphase chromosomes

analysis, where the frequency of chromosomes breaks and gaps were highly induced following treatments. Alternatively, the fast growing nature of the U138 cells may result the rapid loss or dilution of cells in which telomere-specific mutagenic events occurred thus rendering these events undetectable.

4.6 Conclusion

The data presented indicates that changes to telomere length distributions can be detected following the induction of fragile sites. The original hypothesis that the induction of chromosome fragility might result in telomeric deletion events was consistent with the data obtained from SCK fibroblasts where the fragility of telomeres was enhanced by ATR deficiency. Whereas, in MRC5 fibroblasts the induction of chromosome fragility impacted on its upper to lower alleles ratio, with a preferential loss of the longer telomere length distribution.

Chapter 5

Examining the relationship between G-quadruplex stabilisation and telomeric mutation

5.1 Summary

Superimposed on the end replication problem, mutational events have been observed in primary culture cells that create dysfunctional telomeres that are capable of fusion to other chromosome ends. This can lead to genomic instability that may drive tumour progression.

The telomeric G-rich strand renders telomeres prone to form a unique secondary structure called G-quadruplex. The presence such structures at telomeric DNA and their potential resolution as double or single strand breaks could represent a mutational mechanism that may lead to the induction of telomeric dysfunction.

The aim of this study was to determine if G-quadruplex structures, could contribute to telomere erosion and large-scale telomeric deletion. Moreover, the role of ATRX protein and its contributions in resolving G-quadruplex structures was also investigated.

In order to test this hypothesis, G-quadruplex structures were stabilised using the G-quadruplex ligand (RHPS4) in IMR90 fibroblasts, U138 cancer cells, Ntera cells (ATRX+) and (ATRX-) and Hela cells (ATRX+) and (ATRX-). The stabilisation of G-quadruplexes was monitored and the induction of cell-cycle checkpoints, senescence and a reduction in cell growth were observed. Telomere dynamics and stochastic telomeric deletion events were investigated using STELA.

The data showed that an absence of ATRX sensitised cells to RHPS4, but that the stabilisation of G-quadruplexes did not significantly affect the telomere dynamics.

5.2 Introduction

5.2.1 Formation of G-quadruplex

The presence of G-rich single-stranded DNA oriented 5' to 3' toward the chromosome terminus makes telomeres prone to form secondary structures referred to as G-quadruplexes (Tran *et al.*, 2011). Telomeric sequences from different organisms have been shown to fold into several guanine-quadruplex structures by a single strand (intra-molecular) or by two associated strands (bi-molecular) or (tetra-molecular) which form by four associated strands (Williamson *et al.*, 1989). The stability of these structures was identified in the presence of several cations, mainly potassium and sodium (Sen and Gilbert, 1990). In the single cellular eukaryotes *Oxytricha* and *Tetrahymena* telomeric repeats form G-quadruplex structure in sodium (Smith and Feigon, 1992; Wang and Patel, 1994), in human, the structure formed in sodium and in potassium cations and in *Bombyx mori* and *Giardia* formed in potassium (Phan *et al.*, 2007; Amran *et al.*, 2009; Hu *et al.*, 2009). It has also been found that guanines that fold into G-quadruplex structures in the presence of potassium are more stable than in sodium (Tran *et al.*, 2011).

G-quadruplexes consist of hydrogen-bonded guanine tetrads (Hoogsteen hydrogen-bonding arrangement) these structures stack into various structures including a basket-like structure (Figure 5.1) identified in experiments using sodium chloride (Wang and Patel, 1993), whilst in potassium chloride solution experiments revealed two similar structures (hybrid 1 and hybrid 2) (Figure 5.1) (Phan *et al.*, 2007). The difference between these two structures is in their loop orientations. Propeller structures have been found in the solid-state experiments, and in the high concentrations of dehydrating solvents (Figure 5.1) (Parkinson *et al.*, 2002).

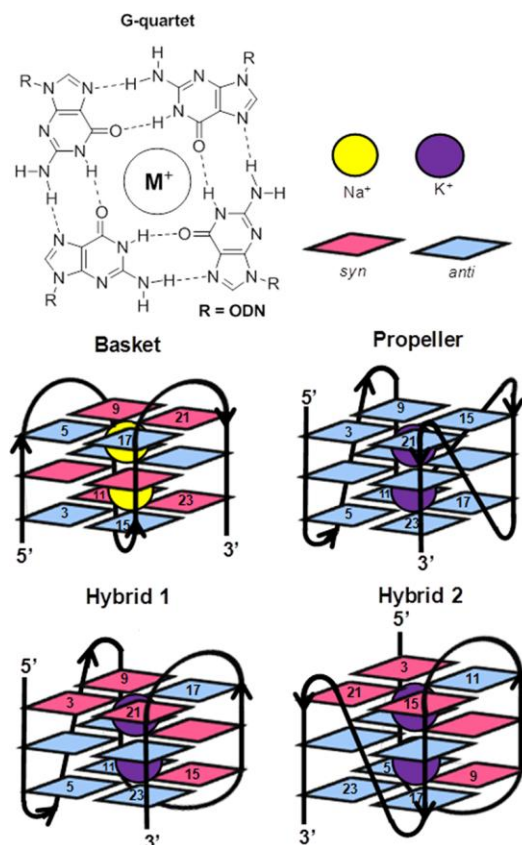


Figure 5.1: Structures of G-quadruplexes. Basket, propeller, hybrid-1 and hybrid-2, are G-quadruplex structures. Purple spheres presented potassium ions, sodium ions are the (yellow spheres), anti G residues are shown in blue, and syn G residues are in magenta. Four guanines form G-quadruplexes, each guanine serves as both hydrogen bonding acceptor and donor and the stacking of guanine tetrads results in G-quadruplex DNA structures. Adapted from (Fleming and Burrows, 2013).

5.2.2 Prevalence of G-quadruplexes in the Genome

Although there is good evidence for G-quadruplex formation *in vitro*, demonstration of their occurrence *in vivo* has been difficult to establish. It has been suggested that the high thermodynamic stability of G-quadruplexes under near-physiological conditions means that these structures could occur in genomic DNA *in vivo* (Biffi *et al.*, 2013). Recent studies have provided evidence of G-quadruplexes in prokaryotic and eukaryotic genomes. The first indication that G-quadruplex formation occurred *in vivo* has been identified at telomeric

repeats of the macronucleus of stichotrichous ciliates using antibodies targeted to G-quadruplex structures (Schaffitzel, 2001). It has been predicted that the human genome contains 376 000 motifs that have the potential to form G-quadruplex structures (Lipps and Rhodes, 2009).

The location of potential G-quadruplex structures is non-random, many studies revealed the prevalence of G-quadruplex in key regulatory regions of the human genome. They have been found frequently in the repetitive DNA regions such as telomeres (Lipps and Rhodes, 2009). Similarly, immunoglobulin switch regions, promoter regions of eukaryotic genes and around 40% of human gene promoters are predicted to contain at least one G-quadruplex motifs including oncogenes and tumour suppressor genes (Biffi *et al.*, 2013; Sen and Gilbert, 1990; Simonsson *et al.*, 2002).

5.2.3 Impact of G-quadruplex Formation in the Genome

Unresolved G-quadruplexes are considered to induce DNA damage responses, senescence and chromosomal end-to-end fusions. It has been found that G-quadruplex structures contribute to the inhibition of cellular proliferation following stabilisation with G-quadruplex ligands (Incles *et al.*, 2004; Salvati *et al.*, 2007). Recently, G-quadruplex structures have attracted attention due to their involvement in telomere-telomere interactions (Giraldo *et al.*, 1994) and in the control of telomerase activity (Zahler *et al.*, 1991). G-quadruplexes are also involved in maintaining chromosome stability and act as negative regulator of telomere elongation (Zahler *et al.*, 1991).

G-quadruplexes are potentially difficult to resolve structures and may lead to replication fork stalling (Leonetti *et al.*, 2004). As described in chapter 4, telomeres resemble fragile sites and replication fork stalling frequently occurs at these sites. The fragility of telomeres combined with G-quadruplex formation may make them susceptible to replication fork

stalling and resolution as a single or double-stranded DNA breaks, resulting in telomeric mutation and deletion events.

5.2.4 G-quadruplex Ligands

Telomerase is potential target for therapeutic intervention (Kelland, 2000), telomerase is up-regulated in approximately 80% of all cancer types (Gunaratnam *et al.*, 2011). G-quadruplex ligands are small molecules designed to fold DNA strand into G-quadruplex structure and prevent the interaction of telomerase with telomeres (De Cian *et al.*, 2007). The original concept of targeting telomerase in cancer treatment was that telomeres would gradually erode until such time that they become critically short and inhibit cellular proliferation (Gowan *et al.*, 2001).

A large number of G-quadruplex- ligands have been reported and designed to stabilise G-quadruplexes. In xenograft models anti-tumour activity has been identified with BRACO-1922 (Burger *et al.*, 2005). More examples of these ligands include: di-substituted aminoalkylamido acridine, pentacyclic acridine (RHPS4) (Figure 5.2); RAPI a protein produced by *Saccharomyces cerevisiae* which is known to bind to G-quadruplex and Gq1 an artificially derived protein which as acts as a G-quadruplex ligand (Haider *et al.*, 2003).

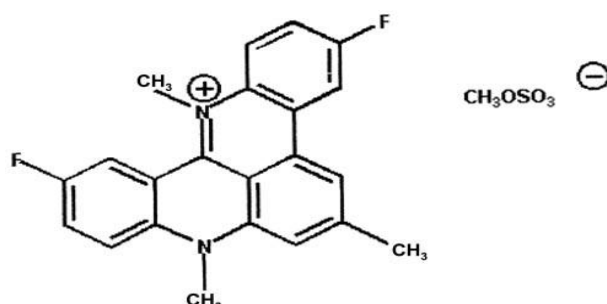


Figure 5.2: RHPS4 structure, adopted from (Leonetti *et al.*, 2004).

5.2.5 G-quadruplex Unwinding

The replication of G-quadruplexes requires that they are resolved by the action of helicases, including the RecQ helicases, BLM and WRN (Fry and Loeb, 1999). RecQ helicase family plays

essential role in genome stability particularly during DNA replication and in telomere metabolism, they contain domains that bind to G-quadruplexes suggesting that these helicases play a role in telomere and genome stability by resolving G-quadruplexes (Huber *et al.*, 2006). Recent studies report that WRN and RTEL helicases also play a role in the regulation of telomeric D-loop structures (Barber *et al.*, 2008).

Mutations in *BLM* result in chromosomal instability, chromosomal fusions and cancer progression (German, 1993). Recent studies have shown that BLM co-localise with telomeric foci within an ALT cell line (Yankiwski *et al.*, 2000). WRN localisation to the telomeres seems to be specifically during the S-phase of the replication cycle. By interacting with TRF2, WRN's 3'-5' exonuclease and weak 3'-5' helicase activities become induced (Opresko *et al.*, 2002) and this may resolve telomeric D-loops. Thus, WRN is involved in normal telomere replication by resolving abnormal secondary telomeric structures during the progression of the replication fork. It has also been reported that RTEL helicase has a role as well in unwinding G-quadruplexes at telomeres (Uringa *et al.*, 2011).

Recently, it has been shown that ATRX binds to telomeric G-rich strand that form secondary structure G-quadruplex *in vivo* (Law *et al.*, 2010) (Biffi *et al.*, 2013). In addition, ATRX together with the histone chaperone DAXX, facilitate the deposition of the histone variant H3.3 into telomere chromatin (Wong *et al.*, 2010). Interestingly, mutations in the ATRX/DAXX/H3.3 complex are found in cancers that display the ALT phenotype, these include pancreatic neuroendocrine tumours (Jiao *et al.*, 2011), oligodendrogliomas and neuroblastomas (Molenaar *et al.*, 2012). It has been suggested that ATRX is a tumour suppressor however; the actual mechanism of ATRX in ALT is still unclear (Clynes *et al.*, 2015).

5.3 This Work

In this chapter, I have examined whether G-quadruplex stabilisation at telomeres has the potential to drive stochastic telomere deletion events. In order to test this hypothesis, G-quadruplex formation was induced and stabilised with using the pentacyclic acridine (RHPS4) G-quadruplex stabilising ligand. The effect of G-quadruplex stabilisation on the cellular proliferation and on the telomere dynamics was examined in the cultured IMR90 fibroblasts and U138 cancer cells. The effect of G-quadruplex formation was also examined in the context of ATRX knockdown in Ntera and Hela cells. Figure 5.3 illustrates the hypothesis, plan and the assays that have been used to test these hypotheses.

IMR90 fibroblasts, U138 cancer cells, Ntera cells (ATRX+ and ATRX-) and Hela cells (ATRX+ and ATRX-), cells were cultured in 6 well plates (35-mm dish) in the presence of G-quadruplex ligand (RHPS4). IMR90 and U138 cells were treated with different concentrations of RHPS4 (1 μ M, 2 μ M, 3 μ M & 4 μ M) for 24 hours and 4 days. Ntera cells (ATRX+ and ATRX-) were treated with a different range of RHPS4 concentrations. Ntera cells treated with 1 μ M of RHPS4 for 24 hours were chosen for DNA extractions and STELA. 5 μ M of RHPS4 for 24 hours treatment was chosen for Hela cells (ATRX+ and ATRX-). Cells were collected for DNA extraction, allowing detailed analysis of telomere dynamics with STELA.

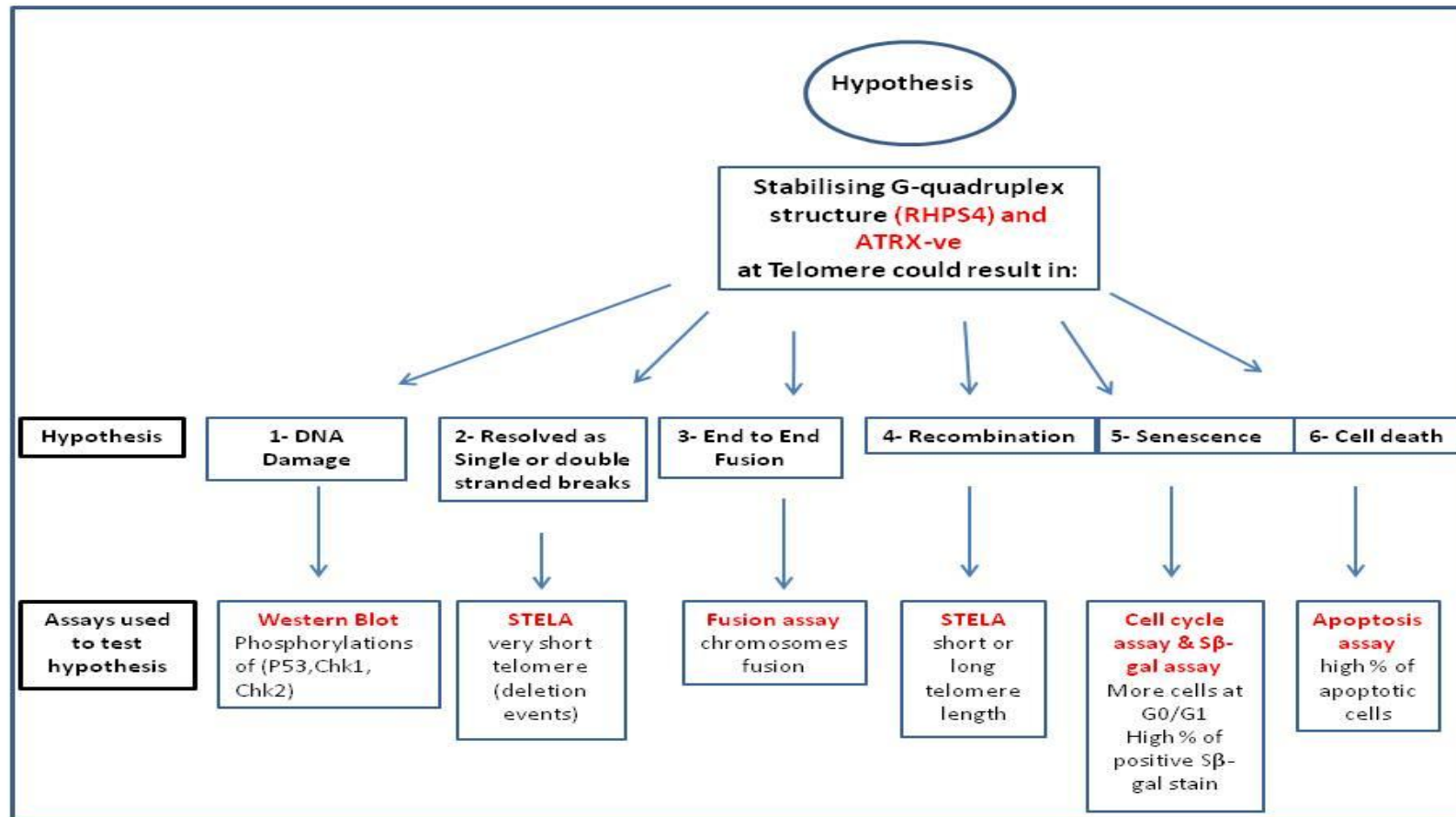


Figure 5.3 Illustrating the hypothesis, plan and the assays that have been used in this chapter.

5.4 Result

5.4.1 Effects of G-quadruplex Stabilisation on Cell Proliferation

In order to monitor the effects of G-quadruplex stabilisation on cellular proliferation of IMR90 fibroblasts and Ntera cells (ATRX+ and ATRX-) cells were seeded in 6 well plates (35-mm dish). 24 hours after plating IMR90 cells, increasing concentrations of freshly dissolved RHPS4, ranging from 1 μ M to 4 μ M, were added to the culture medium and left for 4 days. Then, the drug was released and fresh medium was added and cells left for an additional 6 days. Cell counts were determined daily, from day 1 to day 10 of culture and PD was calculated as shown in figure 5.4.

The data showed that the growth rate of IMR90 fibroblasts in standard culture conditions was determined as 0.255 PD/day. Whereas, the RHPS4 treated IMR90 cells exhibited lower growth rate compared to normal control fibroblasts. The reduction in growth rate was inversely proportional to the concentration of RHPS4, with 0.112 PD/day achieved for cells treated with 4 μ M and 0.163 PD/day for those treated with 3 μ M (Figure 5.4).

To examine the contribution of ATRX protein in resolving G-quadruplex structures, Ntera ATRX+ and Ntera ATRX- cells were exposed to 0.2 μ M, 1 μ M and 5 μ M of RHPS4 for 24 hours. Then, drug was released, fresh medium was added and cells left in culture. Following 24 hours of exposure to 5 μ M RHPS4, ~95% of Ntera cells ATRX- had died, floated and detached from the plate. Whilst in 1 μ M of RHPS4, Ntera ATRX- cells lived longer, ~2 to 3 days after drug released. Furthermore, they lived in culture nearly 21 days following drug released of 0.2 μ M RHPS4. In contrast Ntera ATRX+ cells were more resistant to RHPS4 and displayed cellular proliferation following drug released of different concentrations that have been used.

Ntera cells (ATRX+ and ATRX-) treated with 0.2 μ M of RHPS4 24 hours were passaged serially after treatment and the average of population doublings (PDs) was calculated and plotted in figure 5.5.

The growth rate of Ntera ATRX+ was determined to be on average of 5.77 PD/day after treatment with 0.2 μ M of RHPS4. Interestingly, after day 5 of recovery, Ntera ATRX+ cells resumed their ability to proliferate. Whilst, Ntera cells (ATRX-) displayed lower growth rate (0.0132PD/day) compared to (ATRX+).

These data indicate that the ATRX -ve cells exhibit a specific sensitivity to the G-quadruplex stabilising ligand RHPS4.

Figure 5.4: PDs of IMR90 cells (RHPS4)

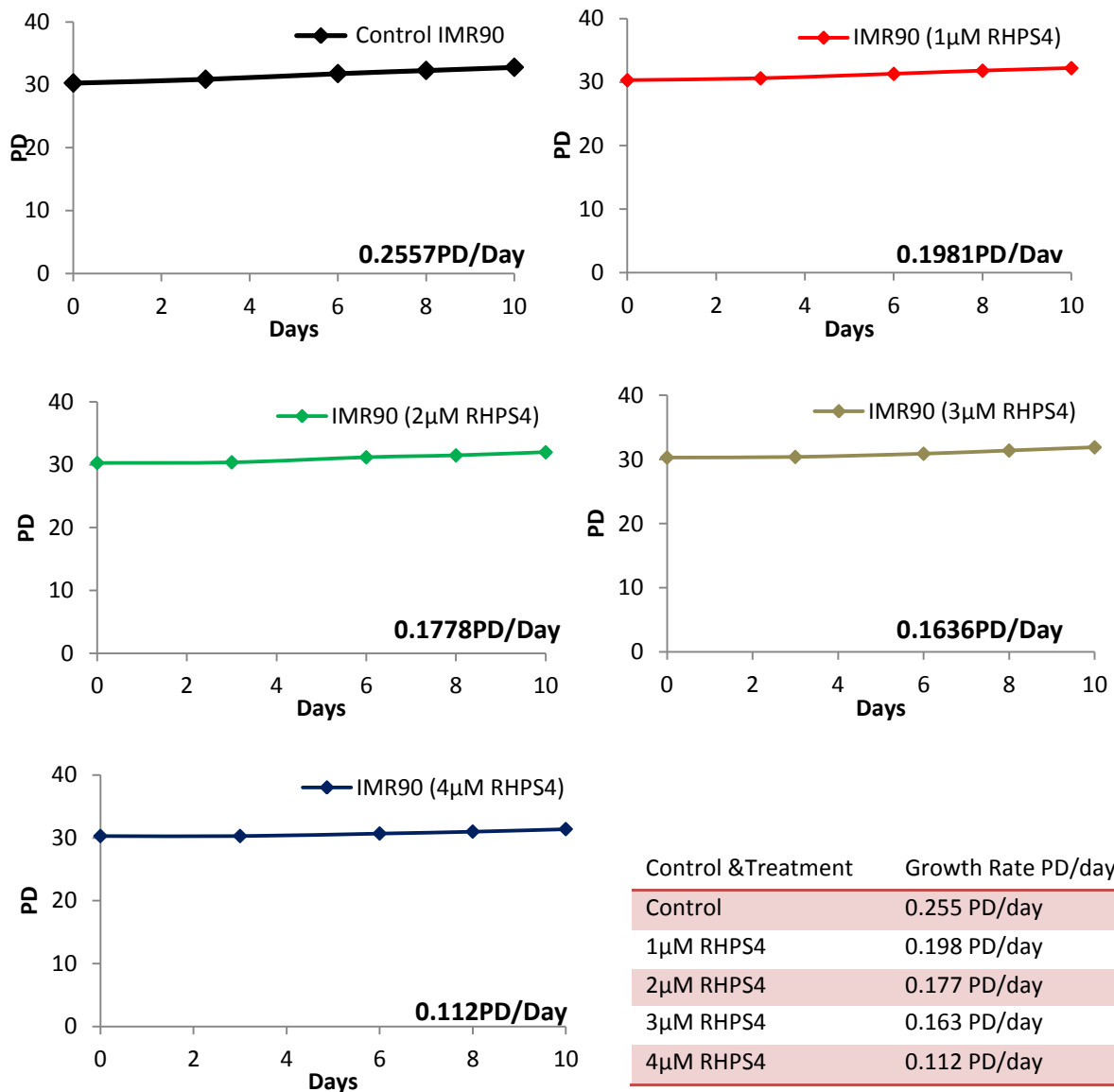
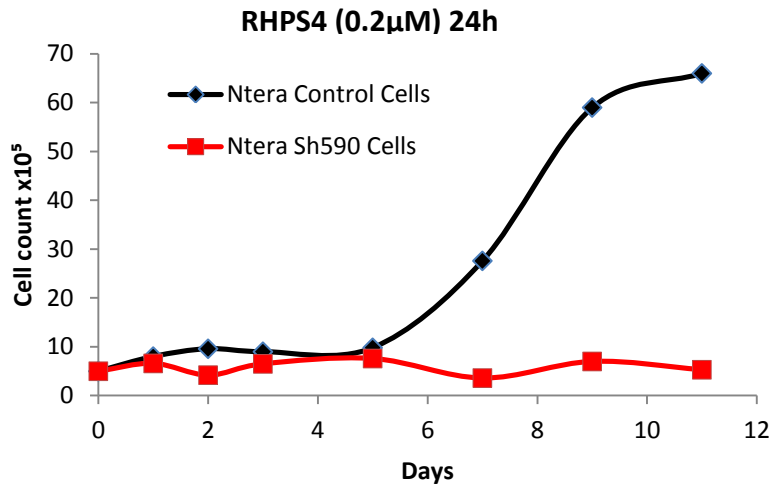


Figure 5.4: Growth curves of IMR90 cells. IMR90 cells were cultured at PD 30.3, control (untreated) (Black Line) and (treated) with different concentrations of RHPS4 (1µM (Red Line), 2µM (Green Line), 3µM (Gray Line) & 4µM (Blue Line)) for 4 days. Plotting growth curves as function of population doublings (PD) versus time in days.

Figure 5.5: PDs of Ntera cells Control (ATRX+) and Sh590 (ATRX-) (RHPS4)



Ntera Cells	Growth Rate PD/day
Ntera cells ATRX+ (RHPS4)	5.77 PD/day
Ntera cells ATRX- (RHPS4)	0.0132PD/day

Figure 5.5: Growth curves of Ntera cells ATRX+ and ATRX-. Ntera control (ATRX+) (Black Line) and (ATRX-) (Red line) were Treated with RHPS4 (0.2μM) (24 hours). Ntera ATRX- cells lived up to ~21 days following drug released. Ntera ATRX+ was more resistant to RHPS4 than Ntera ATRX- cells.

5.4.2 Effects of G-quadruplex Stabilisation on Cell Cycle Progression

In order to investigate the effects of G-quadruplex stabilisation on cell cycle progression and the role of ATRX protein in modulating this structure, cell cycle assay was carried out in Ntera cells (ATRX+) and was compared to Ntera cells (ATRX-). Cell cycle progression was investigated in Ntera cells (ATRX+) and (ATRX-) after 24 hours of 1 μ M RHPS4 treatment (AT) and after 24 hours of recovery (figure 5.6). Cells were collected and fixed in cold 70% ethanol, washed with cold PBS and stained with Propidium Iodide (PI). The percentage of cells in the different phases of cell cycle was analysed by flow cytometry.

As shown in figure 5.6, both Ntera (ATRX+) and (ATRX-) cells post one day treatment of RHPS4, showed an accumulation in G0/G1.

Following drug release the cells were incubated for 24 hours with fresh medium and harvested (Day Recovery) and their cell cycle profile was analysed. These data showed that Ntera (ATRX+) had recovered and progressed through the cell cycle with higher numbers of cells at G2/M and S phases. On contrast, Ntera Sh590 (ATRX-) cells remained accumulated at G0/G1.

Figure 5.6: Cell cycle of Ntera cells Control (ATRX+) and Sh590 (ATRX-) (RHPS4)

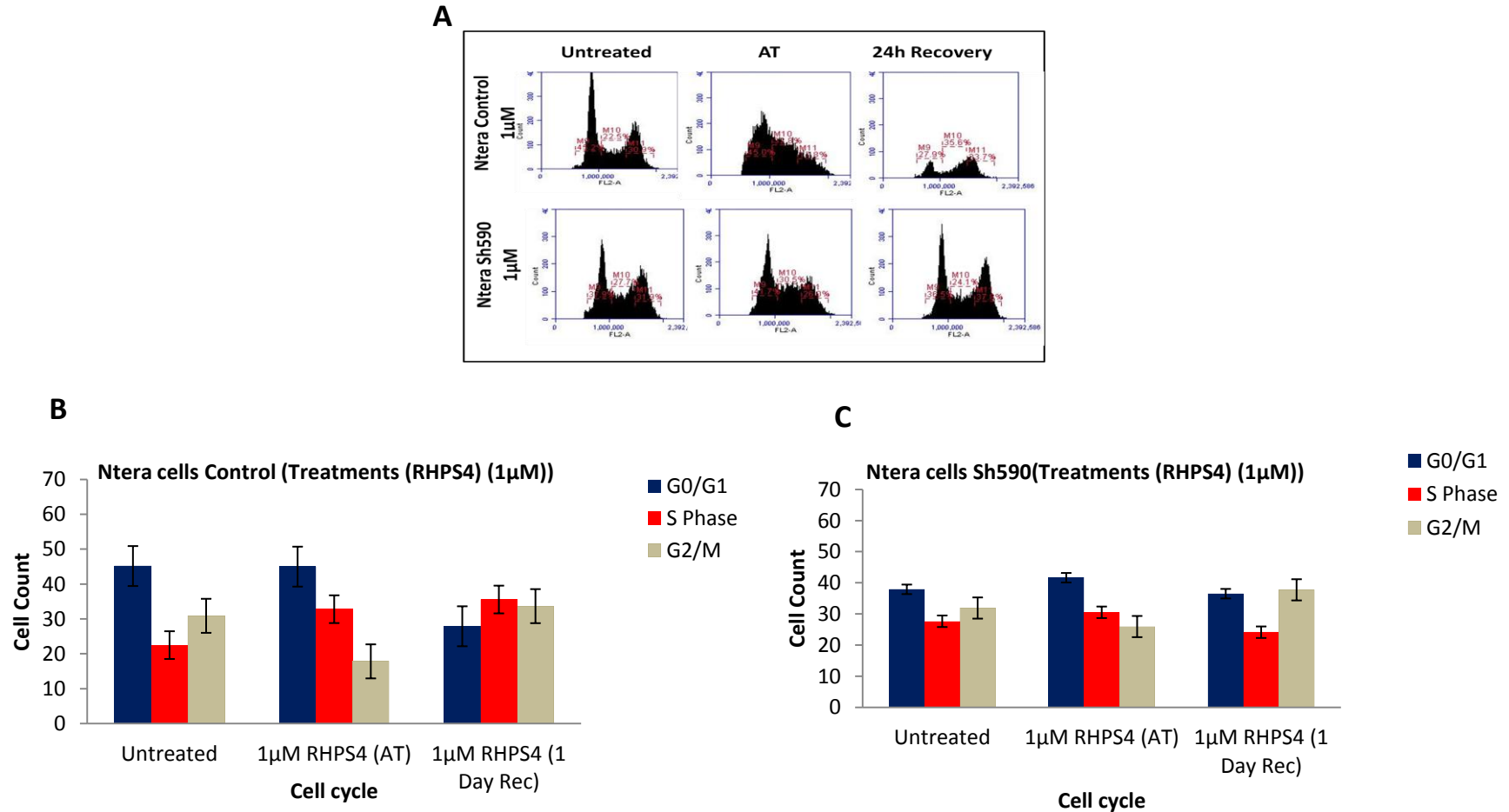


Figure 5.6: Cell cycles of Ntera cells. (A) Ntera control cells were compared to Ntera Sh590 cells. Cells were treated with RHPS4 (1µM). Cell cycle progression was investigated after 24h of (1µM) treatment (AT) and 24h of recovery. As shown Ntera control **(B)** and Sh590 cells **(C)** after adding RHPS4 (AT), cells were accumulated at G0/G1, after drug release (1 Day Recovery) Ntera control cells were progressed through the cell cycle and high numbers of cells were at S phases and G2/M, cells resume their ability of division whereas Ntera Sh590 cells were accumulated at G0/G1. Error bars represent standard error (SE). G0/G1, S and G2/M fraction was calculated by flow cytometry.

5.4.3 Cellular Morphology and Senescence Associated Beta galactosidase Activity (SA β -gal)

In order to examine the impact of G-quadruplex formation on the cellular senescence, morphological changes were tracked in IMR90 fibroblasts, U138 cancer cells and Ntera (ATRX+) and Ntera (ATRX-) cells treated with RHPS4. Cells were compared to their controls under microscope (X20) and pictures were taken regularly (Figure 5.7).

Treated IMR90 fibroblasts changed their morphology becoming larger with a flattened cytoplasm and had bigger nuclei compared to the untreated. These features are consistent with cells undergoing cellular senescence (Toussaint *et al.*, 2000). Moreover, high number of floating cells, dead cells or affected cells were detached from dish, was observed in treated Ntera cells (ATRX+) and (ATRX-) and U138 cells compared to untreated. For those treated cells left in the dishes, stressed cells were observed following treatment directly (Figure 5.7).

Senescence-associated β -galactosidase assay was used to investigate cellular senescence induction in IMR90 cells and U138 cancer cells. Senescent cells were determined by counting 500 cells and the proportions of positive cells were given as percentages of the total counted cells. It was observed that treated (IMR90) cells had higher percentages of activation of senescence-associated β -galactosidase enzyme compared to untreated. This can be clearly seen from the result in figure 5.8. In contrast U138 cells, as tumour cells and P53 deficient cells, no detectable senescence-associated β -galactosidase activity.

Figure 5.7: Cellular Morphology of IMR90, U138 & Ntera cells (ATRX+ and ATRX-) (RHPS4)

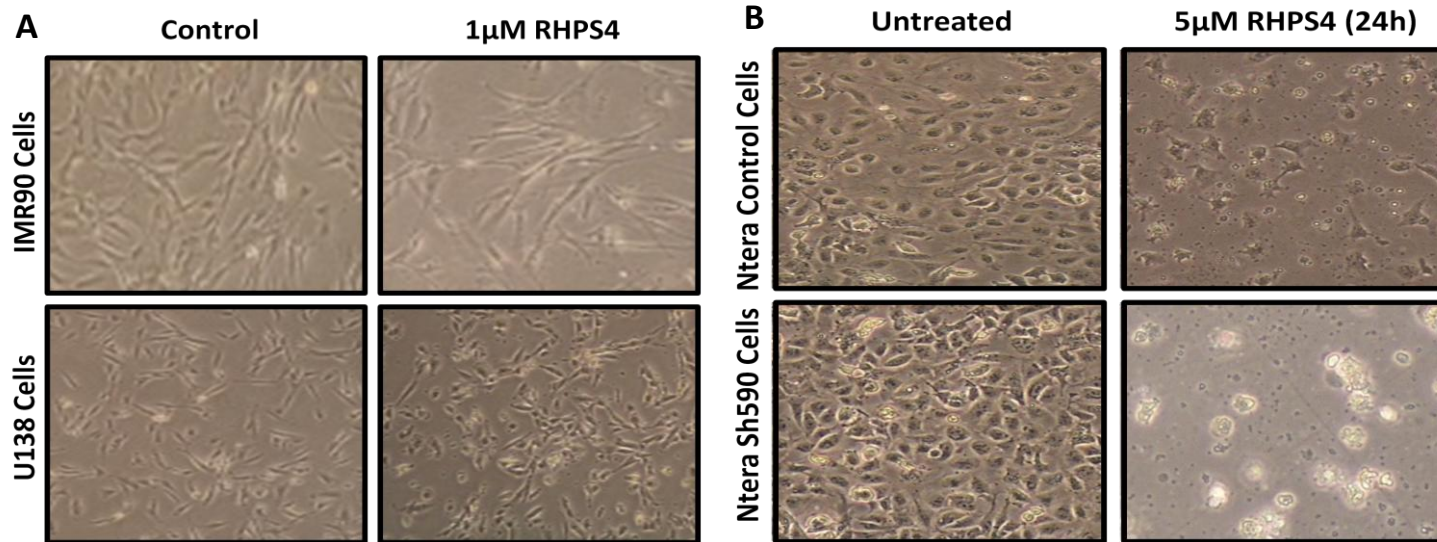


Figure 5.7: Cellular Morphology of IMR90, U138 & Ntera (ATRX+ and ATRX-) Cells. IMR90 and U138 cells (A) were treated with 1 μM of RHPS4 for 24h, morphological changes were monitored and treated cells were compared to the control. Ntera cells ATRX+ and ATRX- (B) were treated with 5 μM of RHPS4 for 24h and were compared to untreated cells.

Figure 5.8: Senescence-Associated β -galactosidase Activity of IMR90 Cells (RHPS4)

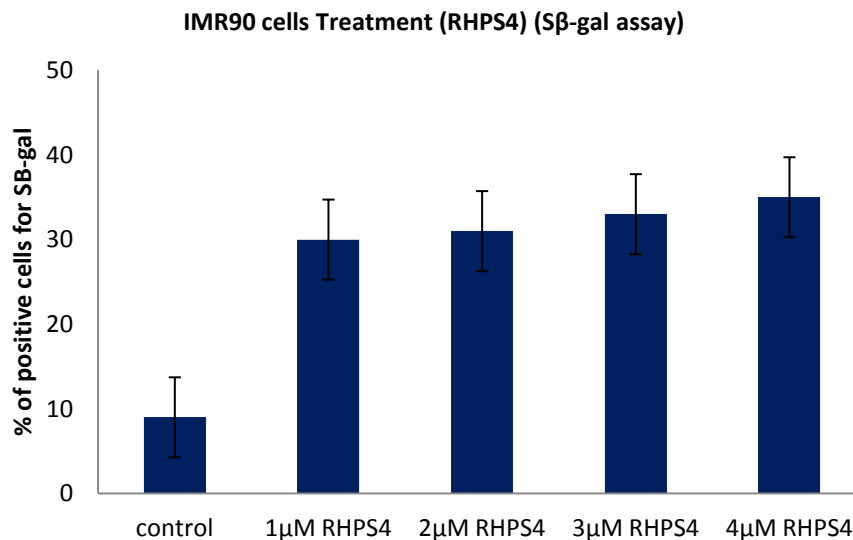


Figure 5.8: The quantification of senescence-associated β -gal-positive for IMR90 cells of total counted 500 cells. Percentage of senescent IMR90 cells treated with 1µM, 2µM, 3µM & 4µM of RHPS4 were compared to the percentage of senescent control cells. $S\beta$ -gal assay was determined by counting positive stained cells under microscope (X20). The proportions of positive cells were given as percentages of the total counted cells. Error bars represent standard error (SE).

5.4.4 G-quadruplex Stabilisation and Cellular Apoptosis

In order to test the impact of G-quadruplex stabilisation on the induction of cellular apoptosis, Ntera cells (ATRX+) and (ATRX-) were cultured in the presence of 5 μ M of RHPS4. Cellular apoptosis assays were carried out in cells (cells treated one hour then left one hour in fresh medium following drug released) and (cells treated six hours then left six hours in fresh medium) (Figure 5.9). Cultured cells were trypsinised, fixed and stained with Propidium Iodide (PI) and the apoptotic cells fractions were determined by flow cytometry. The number of apoptotic cells increased following exposure to RHPS4 in both Ntera cells (ATRX+) and (ATRX-). One hour post-treatment, the apoptotic cell fraction had slightly increased to 1.25% in the Ntera (ATRX+) compared to 1.20% apoptotic cells in untreated Ntera ATRX+. This percentage was higher in treated Ntera cells (ATRX-) at 6.25% and compared to the untreated cells 3.18%. The apoptotic cells increased dramatically following 6 hours exposure to the drug with the apoptotic cell fraction of Ntera ATRX- cells was 37.5% whilst Ntera ATRX+ cells were 9.9%.

These data further show that the absence of ATRX sensitises Ntera cells to treatment with RHPS4.

Figure 5.9: Apoptosis Assay of Ntera cells Control (ATRX+) and Sh590 (ATRX-) (RHPS4)

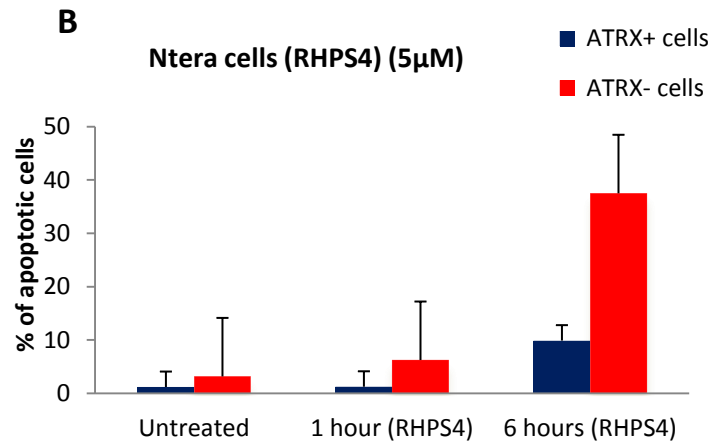
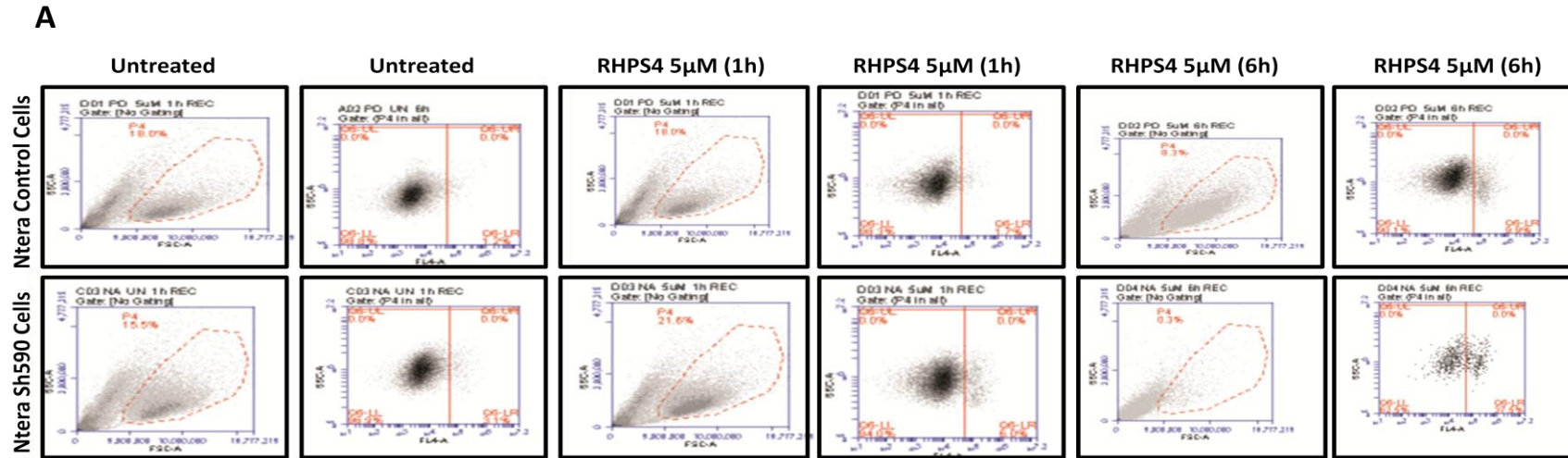


Figure 5.9: Apoptosis Assay of Ntera cells ATRX+ and ARX-. (A)

Apoptosis assay was carried out in Ntera cells ATRX+ and ATRX- treated with 5μM RHPS4 for 1 hour and 6 hours. **(B)** Bar chart display percentage of apoptotic cells (Blue bar represent Ntera ATRX+) (Red bar represent Ntera ATRX-). The proportions of apoptotic cells were calculated by flow cytometry. Error bar represent SE.

5.4.5 Checkpoint Activation

In order to investigate the effect of G-quadruplex stabilisation on key proteins involved with cell cycle checkpoint activation, Ntera cells (ATRX+) and (ATRX-) were treated with 1 μ M of RHPS4 24 hours, protein extracts were obtained for western blot analysis directly after 24 hours of treatment and 24 hours following drug release. The treated Ntera cells (ATRX+) and (ATRX-) were compared to untreated as shown in figure 5.10.

The phosphorylation status of checkpoint proteins was determined using antiphospho Chk1 Ser345, antiphospho Chk2 Thr68 and antiphospho P53 Ser15 antibodies.

The Western blot analysis showed that Chk1, Chk2 and P53 were phosphorylated following exposure to RHPS4 in the Ntera cells (ATRX+). These data indicate that DNA damage checkpoints proteins were activated following drug exposure.

In contrast the Ntera cells (ATRX-), both Chk2 and P53 but not Chk1 were phosphorylated following of 24 hours of treatments. The phosphorylation of both Chk2 and P53 in Ntera ATRX- remained high even 24 hours following drug release.

Figure 5.10: DNA damage Checkpoint Activation in Ntera cells ATRX+ and ATRX-

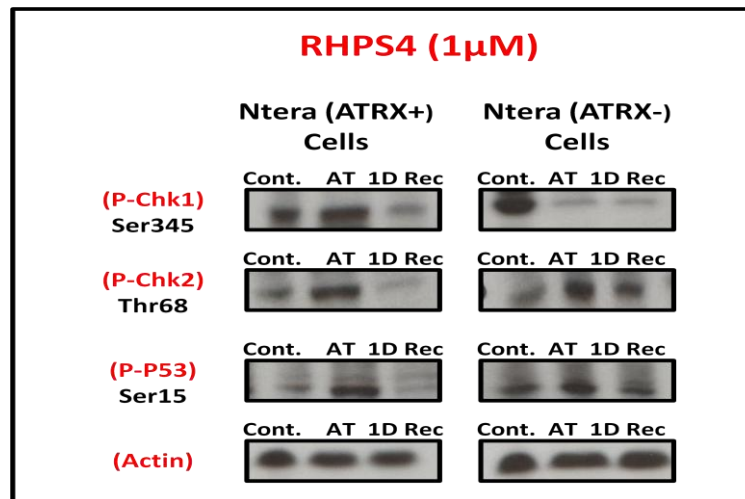


Figure 5.10: DNA damage Checkpoint Activation in Ntera cells ATRX+ and ATRX-. Ntera cells treated with 1 μ M RHPS4 for 24h of treatment and one day of recovery. Equal loading was confirmed by probing with Actin specific antibody.

5.4.6 Analysis of Telomere Dynamics

In order to examine if the stabilisation of G-quadruplexes in the G-rich telomeric strand results in large-scale changes to telomere length, the XpYp telomere length distributions of IMR90, U138 cells, Ntera cells ATRX+, Ntera ATRX- and HeLa cells ATRX+ and ATRX- exposed to RHPS4 were investigated. The role of ATRX in overcoming the effect of such structure was also examined.

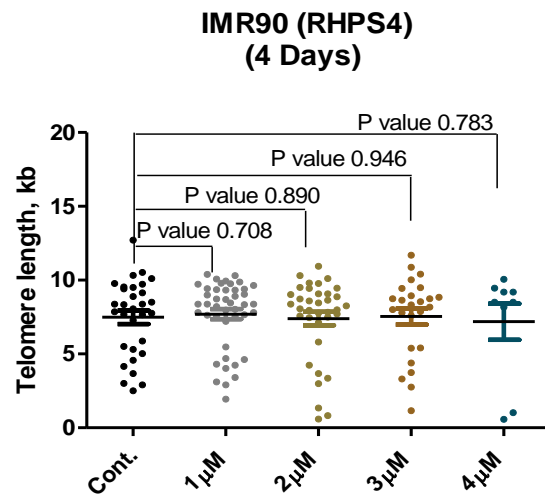
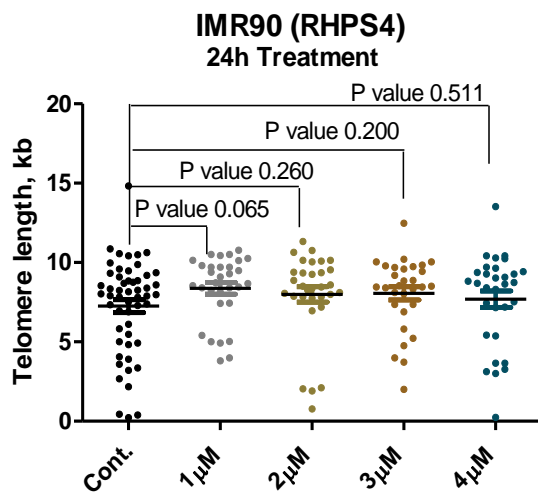
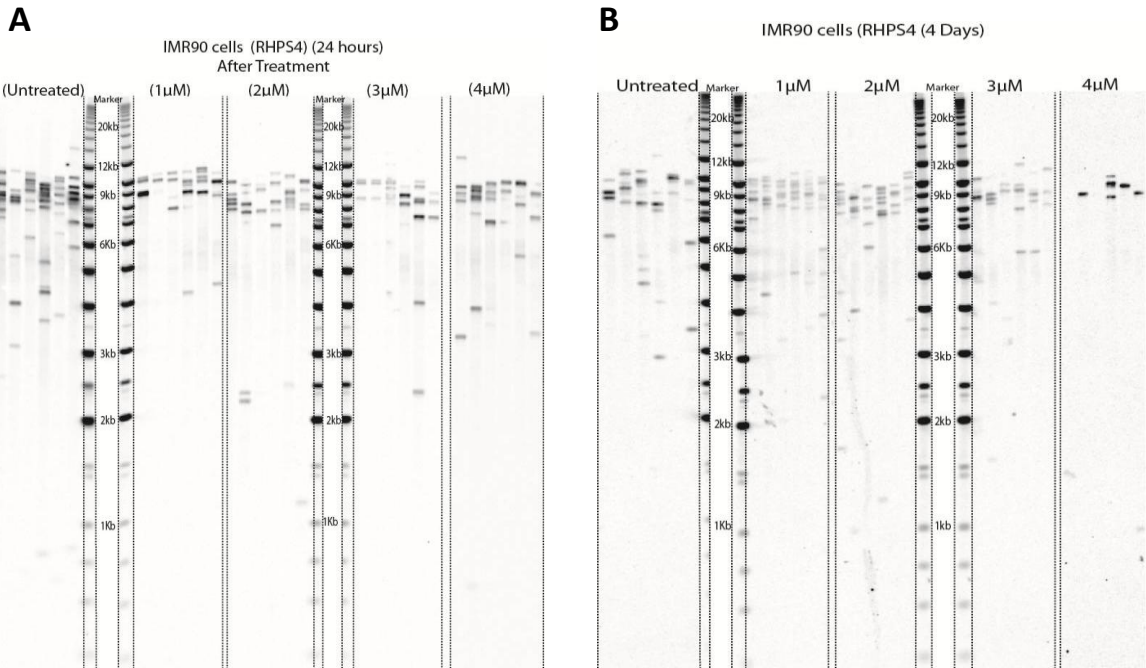
Single telomere length analysis (STELA) was used to track the telomere dynamics with ongoing cell division and to detect the presence of short stochastically deleted telomeres (Baird *et al.*, 2003). STELA for the experiment are shown in figures 5.11, 5.13, 5.15, 5.16 and 5.19.

We have observed that both control and treated IMR90 fibroblasts figures (5.11 and 5.12) displayed uni-modal distributions at the XpYp telomere.

IMR90 fibroblasts showed no significant differences in mean telomere length between treated and untreated cells (figure 5.11). Moreover, the frequencies of short telomeres (below 5 Kb) (figure 5.12) following one day exposure to RHPS4 were lower at treated IMR90 fibroblasts than the control cells. IMR90 fibroblasts treated with 1 μ M of RHPS4 had 9.67% of short telomere frequency, lower than 22.67% of control cells. On the other hand, post-four days treatment, treated cells had more frequencies of short telomere compared to the control. IMR90 fibroblasts treated with 4 μ M of RHPS4 had 22.22% of short telomere frequency, more than 19.35% of control cells. Moreover, IMR90 cells treated with 2 μ M of RHPS4 following one day exposure to drug had 12.90% of short telomere frequency while following 4 days of treatment the frequency increased to reach 19.44%.

Taken together these data indicate that that treatment of IMR90 cells with RHPS4 does not modulate telomere dynamics, either for overall mean telomere length or for the frequency of telomeric deletion events.

Figure 5.11: STELA of IMR90 XpYp Telomere (RHPS4)



RHPS4 (24h)	Untreated	1 μ M	2 μ M	3 μ M	4 μ M
Mean	7.253	8.374	7.986	8.058	7.69
SD	2.95	2.04	2.69	2.27	2.90
SE	0.41	0.37	0.48	0.41	0.52

RHPS4 (4Days)	Untreated	1 μ M	2 μ M	3 μ M	4 μ M
Mean	7.48	7.699	7.39	7.53	7.19
SD	2.58	2.29	2.73	2.70	3.67
SE	0.46	0.35	0.45	0.54	1.22

Figure 5.11: STELA gels of XpYp telomere in the IMR90 untreated and treated with RHPS4 (1 μ M), (2 μ M), (3 μ M) and (4 μ M) for 24 hours treatments (A) and 4 days treatments (B), the tables of descriptive data for telomeres. The gels illustrate the telomere length distributions while the tables give the mean, standard deviations (SD), standard error (SE). Dot Plot made in (Prism) represent dot plots (Telomere length distributions) from the gels, were quantified using Phortetix software, then they were compared (control and treated samples) and p value was calculated using t-test in Prism (P value in Red is Significant) (in Black is NS).

Figure 5.12 Short telomere frequency of IMR90 XpYp (under 5kb)

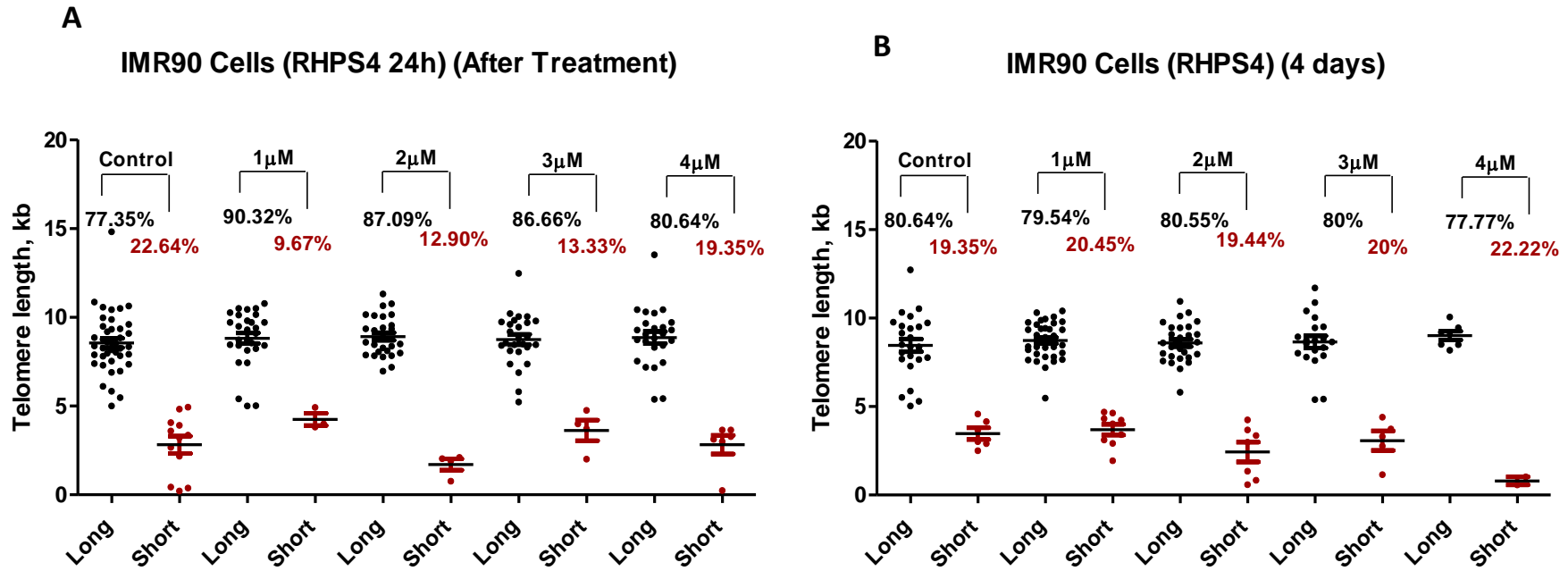
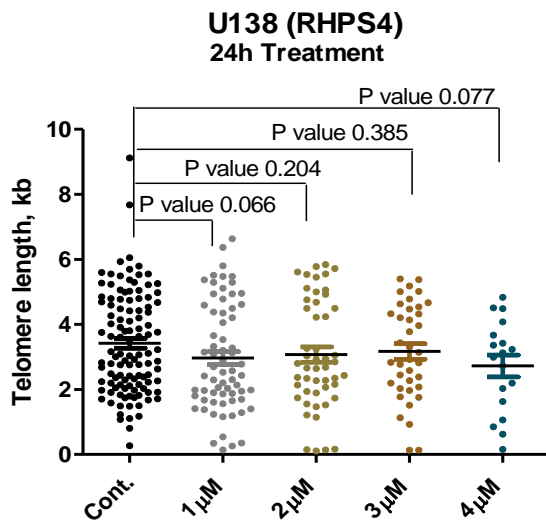
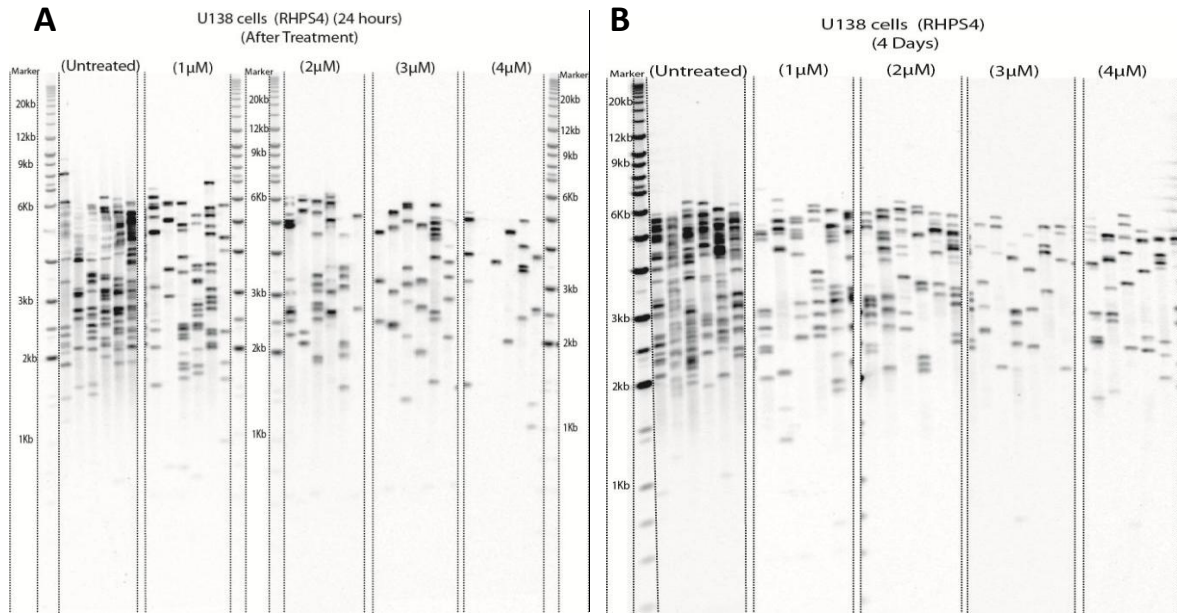


Figure 5.12: Short XpYp telomere frequency in IMR90. Long telomeres (BLACK DOTS) compared to short telomeres (under 5kb) (RED DOTS) for untreated and treated cells with RHPS4 (1μM), (2μM), (3μM) and (4μM) for 24 hours treatment (A) and 4 days treatment (B).

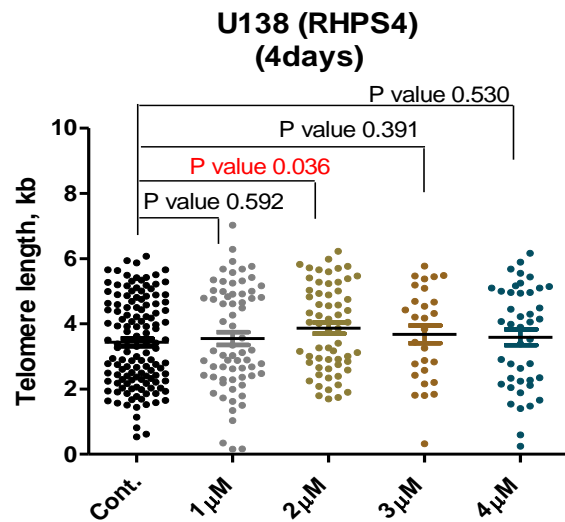
U138 cancer cells displayed a significant difference (p value 0.036) in mean telomere length following 4 days of 2 μ M RHPS4 treatment compared to untreated U138 cells (Figure 5.13). The mean telomere length was longer at treated U138 cells. Furthermore, the frequencies of short telomeres (Figure 5.14) (below 2 Kb) following one day exposure to RHPS4 were higher in treated U138 than the control cells. U138 cancer cells treated with 1 μ M of RHPS4 had 37.31% of short telomere frequency, more than 20.35% of control cells. On the other hand, post-four days treatment, treated U138 cells with 2 μ M had lower frequency of short telomeres (8.19%) compared to the control (15.78%).

As observed with IMR90, the subtle differences observed in the telomere length distribution in U138, are consistent with experimental variation. These data therefore indicate that RHPS4 treatment does not directly affect telomere length.

Figure 5.13: STELA of U138 XpYp Telomere (RHPS4)



RHPS4 (24h)	Untreated	1µM	2µM	3µM	4µM
Mean	3.418	2.963	3.074	3.167	2.72
SD	1.56	1.66	1.66	1.46	1.42
SE	0.15	0.20	0.24	0.24	0.33



RHPS4 (4Days)	Untreated	1µM	2µM	3µM	4µM
Mean	3.432	3.548	3.869	3.677	3.59
SD	1.36	1.60	1.31	1.45	1.57
SE	0.12	0.20	0.17	0.27	0.24

Figure 5.13: STELA gels of XpYp telomere in the U138 untreated and treated with RHPS4 (1µM), (2µM), (3µM) and (4µM) for 24 hours treatments (A) and 4 days treatments (B), the tables of descriptive data for telomeres. The gels illustrate the telomere length distributions while the tables give the mean, standard deviations (SD), standard error (SE). Dot Plot made in (Prism) represent dot plots (Telomere length distributions) from the gels, were quantified using Phortetix software, then they were compared (control and treated samples) and p value was calculated using t-test in Prism (P value in Red is Significant) (in Black is NS).

Figure 5.14 Short telomere frequency of U138 XpYp (under 2kb)

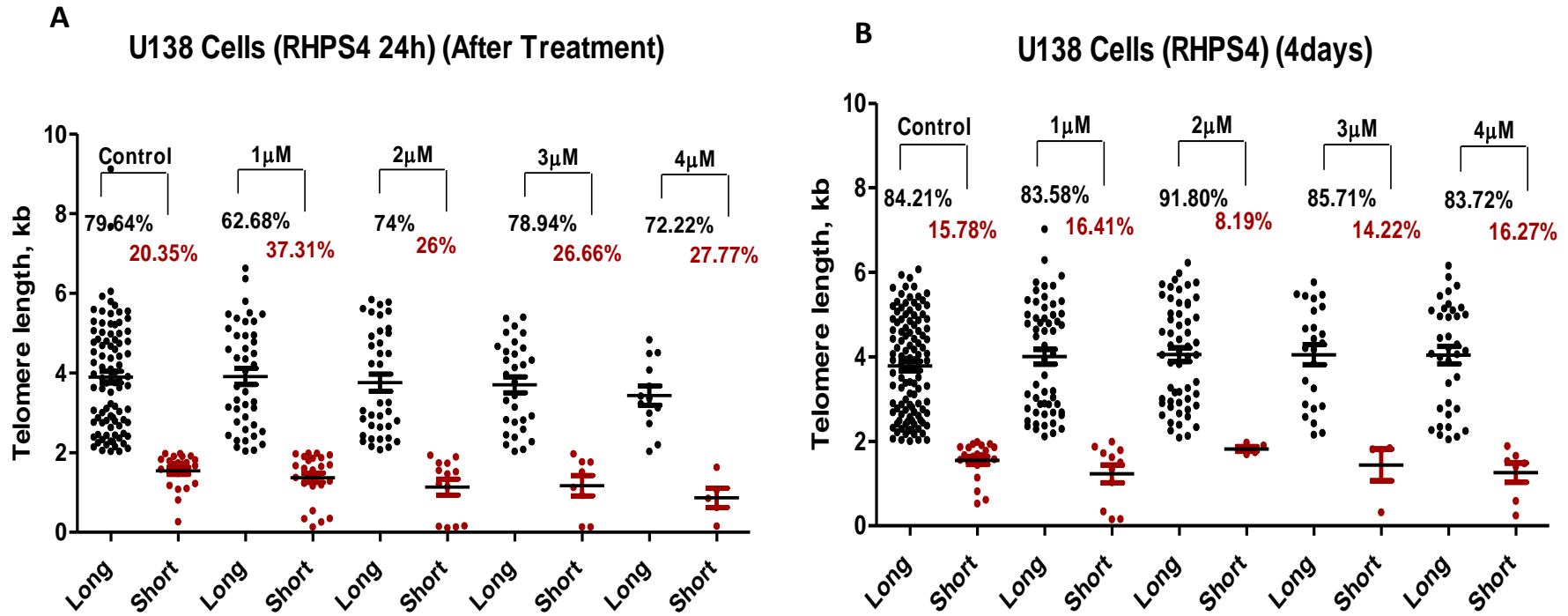
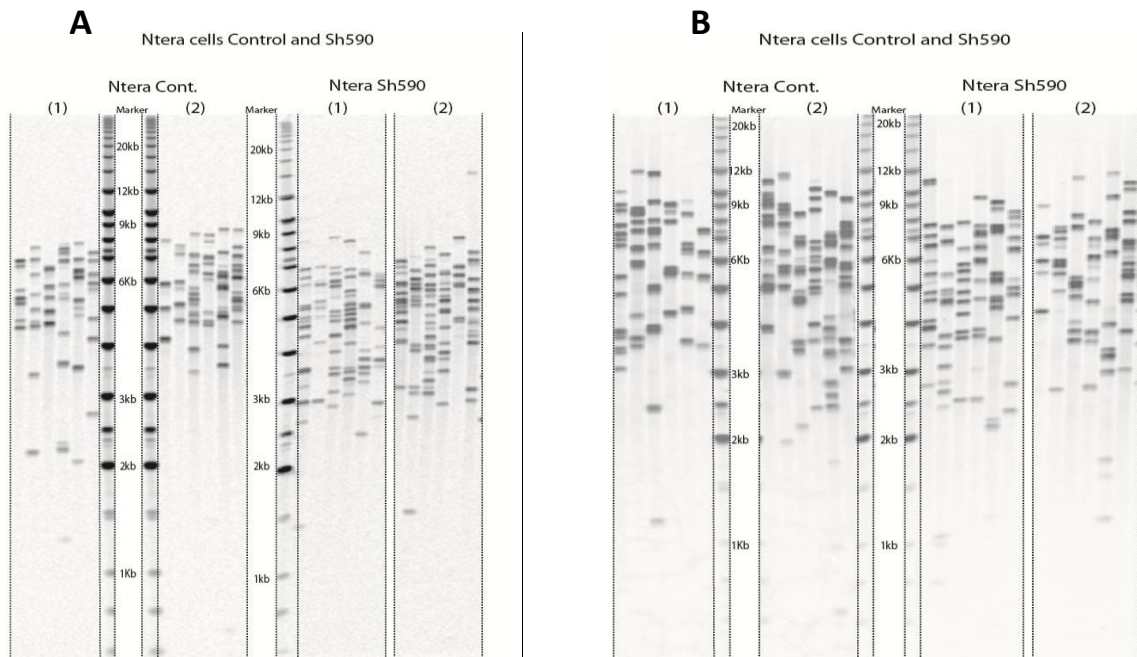


Figure 5.14: Short telomere frequency of U138 XpYp. Long telomere (BLACK DOTS) compared to short telomere (under 2kb) (RED DOTS) for untreated and treated cells with RHPS4 (1μM), (2μM), (3μM) and (4μM) for 24 hours treatments (A) and 4 days treatments (B).

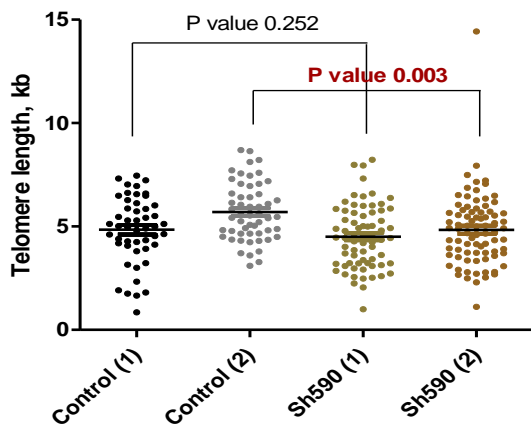
Previously, in our lab, a study was carried out in order to assess the role of ATRX in modulating telomere dynamics. Ntera, MRC5 fibroblasts, HeLa, MDA231, U138, U87, HT1080 and caski cells, were knocked down for ATRX by Dr. Maira Tanikmanova. Cells (ATRX-) were cultured for ~ 52 PDs in a parallel with controls (ATRX+). The study showed that XpYp and 17p STELA analysis revealed no significant difference in mean telomere length between ATRX+ve cells compared to ATRX-ve cells. Interestingly, following 2-3 PDs from ATRX Knockdown in Ntera cells, a significant difference in mean telomere length was observed between Ntera ATRX+ and Ntera ATRX- cells (Figure 5.15). However, this difference in mean telomere length disappeared following 5-10 PDs from ATRX knockdown. This is why Ntera cells were chosen for this study (combination of ATRX deficiency and G-quadruplex stabilisation).

Figure 5.15: STELA of Ntera Control (ATRX+) and Sh590 (ATRX-) XpYp & 17p

Telomere

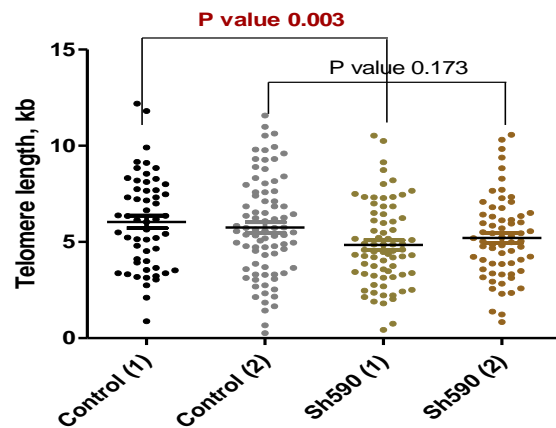


**Ntera cells (Control & Sh590)
(XpYp Telomere)**



Ntera Xp	Cont. (1)	Cont. (2)	Sh590 (1)	Sh590 (2)
Mean	4.843	5.698	4.510	4.837
SD	1.62	1.40	1.52	1.77
SE	0.23	0.19	0.18	0.20

**Ntera cells (Control & Sh590)
(17p Telomere)**



Ntera 17p	Cont. (1)	Cont. (2)	Sh590 (1)	Sh590 (2)
Mean	6.044	5.749	4.841	5.208
SD	2.42	2.56	2.15	2.12
SE	0.33	0.28	0.25	0.26

Figure 5.15: STELA gels of XpYp (A) and 17p (B) telomeres in the Ntera ATRX+ and ATRX- and the tables of descriptive data for telomeres. The gels illustrate the telomere length distributions while the tables give the mean, standard deviations (SD), standard error (SE). Dot Plot made in (Prism) represent dot plots (Telomere length distributions) from the gels, were quantified using Phortetix software, then samples were compared and p value was calculated using t-test in Prism (P value in Red is Significant) (in Black is NS). STELA gels and experiment were done by Dr. Maira Tankimanova.

We examined the effects of a combination G-quadruplex stabilisation and ATRX deficiency on telomere dynamics. Ntera and Hela (ATRX+) and (ATRX-) cells were cultured in the presence of RHPS4 for 24 hours.

No significant difference was observed in the mean telomere length in Ntera ATRX+ cells either following exposure to RHPS4 or after 5 days recovery (figure 5.16). Interestingly, the Ntera ATRX- cells displayed a significant difference in mean telomere length following 24 hours exposure to 1 μ M of RHPS4 compared to untreated ATRX- cells (Figure 5.16). The mean telomere length was longer at treated Ntera ATRX- cells (2.32kb) compared to untreated cells (2.07kb) with p value = 0.006. However, this significant difference in mean telomere length disappeared after 5 days of recovery.

The frequency of short telomeres (figure 5.17) (below 2 Kb) following 5 days of drug released in Ntera ATRX+ cells was higher in treated cells (38.68%) than the control cells (36.77%), although this difference did not reach the statistical significance (p value = 0.228). In the treated ATRX- cells, the short telomere frequency was lower than untreated post-treatment and post 5 days of recovery and these differences were not significant as well, p value was 0.597 and 0.684 respectively.

To examine if telomere dysfunction could be detected, telomere fusion assays were carried out in Ntera cells ATRX+ and ATRX-, no telomere fusion events could be detected (figure 5.18) either in Ntera cells ATRX+ or ATRX- cells.

Treated Hela cells did not display any change in telomere length compared to control either in ATRX+ or ATRX- cells (figure 5.19). Although, Hela cells were treated with higher concentration of RHPS4 (5 μ M) and Ntera cells treated with 1 μ M, Ntera ATRX- cells displayed

greater sensitivity to RHPS4 than HeLa ATRX- cells. The frequency of short telomere significantly increased in HeLa ATRX- following exposure to 5 μ M RHPS4 (figure 5.20) it was determined to be 20.66% compared to untreated HeLa ATRX- (6.77%).

Figure 5.16: STELA of Ntera Control (ATRX+) and Sh590 (ATRX-) XpYp Telomere (RHPS4)

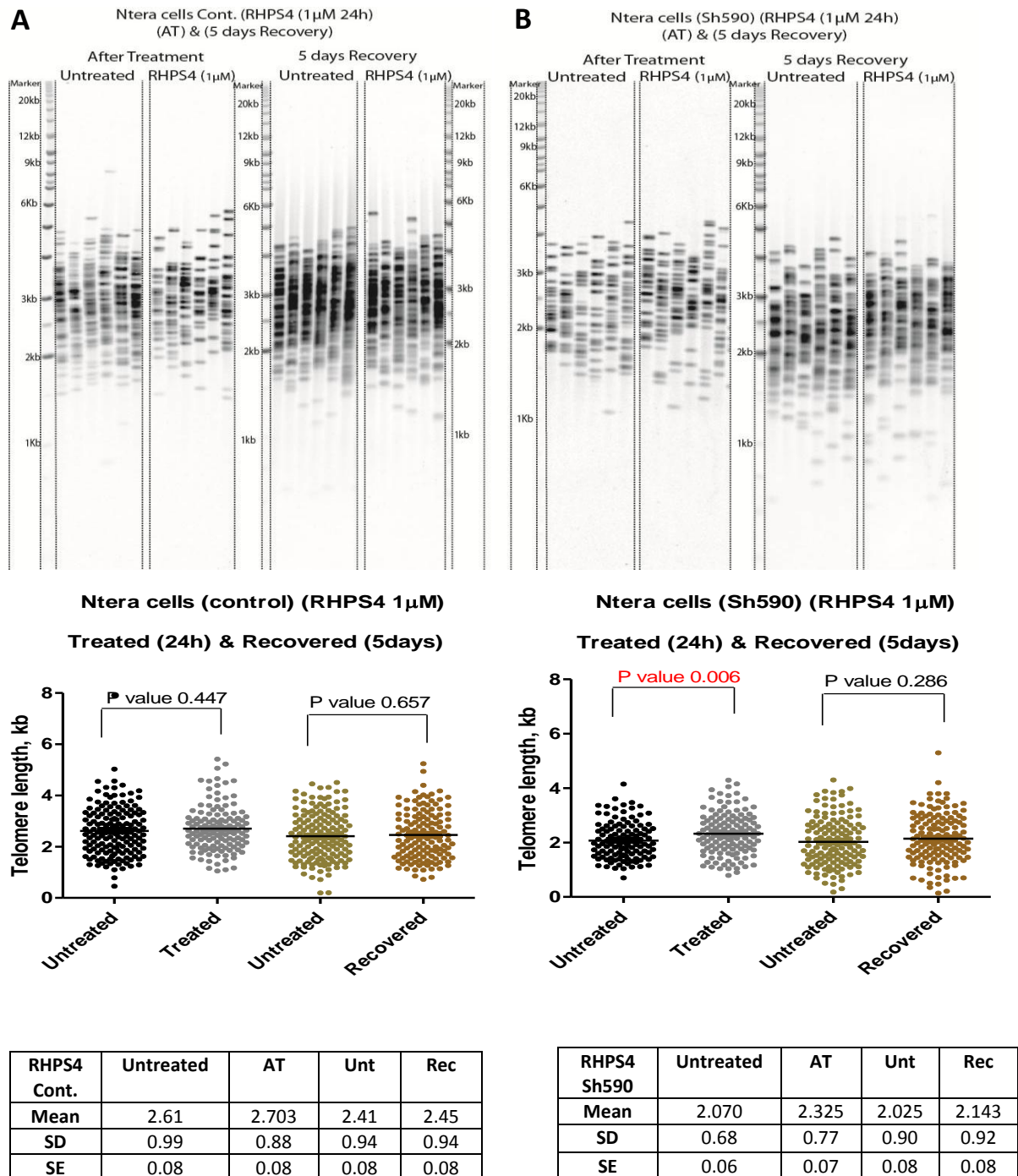


Figure 5.16: STELA gels of XpYp telomere in the Ntera (ATRX+) (A) and (ATRX-) (B) untreated and treated with RHPS4 (1µM) for 24 hours and 5 days of drug released and the tables of descriptive data for telomeres. The gels illustrate the telomere length distributions while the tables give the mean, standard deviations (SD), standard error (SE). Dot Plot made in (Prism) represent dot plots (Telomere length distributions) from the gels, were quantified using Phortetix software, then they were compared (control and treated samples) and p value was calculated using t-test in Prism (P value in Red is Significant) (in Black is NS).

Figure 5.17 Short telomere frequency of Ntera cells Control (ATRX+) and Sh590 (ATRX-) XpYp (under 2kb)

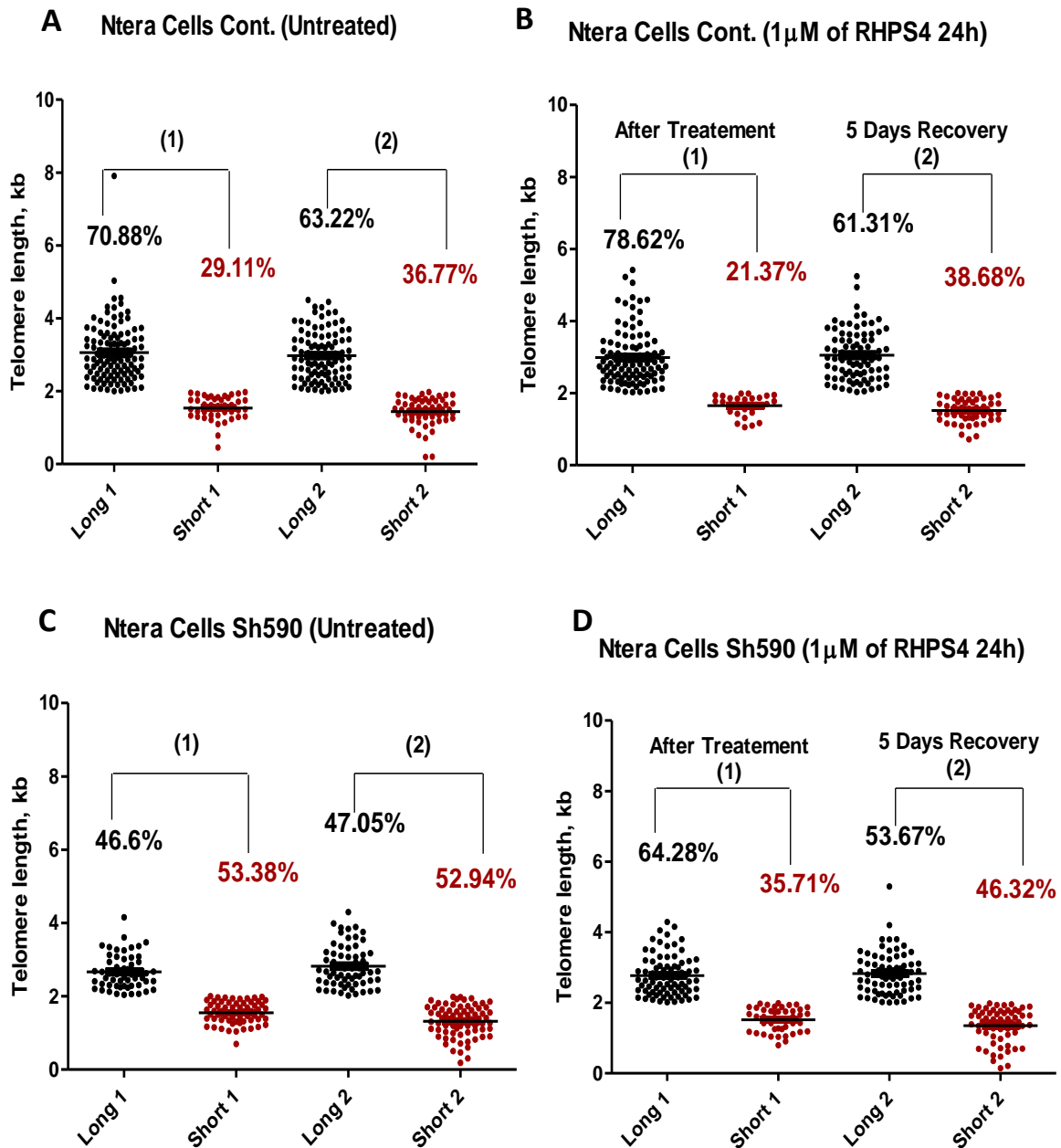


Figure 5.17: Short telomere frequency of Ntera cells Control (ATRX+) and Sh590 (ATRX-) XpYp (under 2kb). Long telomere (BLACK DOTS) compared to short telomere (under 2kb) (RED DOTS) for untreated and treated cells with RHPS4 (1 μ M). **A** Ntera ATRX+ cells untreated, **B** Ntera ATRX+ cells treated with RHPS4, **C** Ntera ATRX- cells untreated and **D** Ntera ATRX- cells treated with RHPS4.

Figure 5.18: STELA of Ntera (Control (ATRX+) and Sh590 (ATRX-) XpYp Telomere (RHPS4)

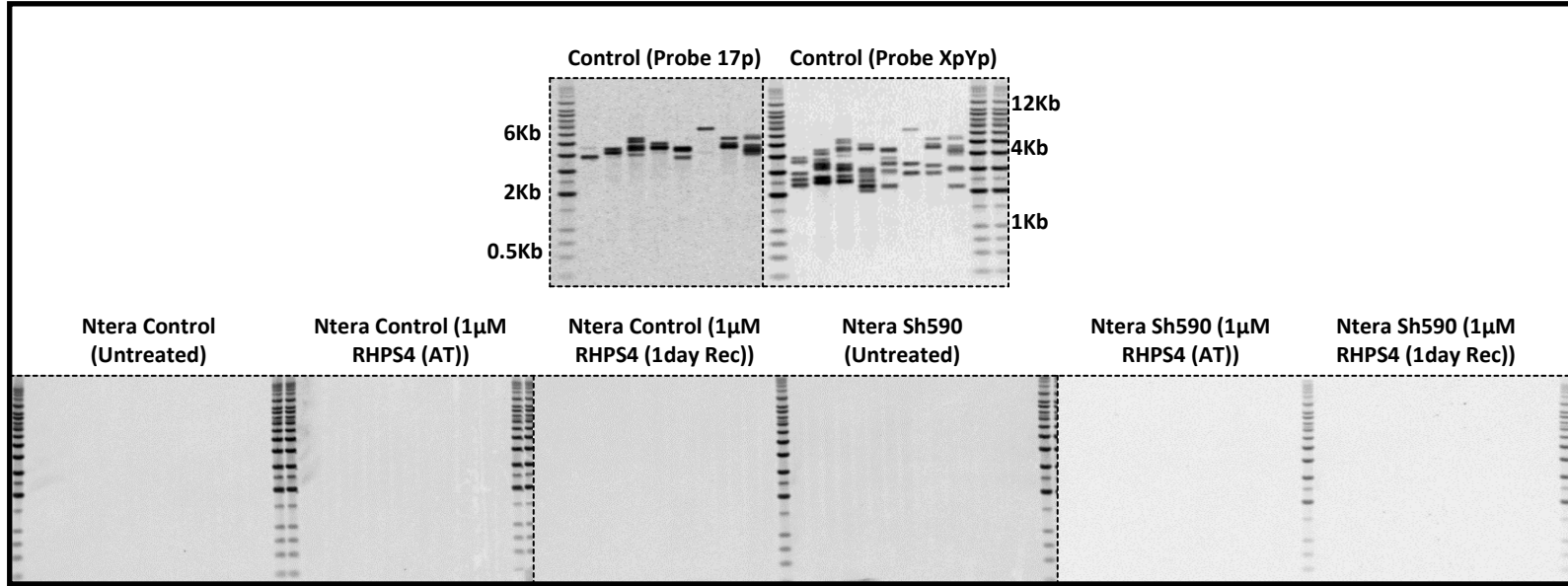
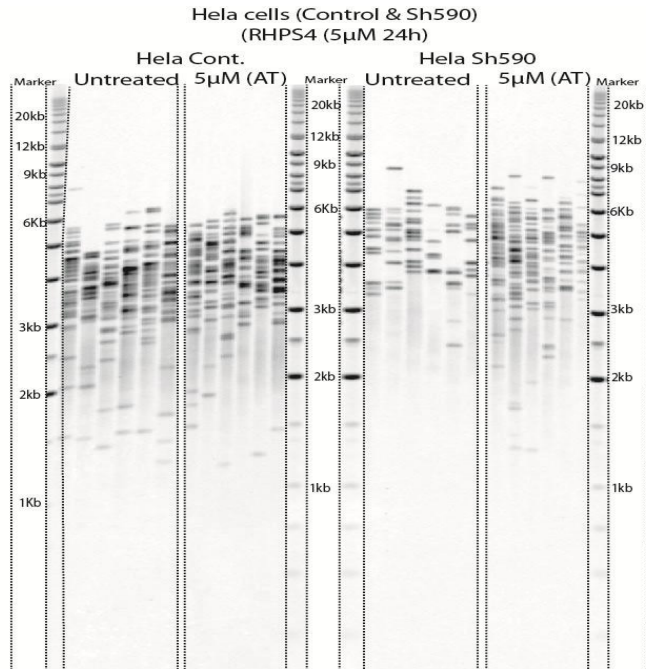
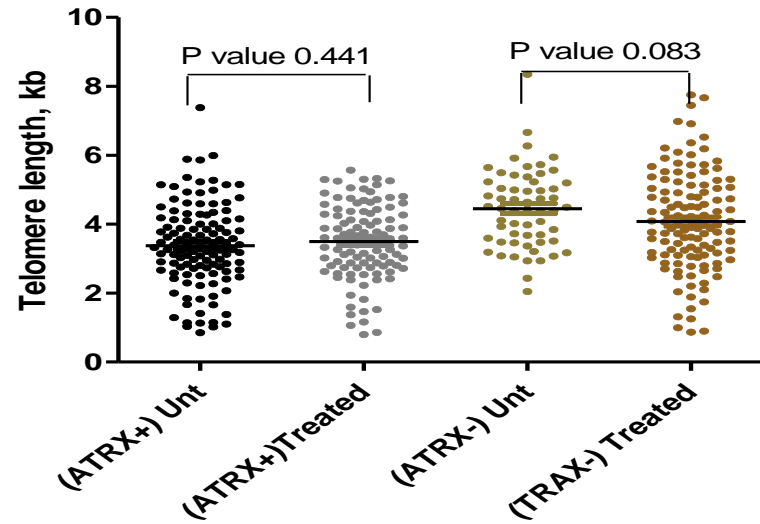


Figure 5.18 Fusion assays in Ntera cells Control (ATRX+) and Sh590 (ATRX-). HEK293 DNA that contains a high frequency of fusion events was used as positive control for the fusion assay. Molecular weight markers are identified on the left and right of the gels. Each reaction contains 50 ng of DNA and is detected by the xyp specific probe. The fusion frequency was 0% after treatment (AT) and 24 hours of drug released for both ATRX+ and ATRX- cells.

Figure 5.19: STELA of HeLa Control (ATRX+) and Sh590 (ATRX-) XpYp Telomere (RHPS4)



**Hela (Cont.) ATRX+ & (sh590) ATRX-
(RHPS4 5µM)
24h Treatment**



RHPS4 (24h)	Untreated Cont	AT Cont.	Unt ATRX-	AT ATRX-
Mean	3.375	3.495	4.450	4.079
SD	1.21	1.09	1.14	1.43
SE	0.11	0.11	0.15	0.13

Figure 5.19: STELA gels of XpYp telomere in the HeLa ATRX+ and ATRX- untreated and treated with RHPS4 (5µM) for 24 hours and the tables of descriptive data for telomeres. The gels illustrate the telomere length distributions while the tables give the mean, standard deviations (SD), standard error (SE). Dot Plot made in (Prism) represent dot plots (Telomere length distributions) from the gels, were quantified using Phortetix software, then they were compared (control and treated samples) and p value was calculated using t-test in Prism (P value in Red is Significant) (in Black is NS).

Figure 5.20 Short telomere frequency of HeLa cells Control (ATRX+) and Sh590 (ATRX-) XpYp (under 3kb)

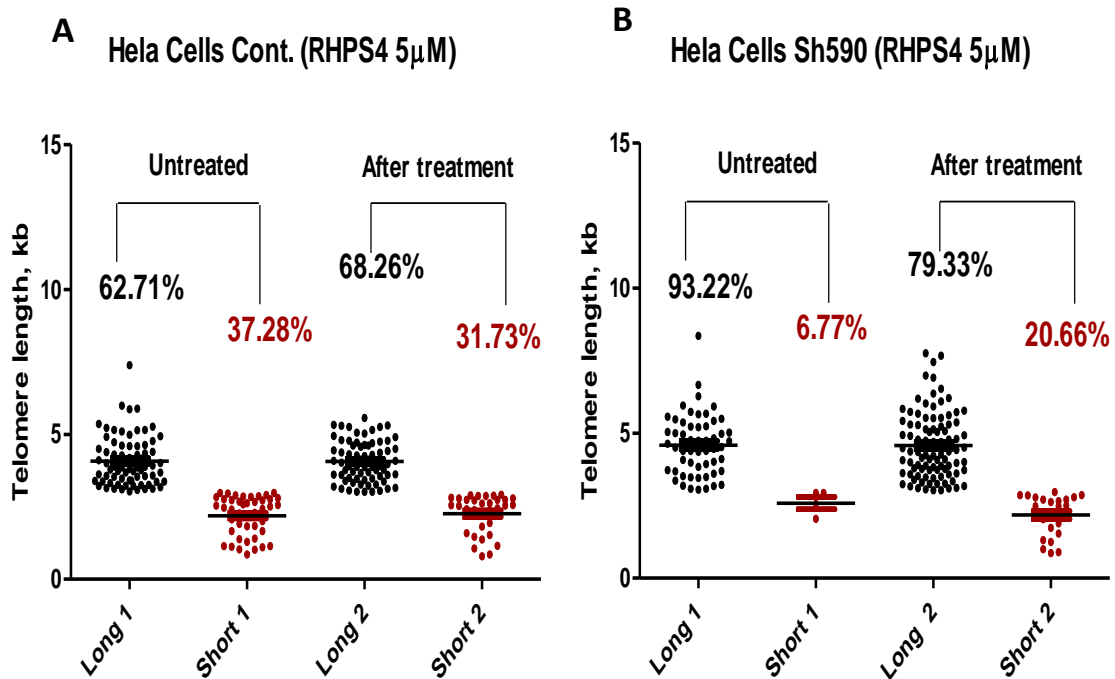


Figure 5.20: Short telomere frequency of HeLa cells Control (ATRX+) (A) and Sh590 (ATRX-) (B) XpYp (under 3kb). Long telomere (BLACK DOTS) compared to short telomere (under 3kb) (RED DOTS) for untreated and treated cells with RHP4 (5µM). After treatment, the frequency of short telomeres of ATRX+ HeLa cells was higher at untreated cells than treated cells. In the untreated ATRX- HeLa cells, short telomere frequency was lower than treated.

5.5 Discussion

Superimposed on the end replication problem, additional mutational mechanisms operate that create dysfunctional telomeres that are capable of fusion (Baird *et al.*, 2003; Capper *et al.*, 2007). The objective of this study was to determine if G-quadruplex structures, which can form in G-rich repeats sequences including those in the G-rich telomeric strand, could contribute to telomere erosion and large-scale telomeric deletion. Moreover, the role of ATRX protein and its contribution in overcoming the effects of such structure was also investigated.

IMR90 fibroblasts, U138 cancer cells, Ntera cells (ATRX+) and (ATRX-) and HeLa cells (ATRX+) and ATRX-) were cultured in the presence of G-quadruplex ligand (RHPS4) for 24 hours, then drug was released and fresh medium was added to cultured cells. In order to monitor any changes in cellular proliferation, DNA damage response, cell cycle arrest, cellular senescence and apoptosis, the untreated cells were compared to treated cells with different concentrations of RHPS4.

5.5.1 Cellular Proliferation

The data showed that the cellular proliferation of treated IMR90 fibroblasts decreased compared to the normal control and IMR90 fibroblasts displayed dose dependent sensitivity to RHPS4. This could be explained by the G-quadruplex ligand RHPS4 stabilising G-quadruplex structures across the genome, inducing replication fork stalling and cellular proliferation inhibition (Rizzo *et al.*, 2009).

The Ntera ATRX- cells displayed a high sensitivity to G-quadruplex ligand RHPS4 and showed a dose dependent viability loss. ~ 95% of Ntera ATRX- cells died following one day of 5 μ M RHPS4 treatment. Ntera cells ATRX- were also treated with 1 μ M of RHPS4 for 24 hours and

they died off following 2 to 3 days of drug released. Whereas, with 24 hours treatment of 0.2 μ M of RHPS4, Ntera ATRX- cells, lived up to 21 days after drug released.

This dose dependency was consistent with recent work on brain tumor cells *in vitro*, where cells exposed to several doses of G-quadruplex ligand RHPS4 showed a dose-dependent inhibition of brain tumor growth (Lagah *et al.*, 2014). They showed that several brain tumor cells exhibit dose-responsive to G-quadruplex ligand RHPS4.

Our data also showed that in contrast to Ntera ATRX-, Ntera ATRX+ cells were more resistant to G-quadruplex ligand RHPS4 with variety of drug concentration (0.2 μ M, 1 μ M and 5 μ M). They were able to resume their proliferation following drug released. This suggests that ATRX may help overcome the effect of G-quadruplex structures, enabling the cells to resume their proliferation and facilitate the replication fork progression. Indeed, it was recently shown that neuroprogenitor cells (ATRX-) display a high sensitivity to G-quadruplex ligand, they suggested that ATRX play a crucial role to overcome the effect of G-quadruplex structure (Watson *et al.*, 2013). However it is unknown yet what part ATRX might play in this. ATRX deficiency is linked to an increase replication fork stalling in different types of cell and this may arise from G-quadruplex formation (Watson *et al.*, 2013; Clynes *et al.*, 2014; Leung *et al.*, 2013). ATRX deficiency together with G-quadruplex stabilising ligands such as RHPS4, enhance replication fork stalling which in turn induces replicative stress, DNA damage response and termination of cellular proliferation (Rizzo *et al.*, 2009; Rodriguez *et al.*, 2012).

5.5.2 Checkpoint Activation and Cell Cycle Arresting

Cell cycle progression was investigated in Ntera cells (ATRX+) and was compared to Ntera cells (ATRX-). Both ATRX+ and ATRX- cells, after 24 hours of treatment (AT), were accumulated at G0/G1. This could be explain that RHPS4 induce and stabilise G-quadruplex formation and replication fork stalled in Ntera cells (ATRX+) and (ATRX-). When, drug was released and after 24 hours of recovery, Ntera (ATRX+) cells were able to replicate and progressed through the cell cycle and higher percentage of cells seen at S phase and G2/M. This suggests that cells were able to resolve the G-quadruplex structure and resume their ability of division. In contrast, Ntera (ATRX-) cells were accumulated at G0/G1. This suggests that cells had difficulty to resolve G-quadruplex and high percentage of cells were not being able to undergo the cellular division. This data support the role of ATRX in contribution of unwinding G-quadruplexes and facilitating replication fork progression (Clynes *et al.*, 2015).

Our data on cell cycle checkpoints proteins revealed that, Chk1, Chk2 and P53 were activated following exposure to RHPS4 (AT) in the Ntera cells (ATRX+). These phosphorylations decreased after 24 hours of drug released. This could explain that due to G-quadruplex stabilisation, replication forks stalled, the checkpoints proteins were activated following drug exposure.

While in Ntera cells (ATRX-), Chk2 and P53 but not Chk1 were phosphorylated following of 24 hours of treatment and the expression of the phsphorylations for both Chk2 and P53 in Ntera ATRX- cells were high even after 24 hours of drug released. This suggests that Ntera ATRX- cells experience replicative stress even after drug released and potentially a consequence of the cells being unable to resolve G-quadruplex structures. Our data from

apoptosis assay support this suggestion, as treated Ntera ATRX- cells displayed higher frequency of apoptotic cells compared to Ntera cells (ATRX+).

5.5.3 Telomere Dynamics

Distinct differences in the responses of ATRX deficient Ntera cells compared to ATRX proficient cells was observed follow the exposure to RHPS4. We therefore examined these cells for differences in telomere dynamics using STELA.

It is known that G-quadruplex structure inhibits the catalytic activity of telomerase, which in turn induce telomere shortening as a consequence (Zahler *et al.*, 1991). In our experiments, data revealed that no telomere shortening was observed in exposed cells to RHPS4, indeed overall it appeared that treatment with RHPS4 did not have an obvious impact on telomere dynamics. The changes that were observed where quite subtle; telomere lengthening was observed in treated cells compared to controls. Such as in U138 cancer cells following 4 days exposure to 2 μ M of RHPS4, its mean telomere length in treated cells was significantly longer than untreated. Moreover, in Ntera ATRX- cells following one day exposure to 1 μ M of RHPS4, mean telomere length was longer as well in these cells compared to their controls.

The following scenario could explain these observations:

Previously, it was shown that ATRX binds to G-rich repeats, including the telomere G-rich strand (Law *et al.*, 2010). It was suggested that ATRX plays a crucial role to overcome the effect of G-quadruplex structures and facilitate the replication of these structure (Watson *et al.*, 2013). It was also revealed that ATRX interacts with MRN complex (MRE11-RAD50-NBS1), which is facilitates chromosomal integrity, DNA replication, restart of stalled replication forks and DNA double strand break repair (Zhong *et al.*, 2007). Indeed, ATRX deficiency has recently been related to a major of replicative stress responses (Wong *et al.*,

2010; Watson *et al.*, 2013; Clynes *et al.*, 2014; Leung *et al.*, 2013). Moreover, recent study suggests the role of ATRX in overcoming G-quadruplex structure, coming from interacting ATRX with DAXX and depositing histone H3.3 at telomeres, which is considered to enable DNA replication progression through G-quadruplex structures. Figure 5.21 showed the role of ATRX in modulating replication through G-quadruplex structure, model was reproduced from (Clynes *et al.*, 2015).

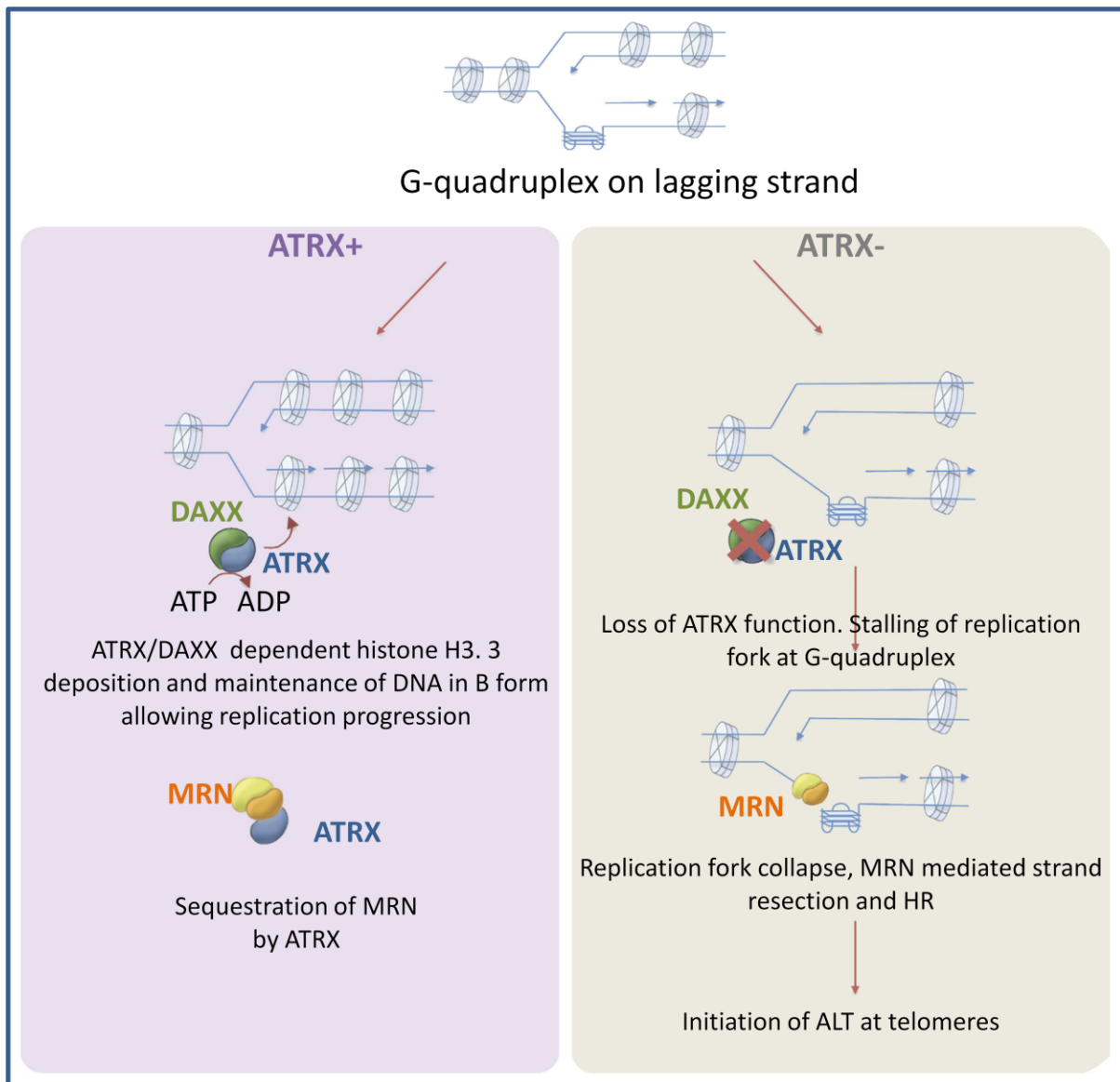


Figure 5.21. Model for telomere length maintenance (ALT pathway) in ATRX proficient and ATRX deficient tumour cells. ATRX with DAXX deposits histone H3.3 at telomeres, facilitate DNA replication progression through G-quadruplexes. The presence of G-quadruplex structures in an ATRX deficient cells results in replication fork stalling, providing a substrate for MRN-dependent homologous recombination and maintenance of telomere length through ALT. ATRX additionally interacts with the MRN complex, facilitating its distribution away from PML bodies and telomeres, further limiting HR. Redrawn from (Clynes *et al.*, 2015).

The presence of G-quadruplex structures which induced by G-quadruplex ligand RHPS4 in Ntera ATRX- cells, result in high frequency of replication fork stalling, facilitating a substrate for MRN dependent homologous recombination (HR) and telomere length maintained through alternative lengthen telomere (ALT) (Clynes *et al.*, 2015). It was reported that ATRX interacts with the MRN complex, to redistribute them away from sites of telomeric recombination and PML bodies, as a further limitation of HR (Clynes *et al.*, 2015).

This scenario could explain why longer telomere was observed in Ntera ATRX- cells. When G-quadruplexes induced and ATRX suppressed, as tumour cells, they have to find a way to maintain their telomere length and proliferation active. Consequently, they might induce ALT to maintain their telomere length. However ALT +ve cells display characteristic heterogeneous telomere length profiles, which were not apparent in the Ntera ATRX- cells. Thus either these cells were in the very early stages of the induction of the ALT phenotype or that a distinct elongation mechanism may be required.

An alternative scenario, which could explain the results:

Cells with short telomeres might display an increased sensitivity to the G-quadruplex ligand RHPS4. In this situation cells with short telomeres preferentially undergo apoptosis in response to the drug, which is consistent with the observed increase in apoptosis observed following drug exposure. This would result in a preferential loss of cells with short telomeres, a skewing of the telomere length distribution and an apparent increase in mean telomere length. This scenario is consistent with the observed telomere length distributions, where there a loss of the telomeres in lower length ranges, but this is not matched by an obvious increase in telomere length in upper length ranges; overall this results in a skewing of the telomere length distribution.

5.6 Conclusions

Overall the data presented in this chapter, show that the treatment of cells with G-quadruplex stabilising ligands exerts a clear cellular phenotype, which is exacerbated in the absence of ATRX. However, the changes to telomere dynamics are subtle and it was apparent that the stabilisation of G-quadruplexes did not directly lead to the induction of stochastic telomeric deletion.

Chapter 6

General Discussion and Future Investigations

6.1 Previous Studies

Superimposed on the end-replication problem, telomere deletion events have been detected both in the presence and in the absence of telomerase (Baird *et al.*, 2003; Britt-compton *et al.*, 2006). This includes spermatogonial stem cells, where the majority of telomeres length are maintained at a mean 12kb in human population by telomerase activity, yet very short telomeres (~10 telomeric repeats) were observed (Baird *et al.*, 2006). Moreover, telomere deletion events have been also detected in telomerase negative cells e.g. normal diploid fibroblasts with an intact DNA damage response, thus it was suggested that cells can endure at least one dysfunctional telomere without cell cycle arrest (Baird *et al.*, 2003; Britt-compton *et al.*, 2006).

Previously, telomeres lacking a fluorescent signal from fluorescently labelled telomere-repeat containing probes have been detected in normal human cells (Callen *et al.*, 2002; Wang *et al.*, 2004; Deng *et al.*, 2007). The presence of telomeres lacking fluorescent signal were consistent with the telomeric deletion events detected using STELA (Baird, 2008).

The data presented in this thesis examines the mutational mechanisms that underlying telomeric deletion events, using the STELA technique. STELA is the only method currently available to detect the extremely short telomeres of the length at which both senescence can be triggered and telomere fusion can occur.

6.2. Research Presented in This Thesis

6.2.1 Oxidative Stress and Telomere Erosion

Many studies have revealed that the replicative lifespan of IMR90 fibroblast is considerably increased in conditions that lower the levels of oxidative stress (Chen et al. 1995 and Saito et al. 1995). Our data are consistent with this view since we observed significant increased of replicative lifespan of IMR90 fibroblast when they grew in standard culture conditions. These data indicate that when cultured in low oxygen, IMR90 cells may display their maximal replicative capacity. These indications are consistent with the view that IMR90 cells, as well as many different primary cells grown in standard conditions, are subjected to oxidative stress. The production of ROS, is limited by oxygen at normal levels within the cell, and will thus rise in high oxygen (Halliwell 2003). In IMR90 cells the levels of oxidative DNA damage, as determined by quantifying oxo8dG in DNA, are higher in senescent compared to young fibroblasts (Chen et al. 1995). This was attributed to decreasing mitochondrial efficiency resulting in an increase in superoxide and hydrogen peroxide production (Chen et al. 1995). A Previous study from our laboratory showed that the ectopic expression of telomerase in IMR90 cells results in IMR90 immortalised in conditions of lower levels of oxidative stress, but not in conditions of high oxidative stress (Britt-Compton, 2009). Thus it was concluded that telomerase is incapable of counteracting telomeric specific damage resulting from oxidative stress. In contrast to IMR90 cells, MRC5 fibroblasts have previously been shown to be immortalised with telomerase in high oxidative stress (20% oxygen) (McSharry *et al.*, 2001). Different cell strains react differently to varying oxygen tensions and that such differences may be due to differing antioxidant capacities (Lorenz, 2001; Britt-Compton, 2009). The role of telomere length in the induction of replicative senescence in

IMR90 has been examined previously and the the key observation made that the telomere length at senescence in IMR90 cells was longer in 20% oxygen compared to 3% oxygen, and that this difference was proportional to the difference in the lifespan (Britt-Compton, 2009).

Our data, together with previously published observations (Britt-Compton, 2009; Chen et al. 1995 and Saito et al. 1995), suggest that IMR90 fibroblast, are not capable of adapting to the high oxygen conditions that they encounter in standard culture, and thus may be subjected to high levels of oxidative stress. It is appears that the replicative capacity of different cells in culture is not always limited by telomere length, and in conditions where the levels of oxidative stress outweigh the antioxidant defences of the cells, senescence can be telomere independent. This conclusion may be important because others have argued that telomere repeat sequences are unusually sensitive to oxidative stress and that this may drive the majority of telomere erosion (von Zglinicki 2002). Thus in conditions of oxidative stress the onset of senescence occurs earlier and is telomere driven. Our data, and data from others also investigating stress-induced premature senescence (SIPS) in fibroblasts, suggest that this may not always be the case. Chen et al. (2001) induced a senescence-like arrest in 100% of IMR90 cells using H₂O₂ and observed no evidence of telomere erosion, either immediately or one week after treatment. These findings were also backed up similar observations using IMR90 cells expressing telomerase (Gorbunova et al. 2002). Another study showed that by using multiple discontinuous subcytotoxic tert-butylhydroperoxide (t-BHP) or a single subcytotoxic H₂O₂ treatment in WI-38 fibroblasts, a significant increase in rates of telomeres erosion was detected (Dumont et al. 2001; de Magalhaes et al. 2002). However, this was accounted for by the cell division of a small proportion of cells that resumed proliferation following treatment and contributed disproportionately to the increase

in the PD of the culture as a whole. Thus it was concluded that SIPS does not arise as a consequence of accelerated telomere erosion, but more likely results from stochastic DNA damage in the rest of the genome (Dumont *et al.* 2001; de Magalhaes *et al.* 2002).

Taken together these data indicate that the original hypothesis that oxidative stress might work as a mutational mechanism and result in telomeric deletion events may not be valid. Instead these data are more consistent with the view that premature senescence does not arise as a consequence of accelerated telomere erosion, but instead more likely results from stochastic DNA damage across the rest of the genome (Dumont *et al.*, 2001; de Magalhaes *et al.*, 2002).

6.2.2 Telomere Fragile Site

Our data showed that SCK fibroblasts display uni-modal distribution at the XpYp telomere and displayed a more homogenous distribution compared to MRC5 cells. In contrast, MRC5 fibroblasts displayed bi-modal distributions at the XpYp telomere, and it's consistent with previous studies that MRC5 containing two differently lengths alleles at XpYp telomere, arise from inter-allelic differences which are set in zygote and resulting of contribution of maternal and paternal telomere alleles (Baird *et al.*, 2003).

Our data also showed that exposure of SCK fibroblasts to APH treatment resulted in significant differences in mean telomere length between cells treated with 0.3 μ M, 1 μ M APH and untreated cells. Treated SCK fibroblasts with APH displayed a longer mean telomere length compared to control. This suggests that cells with shorter telomeres in treated SCK fibroblasts disappeared from the culture; this loss made the mean telomere length higher in these cells than the controls. This might be explained by APH preferentially damaging the

cells with shorter telomeres in cultures of Seckel fibroblasts and that cells in which this occurs subsequently disappear from the culture. As described previously; telomeres repeats pose a challenge to replication process and they resemble the fragile sites characteristics (Sfeir *et al.*, 2009) accordingly, telomeres considered being sensitive to replication inhibition and replication fork stalling that induced by exposure to APH.

The potential fragility of telomere repeats following exposure to APH, which is a replication inhibitor, together with the fact that SCK fibroblasts are deficient for ATR, which plays an important role in the DNA damage response, is consistent with all these factors playing a synergetic effect and to induce damage preferentially in these cells.

In contrast to SCK fibroblasts, the normal diploid fibroblast cell culture MRC5 did not show a statistically significant change in the mean telomere length distribution following treatment with APH. However subtle changes in the proportions of long to short alleles were observed. It is possible that the upper alleles in MRC5 may have been preferentially targeted by APH treatment and that replication fork stalling induced by exposure to APH in these upper alleles were resolved as breaks resulting in a reduction in the length of these alleles. Our western blot data was consistent with this suggestion; as Chk1 was phosphorylated and activated following 1 μ M of APH treatment in MRC5 fibroblasts indicating that replication stress induced DNA-damage occurred. Whereas, the effects of low dose of Aphdicolin (0.3 μ M) concentration was able only to induce the fragile site breakages and SA β -gal activity, but did not signal efficiently to activate and phosphorylate Chk1. This can illustrate that a higher concentration of APH leads to more widespread damage across the genome and they are more likely as single stranded breaks which in turn activate the Chk1 phosphorylation but not Chk2.

Our data also showed that exposure of U138 cancer cells to APH and HU treatments did not produce detectable increases in the proportions of short deleted telomeres or changes in mean telomere lengths. This may arise a consequence of an intrinsic resistance to APH in these cells, or alternatively the fast growing nature of the U138 cells may result the rapid loss or dilution of cells in which telomere-specific mutagenic events occurred thus rendering these events undetectable.

The original hypothesis that the induction of chromosome fragility might result in telomeric deletion events was consistent with the data obtained from SCK fibroblasts where the fragility of telomeres was enhanced by ATR deficiency. Whereas, in MRC5 fibroblasts the induction of chromosome fragility impacted on its upper to lower alleles ratio, with a preferential loss of the longer telomere length distribution.

6.2.3 G-quadruplex Structure at Telomere

Our data revealed that no telomere shortening was observed in exposed cells to RHPS4, indeed overall it appeared that treatment with RHPS4 did not have an obvious impact on telomere dynamics. The changes that were observed were quite subtle; telomere lengthening was observed in treated cells compared to controls. Such as in U138 cancer cells following 4 days exposure to 2 μ M of RHPS4, where mean telomere length in treated cells was significantly longer than the untreated cells. Moreover, in Ntera ATRX- cells following one day exposure to 1 μ M of RHPS4, mean telomere length was longer as well in these cells compared to their controls. Possible scenarios that could explain these observations include:

The G-quadruplex structures induced by ligand RHPS4 in Ntera ATRX- cells, result in high frequency of replication fork stalling, facilitating a substrate for MRN dependent homologous recombination (HR) and telomere-length maintenance via the alternative lengthening of telomeres (ALT) mechanism (Clynes *et al.*, 2015). It was reported that ATRX interacts with the MRN complex, to redistribute them away from sites of telomeric recombination and PML bodies, as a further limitation of HR (Clynes *et al.*, 2015). In the absence of ATRX, ALT might be initiated, however ALT +ve cells display characteristic heterogeneous telomere length profiles, which were not apparent in the Ntera ATRX- cells. Thus either these cells were in the very early stages of the induction of the ALT phenotype or that a distinct elongation mechanism may be required.

An alternative scenario which could explain these observations is that the cells with short telomeres, might display an increased sensitivity to the G-quadruplex ligand RHPS4. In this situation cells with short telomeres preferentially undergo apoptosis in response to the drug, which is consistent with the observed increase in apoptosis observed following drug exposure. This would result in a preferential loss of cells with short telomeres, a skewing of the telomere length distribution and an apparent increase in mean telomere length. This scenario is consistent with the observed telomere length distributions, where there a loss of the telomeres in lower length ranges, but this is not matched by an obvious increase in telomere length in upper length ranges; overall this results in a skewing of the telomere length distribution.

Overall the data show that the treatment of cells with G-quadruplex stabilising ligands exerts a clear cellular phenotype, which is exacerbated in the absence of ATRX. However,

the changes to telomere dynamics are subtle and it was apparent that the stabilisation of G-quadruplexes did not directly lead to the induction of stochastic telomeric deletion.

6.3 Future Investigations

Extension of this work is required to clarify the observations made in this thesis and more studies are possible to illustrate other mechanisms that may play a role in generating telomere deletion events.

Strategies could be employed to examine the genetic requirements for the induction of telomeric deletion. For example, altering the expression of some factors that are responsible for the formation and resolution of secondary structures including G-quadruplexes, T-loops, D-loops and holliday junctions may provide some sight into such mechanisms. For example using RNAi to decrease the expression of proteins involved in recombination, such as loss of RAD52 in yeast which resulted in an increase of telomere deletion (Polotnianka *et al.*, 1998).

Furthermore Ku protein in yeast is thought to regulate the capping of the telomere thus decreasing telomere deletion events. Down regulating its expression may also alter the generation of telomere deletion in human cells (Bulchoc *et al.*, 2001). RNAi could be used as well to reduce the expression of the MRN complex components (MRE11, RAD50, NBS1). This complex is thought to modulate the formation of the secondary structure at telomeres (Zhu *et al.*, 2000), and may relate to the MRX complex in yeast that is postulated to mediate telomere deletions (Bulcholc *et al.*, 2001).

The use of other cells such as WI38 and induce oxidative stress by using hydrogen peroxides in cultures, along with STELA would provide additional evidence of the role of oxidative

stress in generating telomere deletion events. Using antioxidants on the IMR90 cultured in high oxidative stress e.g. 300 μ M of H₂O₂ along with STELA would also provide further evidence that oxidative damage does indeed regulate the entry of IMR90 cells into senescence and it would clarify the role of oxidative stress with regard to replicative senescence.

BLM, WRN, RTEL helicases are known to be required for complete telomere replication, by resolving replication fork stalling within telomeric DNA and facilitating replication fork progression (Crabbe *et al.*, 2004; Opresko *et al.*, 2002). It was shown that the reduction in BLM helicase markedly increases damage in the telomeres (Rizzo *et al.*, 2009). It would be also a great of interest to decrease the expression of BLM, WRN or RTEL by using RNAi in treated cells with RHPS4, Aphidicolin or with Hydroxyurea (drugs induce replication fork stalling), along with STELA may provide evidence that might be consistent with replication fork stalling at telomeres contributing to telomere deletion.

G-quadruplex secondary structures probably form during DNA synthesis, where the duplex strands become separated during DNA replication and single-stranded DNA may fold into G-quadruplex structures (Sarkies *et al.*, 2010). It would be of great interest to follow the G-quadruplex formation during cell-cycle progression by using flow cytometry and synchronising cell populations and treating the cells with the RHPS4 ligand at specific stages of the cell-cycle, including S-G2 phase and G0-G1 phase. This would facilitate the comparison of telomere lengths following treatment in each phase of cell cycle. It may also be informative to synchronise the cell populations at S-G2 phase and applying DNA replication inhibitor e.g. (Aphidicolin) to facilitate more cells to fragility induction and use STELA to provide a clear evidence of the role of replication inhibition at telomeres and

resolving replication fork stalling as single or double stranded telomeric DNA in generating telomere deletion events.

It was shown that the deficiency of ATR, Chk2 or p21 inhibits cell death, and it was suggested that ATR/Chk2/p21 all play important roles during RHPS4-induced telomere damage (Rizzo *et al.*, 2009). It would be interesting to use RNAi to decrease the expression of these proteins ATR/Chk2/p21 and treat with the G-quadruplex stabilising ligand and use STELA to observe if such secondary structures may induce telomeric deletion events.

It was shown that the difference in RHPS4 sensitivity between PFSK-1/ DAOY embryonal cells and C6/GB-1 glioma cells is due to competitive binding of RHPS4 and POT1 to the 3' overhang (Lagah *et al.*, 2014). The less sensitive of C6 and GB-1 cells exhibit higher levels of POT-1 protein at telomeres and it was suggested that potent DNA damage response at telomeres upon RHPS4 exposure is antagonized by overexpression of POT1 or TRF2 (Lagah *et al.*, 2014). Therefore, would be a great interest to see if using RNAi to decrease POT1 or TRF2 expression and facilitating binding site of RHPS4 into telomere would display telomere deletion events that could be detected using STELA.

6.4 Conclusion

Taken together, the data presented in this thesis are not consistent with a role for oxidative stress, or the formation of G-quadruplex structures, in generating large-scale telomeric deletion; however telomeric mutational events may occur following the induction of chromosome fragile sites, specifically in the context of an ATR deficiency. Extension of this

work and more studies are required to illustrate other mechanisms that may play a role in generating telomere deletion events.

References

- Allsopp, R. C., Chang, E., Kashefi-Azham, M., Rogaev, E. I., Piatyszek, M. A., Shay, J. W., & Harley, C. B. (1995). Telomere shortening is associated with cell division in vitro and in vivo. *Experimental cell research*, 220(1), 194-200.
- Almeida, C., Azevedo, N. F., Fernandes, R. M., Keevil, C. W., & Vieira, M. J. (2010). Fluorescence in situ hybridization method using a peptide nucleic acid probe for identification of *Salmonella* spp. in a broad spectrum of samples. *Applied and environmental microbiology*, 76(13), 4476-4485.
- Amann, R., & Fuchs, B. M. (2008). Single-cell identification in microbial communities by improved fluorescence in situ hybridization techniques. *Nature Reviews Microbiology*, 6(5), 339-348.
- Ames, B. N. (1989). Endogenous oxidative DNA damage, aging, and cancer. *Free Radical Research*, 7(3-6), 121-128.
- Amran S, Ang W, Tan M, Li C, Lim K, Lim M, Lim W and Phan T (2009) A novel chair-type G-quadruplex formed by a *Bombyx mori* telomeric sequence. *Nucleic Acids Res.*, 37, 931–938.
- Arlt M.F, Miller D.E., Beer D.G. and Glover T.W (2002). Molecular characterization of FRAXB and comparative common fragile site instability in cancer cells. *Genes Chromosomes Cancer* 33:82–92.
- Arosio, D., Cui, S., Ortega, C., Chovanec, M., Di Marco, M., Baldini, G., Falaschi, A. & Vindigni, A. (2002) Studies On The Mode Of Ku Interaction With Dna.J *Biol Chem*, 277, 9741-8.
- Artandi, S. E. & Depinho, R. A. (2000) A critical role for telomeres in suppressing and facilitating carcinogenesis. *Curr Opin Genet Dev*, 10, 39-46.
- Attwooll, C. L., Akpınar, M. & Petrini, J. H. (2009) The Mre11 Complex And The Response To Dysfunctional Telomeres. *Mol Cell Biol*, 29, 5540-51.

- Ball, A. J., & Levine, F. (2005). Telomere-independent cellular senescence in human fetal cardiomyocytes. *Aging cell*, 4(1), 21-30.
- Banik, S. S. & Counter, C. M. (2004) Characterization of interactions between PinX1 and human telomerase subunits hTERT and hTR. *J Biol Chem*, 279, 51745-8.169.
- Barber, L.J. et al. (2008) RTEL1 maintains genomic stability by suppressing homologous recombination. *Cell* 135, 261–271.
- Bartek J, Falck J and Lukas J. (2001). CHK2 KINASE. *Nature* 877- 886.
- Bass, H. W., Marshall, W. F., Sedat, J. W., Agard, D. A. & Cande, W. Z. (1997) Telomeres cluster de novo before the initiation of synapsis: a three-dimensional spatial analysis of telomere positions before and during meiotic prophase. *J Cell Biol*, 137, 5-18.
- Bailey, S. M., Brenneman, M. A. & Goodwin, E. H. (2004) Frequent Recombination In Telomeric Dna May Extend The Proliferative Life Of Telomerase-Negative Cells. *Nucleic Acids Res*, 32, 3743-51.
- Baird DM (2008) Telomere dynamics in human cells. *Biochimie* 90:116–121.
- Baird DM, Britt-Compton B, Rowson J, Amso NN, Gregory L, Kipling D. (2006). Telomere instability in the male germline. *Hum Mol Genet* 15:45–51.
- Baird, D. M., Coleman, J., Rosser, Z. H. & Royle, N. J. (2000). High levels of sequence polymorphism and linkage disequilibrium at the telomere of 12q: implications for telomere biology and human evolution. *Am J Hum Genet*, 66, 235-50.
- Baird, D. M., Davis, T., Rowson, J., Jones, C. J. & Kipling, D. (2004). Normal telomere erosion rates at the single cell level in Werner syndrome fibroblast cells. *Hum Mol Genet*, 13, 1515-24.
- Baird, D. M. & Farr, C. J. (2006) The organization and function of chromosomes. *EMBO Rep*, 7, 372-6.

- Baird, D. M., Jeffreys, A. J. & Royle, N. J. (1995) Mechanisms underlying telomere repeat turnover, revealed by hypervariable variant repeat distribution patterns in the human Xp/Yp telomere. *Embo J*, 14, 5433-43.
- Baird, D. M., Rowson, J., Wynford-Thomas, D. & Kipling, D. (2003) Extensive Allelic Variation and Ultrashort Telomeres In Senescent Human Cells. *Nat Genet*, 33, 203-7.
- Balin, A. K., Fisher, A. J. & Carter, D. M. (1984) Oxygen Modulates Growth Of Human Cells At Physiologic Partial Pressures. *J Exp Med*, 160, 152-66.
- Barzilai, A., & Yamamoto, K. I. (2004). DNA damage responses to oxidative stress. *DNA repair*, 3(8), 1109-1115.
- Baumann, P. & Cech, T. R. (2001) Pot1, the putative telomere end-binding protein in fission yeast and humans. *Science*, 292, 1171-5.
- Beachy, P. A., Karhadkar, S. S. & Berman, D. M. (2004) Tissue repair and stem cell renewal in carcinogenesis. *Nature*, 432, 324-31.
- Biffi G, Tannahill D, McCafferty J and Balasubramanian S (2013) Quantitative visualization of DNA G-quadruplex structures in human cells. *NATURE CHEMISTRY* 5: 182-186.
- Blackburn, E. H. & Gall, J. G. (1978) A tandemly repeated sequence at the termini of the extrachromosomal ribosomal RNA genes in Tetrahymena. *J Mol Biol*, 120, 33-53.
- Blackburn, E. H. (1994). Telomeres: no end in sight. *Cell*, 77(5), 621-623.
- Block, W. D., Yu, Y., Merkle, D., Gifford, J. L., Ding, Q., Meek, K. & Lees-Miller, S. P. (2004) Autophosphorylation-Dependent Remodeling Of The Dna-Dependent Protein Kinase Catalytic Subunit Regulates Ligation Of Dna Ends. *Nucleic Acids Res*, 32, 4351-7.
- Bloom, D. (1954) Congenital telangiectatic erythema resembling lupus erythematosus in dwarfs; probably a syndrome entity. *AMA Am J Dis Child*, 88, 754-8.
- Bodnar, A. G., Ouellette, M., Frolkis, M., Holt, S. E., Chiu, C. P., Morin, G. B., Harley, C. B., Shay, J. W., Lichtsteiner, S. & Wright, W. E. (1998) Extension of life-span by introduction of telomerase into normal human cells. *Science*, 279, 349-52.

- Boiteux, S., & Radicella, J. P. (2000). The human OGG1 gene: structure, functions, and its implication in the process of carcinogenesis. *Archives of biochemistry and biophysics*, 377(1), 1-8.
- Boonstra, J., & Post, J. A. (2004). Molecular events associated with reactive oxygen species and cell cycle progression in mammalian cells. *Gene*, 337, 1-13.
- Bottari, B., Santarelli, M., Neviani, E., Gatti, M., 2010. Natural whey starter for Parmigiano Reggiano: culture-independent approach. *Journal Applied Microbiology* 108, 1676-1684.
- Bowers, J.E., Chapman, B.A., Rong, J., Paterson, A.H. (2003) Unravelling angiosperm genome evolution by phylogenetic analysis of chromosomal duplication events. *Nature*, 422:433–438.
- Brackertz, M., Kubbies, M., Feige, A., & Salk, D. (1983). Decreased oxygen supply enhances growth in culture of human mid-trimester amniotic fluid cells. *Human genetics*, 64(4), 334-338.
- Braig, M. & Schmitt, C. A. (2006) Oncogene-induced senescence: putting the brakes on tumor development. *Cancer Res*, 66, 2881-4.
- Britt-Compton, B., Capper, R., Rowson, J. & Baird, D. M. (2009) Short Telomeres Are Preferentially Elongated By Telomerase In Human Cells. *Febs Lett*, 583, 3076-80.
- Britt-Compton B, Rowson J, Locke M, Mackenzie I, Kipling D, Baird DM (2006) Structural stability and chromosome specific telomere length is governed by cis-acting determinants in humans. *Hum Mol Genet* 15:725–733.
- Broccoli, D., Smogorzewska, A., Chong, L. & De Lange, T. (1997) Human telomeres contain two distinct Myb-related proteins, TRF1 and TRF2. *Nat Genet*, 17, 231-5.
- Bryan, T. M., Englezou, A., Dalla-Pozza, L., Dunham, M. A. & Reddel, R. R. (1997) Evidence for an alternative mechanism for maintaining telomere length in human tumors and tumor-derived cell lines. *Nat Med*, 3, 1271-4.

- Bucholc, M., Park, Y., & Lustig, A. J. (2001). Intrachromatid excision of telomeric DNA as a mechanism for telomere size control in *Saccharomyces cerevisiae*. *Molecular and cellular biology*, 21(19), 6559-6573.
- Buis, J., Wu, Y., Deng, Y., Leddon, J., Westfield, G., Eckersdorff, M., Sekiguchi, J.M., Chang, S., and Ferguson, D.O. (2008).
- Burger AM, Dai F, Schultes CM, Reszka AP, Moore MJ, Double JA, Neidle S (2005) The G-quadruplex-interactive molecule BRACO-19 inhibits tumor growth, consistent with telomere targeting and interference with telomerase function. *Cancer Res* 65(4):1489-96.
- Cahill, D. P., Kinzler, K. W., Vogelstein, B. & Lengauer, C. (1999) Genetic instability and darwinian selection in tumours. *Trends Cell Biol*, 9, M57-60.
- Callén, E., Samper, E., Ramírez, M. J., Creus, A., Marcos, R., Ortega, J. & Surrallés, J. (2002). Breaks at telomeres and TRF2-independent end fusions in Fanconi anemia. *Human molecular genetics*, 11(4), 439-444.
- Campisi, J. (2005). Senescent cells, tumor suppression, and organismal aging: good citizens, bad neighbors. *Cell*, 120(4), 513-522.
- Campisi, J. & d'Adda di Fagagna, F. (2007). Cellular senescence: when bad things happen to good cells. *Nat. Rev. Mol. Cell Biol.*, 8, 729–740.
- Capper, R., Britt-Compton, B., Tankimanova, M., Rowson, J., Letsolo, B., Man, S., Haughton, M. & Baird, D. M. (2007) The Nature Of Telomere Fusion And A Definition Of The Critical Telomere Length In Human Cells. *Genes Dev*, 21, 2495-508.
- Casper AM, Durkin SG, Arlt MF, Glover TW. (2004). Chromosomal instability at common fragile sites in Seckel syndrome. *Am. J. Hum. Genet.* 75:654–60.
- Casper AM, Nghiem P, Arlt MF and Glover TW (2002). ATR regulates fragile site stability. *Cell* 111:779–89.
- Cawthon, R. M. (2002). Telomere measurement by quantitative PCR. *Nucleic acids research*, 30(10), e47-e47.

- Cawthon, R. M., Smith, K. R., O'Brien, E., Sivatchenko, A., & Kerber, R. A. (2003). Association between telomere length in blood and mortality in people aged 60 years or older. *The Lancet*, 361(9355), 393-395.
- Celli, G. B. & De Lange, T. (2005) DNA processing is not required for ATM-mediated telomere damage response after TRF2 deletion. *Nat Cell Biol*, 7, 712-8.
- Cesare, A. J. & Griffith, J. D. (2004) Telomeric DNA in ALT cells is characterized by free telomeric circles and heterogeneous t-loops. *Mol Cell Biol*, 24, 9948-57.
- Cesare, A. J., Quinney, N., Willcox, S., Subramanian, D. & Griffith, J. D. (2003) Telomere looping in *P. sativum* (common garden pea). *Plant J*, 36, 271-9.
- Chainiaux, F., Magalhaes, J. P., Eliaers, F., Remacle, J., & Toussaint, O. (2002). UVB-induced premature senescence of human diploid skin fibroblasts. *The international journal of biochemistry & cell biology*, 34(11), 1331-1339.
- Chandel, N. S., Maltepe, E., Goldwasser, E., Mathieu, C. E., Simon, M. C., & Schumacker, P. T. (1998). Mitochondrial reactive oxygen species trigger hypoxia-induced transcription. *Proceedings of the National Academy of Sciences*, 95(20), 11715-11720.
- Chang, P., Coughlin, M. & Mitchison, T. J. (2005) Tankyrase-1 polymerization of poly(ADP-ribose) is required for spindle structure and function. *Nat Cell Biol*, 7, 1133-9.
- Cheng, M. L., Ho, H. Y., Wu, Y. H. & Chiu, D. T. (2004) Glucose-6-Phosphate Dehydrogenase-Deficient Cells Show An Increased Propensity For Oxidant-Induced Senescence. *Free Radic Biol Med*, 36, 580-91.
- Chen Y, et al. (2008) A shared docking motif in TRF1 and TRF2 used for differential recruitment of telomeric proteins. *Science* 319: 1092–1096.
- Chen, Q., Fischer, A., Reagan, J. D., Yan, L. J. & Ames, B. N. (1995) Oxidative Dna Damage And Senescence Of Human Diploid Fibroblast Cells. *Proc Natl Acad Sci U S A*, 92, 4337-41.
- Chen, C. Y., Huang, Y. L. & Lin, T. H. (1998) Association Between Oxidative Stress And Cytokine Production In Nickel-Treated Rats. *Arch Biochem Biophys*, 356, 127-32.

- Chen, L. Y., Liu, D. & Songyang, Z. (2007) Telomere Maintenance Through Spatial Control of telomeric proteins. *Mol Cell Biol*, 27, 5898-909.
- Chen, Q. M., Prowse, K. R., Tu, V. C., Purdom, S. & Linskens, M. H. (2001) Uncoupling The Senescent Phenotype From Telomere Shortening In Hydrogen Peroxide-Treated Fibroblasts. *Exp Cell Res*, 265, 294-303.
- Chen, L., Trujillo, K., Sung, P. & Tomkinson, A. E. (2000) Interactions Of The Dna Ligase Iv-Xrcc4 Complex With Dna Ends And The Dna-Dependent Protein Kinase. *J Biol Chem*, 275, 26196-205.
- Chiurillo, M. A., Cano, I., Da Silveira, J. F. & Ramirez, J. L. (1999) Organization of telomeric and sub-telomeric regions of chromosomes from the protozoan parasite Trypanosoma cruzi. *Mol Biochem Parasitol*, 100, 173-83.
- Clynes, D. et al. (2014). ATRX dysfunction induces replication defects in primary mouse cells. *PLoS ONE* 9, e92915.
- Clynes D, Jelinska C, Xella B, Ayyub H, Scott C, Mitson M, Taylor S, Higgs D & Gibbons R. (2015). Suppression of the alternative lengthening of telomere pathway by the chromatin remodelling factor ATRX. *Nature* DOI: 10.1038/ncomms8538 <http://www.nature.com/naturecommunications>.
- Cohen, S. B., Graham, M. E., Lovrecz, G. O., Bache, N., Robinson, P. J. & Reddel, R. R. (2007) Protein composition of catalytically active human telomerase from immortal cells. *Science*, 315, 1850-3.
- Cook, B. D., Dynek, J. N., Chang, W., Shostak, G. & Smith, S. (2002) Role for the related poly(ADP-Ribose) polymerases tankyrase 1 and 2 at human telomeres. *Mol Cell Biol*, 22, 332-42.175
- Coquelle, A., Pipiras, E., Toledo, F., Buttin, G., & Debatisse, M. (1997). Expression of fragile sites triggers intrachromosomal mammalian gene amplification and sets boundaries to early amplicons. *Cell*, 89(2), 215-225.

- Crabbe, L., Verdun, R. E., Haggblom, C. I. & Karlseder, J. (2004) Defective telomere lagging strand synthesis in cells lacking WRN helicase activity. *Science*, 306, 1951-3.
- D'adda Di Fagagna, F., Reaper, P. M., Clay-Farrace, L., Fiegler, H., Carr, P., Von Zglinicki, T., Saretzki, G., Carter, N. P. & Jackson, S. P. (2003) A DNA damage checkpoint response in telomere-initiated senescence. *Nature*, 426, 194-8.
- David, S. S., O'shea, V. L. & Kundu, S. (2007) Base-Excision Repair Of Oxidative Dna Damage. *Nature*, 447, 941-50.
- De Cian A, Cristofari G, Reichenbach P, De Lemos E, Monchaud D, et al. (2007) Reevaluation of telomerase inhibition by quadruplex ligands and their mechanisms of action. *Proceedings of the National Academy of Sciences of the United States of America* 104: 17347–17352.
- De Jager, M., Van Noort, J., Van Gent, D. C., Dekker, C., Kanaar, R. & Wyman, C. (2001) Human Rad50/Mre11 Is A Flexible Complex That Can Tether Dna Ends. *Mol Cell*, 8, 1129-35.
- De Lange, T. (2005) Shelterin: the protein complex that shapes and safeguards human telomeres. *Genes Dev*, 19, 2100-10.
- de Magalhães, J. P., Chainiaux, F., Remacle, J., & Toussaint, O. (2002). Stress-induced premature senescence in BJ and hTERT-BJ1 human foreskin fibroblasts. *FEBS letters*, 523(1), 157-162.
- Demyttenaere, K., Bruffaerts, R., Posada-Villa, J., Gasquet, I., Kovess, V., Lepine, J. & Chatterji, S. (2004). Prevalence, severity, and unmet need for treatment of mental disorders in the World Health Organization World Mental Health Surveys. *JAMA: the journal of the American Medical Association*, 291(21), 2581-2590.
- Denchi, E. L. & De Lange, T. (2007) Protection of telomeres through independent control of ATM and ATR by TRF2 and POT1. *Nature*, 448, 1068-71.
- Denchi, E. L. (2009) Give me a break: how telomeres suppress the DNA damage response. *DNA Repair (Amst)*, 8, 1118-26.

- Deng, Z., Dheekollu, J., Broccoli, D., Dutta, A., & Lieberman, P. M. (2007). The origin recognition complex localizes to telomere repeats and prevents telomere-circle formation. *Current Biology*, 17(22), 1989-1995.
- Deng, Y., Guo, X., Ferguson, D. O. & Chang, S. (2009) Multiple Roles For Mre11 At Uncapped Telomeres. *Nature*, 460, 914-8.
- Di Leonardo, A., Linke, S. P., Clarkin, K. & Wahl, G. M. (1994) DNA damage triggers a prolonged p53-dependent G1 arrest and long-term induction of Cip1 in normal human fibroblasts. *Genes Dev*, 8, 2540-51.
- Di Micco, R., Fumagalli, M., Cicalese, A., Piccinin, S., Gasparini, P., Luise, C., Schurra, C., Garre, M., Nuciforo, P. G., Bensimon, A., Maestro, R., Pelicci, P. G. & D'adda Di Fagagna, F. (2006) Oncogene-induced senescence is a DNA damage response triggered by DNA hyper-replication. *Nature*, 444, 638-42.
- Dimitrova, N. & De Lange, T. (2009) Cell Cycle-Dependent Role Of Mrn At Dysfunctional Telomeres: Atm Signaling-Dependent Induction Of Nonhomologous End Joining (Nhej) In G1 And Resection-Mediated Inhibition Of Nhej In G2. *Mol Cell Biol*, 29, 5552-63.
- Dimri GP, Lee X, Basile G, Acosta M, Scott G, Roskelley C, Medrano EE, Linskens M, Rubelj I, Pereira-Smith O. (1995). "A biomarker that identifies senescent human cells in culture and in aging skin in vivo". *Proc. Natl. Acad. Sci. U.S.A.* 92 (20): 9363–7.
- Dimri, G. P., Itahana, K., Acosta, M. & Campisi, J. (2000) Regulation of a senescence checkpoint response by the E2F1 transcription factor and p14(ARF) tumor suppressor. *Mol Cell Biol*, 20, 273-85.
- Dionne, I. & Wellinger, R. J. (1998) Processing of telomeric DNA ends requires the passage of a replication fork. *Nucleic Acids Res*, 26, 5365-71.178.
- Dumont, P., Balbeur, L., Remacle, J. & Toussaint, O. (2000) Appearance of biomarkers of in vitro ageing after successive stimulation of WI-38 fibroblasts with IL-1alpha and TNF-alpha:

senescence associated beta-galactosidase activity and morphotype transition. *J Anat*, 197 Pt 4, 529-37.

- Dunbar, J., Ticknor, L. O., & Kuske, C. R. (2000). Assessment of microbial diversity in four southwestern United States soils by 16S rRNA gene terminal restriction fragment analysis. *Applied and Environmental Microbiology*, 66(7), 2943-2950.
- Durkin S, Arlt M, Howlett N and Glover T. (2006). Depletion of CHK1, but not CHK2, induces chromosomal instability and breaks at common fragile sites. *Nature* 25, 4381–4388.
- Durkin S and Glover T (2007). Chromosome Fragile Sites. *Annu. Rev. Genet.* 1:169–192.
- Egholm, M., Buchardt, O., Christensen, L., Behrens, C., Freier, S. M., Driver, D. A., Nielsen, P. E. (1993). PNA hybridizes to complementary oligonucleotides obeying the Watson-Crick hydrogen-bonding rules. *Nature*, 365(6446), 566-568.
- Ellis, n. a., groden, j., ye, t. z., straughen, j., lennon, d. j., ciocci, s., proytcheva, m. & german, j. (1995) The Bloom's syndrome gene product is homologous to RecQ helicases. *Cell*, 83, 655-66.
- Ellis, N. A., Groden, J., Ye, T. Z., Straughen, J., Lennon, D. J., Ciocci, S., Proytcheva, M. & German, J. (1995) The Bloom's syndrome gene product is homologous to RecQ helicases. *Cell*, 83, 655-66.
- Ellis, N.A., Groden, J., Ye, T.Z., Straughen, J., Lennon, D.J., Ciocci, S., Proytcheva, M. and German, J. (1995). The Bloom's syndrome gene product is homologous to RecQ helicases. *Cell*, 83, 655–666.
- Elsa Callén, Enrique Samper, María J. Ramírez, Amadeu Creus, Ricard Marcos, Juan J. Ortega, Teresa Olivé, Isabel Badell, María A. Blasco, and Jordi Surrallés (2002) Breaks at telomeres and TRF2-independent end fusions in Fanconi anemia. *Hum. Mol. Genet.* 11 (4): 439-444 doi:10.1093/hmg/11.4.439
- Euling, S., and Ambros, V. (1996b). Reversal of cell fate determination in *Caenorhabditis elegans* vulval development. *Development*, 122, 2507–2515.

- Fajkus, J., Sykorova, E. & Leitch, A. R. (2005) Telomeres in evolution and evolution of telomeres. *Chromosome Res*, 13, 469-79.
- Falck, J., Coates, J. & Jackson, S. P. (2005) Conserved Modes Of Recruitment Of Atm, Atr And Dna-Pkcs To Sites Of Dna Damage. *Nature*, 434, 605-11.179
- Fay, D.S., Keenan, S., and Han, M. (2002). fzf-1 and lin-35/Rb function redundantly to control cell proliferation in *C. elegans* as revealed by a nonbiased synthetic screen. *Genes Dev.*, 16, 503–517.
- Finato, A. O., Varella-Garcia, M., Tajara, E. H., Taddei, V. A., & Morielle-Versute, E. (2000). Intrachromosomal distribution of telomeric repeats in *Eumops glaucinus* and *Eumops perotis* (Molossidae, Chiroptera). *Chromosome Research*, 8(7), 563-569.
- Fleming A and Burrows C (2013) G-Quadruplex Folds of the Human Telomere Sequence Alter the Site Reactivity and Reaction Pathway of Guanine Oxidation Compared to Duplex DNA. *Chem. Res. Toxicol.* 26:593–607.
- Forsyth, N. R., Evans, A. P., Shay, J. W. & Wright, W. E. (2003) Developmental Differences In The Immortalization Of Lung Fibroblasts By Telomerase. *Aging Cell*, 2, 235-43.
- Fry, M. and Loeb, L.A. (1999) Human werner syndrome DNA helicase unwinds tetrahelical structures of the fragile X syndrome repeat sequence d(CGG)_n. *J. Biol. Chem.* 274, 12797–12802.
- Fu, D. & Collins, K. (2007) Purification of human telomerase complexes identifies factors involved in telomerase biogenesis and telomere length regulation. *Mol Cell*, 28, 773-85.
- Fukuchi, K., Martin, G. M. & Monnat, R. J., Jr. (1989) Mutator phenotype of Werner syndrome is characterized by extensive deletions. *Proc Natl Acad Sci U S A*, 86, 5893-7.
- German, J. (1993). Bloom syndrome: a mendelian prototype of somatic mutational disease. *Medicine (Baltimore)*, 72, 393–406.
- German, J., Archibald, R. & Bloom, D. (1965) Chromosomal Breakage in a Rare and Probably Genetically Determined Syndrome of Man. *Science*, 148, 506-7.

- German, J., Schonberg, S., Louie, E. & Chaganti, R. S. (1977) Bloom's syndrome. IV. Sister-chromatid exchanges in lymphocytes. *Am J Hum Genet*, 29, 248-55.
- Gil, M. E., & Coetzer, T. L. (2004). Real-time quantitative PCR of telomere length. *Molecular biotechnology*, 27(2), 169-172.
- Giraldo R and Rhodes D (1994) The yeast telomere-binding protein RAP1 binds to and promotes the formation of DNA quadruplexes in telomeric DNA. *EMBO J.* 13,2411–2420.
- Gire, V., Roux, P., Wynford-Thomas, D., Brondello, J. M. & Dulic, V. (2004) DNA damage checkpoint kinase Chk2 triggers replicative senescence. *Embo J*, 23, 2554-63.
- Glover T. (2006). Common fragile sites. *Cancer Letters* 232:4–12.
- Gorgoulis VG, Vassiliou LV, Karakaidos P, Zacharatos P, Kotsinas A. (2005). Activation of the DNA damage checkpoint and genomic instability in human precancerous lesions. *Nature* 434:907–13.
- Gorman, J., & Greene, E. C. (2008). Visualizing one-dimensional diffusion of proteins along DNA. *Nature structural & molecular biology*, 15(8), 768-774.
- Gowan SM, Harrison JR, Patterson L, Valenti M, Read MA, et al. (2002) A Gquadruplex-interactive potent small-molecule inhibitor of telomerase exhibiting in vitro and in vivo antitumor activity. *Molecular Pharmacology* 61: 1154–1162.
- Gowan, S. Heald G, Stevens M, And Kelland L (2001) Potent Inhibition of Telomerase by Small-Molecule Pentacyclic Acridines Capable of Interacting with G-Quadruplexes. *Molecular Pharmacology* (60)5:981-988.
- Greider, C. W. & Blackburn, E. H. (1985) Identification of a specific telomere terminal transferase activity in Tetrahymena extracts. *Cell*, 43, 405-13.
- Greider, C. W. & Blackburn, E. H. (1996) Telomeres, telomerase and cancer. *Sci Am*, 274, 92-7.
- Griffith, J. D., Comeau, L., Rosenfield, S., Stansel, R. M., Bianchi, A., Moss, H. & De Lange, T. (1999) Mammalian telomeres end in a large duplex loop. *Cell*, 97, 503-14.

- Grand CL, Bearss DJ, Von Hoff DD, Hurley LH (2002) Quadruplex formation in the c-MYC promoter inhibits protein binding and correlates with in vivo promoter activity. *European Journal of Cancer* 38: S106–S107.
- Gunaratnam M, Fuente M, Hampel S, Todd A, Reszka A, Schätzlein A and Neidle S (2011) Targeting pancreatic cancer with a G-quadruplex ligand. *Bioorg. Med. Chem.* 19:7151–7157.
- Hahn WC, Stewart SA, Brooks MW, York SG, Eaton E, et al. (1999) Inhibition of telomerase limits the growth of human cancer cells. *Nature Medicine* 5: 1164–1170.
- Haider, S. M., Parkinson, G. N., & Neidle, S. (2003). Structure of a G-quadruplex–ligand complex. *Journal of molecular biology*, 326(1), 117-125.
- Hammarsten, o. & Chu, g. (1998) DNA-dependent protein kinase: DNA binding and activation in the absence of Ku. *Proc Natl Acad Sci U S A*, 95, 525-30.
- Han, H., & Hurley, L. H. (2000). G-quadruplex DNA: a potential target for anti-cancer drug design. *Trends in pharmacological sciences*, 21(4), 136-142.
- Harper, L., Golubovskaya, I. & Cande, W. Z. (2004) A bouquet of chromosomes. *J Cell Sci*, 117, 4025-32.
- Hartlerode, A. J. & Scully, R. (2009) Mechanisms Of Double-Strand Break Repair In Somatic Mammalian Cells. *Biochem J*, 423, 157-68.
- Hartmann, M., Frey, B., Kölliker, R., & Widmer, F. (2005). Semi-automated genetic analyses of soil microbial communities: comparison of T-RFLP and RISA based on descriptive and discriminative statistical approaches. *Journal of Microbiological Methods*, 61(3), 349-360.
- Hayflick, L. (1965). The Limited In Vitro Lifetime Of Human Diploid Cell Strains. *Exp Cell Res*, 37, 614-36.
- Hedglin, M., & O'Brien, P. J. (2010). Hopping enables a DNA repair glycosylase to search both strands and bypass a bound protein. *ACS chemical biology*, 5(4), 427-436.

- Henderson, S., Allsopp, R., Spector, D., Wang, S. S. & Harley, C. (1996) In Situ Analysis Of Changes In Telomere Size During Replicative Aging And Cell Transformation. *J Cell Biol*, 134, 1-12.
- Henderson E, Hardin C, Walk K, Tinoco r and Blackburn H (1987) Telomeric DNA oligonucleotides form novel intramolecular structures containing guanine-guanine base pairs. *Cell*, (51) 899–908.
- Herbig, U., Jobling, W. A., Chen, B. P., Chen, D. J. & Sedivy, J. M. (2004) Telomere shortening triggers senescence of human cells through a pathway involving ATM, p53, and p21(CIP1), but not p16(INK4a). *Mol Cell*, 14, 501-13.
- Hills, M., Lücke, K., Chavez, E. A., Eaves, C. J., & Lansdorp, P. M. (2009). Probing the mitotic history and developmental stage of hematopoietic cells using single telomere length analysis (STELA). *Blood*, 113(23), 5765-5775.
- Hiyama, E. & Hiyama, K. (2002) Clinical utility of telomerase in cancer. *Oncogene*, 21, 643-9.
- Hoekstra, M. F. (1997) Responses to DNA damage and regulation of cell cycle checkpoints by the ATM protein kinase family. *Curr Opin Genet Dev*, 7, 170-5.
- Holt, S. E. & Shay, J. W. (1999) Role of telomerase in cellular proliferation and cancer. *J Cell Physiol*, 180, 10-8.
- Hopfner, K. P., Karcher, A., Craig, L., Woo, T. T., Carney, J. P. & Tainer, J. A. (2001) Structural Biochemistry And Interaction Architecture Of The Dna Double-Strand Break Repair Mre11 Nuclease And Rad50-Atpase. *Cell*, 105, 473-85.
- Hopfner, K. P., Karcher, A., Shin, D., Fairley, C., Tainer, J. A. & Carney, J. P. (2000) Mre11 And Rad50 From Pyrococcus Furiosus: Cloning And Biochemical Characterization Reveal An Evolutionarily Conserved Multiprotein Machine. *J Bacteriol*, 182, 6036-41.
- Hopfner, K. P., Putnam, C. D. & Tainer, J. A. (2002) Dna Double-Strand Break Repair From Head To Tail. *Curr Opin Struct Biol*, 12, 115-22.

- Horvath, M.P., Schweiker, V.L., Bevilacqua, J.M., Ruggles, J.A. & Schultz, S.C. (1998). Crystal structure of the *Oxytricha nova* telomere end binding protein complexed with single strand DNA. *Cell*, 95, 963–974
- Houghtaling, B. R., Cuttonaro, L., Chang, W. & Smith, S. (2004) A dynamic molecular link between the telomere length regulator TRF1 and the chromosome end protector TRF2. *Curr Biol*, 14, 1621-31.
- Hsiao, S. J. & Smith, S. (2009) Sister telomeres rendered dysfunctional by persistent cohesion are fused by NHEJ. *J Cell Biol*, 184, 515-26.
- Hu L, Lim W , Bouaziz S and Phan T (2009) Giardia telomeric sequence d(TAGGG)₄ forms two intramolecular G-quadruplexes in K⁺ solution: effect of loop length and sequence on the folding topology. *J. Am. Chem. Soc.*, 131, 16824–16831.
- Huber, M.D. et al. (2006) A conserved G4 DNA binding domain in RecQ family helicases. *J. Mol. Biol.* 358, 1071–1080
- Hug, N, Lingner, J. (2006) Telomere length homeostasis. *Chromosoma*, 115:413–425.10.1007/s00412-006-0067-3.
- Hunter N. Meiotic recombination. In: Aguilera A, Rothstein R. (2007). Homologous recombination hybridization method using a peptide nucleic acid probe for the identification of *Salmonella* spp. in a broad spectrum of samples. *Applied and Environmental Microbiology* 76, 4476-4485.
- Incles CM, Schultes CM, Kempinski H, Koehler H, Kelland LR, et al. (2004) A G-quadruplex telomere targeting agent produces p16-associated senescence and chromosomal fusions in human prostate cancer cells. *Molecular Cancer Therapeutics* 3: 1201–1206.
- Itahana K, Campisi J, Dimri GP (2007). "Methods to detect biomarkers of cellular senescence: the senescence-associated beta-galactosidase assay". *Methods Mol. Biol. Methods in Molecular Biology* 371: 21–31.

- Itahana, K., Dimri, G., & Campisi, J. (2001). Regulation of cellular senescence by p53. *European Journal of Biochemistry*, 268(10), 2784-2791.
- Jackson, S. P. & Bartek, J. (2009) The Dna-Damage Response In Human Biology And Disease. *Nature*, 461, 1071-8.
- Jiao, Y. et al. (2011) DAXX/ATRAX, MEN1, and mTOR pathway genes are frequently altered in pancreatic neuroendocrine tumors. *Science* 331, 1199–1203.
- Jiricny, J. (2006) The Multifaceted Mismatch-Repair System. *Nat Rev Mol Cell Biol*, 7, 335-46.
- Johnson, F. B., Marciniak, R. A., McVey, M., Stewart, S. A., Hahn, W. C. and Guarente, L. (2001). The *Saccharomyces cerevisiae* WRN homolog Sgs1p participates in telomere maintenance in cells lacking telomerase. *EMBO J.*, 20, 905-913.
- Johnson, F.B., Lombard, D.B., Neff, N.F., Mastrangelo, M.A., Dewolf, W., Ellis, N.A., Marciniak, R.A., Yin, Y., Jaenisch, R. and Guarente, L. (2000) Association of the Bloom syndrome protein with topoisomerase IIIalpha in somatic and meiotic cells. *Cancer Res.*, 60, 1162–1167.
- Justé A, Thommad B, Lievens B. Recent advances in molecular techniques to study microbial communities in food-associated matrices and processes. *Food Microbiol.* 2008;13:745.
- Kapoor V. and Telford W. (2004) *Methods Mol. Biol.*, 263, 385-398
- Kapoor, V., & Telford, W. G. (2004). Telomere length measurement by fluorescence in situ hybridization and flow cytometry. In *Flow Cytometry Protocols* (pp. 385-398). Humana Press.
- Karlseder, J., Broccoli, D., Dai, Y., Hardy, S. & De Lange, T. (1999) p53- and ATM-dependent apoptosis induced by telomeres lacking TRF2. *Science*, 283, 1321-5.
- Karow, J. K., Constantinou, A., Li, J. L., WEST, S. C. & HICKSON, I. D. (2000) The Bloom's syndrome gene product promotes branch migration of holliday junctions. *Proc Natl Acad Sci U S A*, 97, 6504-8.

- Karow, J.K., Constantinou, A., Li, J.L., West, S.C. and Hickson, I.D. (2000). The Bloom's syndrome gene product promotes branch migration of holiday junctions. *Proc. Natl Acad. Sci. USA*, 97, 6504–6508.
- Keegan, K. S., D. A. Holtzman, A. W. Plug, E. R. Christenson, E. E. Brainerd, G. Flaggs, N. J. Bentley, E. M. Taylor, M. S. Meyn, S. B. Moss, A. M. Carr, T. Ashley, and M. F. Hoekstra. (1996). The Atr and Atm protein kinases associate with different sites along meiotically pairing chromosomes. *Genes Dev.* 10:2423–2437.
- Keith, W. N., Bilisland, A., Hardie, M. & Evans, T. R. (2004) Drug insight: Cancer cell immortality-telomerase as a target for novel cancer gene therapies. *Nat Clin Pract Oncol*, 1, 88-96.
- Kelland LR (2000) Telomerase inhibitors targeting the vulnerable end of cancer? *Anticancer Drugs* 11:503–513.
- Kim, H., & D'Andrea, A. D. (2012). Regulation of DNA cross-link repair by the Fanconi anemia/BRCA pathway. *Genes & development*, 26(13), 1393-1408.
- Kim, S. H., Beausejour, C., Davalos, A. R., Kaminker, P., Heo, S. J. & Campisi, J. (2004) TIN2 mediates functions of TRF2 at human telomeres. *J Biol Chem*, 279, 43799-804.
- Kitts, C. L. (2001). Terminal restriction fragment patterns: a tool for comparing microbial communities and assessing community dynamics. *Biological Sciences*, 69. microbial communities in food-associated matrices and processes. *Food Microbiology* 25, 745-761.
- Kolberg M, Strand KR, Graff P, Andersson KK. (2004). Structure, function, and mechanism of ribonucleotide reductases. *Biochim Biophys Acta.* 1;1699(1-2):1-34.
- Kremer EJ, Pritchard M, Lynch M, Yu S and Holman K, (1991) Mapping of DNA instability at the fragile X to a trinucleotide repeat sequence p(CCG)n. *Science* 252:1711–14.
- Krtolica, A., Parrinello, S., Lockett, S., Desprez, P. Y., & Campisi, J. (2001). Senescent fibroblasts promote epithelial cell growth and tumorigenesis: a link between cancer and aging. *Proceedings of the National Academy of Sciences*, 98(21), 12072-12077.

- Kysela, B., Chovanec, M. & Jeggo, P. A. (2005) Phosphorylation Of Linker Histones By DNA-Dependent Protein Kinase Is Required For DNA Ligase IV-Dependent Ligation In The Presence Of Histone H1. *Proc Natl Acad Sci U S A*, 102, 1877-82.
- Lagah S, Tan I-L, Radhakrishnan P, Hirst RA, Ward JH, et al. (2014) RHPS4 G-Quadruplex Ligand Induces Anti-Proliferative Effects in Brain Tumor Cells. *PLoS ONE* 9(1): e86187. doi:10.1371/journal.pone.0086187.
- Lahtinen, S., Gueimonde, M., Ouwehand, A., Reinikainen, J., Salminen, S., 2005. Probiotic bacteria may become dormant during storage. *Applied and Environmental Microbiology* 71, 1662-1663.
- Lansdorp, P. M., Verwoerd, N. P., van de Rijke, F. M., Dragowska, V., Little, M. T., Dirks, R. W., & Tanke, H. J. (1996). Heterogeneity in telomere length of human chromosomes. *Human molecular genetics*, 5(5), 685-691.
- Law, M. J. et al. (2010) ATR-X Syndrome Protein Targets Tandem Repeats and Influences Allele-Specific Expression in a Size-Dependent Manner. *Cell* 143, 367–378.
- LeBeau MM, Rowley JD. (1984). Heritable fragile sites in cancer. *Nature* 308:607–608.
- Leonetti, C., Amodei, S., Angelo, C., Rizzo, A., Benassi, B., Antonelli, A., Elli, R., Stevens, M., D’Incalci, M., Zupi, G. and Biroccio, A.(2004) Biological Activity of the G-Quadruplex Ligand RHPS4 (3,11-Difluoro-6,8,13-trimethyl-8H-quino[4,3,2-kl]acridinium methosulfate) Is Associated with Telomere Capping Alteration. *Mol Pharmacol*; 66:1138–1146.
- Letsolo, B. T., Rowson, J. & Baird, D. M. (2009) Fusion Of Short Telomeres In Human Cells Is Characterized By Extensive Deletion And Microhomology, And Can Result In Complex Rearrangements. *Nucleic Acids Res*, 38, 1841-52.
- Leung, J. W. et al. (2013). Alpha thalassemia/mental retardation syndrome X-linked gene product ATRX is required for proper replication restart and cellular resistance to replication stress. *J. Biol. Chem.* 288, 6342–6350.

- Li, B. & Comai, L. (2002) Displacement Of Dna-Pkcs From Dna Ends By The Werner Syndrome Protein. *Nucleic Acids Res*, 30, 3653-61.
- Li, B. & De Lange, T. (2003) Rap1 affects the length and heterogeneity of human telomeres. *Mol Biol Cell*, 14, 5060-8.
- Li, B. & Lustig, A. J. (1996) A Novel Mechanism For Telomere Size Control In *Saccharomyces Cerevisiae*. *Genes Dev*, 10, 1310-26.
- Lieber, M. R. (2010) The mechanism of double-strand DNA break repair by the nonhomologous DNA end-joining pathway. *Annu Rev Biochem*, 79, 181-211
- Lieber, M. R., Ma, Y., Pannicke, U. & Schwarz, K. (2003) Mechanism And Regulation Of Human Non-Homologous Dna End-Joining. *Nat Rev Mol Cell Biol*, 4, 712-20.
- Lin, K. W., & Yan, J. (2005). The telomere length dynamic and methods of its assessment. *Journal of cellular and molecular medicine*, 9(4), 977-989.
- Lingner, J., Cech, T. R., Hughes, T. R. & Lundblad, V. (1997) Three Ever Shorter Telomere (EST) genes are dispensable for in vitro yeast telomerase activity. *Proc Natl Acad Sci U S A*, 94, 11190-5.
- Lipps H and Rhodes D (2009) G-quadruplex structures: in vivo evidence and function. *Cell Biology* (19)8:414-422
- Liu, Y., Fiskum, G., & Schubert, D. (2002). Generation of reactive oxygen species by the mitochondrial electron transport chain. *Journal of neurochemistry*, 80(5), 780-787.
- Loayza, D., Parsons, H., Donigian, J., Hoke, K. & De Lange, T. (2004) DNA binding features of human POT1: a nonamer 5'-TAGGGTTAG-3' minimal binding site, sequence specificity, and internal binding to multimeric sites. *J Biol Chem*, 279, 13241-8.
- Loeb, L. A. & Monnat, R. J., Jr. (2008) Dna Polymerases And Human Disease. *Nat Rev Genet*, 9, 594-604.
- Loft, S., & Poulsen, H. E. (1996). Cancer risk and oxidative DNA damage in man. *Journal of molecular medicine*, 74(6), 297-312.

- Loft, S., Vistisen, K., Ewertz, M., Tjønneland, A., Overvad, K., & Poulsen, H. E. (1992). Oxidative DNA damage estimated by 8-hydroxydeoxyguanosine excretion in humans: influence of smoking, gender and body mass index. *Carcinogenesis*, 13(12), 2241-2247.
- Luderus, M. E., Van Steensel, B., Chong, L., Sibon, O. C., Cremers, F. F. & De Lange, T. (1996) Structure, subnuclear distribution, and nuclear matrix association of the mammalian telomeric complex. *J Cell Biol*, 135, 867-81.
- Lukusa T and Fryns J.P (2008). Human chromosome fragility. *Biochimica et Biophysica Acta* 1779:3–16.
- Ma, Y., Lu, H., Tippin, B., Goodman, M. F., Shimazaki, N., Koiwai, O., Hsieh, C. L., Schwarz, K. & Lieber, M. R. (2004) A Biochemically Defined System For Mammalian Nonhomologous Dna End Joining. *Mol Cell*, 16, 701-13.
- Ma, Y., Schwarz, K. & Lieber, M. R. (2005) The Artemis:Dna-Pkcs Endonuclease Cleaves Dna Loops, Flaps, And Gaps. *Dna Repair (Amst)*, 4, 845-51.
- Magenis RE, Hecht F and Lovrien EW (1970). Heritable fragile site on chromosome 16:probable localization of haptoglobin locus in man. *Science* 179:85–87.
- Marrone, A. & Mason, P. J. (2003) Dyskeratosis congenita. *Cell Mol Life Sci*, 60, 507-17.
- Marsh TL (1999) Terminal restriction fragment length polymorphism (T-RFLP): an emerging method for characterizing diversity among homologous populations of amplification products. *Curr Opin Microbiol* 2: 323–327.
- Martin, G. M. (1982) Syndromes of accelerated aging. *Natl Cancer Inst Monogr*, 60, 241-7.
- Martin, G. M. and Oshima, J. (2000). Lessons from human progeroid syndromes. *Nature*, 408, 263-266.
- Masutomi, K. & Hahn, W. C. (2003) Telomerase and tumorigenesis. *Cancer Lett*, 194, 163-72.
- McClintock, B. (1939) The Behavior in Successive Nuclear Divisions of a Chromosome Broken at Meiosis. *Proc Natl Acad Sci U S A*, 25, 405-16.193

- Mckee, B. D. (2004) Homologous pairing and chromosome dynamics in meiosis and mitosis. *Biochim Biophys Acta*, 1677, 165-80.
- McSharry, B. P., Jones, C. J., Skinner, J. W., Kipling, D., & Wilkinson, G. W. G. (2001). Human telomerase reverse transcriptase-immortalized MRC-5 and HCA2 human fibroblasts are fully permissive for human cytomegalovirus. *Journal of General Virology*, 82(4), 855-863.
- Metcalfe, J. A., Parkhill, J., Campbell, L., Stacey, M., Biggs, P., Byrd, P. J. & Taylor, A. M. (1996) Accelerated telomere shortening in ataxia telangiectasia. *Nat Genet*, 13, 350-3.
- Meyn, M. S. (1999) Ataxia-telangiectasia, cancer and the pathobiology of the ATM gene. *Clin Genet*, 55, 289-304.
- Mirkin, E. V., & Mirkin, S. M. (2007). Replication fork stalling at natural impediments. *Microbiology and Molecular Biology Reviews*, 71(1), 13-35.
- Mitchell, J. R., Wood, E. & Collins, K. (1999) A telomerase component is defective in the human disease dyskeratosis congenita. *Nature*, 402, 551-5.
- Moeseneder, M. M., Arrieta, J. M., Muyzer, G., Winter, C., & Herndl, G. J. (1999). Optimization of terminal-restriction fragment length polymorphism analysis for complex marine bacterioplankton communities and comparison with denaturing gradient gel electrophoresis. *Applied and environmental microbiology*, 65(8), 3518-3525.
- Molenaar, J. J. et al. (2012) Sequencing of neuroblastoma identifies chromothripsis and defects in neuritogenesis genes. *Nature* 483, 589–593.
- Munoz-Jordan, J. L., Cross, G. A., De Lange, T. & Griffith, J. D. (2001) t-loops at trypanosome telomeres. *Embo J*, 20, 579-88.
- Nasir, M., Fatihah, N., Ponnuraj Kannan, T., Sulaiman, S. A., Shamsuddin, S., Ahmad, A., & Stangaciu, S. (2014). Telomeres and Oxidative Stress. *British Journal of Medicine & Medical Research*, 4(1). 34-48.

- Nielsen, J., & Wohler, M. (1991). Chromosome abnormalities found among 34910 newborn children: results from a 13-year incidence study in Århus, Denmark. *Human genetics*, 87(1), 81-83.
- O'Driscoll M, Ruiz-Perez VL, Woods CG, Jeggo PA, Goodship JA. (2003). A splicing mutation affecting expression of ataxia-telangiectasia and Rad3-related protein (ATR) results in Seckel syndrome. *Nat. Genet.* 33:497–501.
- Olovnikov, A. M. (1971) [Principle of marginotomy in template synthesis of polynucleotides]. *Dokl Akad Nauk SSSR*, 201, 1496-9.
- O'Malley, R.C. & Ecker, J.R. (2010). Linking genotype to phenotype using the Arabidopsis unimutant collection. *Plant J.* 61: 928–940.
- Opresko, P. L., Fan, J., Danzy, S., Wilson, D. M., & Bohr, V. A. (2005). Oxidative damage in telomeric DNA disrupts recognition by TRF1 and TRF2. *Nucleic acids research*, 33(4), 1230-1239.
- Opresko, P. L., Von Kobbe, C., Laine, J. P., Harrigan, J., Hickson, I. D. & Bohr, V. A. (2002) Telomere-binding protein TRF2 binds to and stimulates the Werner and Bloom syndrome helicases. *J Biol Chem*, 277, 41110-9.
- Opresko, P. L., von Kobbe, C., Laine, J. P., Harrigan, J., Hickson, I. D. and Bohr, V. A. (2002). Telomere-binding protein TRF2 binds to and stimulates the Werner and Bloom syndrome helicases. *J. Biol. Chem.*, 277, 41110-41119.
- Orren, D. K. (2006). Werner syndrome: molecular insights into the relationships between defective DNA metabolism, genomic instability, cancer and aging. *Front. Biosci.*, 11, 2657-2671.
- Osborn AM, Moore ERB & Timmis KN (2000) An evaluation of terminal-restriction fragment length polymorphism (T-RFLP) analysis for the study of microbial community structure and dynamics. *Environ Microbiol* 2: 39–50.

- Packer, L., & Fuehr, K. (1977). Low oxygen concentration extends the lifespan of cultured human diploid cells.
- Palm, W. & De Lange, T. (2008) How shelterin protects mammalian telomeres. *Annu Rev Genet*, 42, 301-34.
- Parrinello, S., Samper, E., Krtolica, A., Goldstein, J., Melov, S. & Campisi, J. (2003) Oxygen sensitivity severely limits the replicative lifespan of murine fibroblasts. *Nat Cell Biol*, 5, 741-7.
- Parkinson N, Lee H and Neidle S (2002) Crystal structure of parallel quadruplexes from human telomeric DNA. *Nature* (417) 876–880.
- Patel D, Phan A and Kuryavyi V (2007) Human telomere, oncogenic promoter and 5'-UTR G-quadruplexes: diverse higher order DNA and RNA targets for cancer therapeutics *Nucleic Acids Research*, (35)22: 7429–7455
- Petkova, R., Chicheva, Z., & Chakarov, S. (2011). Measuring telomere length- from ends to means. *Biotechnology and Biotechnological Equipment*, 25(4), 2576-2582.
- Phan T, Kuryavyi V, Luu N and Patel J (2007) Structure of two intramolecular G-quadruplexes formed by natural human telomere sequences in K⁺ solution. *Nucleic Acids Res.* 35, 6517–6525.
- Pich, U., Fuchs, J. & Schubert, I. (1996) How do Alliaceae stabilize their chromosome ends in the absence of TTTAGGG sequences? *Chromosome Res*, 4, 207-13.
- Polotnianka, R. M., Li, J., & Lustig, A. J. (1998). The yeast Ku heterodimer is essential for protection of the telomere against nucleolytic and recombinational activities. *Current biology*, 8(14), 831-835.
- Pritchett, C. J., Senior, P. V., Sunter, J. P., Watson, A. J., Wilson, R. G. & Appleton, D. R. (1985) Cell Proliferation In Human Colorectal Mucosa In Organ Culture: The Early Adaptive Changes. *J Anat*, 141, 171-9.

- Rizzo, A. et al. (2009) Stabilization of quadruplex DNA perturbs telomere replication leading to the activation of an ATR-dependent ATM signaling pathway. *Nucleic Acids Res.* 37, 5353–5364
- Roberson, R. S., Kussick, S. J., Vallieres, E., Chen, S. Y. & Wu, D. Y. (2005) Escape from therapy-induced accelerated cellular senescence in p53-null lung cancer cells and in human lung cancers. *Cancer Res*, 65, 2795-803.
- Rodriguez, R. et al. (2012) Small-molecule-induced DNA damage identifies alternative DNA structures in human genes. *Nat. Chem. Biol.* 8, 301–310
- Ruiz-Herrera, A., Garcia, F., Giulotto, E., Attolini, C., Egozcue, J., Ponsa, M., & Garcia, M. (2004). Evolutionary breakpoints are co-localized with fragile sites and intrachromosomal telomeric sequences in primates. *Cytogenetic and genome research*, 108(1-3), 234-247.
- Sagi J (2013) G-quadruplexes incorporating modified constituents: a review. *J Biomol Struct Dyn.*
- Saito, I., Takayama, M., Sugiyama, H., Nakatani, K., Tsuchida, A., & Yamamoto, M. (1995). Photoinduced DNA Cleavage Via Electron Transfer: Demonstration That Guanine Residues Located 5'to Guanine Are The Most Electron-Donating Sites. *Journal Of The American Chemical Society*, 117(23), 6406-6407.
- Salk, D. (1982) Werner's syndrome: a review of recent research with an analysis of connective tissue metabolism, growth control of cultured cells, and chromosomal aberrations. *Hum Genet*, 62, 1-5.
- Salvati E, Leonetti C, Rizzo A, Scarsella M, Mottolese M, Galati R, Sperduti I, Stevens M, D’Incalci M, Blasco M, Chiorino G, Bauwens S, Horard B, Gilson E, Stoppacciaro A, Zupi G, and Biroccio A (2007) Telomere damage induced by the G-quadruplex ligand RHPS4 has an antitumor effect. *The Journal of Clinical Investigation* (117)11:3236-3247.

- Saretzki, G., & Zglinicki, T. (2002). Replicative aging, telomeres, and oxidative stress. *Annals of the New York Academy of Sciences*, 959(1), 24-29.
- Sarkies, P., Reams, C., Simpson, L. J. & Sale, J. E. (2010) Epigenetic instability due to defective replication of structured DNA. *Mol. Cell* 40, 703–713
- Sarthy, J., Bae, N. S., Scrafford, J. & Baumann, P. (2009) Human RAP1 inhibits non-homologous end joining at telomeres. *Embo J*, 28, 3390-9.
- Savitsky, K., Sfez, S., Tagle, D. A., Ziv, Y., Sartiel, A., Collins, F. S., Shiloh, Y. & Rotman, G. (1995) The complete sequence of the coding region of the ATM gene reveals similarity to cell cycle regulators in different species. *Hum Mol Genet*, 4, 2025-32.
- Sawada, M., Sun, W., Hayes, P., Leskov, K., Boothman, D. A. & Matsuyama, S. (2003) Ku70 Suppresses The Apoptotic Translocation Of Bax To Mitochondria. *Nat Cell Biol*, 5, 320-9.200.
- Schaffitzel C (2001) In vitro generated antibodies specific for telomeric guaninequadruplex DNA react with *Stylyonchia lemnae* macronuclei. *Proc. Natl. Acad. Sci.* 98, 8572–8577.
- Scherthan, H. (2001) A bouquet makes ends meet. *Nat Rev Mol Cell Biol*, 2, 621-7.
- Schmitt, C. A., Fridman, J. S., Yang, M., Lee, S., Baranov, E., Hoffman, R. M. & Lowe, S. W. (2002) A senescence program controlled by p53 and p16INK4a contributes to the outcome of cancer therapy. *Cell*, 109, 335-46.
- Sen, D., & Gilbert, W. (1990). A sodium-potassium switch in the formation of four-stranded G4-DNA. *Nature*, 344(6265), 410-414.
- Serrano, M., Lin, A. W., Mccurrach, M. E., Beach, D. & Lowe, S. W. (1997) Oncogenic ras provokes premature cell senescence associated with accumulation of p53 and p16INK4a. *Cell*, 88, 593-602.
- Sfeir, A., Kosiyatrakul, S. T., Hockemeyer, D., MacRae, S. L., Karlseder, J., Schildkraut, C. L., & de Lange, T. (2009). Mammalian telomeres resemble fragile sites and require TRF1 for efficient replication. *Cell*, 138(1), 90-103.

- Shay, J.W. & Wright, W.E. Hayflick, his limit, and cellular ageing. *Nat. Rev. Mol. Cell Biol.*, 1, 72–76 (2000).
- Sherr, C. J., & DePinho, R. A. (2000). Cellular Senescence: Minireview Mitotic Clock or Culture Shock?. *Cell*, 102(4), 407-410.
- Shiloh, Y. (2006) The ATM-mediated DNA-damage response: taking shape. *Trends Biochem Sci*, 31, 402-10.
- Simonsen, J. L., Rosada, C., Serakinci, N., Justesen, J., Stenderup, K., Rattan, S. I., ... & Kassem, M. (2002). Telomerase expression extends the proliferative life-span and maintains the osteogenic potential of human bone marrow stromal cells. *Nature biotechnology*, 20(6), 592-596.
- Smith, S. & De Lange, T. (2000) Tankyrase promotes telomere elongation in human cells. *Curr Biol*, 10, 1299-302.
- Smith W and Feigon J (1992) Quadruplex structure of Oxytricha telomeric DNA oligonucleotides. *Nature*, 356, 164–168.
- Sohier, D., Lonvaud-Funel, A., 1998. Rapid and sensitive *in situ* hybridization method for detecting and identifying lactic acid bacteria in wine. *Food Microbiology* 15, 391-397.
- Sutherland GR (1977). Fragile sites on human chromosomes: demonstration of their dependence on the type of tissue culture medium. *Science* 197:265–66
- Sutherland GR (1979). Heritable fragile sites on human chromosomes I. Factors affecting expression in lymphocyte culture. *Am. J. Hum. Genet.* 31:125–35.
- Sutherland, G. R., Baker, E., & Richards, R. I. (1998). Fragile sites still breaking. *Trends in Genetics*, 14(12), 501-506.
- Swiggers, S. J., Nibbeling, H. A., Zeilemaker, A., Kuijpers, M. A., Mattern, K. A. & Zijlmans, J. M. (2004) Telomerase activity level, but not hTERT mRNA and hTR level, regulates telomere length in telomerase-reconstituted primary fibroblasts. *Exp Cell Res*, 297, 434-43.

- Sykorova, E, Leitch, A.R., Fajkus, J. (2000) Asparagales telomerases which synthesize the human type of telomeres. *Plant Mol Biol.*, 60:633–646.
- Takai, H., Smogorzewska, A. & De Lange, T. (2003) DNA damage foci at dysfunctional telomeres. *Curr Biol*, 13, 1549-56.
- Tallec B, Koundrioukoff S, Wilhelm T, Letessier A, Brison O and Debatisse M (2014) Updating the mechanisms of common fragile site instability: how to reconcile the different views? *Cell. Mol. Life Sci.* 71:4489–4494.
- Tahara H, Seimiya H, Shin-ya K, Ide T (2006) New screening technology for development of effective anti-cancer drugs targeting telomere G-tail. *Ejc Supplements* 4: 189–189.
- Toledo F, Coquelle A, Svetlova E and Debatisse M (2000) Enhanced flexibility and aphidicolin-induced DNA breaks near mammalian replication origins: implications for replicon mapping and chromosome fragility. *Nucleic Acids Research* 2000 Vol. 28. NO. 23:4805-4813.
- Tollefsbol, T. O. & Cohen, H. J. (1984) The effect of age on the accumulation of labile triosephosphate isomerase and thymidine incorporation in pokeweed mitogen stimulated human lymphocytes. *J Gerontol*, 39, 398-405.
- Torres, J. Z., Schnakenberg, S. L., & Zakian, V. A. (2004). *Saccharomyces cerevisiae* Rrm3p DNA helicase promotes genome integrity by preventing replication fork stalling: viability of rrm3 cells requires the intra-S-phase checkpoint and fork restart activities. *Molecular and cellular biology*, 24(8), 3198-3212.
- Toussaint, O., Dumont, P., Dierick, J. F., Pascal, T., Fripiat, C., Chainiaux, F., Sluse, F., Eliaers, F., and Remacle, J. (2000). "Stress-induced premature senescence. Essence of life, evolution, stress, and aging." *Ann N Y Acad Sci* 908:85-98.
- Tran P, Mergny J, and Alberti P (2011) Stability of telomeric G-quadruplexes. *Nucleic Acids Research* (39)8: 3282–3294.
- Turner G, Till R and Daniel A (1978). Marker X chromosomes, mental retardation and macroorchidism. *N. Engl. J. Med.* 299:1472.

- Turrens, J. F. (2003). Mitochondrial formation of reactive oxygen species. *The Journal of physiology*, 552(2), 335-344.
- Uringa, E.-J., Youds, J. L., Lisaingo, K., Lansdorp, P. M., & Boulton, S. J. (2011). RTEL1: an essential helicase for telomere maintenance and the regulation of homologous recombination. *Nucleic Acids Research*, 39(5), 1647–1655. doi:10.1093/nar/gkq1045
- Van Steensel, B. & De Lange, T. (1997) Control of telomere length by the human telomeric protein TRF1. *Nature*, 385, 740-3.
- Von Zglinicki, T. (2002) Oxidative Stress Shortens Telomeres. *Trends Biochem Sci*, 27, 339-44.
- Von Zglinicki, T., Saretzki, G., Döcke, W., & Lotze, C. (1995). Mild hyperoxia shortens telomeres and inhibits proliferation of fibroblasts: a model for senescence?. *Experimental cell research*, 220(1), 186-193.
- Venteicher, A. S., Abreu, E. B., Meng, Z., Mccann, K. E., Terns, R. M., Veenstra, T. D., Terns, M. P. & Artandi, S. E. (2009) A human telomerase holoenzyme protein required for Cajal body localization and telomere synthesis. *Science*, 323, 644-8.
- Verdun, R. E., Crabbe, L., Haggblom, C. & Karlseder, J. (2005) Functional human telomeres are recognized as DNA damage in G2 of the cell cycle. *Mol Cell*, 20, 551-61.
- Verdun R.E. and Karlseder J (2006). The DNA damage machinery and homologous recombination pathway act consecutively to protect human telomeres. *Cell* 127:709–720.
- Vulliamy, T. J., Walne, A., Baskaradas, A., Mason, P. J., Marrone, A. & Dokal, I. (2005) Mutations in the reverse transcriptase component of telomerase (TERT) in patients with bone marrow failure. *Blood Cells Mol Dis*, 34, 257-63.
- Waga, S. & Stillman, B. (1998) The DNA replication fork in eukaryotic cells. *Annu Rev Biochem*, 67, 721-51.
- Walpita, D., Plug, A.W., Neff, N.F., German, J. and Ashley, T. (1999). Bloom's syndrome protein, BLM, colocalizes with replication protein A in meiotic prophase nuclei of mammalian spermatocytes. *Proc. Natl Acad. Sci. USA*, 96, 5622–5627.

- Wang, Y., and Patel, D. J. (1993) Solution structure of the human telomeric repeat d[AG3(T2AG3)3] G-tetraplex. *Structure* (1)263–282.
- Wang Y and Patel J (1994) Solution structure of the Tetrahymena telomeric repeat d(T2G4)4 G-tetraplex. *Structure* 2, 1141–1156.
- Watson, L. A. et al. (2013) Atrx deficiency induces telomere dysfunction, endocrine defects, and reduced life span. *J. Clin. Invest.* 123, 2049–2063.
- Watson, J. M. & Riha, K. (2010) Comparative biology of telomeres: Where plants stand. *FEBS Lett*, 584, 3752-3759.206
- Weterings, E. & Chen, D. J. (2008) The Endless Tale Of Non-Homologous End-Joining. *Cell Res*, 18, 114-24.
- Williams, R. S., Dodson, G. E., Limbo, O., Yamada, Y., Williams, J. S., Guenther, G., Classen, S., Glover, J. N., Iwasaki, H., Russell, P. & Tainer, J. A. (2009) Nbs1 Flexibly Tethers Ctp1 And Mre11-Rad50 To Coordinate Dna Double-Strand Break Processing And Repair. *Cell*, 139, 87-99.
- Williams, R. S., Moncalian, G., Williams, J. S., Yamada, Y., Limbo, O., Shin, D. S., Groocock, L. M., Cahill, D., Hitomi, C., Guenther, G., Moiani, D., Carney, J. P., Russell, P. & Tainer, J. A. (2008). Mre11 Dimers Coordinate Dna End Bridging And Nuclease Processing In Double-Strand-Break Repair. *Cell*, 135, 97-109.
- Williamson R, Raghuraman K and Cech R (1989) Monovalent cation-induced structure of telomeric DNA: the G-quartet model. *Cell*, 59: 871–880.
- Williams, R. S., Williams, J. S. & Tainer, J. A. (2007). Mre11-Rad50-Nbs1 Is A Keystone Complex Connecting Dna Repair Machinery, Double-Strand Break Signaling, And The Chromatin Template. *Biochem Cell Biol*, 85, 509-20.
- Wong, L. H. et al. (2010). ATRX interacts with H3.3 in maintaining telomere structural integrity in pluripotent embryonic stem cells. *Genome Res.* 20, 351–360.

- Wu, G. J., Sinclair, C. S., Paape, J., Ingle, J. N., Roche, P. C., James, C. D. & Couch, F. J. (2000) 17q23 amplifications in breast cancer involve the PAT1, RAD51C, PS6K, and SIGma1B genes. *Cancer Res*, 60, 5371-5.
- Wu, L., Davies, S. L., Levitt, N. C. & Hickson, I. D. (2001) Potential role for the BLM helicase in recombinational repair via a conserved interaction with RAD51. *J Biol Chem*, 276, 19375-81.207
- Xin, H., Liu, D., Wan, M., Safari, A., Kim, H., Sun, W., O'connor, M. S. & Songyang, Z. (2007) TPP1 is a homologue of ciliate TEBP-beta and interacts with POT1 to recruit telomerase. *Nature*, 445, 559-62.
- Yankiwski, V., Marciniak, R.A., Guarente, L. and Neff, N.F. (2000). Nuclear structure in normal and Bloom syndrome cells. *Proc. Natl Acad. Sci. USA*, 97, 5214–5219.
- Ye, J. Z., Donigian, J. R., Van Overbeek, M., Loayza, D., Luo, Y., Krutchinsky, A. N., Chait, B. T. & De Lange, T. (2004a) TIN2 binds TRF1 and TRF2 simultaneously and stabilizes the TRF2 complex on telomeres. *J Biol Chem*, 279, 47264-71.
- Ye, J. Z., Hockemeyer, D., Krutchinsky, A. N., Loayza, D., Hooper, S. M., Chait, B. T. & De Lange, T. (2004b) POT1-interacting protein PIP1: a telomere length regulator that recruits POT1 to the TIN2/TRF1 complex. *Genes Dev*, 18, 1649-54.
- Yeager, T. R., Neumann, A. A., Englezou, A., Huschtscha, L. I., Noble, J. R. & Reddel, R. R. (1999) Telomerase-negative immortalized human cells contain a novel type of promyelocytic leukemia (PML) body. *Cancer Res*, 59, 4175-9.
- Yoo, J.E., Oh, B.K. & Park, Y.N. (2009). Human PinX1 mediates TRF1 accumulation in nucleolus and enhances TRF1 binding to telomeres. *J. Mol. Biol.* 388: 928–940.
- Yuan, K., et al. (2009). PinX1 is a novel microtubule-binding protein essential for accurate chromosome segregation. *J. Biol. Chem.* 284: 23072–23082.
- Yunis JJ, Soreng AL. (1984). Constitutive fragile sites and cancer. *Science* 226:1199–1204.

- Zahler, A. M. & Prescott, D. M. (1988) Telomere terminal transferase activity in the hypotrichous ciliate *Oxytricha nova* and a model for replication of the ends of linear DNA molecules. *Nucleic Acids Res*, 16, 6953-72.208.
- Zahler AM, Williamson JR, Cech TR, and Prescott DM (1991). Inhibition of telomerase by G-quartet DNA structures. *Nature* 350: 718–720.
- Zeng Z, et al. (2010). Structural basis of selective ubiquitination of TRF1 by SCFFbx4. *Dev. Cell*, 18: 214–225.
- Zhao H And Piwnica H. (2001). ATR-Mediated Checkpoint Pathways Regulate Phosphorylation and Activation of Human Chk1. *Molecular And Cellular Biology* 21;(13) 63110-1093.
- Zhong, Z. H. et al. (2007) Disruption of telomere maintenance by depletion of the MRE11/RAD50/NBS1 complex in cells that use alternative lengthening of telomeres. *J. Biol. Chem.* 282, 29314–29322.
- Zhong, S., Hu, P., Ye, T.Z., Stan, R., Ellis, N.A. and Pandolfi, P.P. (1999). A role for PML and the nuclear body in genomic stability. *Oncogene*, 18, 7941–7947.
- Zhou, X.Z., et al. (2011). The telomerase inhibitor PinX1 is a major haploinsufficient tumor suppressor essential for chromosome stability in mice. *J. Clin. Invest.* 121: 1266–1282.
- Zhu, J., Woods, D., McMahon, M. & Bishop, J. M. (1998) Senescence of human fibroblasts induced by oncogenic Raf. *Genes Dev*, 12, 2997-3007.
- Zhu, X. D., Küster, B., Mann, M., Petrini, J. H., & de Lange, T. (2000). Cell-cycle-regulated association of RAD50/MRE11/NBS1 with TRF2 and human telomeres. *Nature genetics*, 25(3), 347-352.
- Zhuang, J., Jiang, G., Willers, H. & Xia, F. (2009). Exonuclease Function Of Human Mre11 Promotes Deletional Nonhomologous End Joining. *J Biol Chem*, 284, 30565-73.

- Zlotorynski E, Rahat A, Skaug J, Ben-Porat N, Ozeri E, Hershberg R, Levi A, Scherer SW, Margalit H And Kerem B (2003). Molecular basis for expression of common and rare fragile sites. *Mol Cell Biol* 23(20):7143–7151.